The use of platelet-rich biopolymers in the enhancement of synthetic scaffolds for ligament tissue engineering applications

Rachael Amanda Bell

Submitted in accordance with the requirements for the degree of
Doctor of Philosophy

Department of Oral Biology, School of Dentistry
Faculty of Medicine and Health
The University of Leeds

August, 2018

The candidate confirms that the work submitted is her own and that appropriate credit has been given where reference has been made to the work of others.

Acknowledgements

Firstly, I need to thank my parents, without whom this thesis could not exist. I am particularly grateful for their unconditional belief in my capabilities, and for putting up with my rants. I would also like to thank them for housing me during the write-up phase, and for accepting that this phase was a lot longer than planned.

I would also like to thank Fatima, for being the greatest friend anyone could wish for. Without her endless support and generosity this would have felt impossible. Thanks for all the junk food, coffee and excellent company, as well as your lab-related wisdom.

Many thanks to Phil for his help with the rheology work, and to Shane and Georg for their commitment to the necessary Friday evening pub sessions. I extend my gratitude to everyone in Oral Biology for their help over these three years.

Abstract

Introduction: Rupture of the anterior cruciate ligament (ACL) of the knee is a common injury among athletes, leading to instability of the knee. Due to the poor healing capacity of this ligament, reconstruction is currently the only suitable method of treatment. At present, material for reconstruction is most often harvested from the donor's patellar tendon, which can lead to issues with donor site morbidity and further knee instability. This has led to the development of synthetic ligaments, which have demonstrated varying levels of success. Xiros Ltd. (Leeds) have developed a woven polyethylene terephthalate (PET) ligament prosthesis able to induce tissue formation *in vivo*. However, tissue induction is slow, leaving the material exposed to abrasive forces upon implantation, which eventually leads to graft failure.

Objective: To assess whether a hybrid construct, composed of the Xiros PET ligament and a platelet-rich biopolymer coating, can enhance synovial cell proliferation, infiltration and expression of extracellular matrix genes, which may indicate promotion of tissue induction.

Methods: Primary bovine synovial cell (bSC) cultures were established from the metatarsophalangeal joints of 12-18 month old bovines. Venous blood was taken from healthy human donors and platelet-rich and platelet-poor plasma fractions were extracted. 3D cell-seeded hybrid ligament constructs were fabricated by seeding bSCs onto sections of Xiros Ltd. PET scaffold before coating them with various combinations of plasma, collagen and alginate. Cells were monitored within coated constructs using confocal microscopy, DNA content analysis and Live/dead staining. Biopolymers were characterised using scanning electron microscopy (SEM) and rheology. Coating longevity was assessed using light microscopy image analysis. Cyclic tensile strain (5% strain at a frequency of 1 Hz) was applied to the three most promising coated constructs using an in-house house developed bioreactor, and qRT-PCR was used to measure changes in expression of ligament and non-ligament associated genes. The effect of cyclic tensile strain on *tPA* and *PAI-1* gene expression was analysed using qRT-PCR and secreted PAI-1 protein was assessed using Western blot.

Results: Alginate-based coatings demonstrated the greatest stability, but significantly inhibited cell infiltration and proliferation. In contrast both plasma and collagen coatings had poor longevity, but promoted cell infiltration, in comparison with the non-coated control scaffold. All constructs supported good cell viability. PDGF-AB and IGF-1 release from coatings occurred up to 3 days. Changes in expression of ECM and transcription factor genes

were inconsistent between donors. Cyclic tensile strain increased cell proliferation in all constructs. The longevity of the 100% plasma (P100) coating was greatly enhanced by the application of cyclic tensile strain, leading to selection of this construct for final studies. Strain induced no change in *tPA* gene expression but caused a significant upregulation of *PAI-1* gene expression and protein secretion, indicating a possible mechanism of enhanced coating longevity. Increasing the platelet density of the P100 coating had no significant effect on cell proliferation nor transcription of ECM genes.

Discussion: This study has demonstrated that bovine synovial cell-seeded 3D hybrid ligament constructs composed of the Xiros Ltd. PET scaffold and a biopolymer coating, can be successfully fabricated, and are compatible with the cyclic strain bioreactor utilised for this work. The 100% plasma-coated construct was the most successful candidate due to its ability to promote cellular infiltration, as well as its superior longevity when subjected to cyclic tensile strain. Application of cyclic tensile strain to cell-seeded constructs resulted in upregulation of PAI-1, which may have contributed to this increase in coating longevity.

Conclusion: These findings demonstrate the potential of a PET-fibrin construct for ligament regeneration purposes, and indicate the importance of regular exercise of the knee immediately following ACL reconstruction. Further studies should focus on the behaviour of this construct *in vivo*.

Contents

List of Figures

List of Tables

List of Abbreviations

2D	Two-dimensional
3D	Three-dimensional
ACL	Anterior cruciate ligament
AMB	Anteromedial bundle
ANC-1	Nuclear anchorage protein
ANOVA	Analysis of variance
bFGF	Basic fibroblast growth factor
bHLH	Basic helix-loop-helix
BMSC	Bone marrow stem cells
BSA	Bovine serum albumin
bSC	Bovine synovial cells
CD	Cluster of differentiation
cDNA	Complementary Deoxyribonucleic acid
COL1A1	Collagen type I alpha I
COL3A1	Collagen type III alpha I
DAPI	4′,6-diamidino-2-phenylindole
DMEM	Dulbecco's Modified Eagles Medium
DMSO	Dimethyl sulfoxide
dNTPs	Deoxyribonucleotides
ECM	Extracellular matrix
EDTA	Ethylenediaminetetraacetic acid
EGF	Epitdermal growth factor
ELISA	Enzyme-linked immunosorbent assay
FBS	Foetal bovine serum
FDA	Food and drug Administration
FDP	Fibrin degradation products

FpA	Fibrinopeptide A
FpB	Fibrinopeptide B
GAG	Glycosaminoglycan
GAPDH	Glyceraldehyde-3-phosphate dehydrogenase
GTP-ases	Guanosine triphosphate-ases
HDF	Human dermal fibroblasts
HPRT1	Hypoxanthine Phosphoribosyltransferase I
HSCT	Haematopoietic stem cell transplantation
IGF-1	Insulin-like growth factor-I
KASH	Klarsicht/ANC-1/Syne Homology
LDH	Lactate dehydrogenase
LINC	Linker of Nucleoskeleton and Cytoskeleton
LK	Leeds-Keio
LVER	Linear viscoelastic region
MCL	Medial collateral ligament
MMP	Matrix metalloprotease
mRNA	Messenger RNA
MSC	Mesenchymal stem cells
NBF	Neutral buffered formalin
NCBI	National Centre for Biotechnology Information
NPC	Nuclear pore complex
PAI-1	Plasminogen activator inhibitor-I
PB-MSC	Phosphate buffered saline
PBS	Peripheral blood-derived MSCs
PCL	Posterior cruciate ligament
PCR	Polymerase chain reaction
PDGF	Platelet-derived growth factor
PET	Polyethylene terephthalate

PLB	Posterolateral bundle
PPP	Platelet-poor plasma
PRF	Platelet-rich fibrin
PRGF	Preparations rich in growth factors
PRP	Platelet-rich plasma
qRT-PCR	Quantitative real time PCR
RGD	Arginine-glycine-aspartic acid
rhVEGF	Ribonucleic acid
RNA	Recombinant human VEGF
ROCK	Rho-associate protein kinase
RUNX2	Runt-related transcription factor 2
SCX	Scleraxis
SEM	Scanning electron microscopy
Strep-HRP	Streptavidin-Horseradish peroxidase
SUN	Domain containing Sad1 and UNC84
TBS+T	Tris buffered saline + 1% Tween 20
TGF-β	Transforming growth factor-beta
TMB	Tetramethylbenzidine
TNC	Tenascin-C
tPA	Tissue-type plasminogen activator
VEGF	Vascular endothelial growth factor

Chapter 1

Introduction and literature review

Tissue engineering, also commonly referred to as regenerative medicine, is an interdisciplinary field which aims to maintain and/or restore tissue function and integrity as an alternative to transplantation (Fergal, 2011). Transplantation generally involves the use of either allogenic tissue (from a donor), or autogenic tissue (from a healthy area of the patient). In addition to the limited availability of donor tissues, allogenic tissue transplantation can give rise to immunological rejection in the recipient, creating the need for immunosuppressive therapy. Even in circumstances where an autologous transplant is possible, morbidity at the donor site presents an additional problem, by creating a second area of deficient tissue (Laurencin *et al*., 1999).

Tissue engineering is considered to include three main strategies. The first involves the direct injection of bolus cells or growth factors, either into the tissue of interest, or into the systemic circulation. Examples include haematopoietic stem cell transplantation (HSCT), which has been indicated for a number of blood diseases (Majhail *et al.*, 2012), and intravenous recombinant human vascular endothelial growth factor (rhVEGF) infusion for treatment of angina through the revascularisation of the infarcted heart *(*Henry *et al.*, 2003). The second strategy involves incorporating signalling molecules, such as growth factors, into a biological or synthetic scaffold which can then be implanted. The intention is that this will promote tissue growth over the scaffold. The final and most challenging method involves the *ex vivo* production of three dimensional tissues using a scaffold, cells, molecular signalling, and a bioreactor. Engineered biological tissues may then be grafted into the damaged area (Lee *et al*., 2011).

Significant advances have been made in fields of orthopaedic tissue engineering; an area of medical research which is becoming increasingly important due to the ageing population. In particular, research associated with bone tissue engineering has shown promising results (Amini *et al*., 2012). A field which is currently less prominent is that of ligament tissue engineering. A literature search conducted using PubMed in October 2017 produced 36,383 results for ‘bone tissue engineering,’ and 10,418 results for ‘cartilage tissue engineering,’ whereas searching ‘ligament tissue engineering’ only generated 1,941 results. This demonstrates the comparative lack of research in this field and thus the requirement for further work.

Of particular significance are the clinical problems associated with damage to the anterior cruciate ligament (ACL) of the knee which connects the femur to the tibia. ACL injury is incredibly common in athletes, accounting for approximately 40% of all serious injuries. In

the case of a complete tear, the ACL is incapable of self-healing and will require surgical intervention to repair the ligament (NHS, 2013). This inability to heal has been associated with its limited blood supply resulting from its intra-articular position. Within the joint, there is an absence of clot formation, which normally aids healing by acting as a scaffold for cellular ingrowth, and providing growth factors necessary for effective repair (Murray *et al*., 2007).

1.1 Current approaches to ACL repair

Over the years, orthopaedic surgery has seen a number of approaches to reconstructing a ruptured ACL. Primary repair consists of suturing the native ligament back together at the rupture site, but this procedure is no longer recommended due to the repaired ligaments becoming functionally inadequate in a high proportion of cases (Fu *et al.*, 2000). Augmented primary repair involves placing additional tissue in an extra-articular position, in an attempt to further stabilise the reconstruction. However, the tissue used is generally weaker than ligament tissue and its placement at non-anatomical sites has not been found to enhance joint stability. Alternative augmentation methods involve placing an artificial support over the top of the primary repair. Although a study using a PET augmentation device reported an improvement in ACL tensile strength, and decreased joint laxity by 16 weeks post-surgery (Seitz *et al.*, 2013), it is now widely accepted that both non-augmented and augmented primary repair is not a suitable treatment method, and that complete replacement of the damaged ACL with a graft is preferable (Kiapour and Murray, 2013).

1.1.1 Biologic ACL grafts

Biologic grafts may be in the form of either autografts (harvested from another site within the patient) or allografts (harvested from a cadaver). Choices for autografts include patellar tendon, semitendinosus/gracilis tendon and quadriceps tendon. For allografts, the options include Achilles tendon, patellar tendon and hamstring tendon (Fu *et al.*, 2000). The current gold standard treatment for reconstruction uses the middle third of the autologous patellar tendon, which is used to form a bone-tendon-bone graft in the place of the ACL. However, there are still significant problems associated with this method. Firstly, this treatment fails to restore the normal mechanics of the knee, leading to reduced joint flexion and uneven loadbearing (Hall *et al*., 2012). A study conducted between 1991 and 1994 found that 30.5% of patients that underwent ACL reconstruction presented with early complications post-surgery, with 26.7% of patients requiring reoperations (Kartus *et al.*, 1999). Consecutive operations are less likely to be successful and instability of the knee predisposes the patient to osteoarthritis (OA).

Secondly, the use of an autograft requires tissue to be harvested from an otherwise healthy area, often leading to donor site morbidity. Allograft material is associated with high rates of

immunological rejection and disease transmission, as well as issues with material availability (Kiapour and Murray, 2013). Both autograft and allograft material must be attached to bones, and this is where the breaking load greatly decreases. Surgical fixation, by suture or stapling, results in a breaking load of less than 200 N, whereas breaking loads of human ACLs have been reported to be as high as 1725-2160 N. Even by using screws to attach the grafted tissue to the bone, the breaking load does not exceed around 600 N (Dunn, 1998).

1.1.2 Synthetic ACL grafts

To try to address some of the issues associated with biologic grafts, a number of materials have been used as artificial ligaments since the early 1900s. Silver wire, silk strings and nylon were some of the first examples used, however early rupture meant that they were never advanced to clinical trial. In the latter half of the twentieth century, ligaments composed of Teflon and polypropylene were used to replace human ligaments. However, high rupture rate and inflammatory responses from surrounding tissues meant that use of these materials was soon abandoned (Legnani *et al.* 2010). A carbon fibre ligament was developed in 1977 by Jenkins *et al.*, which was eventually used to replace the human ACL in 1981, after promising results were reported in a rabbit model. Yet, after initially encouraging results, it was found that the material had poor resistance to torsion forces, which resulted in early rupture and subsequent carbon deposition within the knee joint, as well as in the liver (Rushton *et al.*, 1983). All later artificial ligaments, including those composed of Gore-Tex and Dacron, which were initially approved by the Food and Drug Administration (FDA), were abandoned due to unsatisfactory results. Mechanical fatigue, as well as formation of detrimental wear debris, were the main problems associated with artificial ligaments.

In 1982, the Leeds-Keio (LK) ligament was developed by a collaboration between the University of Leeds (UK) and Keio University (Japan), and is now commercially available as a product from Xiros Ltd., a company based near Leeds. This is a woven polyethylene terephthalate (PET) tape comprising of 9 yarns, each consisting of 96 monofilaments with diameters of 20 μm. Its maximum tensile strength has been reported at 820 N, increasing to 2000 N after sufficient tissue ingrowth. The stiffness of the Xiros ligament has been measured at 200 N/mm^2 (Fujikawa *et al*., 2000), which is relatively similar to the 242 N/mm^2 reported for young ACL tissue (Woo *et al.,* 1999). Due to its woven structure, cells are able to integrate into this scaffold-based prosthesis, allowing the formation of new tissue. The ligament was approved for use as an ACL substitute and has been implanted in over 50,000 patients worldwide (Legnani *et al*., 2010). However, a number of follow-up studies indicated unsatisfactory performance of the synthetic graft due to high rates of knee instability and ligament rupture before 5 years post operation. This led to many studies concluding that the

Xiros ligament is not suitable as an ACL substitute (Engstrom *et al.,* 1993; Denti *et al*., 1995; Rading and Peterson, 1995; Murray and Macnicol, 2004).

Studies have shown that tissue induction in the Xiros ligament is relatively slow (Shroven *et al.,* 1994), leading to exposed areas of the material which are susceptible to abrasive forces when in contact with bone. This can lead to accumulation of wear debris, which may subsequently cause synovitis within the joint (Chen *et al.,* 2014). One possible method for enhancing tissue induction is by promoting the bioactivity of the extracellular environment, by combining the Xiros ligament with a bioactive polymer component such as platelet-rich plasma (PRP), which provides growth factors capable of stimulating cellular activity at concentrations which are physiologically relevant. The main advantages of using PRP over recombinant factors are as follows. Firstly, by using an autologous plasma product, the complications associated with regulations and approval are removed. Secondly, the risks of immunological reactions or carcinogenesis are reduced. Finally, recombinant growth factors are expensive, whereas autologous PRP may be derived simply and cheaply from the patient (Sun *et al*., 2010).

Other biological materials which have shown promise as cell substrates for the purposes of tissue engineering include collagen and alginate. The aim of the work presented in this thesis was to combine the Xiros ligament with different mixes of PRP, collagen and alginate biopolymers in order to speed up tissue induction throughout the ligament. The objective was to develop an optimum hybrid construct which induced maximum cell proliferation and migration, whilst also being stable enough to support cell growth until a *de novo* ECM has been synthesised.

The importance of applying relevant mechanical forces to the developing ligament has been extensively demonstrated, as discussed in further detail in this chapter (section 1.3). As such, the hybrid constructs were also subjected to cyclic strain using an in-house developed bioreactor. By exposing the constructs to an environment which mimics the *in vivo* one, it was anticipated that effective selection of an optimum hybrid construct could be achieved.

1.2 Ligament structure

Skeletal ligaments are composed of tightly packed collagen fibres (85% of which is collagen type I) which attach to the ends of bones forming a joint. Their purpose is to support the joint and allow correct movement. A small population of fibroblasts are responsible for the synthesis and maintenance of this collagenous matrix. Other components of the matrix include proteins such as elastin, actin, lamanin, and integrins (Frank *et al*., 2004).

Further analysis of ligament structure, using polarizing light, has shown the collagen fibres to be arranged into bundles along the length of the ligament. The presence of a sinusoidal wave-

like architecture has also been demonstrated, which is known as 'crimp.' The presence of crimp is believed to allow loading of the ligament without causing damage, as these wavy regions can straighten during stretching of the ligament.

It has often been noted that ligaments and tendons share many characteristics, and this has led to the use of tendons for the purpose of ligament reconstruction (Webster *et al.,* 2016). However, a histological and biochemical comparison carried out by Amiel *et al.* (1984), demonstrated a higher cell density in rabbit ligaments in comparison with their tendons, with ligament cell populations appearing more heterogeneous. In addition, ligaments contained less collagen type I and more glycosaminoglycans (GAGs), leading to the authors hypothesising that the ligament differentiation process is slower than that of tendons. It is worth noting that there was significant variation found between different ligaments and between different tendons, making it difficult to determine the fundamental differences between the two tissues. Ligaments are generally considered to be more metabolically active than tendons (Ng, 2002).

The ACL, posterior cruciate ligament (PCL) and medial collateral ligament (MCL) of the knee connect the femur to the tibia, and are all key structures in stabilisation of the knee joint. The ACL in particular is responsible for restricting forward motion of the tibia and resisting rotational loads on the knee (Duthon *et al.,* 2006). From its attachment at the femur, the ACL runs diagonally through the joint, such that it is anterior, medial and distal to the tibia. The total length of the ACL ranges from 22-41mm, and its width from 7-12 mm (Amis and Dawkins, 1991). From the femur to the tibia, the cross-sectional area of the ACL increases, with the ligament and fans out as it attaches to the tibia (Bernard *et al.,* 1997). Girgis *et al.* (1975) functionally separated the ACL into a two bundle model which has been widely accepted by those in the field. This model describes an anteromedial bundle (AMB) and a posterolateral bundle (PLB), which are loaded independently upon knee flexion and extension (Figure 1.1). The ACL rotates slightly upon flexion and fibres of the AMB spiral around the rest of the ligament. Fibres of the AMB tighten and extend with 30˚ of flexion, whereas the PLB becomes slack. When the joint surpasses 90˚ of flexion, the AMB fibres continue to extend, and the PLB fibres also then start to tighten as the joint becomes fully flexed (Amis and Dawkins, 1991).

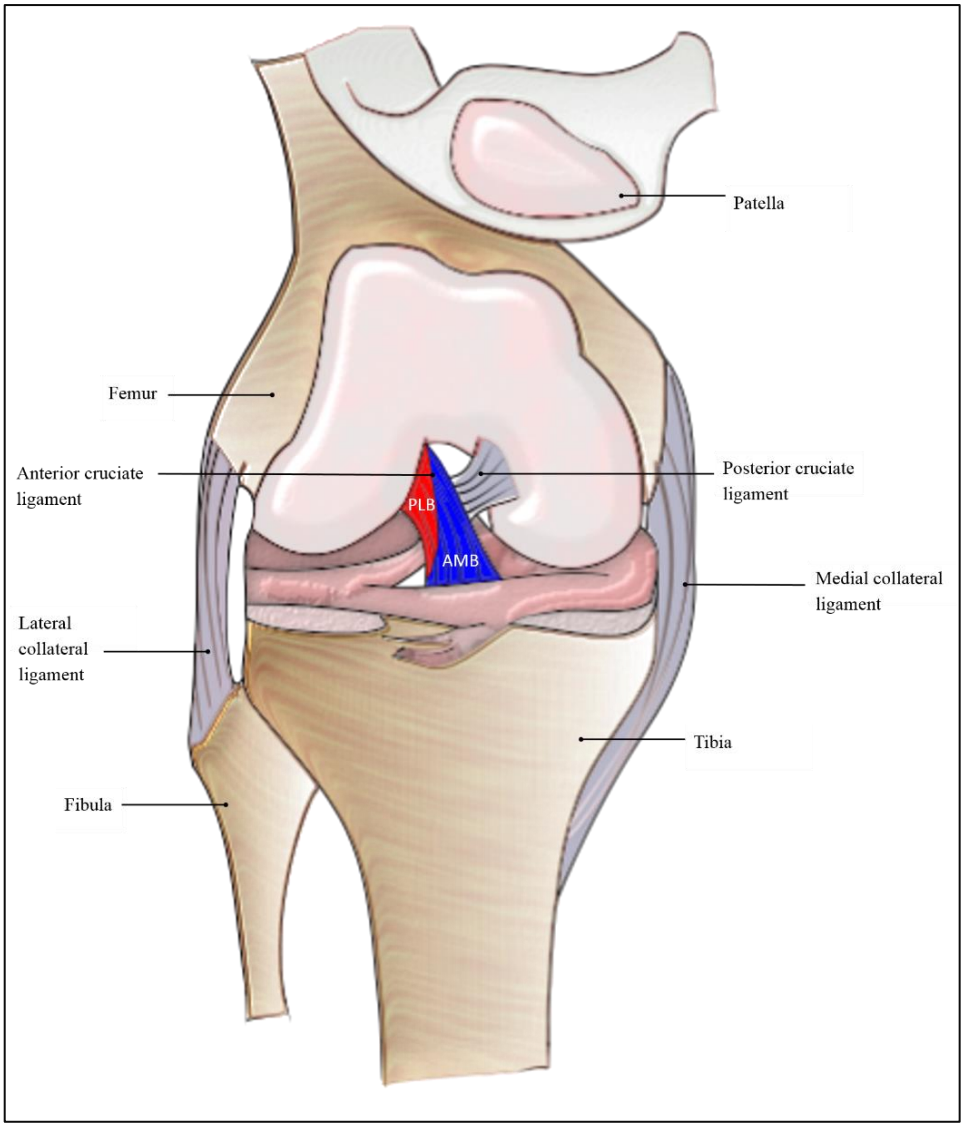

Figure 1.1 Position of the anterior cruciate ligament.
The knee joint, showing the position of the anterior cruciate ligament connecting the femur to the tibia. The anteromedial bundle (AMB) and posterolateral bundle (PLB) of the two-bundle model are shown in blue and red respectively. Adapted from (Tandeter and Shvartzman, 1999).

At the microscopic level, ACL tissue can be divided into three key areas (Figure 1.2). The proximal section (where the ACL connects to the femur), is highly cellular, containing ovoid cells as well as spindle-like fibroblasts. This fibrocartilage region contains collagen type II, which is normally associated with cartilage tissue, as well as glycoproteins such as fibronectin and laminin (Duthon *et al.*, 2006).

The central mid-substance of the ACL has very few cells, but those which are present are spindle-like fibroblasts responsible for maintaining the dense collagen fibres to which they attach. It is in this region that the collagen crimp pattern, characteristic of ligament tissue, is evident. Fibroblasts seem to be positioned such that they follow these crimp wave patterns (Murray and Spector, 1999).

The distal region of the ACL, where it connects to the tibia, is the toughest section of the ligament. Here, the tissue is rich with chondrocytes and ovoid fibroblasts, which resemble cells of articular cartilage. Cells in this region are highly active, as indicated by their relative abundance of organelles. Collagen fibres in this region are less dense than in the central region (Duthon *et al.,* 2006).

The large collagen bundles which compose the ACL are described as fascicles, and each fascicle is enveloped by connective tissue known as the paratenon. The fascicles are composed of a number of fibrils, each of which is wrapped in an epitenon. Further down this hierarchy are the sub-fibrils, which comprise the fibrils. These units are surrounded by loose endotenon connective tissue, and are composed of micro-fibrils. Finally, these micro-fibrils are made up of collagen fibrils which have a similar hierarchical structure (Figure 1.3), as described later on in this chapter (Strocchi *et al.,* 1992).

The blood vessels which supply the ACL are not homogenously distributed. The proximal end, near to the femur, is relatively vascular in comparison with the distal end. In one area of the ligament in particular, near to the tibial attachment site, the tissue is entirely avascular, and it is believed that this poor vascularity contributes significantly to the limited healing capacity of the ACL (Scapinelli, 1997).

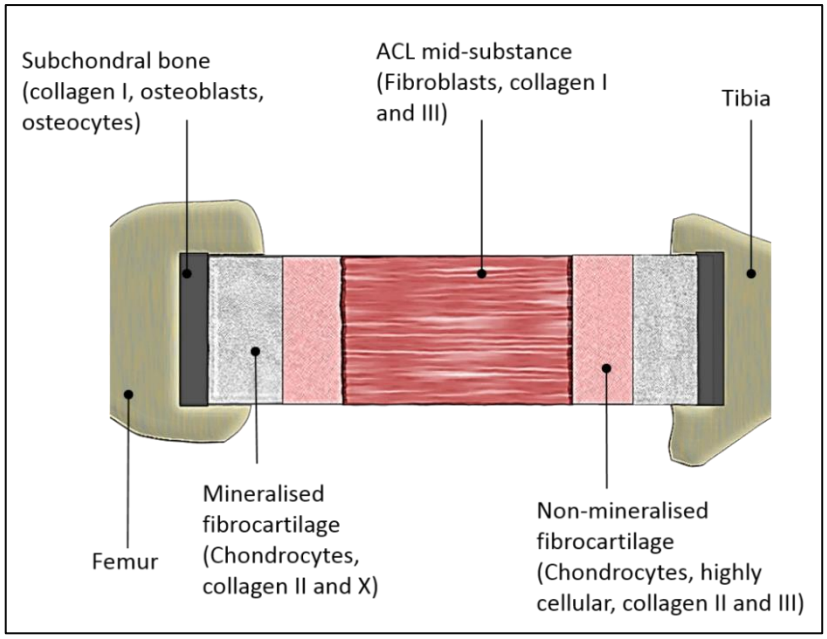

Figure 1.2 Macrostructure of the anterior cruciate ligament.

The image shows the transition from bone to mineralised cartilage, non-mineralised cartilage, through to the ACL midsubstance. Near to the bone, the tissue is highly cellular and the ECM is rich in collagen II. Whereas, in the midsubstance, there is a sparse population of fibroblasts and the ECM is primarily composed of collagen I. Adapted from (Wudebwe *et al.*, 2014).

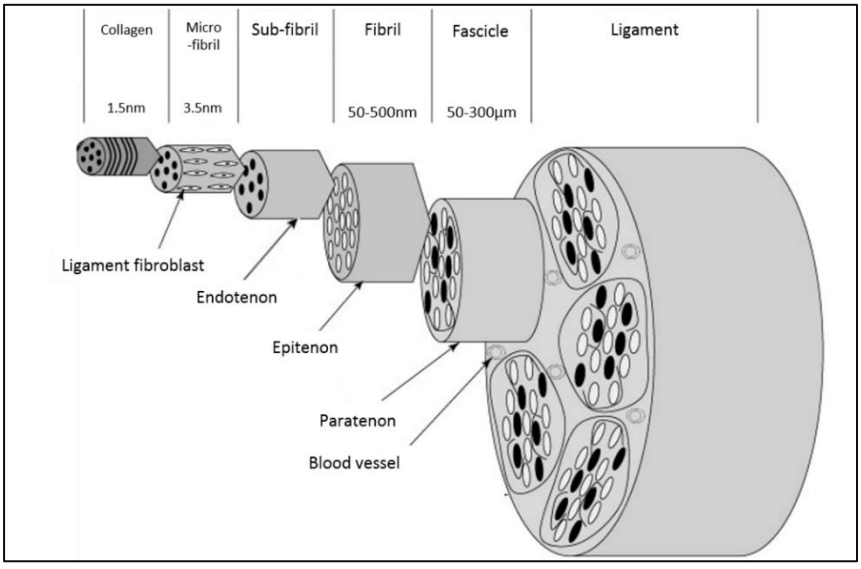

Figure 1.3 The hierarchical microstructure of a ligament.

The ligament is composed of a number of fascicles, which are themselves composed of a number of fibrils. These fibrils are composed of sub-fibrils, which are composed of micro-fibrils. Finally, collagen fibres, which compose the micro-fibrils, are the basic subunit of ligaments (the structure of collagen is described later in section 1.6.2). Taken from (Richardson *et al.*, 2007) with modifications.

1.3 Effect of exercise on ACL repair

The first published ACL reconstruction took place over a century ago (Hey Groves, 1917), and at this time, little was known about effective rehabilitation post operation. Up until the late twentieth century, the knee was commonly immobilised for six weeks or more post-surgery, until inflammation had subsided and the graft had healed (Beynnon *et al*., 2005). However, this leads to adverse effects including collagen degradation, glycosaminoglycan (GAG) reduction, and joint stiffness (Amiel *et al.*, 1994). It has been well established that long-term immobilisation of joints leads to atrophy of a number of tissues associated with that joint (Ng, 2002; Beynnon *et al*., 2005). However, there is no definitive conclusion on what intensity of exercise is required for optimum rehabilitation.

A study conducted in 1992 compared active mobilisation with passive mobilisation (using a continuous passive motion (CPM) device). No statistically significant difference in joint stability or range of motion was reported between groups during a 6 month period post-surgery (Rosen *et al.*, 1992). Additionally, a randomized, double-blind study conducted with 25 patients compared an accelerated and non-accelerated exercise regime post-repair of the ACL. No significant difference was seen in functional performance of the knee or in cartilage metabolism between groups (Beynnon *et al.*, 2005). These studies suggest that the intensity of exercise following ACL reconstruction does not significantly affect repair as long as the joint is mobilised within a month of surgery, and is exercised daily. In the context of *in vitro* studies, this demonstrates the importance of applying mechanical loads to ligament constructs.

The application of mechanical forces to tissue is crucial for normal ligament development. This has been demonstrated *in vivo* by ACL grafts which have become slack after implantation. Those which remain taut are exposed to mechanical tensile forces, and subsequently show good tissue induction and maturation. However, those which are implanted slack, or become loose after surgery have poor tissue induction and maturation (Fujikawa *et al.*, 1989). The effect of cyclic strain on cell proliferation and differentiation has been investigated extensively *in vitro*, and is discussed in this section.

One of the first investigations into the effect of cyclic strain on cells was published in 1976 (Leung *et al.*, 1976). In this study rabbit aortic medial cells were cultured on elastin membranes which were exposed to cycles of elongation and relaxation. The authors reported a two to four-fold increase in synthesis of matrix components in comparison with cells grown on non-stretched membranes. Interestingly, no difference in cell proliferation rate was measured.

The stimulatory effect of cyclic strain was also demonstrated in fibroblasts derived from the human patellar tendon, by Johannes *et al.* (2000). Cells were cultured on silicon dishes and

subjected to 5% strain at a frequency of 1 Hz. Results from the study showed an increase in proliferation compared with static controls when cells were subjected to 15 minutes or 1 hour of strain. This change in proliferation was not found when cells were exposed to strain for 30 minutes, possibly indicating that intermediate durations of strain can be detrimental to cells.

Berry *et al.* (2003) investigated the effect of cyclic strain on human dermal fibroblasts seeded in collagen gels. Strain was applied using a novel, in-house developed system, whereby the collagen construct was moulded in a ring shape, and held between two stainless steel posts which transferred the mechanical force. Application of 10% cyclic strain at 1 Hz was found to significantly increase cell proliferation.

Raif *et al.* (2005) also demonstrated the effect of cyclic strain on cell proliferation *in vitro*. Cells used for the study were harvested from the synovial membrane of bovines, and were seeded on woven polyester scaffolds. Cyclic strain was applied to the scaffolds at 1 Hz using an in-house developed bioreactor. The study demonstrated an optimal strain application time of 1 hour, and also found that proliferation rate positively correlated with strain amplitude up to 4.5%. A later study was conducted using the same bioreactor, and the subsequent results showed a three-fold upregulation of matrix metalloproteinase-3 (*MMP-3*) when cells were subjected to strain of 4.5% at 1 Hz, for a single 1 hour session. Upregulation of *MMP-3* is associated with matrix degradation, and is indicative of a catabolic environment (Raif, 2008).

Webb *et al*. (2006) produced a mechanical bioreactor system which applied cyclic strain or static strain to tracheal fibroblasts seeded onto polyurethane scaffolds. Strain was applied at an amplitude of 10%, and the cyclic strain was conducted at a frequency of 0.25 Hz, for 8 hours per day. The results showed a greater stimulatory effect from cyclic strain than from static tension, indicated by an increased proliferation response as well as increased expression of matrix-related genes. Cyclic strain also increased the elastic modulus of the scaffold-fibroblast constructs in comparison with statically tensioned constructs. This work demonstrates the importance of the application of strain in a cyclic manner, mimicking the *in vivo* experience.

The effect of cyclic strain on matrix synthesis was extensively examined by Sun *et al.* (2016). Rabbit bone marrow mesenchymal stem cells (BMSCs) and ACL fibroblasts were cultured in a Flexcell Strain Unit and subjected to 5 days of cyclic strain for 8 hours per day, with 15 minutes of rest every 2 hours. The strain amplitude and frequency were varied to determine which parameters were optimal. Strain was applied at 5, 10 or 15%, at a frequency of 0.1, 0.5, or 1 Hz. The results showed that a strain frequency of 0.1% reduced proliferation and collagen synthesis at all amplitudes in both BMSCs and ACL fibroblasts. A frequency of 0.5 Hz was optimal for greatest proliferation rate and collagen synthesis in both BMSCs and ACL

fibroblasts, at any strain amplitude. A strain amplitude of 15% was found to induce greatest proliferation and collagen synthesis at this frequency. Interestingly, by increasing the frequency to 1 Hz, the optimum strain amplitude decreased to 10%. This suggests that strain frequency and amplitude are not independent factors, but have a combined effect on cells.

The studies discussed here demonstrate the stimulatory effect that cyclic strain has on both proliferation and matrix synthesis in a number of different cell types. When selecting cyclic strain parameters for *in vitro* investigations, the strain amplitude and frequency should be reflective of those experienced by the tissue of interest. In the case of the ACL, a frequency of 1 Hz is appropriate as this is representative of walking pace. A suitable strain amplitude is more challenging to select due to difficulties in accurately measuring elongation of the native ACL. Luque-Seron and Medina-Porqueres (2016) reviewed a number of studies which measured graft strain during rehabilitation exercises, after ACL reconstruction. The greatest strain measured was 4.4%, during isometric seated knee extensions using a 30 Nm torque as resistance (Beynnon *et al.,* 1995). Based on these findings, a strain amplitude of 4-5% is reflective of the maximum strain likely to be applied to the graft during normal activities, including walking and stair climbing. It is essential that any material considered as an ACL graft is able to withstand such forces.

1.4 Overview of tissue engineered ligaments

The ideal material to replace the ACL should be strong enough to endure the forces associated with the knee joint. It must also be biocompatible, meaning that it is non-toxic and does not promote a detrimental immunological reaction. Thus far, no artificial ligament has met these criteria, and so the approach has shifted to one which attempts to restore the biological tissue using tissue engineering methods. In this instance, the scaffold must also promote cell integration as well as tissue induction, and must create an extracellular environment which favours development of ligamentous tissue.

One of the first materials investigated for use in ligament regeneration was collagen, since it is the main component of the extracellular matrix. In 1993, Huang *et al.* published their work which involved seeding fibroblasts onto a collagen matrix, and they observed a 30 fold increase in matrix strength between weeks 1 and 12. Furthermore, collagen is easily degraded by the body, making it particularly suitable for tissue engineering purposes (Yilgor *et al*., 2012).

Silk fibroin, a protein excreted by silk worms, is another material which has been used in this setting. Altman *et al*. (2002) used a silk fibroin matrix seeded with human bone marrow MSCs and found that these scaffolds encouraged differentiation of the cells towards ligament

lineages. As well as degrading slowly *in vivo*, the material is also biocompatible and possesses suitable mechanical properties for ligament regeneration.

Polyhydroxyesters, such as poly(lactic acid), have also shown promise in ligament tissue engineering due to their slow degradation rate, cell attachment, and their ability to induce cell proliferation (Yilgor *et al.,* 2012). More recently, poly(urethane urea), a relatively new synthetic polymer, was tested as an ACL prosthesis in a rabbit model. The study showed migration of native cells into the prosthesis as well as neovascularisation between the fibres. After 24 months, the function of the knee remained intact suggesting that this material holds good promise for ligament tissue engineering applications (Liljensten *et al*., 2002).

Cooper et al. (2008) attempted to reconstruct a rabbit ACL by seeding ACL fibroblasts onto a biodegradable biomimetic scaffold produced by 3D braiding technology. The addition of cells produced better results than the implantation of the synthetic ligament alone. The study demonstrated infiltration of cells into the ligament, as well as collagen remodelling, indicating that combining scaffold and cells holds good potential for induction of tissue with appropriate structural integrity.

Work by Murray *et al.* (2007) suggested that reduced healing of the ACL was associated with a deficiency of growth factors. Platelet-rich plasma (PRP) is a concentrated platelet preparation suspended in a small amount of blood plasma, and contains a number of growth factors involved in wound healing. Incorporation of PRP into collagen hydrogels, followed by implantation into canine ACL wound sites, resulted in enhanced ACL healing, suggesting that incorporation of endogenous growth factors into a scaffold is a promising technique for promoting the repair of non-healing ligaments.

1.5 Platelet-rich plasma

Platelet-rich plasma (PRP) is derived by centrifugation of a whole blood sample to separate its components into three distinct bands based on their relative densities. Erythrocytes settle in the lowest band since they contain large quantities of iron-rich haemoglobin. Leukocytes form a thin white band just above the erythrocyte layer, known as the buffy coat, and the plasma layer, containing fibrinogen and other plasma proteins, forms the uppermost band. Platelets are found in greatest density within the buffy coat and the lower portion of the plasma layer (see Figure 1.4). Following the initial centrifugation step, the plasma layer is extracted and further processed to concentrate the platelets. This may be achieved by performing a second centrifugation step to pellet the platelets before removing a portion of the top, platelet poor, plasma (preparation of PRP is described in detail in section 3.1.2.1). Alternatively, specialised filtration methods can be used to remove large portions of liquid, thereby

concentrating the platelets. The result is a high concentration of platelets in a small volume of plasma (Visser *et al*., 2010).

PRP is used clinically and cosmetically, but in all cases it is derived from the patient's own blood. This use of autologous preparations prevents immunological rejection caused by extracellular antigen present on non-autologous platelets (Marx, 2014). Within the dense granules and α-granules of the platelets reside a number of growth factors which promote wound healing and regulate cell proliferation (Blair and Flaumenhaft, 2009). The preparations also contain fibrinogen, fibronectin and vitronectin, which are components in bone and connective tissues, and which also promote epithelial migration (Saucedo *et al*., 2012). Upon addition of an activation agent, such as $CaCl_2$, thrombin, collagen type I or batroxobin, fibrinogen monomers are polymerised into insoluble fibrin strands which are then cross-linked by factor XIII to form a strong fibrin mesh (Weisel and Litvinov, 2013). A number of names have been given to similar preparations, such as 'concentrated plasma', 'platelet-rich fibrin' (PRF), and 'preparations rich in growth factors' (PRGF) (Foster *et al*., 2009).

The use of PRP in regeneration of tissues is a relatively recent development, with the first experiments being aimed at bone regeneration (Marx *et al.*, 1998). The study observed improved graft integration in patients with the addition of PRP in comparison with those without PRP. This finding encouraged a shift from using recombinant growth factors, which are expensive and have a short life span, to PRP which can be prepared from patient blood samples, and which contains growth factors at physiologically relevant ratios. (Dhillon *et al*., 2014).

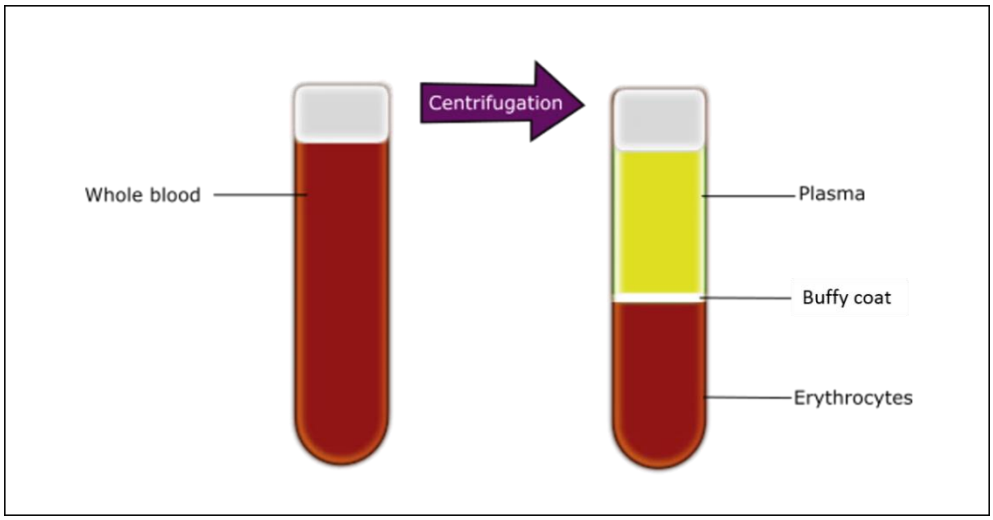

Figure 1.4 Illustration of blood fractions following centrifugation.
Centrifuging whole blood at a low speed of approximately 200 × *g* results in formation of three distinct fractions. Platelets are found in greatest density low down in the plasma fraction and within the buffy coat. Leukocytes are also found in the buffy coat, while erythrocytes separate into the lowest fraction due to their high density.

1.5.1 Components of PRP

Platelets are the main cellular component of PRP and are responsible for the release of the desired growth factors. Leukocytes are also commonly found in PRP preparations and there is conflict in the literature as to whether the presence of leukocytes is beneficial or detrimental. One study showed that the presence of mononuclear lymphocytes enhanced proliferation of ACL fibroblasts, as well as increasing collagen type I and III expression. Upregulation of interleukin-6, a collagen synthesis stimulatory cytokine, was also observed (Yoshida *et al*., 2013). On the other hand, leukocytes also release inflammatory cytokines such as IL-1β and TNF-α, which promote cellular breakdown and would thus be detrimental in a tissue engineering setting (Anitua *et al*., 2011).

In addition, blood plasma is composed of a vast array of proteins involved in a number of processes. Albumins, which regulate oncotic pressure as well as acting as transporters for insoluble molecules, make up the greatest proportion of the proteins in plasma. Globulins, involved in immune function, are the second most abundant, followed by fibrinogen, which is the clot-forming component. Regulatory proteins and clotting factors are also present, each making up less than 1% of the total protein mass (Buzanovskii, 2017).

1.5.2 Growth factors present in PRP

The growth promoting activity of serum was first attributed to factors derived from platelets during the early 1970s (Ross *et al.*, 1974). This section details some of the main growth factors contained in the alpha granules of platelets, with particular focus on those which have been implicated in ligament differentiation and regeneration. Upon activation of platelets, these growth factors are released into the extracellular environment, where they interact with cells and invoke various responses (Molloy *et al.* 2003).

1.5.2.1 Platelet-derived growth factor (PDGF)

PDGF is heavily associated with ligament healing by regulation of chemotaxis, angiogenesis and fibroblast proliferation (Molloy *et al.*, 2003). A PDGF-B gene transfer model was used to induce PDGF expression in rats with patellar ligament injury. After a week, ligaments subjected to gene transfer had significantly greater laminin deposition than control ligaments. By week 4, there was approximately twice as much collagen-I deposition as control ligaments. Induced PDGF expression also resulted in greater angiogenesis (Nakamura *et al.*, 1998).

A study which evaluated the effect of different growth factors on the proliferation of rabbit MCL and ACL fibroblasts found that PDGF-BB, but not PDGF-AA, induced proliferation in both fibroblast types (Schmidt *et al.* 1995).

1.5.2.2 Transforming growth factor-beta (TGF- β)

TGF- β is a highly multifunctional cytokine which belongs to the transforming growth factor superfamily. There are 30 members of the TGF- β family, which are secreted by a number of cells in their latent form, in which they are complexed with latent TGF- β binding protein (LTBP) and latency associated peptide (LAP). TGF- β signal transduction pathways initiate different responses depending on the context of the signal. For example, different cell types respond differently to TGF- β due to varying expression levels of TGF- β ligands, receptors and regulators, which leads to differences in the signal intensity. Moreover, differences in the epigenetics of the cell, pertaining to chromatin folding, leaves different genes exposed to TGF- β mediated regulation. (Massagué, 2014).

A study by Spindler *et al.* (2003) used fibrin clots containing recombinant human TGF- β2 as a growth factor delivery system in an MCL deficient rabbit model. Delivery of 0.1 µg TGF- β2 to the injured ligament resulted in a significant increase in ligament stiffness (in comparison with the contralateral control ligament). Treated ligaments were also associated with greater scar tissue formation, as indicated by gross observation, but this did not reduce the maximum tensile load of the ligaments.

An *in vitro* study published in 2007 looked at the effect of different concentrations of recombinant TGF- β1 on human bone marrow stromal cells cultured on woven scaffolds composed of poly(L-lactide/glycolide) fibres. Treatment with TGF- β1 was found to increase cell proliferation significantly at all concentrations (1, 5 and 10 ng/ml). By the sixth day of culture, significantly more collagen had been synthesised by cells treated with 5 and 10 ng/ml TGF- β1, in comparison with the control (Jenner *et al.*, 2007).

1.5.2.3 Vascular endothelial growth factor (VEGF)

VEGF, also referred to as VEGFA, belongs to a gene family which includes a number of other growth factors, including VEGFB, VEGFC and VEGFD. While VEGFA primarily regulates blood vessel formation, other members of this family regulate formation of other components of the vascular system, such as lymphatic vessels (Ferrara *et al.*, 2003). As well as inducing a potent angiogenic response *in vivo*, VEGF has also been shown to stimulate *in vitro* proliferation of endothelial cells originating from blood vessels (Ferrara and Davis-Smyth, 1997).

VEGF has been reported to decrease the strength of grafted tissue as the newly formed vessels can create weaknesses in the structure (Molloy *et al.*, 2003). However, Ju *et al.* (2006) published work in which they subjected *in situ* rabbit ACLs to a freeze-thaw process to kill intrinsic fibroblasts, before treating the ligament with 30 µg VEGF. As expected the VEGF treated ACLs showed significantly greater vascularisation. Unexpectedly, the treated

ligaments showed no significant difference in mechanical properties, in comparison with controls. It is likely that an optimal level of angiogenesis can be achieved, in which sufficient vascularisation is stimulated to be beneficial for tissue development, but not so much as to compromise the mechanical properties.

1.5.2.4 Insulin-like growth factor-I (IGF-1)

The effect of IGF-1 on ACL fibroblasts was investigated by adenoviral gene transfer (Steinert *et al.*, 2008). A gene delivery system was developed to transfer an IGF-1 gene into human ACL fibroblasts cultured in collagen-I hydrogels. Using histology, it was found that hydrogels containing IGF-1 transduced cells had greater cellularity, as well as increased collagen-I, collagen-III, elastin, vimentin, fibronectin, and tenascin deposition.

Another study compared the effect of combinations of growth factors, at varying concentrations, on collagen synthesis and tensile strength of engineered human ligaments (Hagerty *et al.*, 2012). The ligaments were produced by seeding fibrin gels with human ACL fibroblasts. The study found a positive relationship between IGF-1 concentration and maximum tensile load. In addition, IGF-1 was found to significantly increase collagen content in the engineered ligaments.

1.5.2.5 Epidermal growth factor (EGF)

A study previously mentioned, looking at the effect of growth factors on MCL and ACL fibroblast proliferation *in vitro*, also assessed the effect of EGF. The work demonstrated that EGF had a significant positive effect on proliferation of both fibroblast types (Schmidt *et al.* 1995).

Another study, conducted in 1999, investigated the effect of growth factors on migration of cells from intra-articular and extra-articular ligaments. EGF caused a 200% increase in migration of cells from the intra-articular ligaments (ACL and PCL), and just a 100% increase in migration of cells from extra-articular ligaments (MCL and LCL) (Hannafin *et al.*, 1999).

1.5.2.6 Basic Fibroblast growth factor (bFGF)

The role of bFGF in promoting ligament fibroblast proliferation was demonstrated by Scmidt *et al.* (1995). Incubation of rabbit ACL and MCL fibroblasts with bFGF was found to significantly increase cell proliferation.

Leong *et al.* 2015) used an electrospun polycaprolactone scaffold loaded with bFGF to replace the ACL in an *in vivo* rat model. The presence of bFGF induced greater cell infiltration into acellular grafts in comparison with the control. In addition, grafts loaded with bFGF had a significantly higher stiffness and maximum tensile load than control grafts.

1.5.3 PRP use *in vivo*

Use of platelet-rich plasma as a therapeutic agent has been documented since the mid-1900s. There has been considerable variations reported in the exact composition of PRP and investigations have used quite different delivery methods which have led to contradiction in the literature. For example, PRP may be delivered in either an activated or inactivated form. For surgical use, PRP is often mixed with either thrombin or $CaCl_2$ so that it coagulates to form a gel-like substance at the repair site. When PRP is activated with thrombin, growth factors are released from the platelets quickly, within a few hours, which is thought to decrease the efficacy of the treatment. The use of $CaCl_2$ instead slows down this process as calcium ions stimulate autogenous production of thrombin from pro-thrombin. According to Sell *et al.* (2011), this can extend the growth factor release time to up to 7 days. Activation has also been achieved by combining PRP with soluble type I collagen (Fufa *et al*., 2008). This slowed down degradation of the fibrin gel as well as equalising the release of growth factors. Further attempts to extend growth factor release time have been made by using gelatin gel microspheres (Bir *et al*., 2009), lyophilized PRP (Pietramaggiori *et al*., 2007), and alginate beads (Lu *et al*., 2008); all of which have been shown to improve wound healing, implying that extending the time period of growth factor release increases the efficacy of PRP.

One of the first successful therapeutic uses of autologous PRP was in the setting of chronic wound healing. Although the production of PRP was one of the steps in making the therapeutic agent, the plasma fraction was actually discarded to leave just the platelets. The platelets were then activated with thrombin to release the growth factors (described in the study as platelet-derived wound healing factors (PDWHF)), which were mixed into a microcrystalline collagen salve. Patients applied the salve topically to chronic non-healing cutaneous ulcers which had previously been treated with conventional wound healing methods for an average of 198 weeks. Daily treatment with the salve containing PDWHF resulted in a mean total healing time of 10.6 weeks, with no signs of hypertrophic scarring (Knighton *et al.,* 1986). Since no control group was present in this study it is difficult to fully confirm that PDWHF was responsible for wound healing. However, given the persistence of these wounds prior to treatment it is highly likely that PDWHF played a significant role in augmentation of the healing process.

Anitua *et al.* (1999) published a preliminary study which evaluated the use of autologous plasma rich in growth factors (PRGF) for preparing sites for dental implants. Although termed PRGF in this study, the methodology describes the production of PRP, whereby the final product is autologous plasma containing a higher platelet density than whole blood. The preparation was then activated with $CaCl_2$ to form a gel shortly before being placed in defects following tooth extraction. The study concluded that superior epithelialisation occurred in

PRP treated patients in comparison with controls. In addition, greater regeneration of bone defects was found to occur at PRP treated sites.

Murray *et al.* (2006) published a study using a method for healing a central defect in the canine ACL (Murray *et al.*, 2006). The method involved incorporating PRP into a collagenous scaffold. First attempts of this technique were carried out by placing the collagen sponge scaffold into the defect and then covering this with PRP. Since this did not cause full absorption of the PRP into the collagen, the method was improved upon by first soaking the collagen sponge in PRP before insertion into the defect. Murray *et al.* (2006) suggested that the inability of intra-articular tissues to repair is due to an inability to form a fibrin-platelet scaffold within the defect, and proposed that this is due to the presence of plasmin within the synovial fluid, which degrades the fibrin-platelet scaffold, preventing cells from repairing the damage. If this is the case it would suggest that research should focus on producing a stable scaffold which supports cell attachment and synthesis of new ligament tissue.

A year later, the same group combined PRP with collagen to form a mixed hydrogel that was used to enhance primary repair in porcine ACLs (Murray *et al.*, 2006). The ACL was transected in both knees before being sutured back together. In one knee, the repair site was additionally treated with a strip of Gelfoam gelatine sponge soaked in a mixture of rat tail collagen/autologous PRP. The bone-ACL-bone complex was tested mechanically after 4 weeks, and all ACLs repaired by suture alone failed at a point within the ligament tissue (midsubstance). Intact knees were also tested, all of which failed at the bone-ligament interface. Out of the five knees treated with the collagen/PRP soaked sponge, two failed at the bone-ligament interface (similarly to the intact knees) rather than the midsubstance, demonstrating the efficacy of the ACL repair in these cases.

Interestingly, Murray *et al.* (2009) also published a study in which they concluded that PRP alone was not sufficient to enhance primary ACL repair by suture, in a porcine model. However, PRP was injected around the suture material without prior activation. The authors explain that exposed collagen from the ligament would initiate gelation, but the surgical site was closed without confirmation of this. If gelation had occurred successfully, the PRP gel may not have remained within the defect area. The benefit of using a solid sponge material soaked in PRP is that the therapeutic component is confined to the damaged area. Furthermore, the collagen and gelatine sponges mentioned in previous studies (Murray *et al.*, 2006 and 2007 respectively) would likely have been more durable than a plasma gel. It is clear that, although PRP contains the components necessary to induce tissue healing, it does not possess the strength to support a load-bearing tissue unless supported by additional materials.

PRP has also been used to improve healing of load-bearing tissues which are able to heal without surgical intervention. A study by Parafioriti *et al*. (2011) showed that a single injection of PRP into rat Achilles tendon tear models improved coordination of the repair process after 1 week. Although after 2 weeks there was no histological difference between treated and control groups, the study does suggest that the rate of healing is improved in the presence of PRP. In addition, the Achilles tendon is an extra-articular tissue, which is well supplied by blood vessels, and thus may not benefit from PRP treatment in the same way as intra-articular tissues such as the ACL.

A contradictory study carried out by Martinello *et al.* (2013) compared the use of autologous peripheral blood-derived MSCs (PB-MSCs) alone, with the use of these cells with the addition of PRP for the treatment of lesions of the digital flexor tendons in sheep. Results of the study suggested that the addition of PRP had no benefit for lesion healing, and that PB-MSCs on their own were just as effective. However, the methods section of this paper did not indicate the exact source of the PRP and only stated that it was produced from blood harvested from the jugular vein of 12 sheep. It does not mention whether autologous PRP preparations were used on each sheep, and the use of non-autologous preparations of PRP on the lesions would cause a marked reduction in PRP function. In fact, a review paper published by Marx (2004) discussed how non-autologous PRP treatment would result in platelets that were not viable and thus would not secrete the growth factors crucial for PRP activity. In addition, antigen present on the platelet membranes could promote the synthesis of anti-platelet antibodies, thereby eliminating the PRP. It is important to ensure that any PRP used for *in vivo* applications is autologous in order to give a true representation of its activity.

Clinical trials have also been conducted to assess the use of PRP therapy in humans. A clinical study conducted by Kim *et al.* (2013) applied autologous PRP to various long-term (1-36 months) ulcers. By applying PRP every 1-2 weeks, skin lesions showed a significant increase in healing with complete epithelialisation occurring within 30 days.

Of particular debate is the efficacy of PRP as a treatment for chronic lateral epicondylar tendinopathy (tennis elbow). The treatment method involves multiple injections of autologous PRP into the extensor carpi radialis brevis tendon. One study using this technique found that the treatment significantly reduced pain and concluded that it should be considered before surgical intervention (Mishra *et al.,* 2006). A later study by the same authors used the same treatment method to assess the efficacy of PRP in treating chronic tennis elbow. The authors reported a significant decrease in pain and increase in joint functionality in comparison with controls, by 24 weeks (Mishra *et al.,* 2014).

A study published in 2011 investigated the use of PRP to reduce morbidity of the patellar tendon after harvesting for ACL reconstruction. Autologous PRP was applied to the remaining patellar tendon after harvesting. The authors reported a reduction in pain in patients treated with PRP, but appreciate a need for further investigation of the technique (Cervellin *et al.*, 2011).

PRP was used to treat partial tears of the ulnar collateral ligament (UCL) in a study published by Podesta *et al.* (2013). A single injection of autologous leukocyte-rich PRP was administered into the UCL of each patient under ultrasound guidance. 88% of patients returned to the same level of sporting activity within 10-15 weeks post treatment, indicating PRP as an effective treatment for such injuries.

In 2010, PRP was used to coat grafts after ACL reconstruction using either autologous patellar tendon or hamstring grafts. Magnetic resonance imaging (MRI) of the patient's knees was used to determine the point at which the graft had fully integrated into the bone (described by the authors as 'a completely homogenous intra-articular segment'). In the absence of PRP treatment this was found to take an average of 369 days, whereas in PRP treated grafts, this took an average of just 177 days (Radice *et al.*, 2010).

These studies demonstrate the potential of PRP in the healing of defects in numerous different tissues, by stimulating regenerative activity in epithelial cells, tenocytes, as well as ligament fibroblasts. Further understanding of the stimulatory effects of PRP might be obtained from *in vitro* studies, in which cells are seeded onto synthetic scaffolds, without the benefit of a native ECM, nor the endogenous regenerative cues of an *in vivo* system.

1.5.4 PRP use *in vitro*

PRP has been used extensively *in vitro* with a number of cell types, including stem cells as well as terminally differentiated cells. Investigations into the effects of PRP use have considered the response of MSCs to a platelet-rich environment. A study by Goedecke *et al.* (2011) compared the response of human MSCs cultured in media supplemented with 5 or 10% non-autologous PRP, with those supplemented with 5% foetal calf serum (FCS). At passage 1, culture with 5% or 10% PRP resulted in a 744% and 771% average increase in MSCs respectively, whereas culture with 10% FBS resulted in an average increase of just 300%.

A study published in 2005 looked at the response of human periodontally related cells to PRP. The authors reported a significant increase in proliferation of periodontal ligament cells, as well as an upregulation of *COL1* expression. Increased proliferation was also observed in gingival fibroblasts, but interestingly PRP caused a 40% decrease in keratinocyte growth.

Ishida *et al.* (2007) assessed the effect of different concentrations of PRP on the viability of meniscal cells, and found the viability to increase in a dose dependent manner. In addition, PRP was found to increase GAG synthesis as well as upregulate collagen type I, biglycan and decorin gene expression in comparison with platelet-poor plasma.

Two years later an article was published on the effect of autologous PRP on gene expression in horse tendon and ligament explants. In suspensory ligament explants, PRP induced a significant upregulation of collagen type I and cartilage oligomeric matrix protein (*COMP*), and interestingly a downregulation of collagen type III expression. This same trend was evident in explants of the flexor digitorum superficialis tendon (McCarrel and Fortier, 2009).

A study conducted by Visser *et al.* (2010) incorporated preparations rich in growth factors (PRGF) into a synthetic scaffold. PRGF is derived from PRP by a freeze-thaw-freeze process, to lyse the platelets. The PRGF was pipetted onto the surface of biodegradable poly-L-lactic acid scaffolds which were left to incubate in humid conditions for 10 minutes at 37°C. Canine fibroblasts were seeded onto the scaffolds and calcium within the media caused the formation of thrombin from prothrombin, which in turn activated the coagulation cascade. The result was a thin coating of fibrin over the surface of the synthetic scaffold and a significantly higher cell density was observed on these PRGF-treated scaffolds compared with untreated and serum-treated scaffolds.

Sell *et al.* (2011) incorporated PRGF into 3 different scaffolds; silk fibroin, poly(glycolyic acid), and polycaprolactone. An additional step was carried out in which the PRGF was dried by lyophilisation to form a powder. This powder was then added to solutions of the three polymers and the mixtures were electrospun to produce fibrous scaffolds with a 1:1 ratio of polymer fibres to PRGF fibres. The results showed that the scaffolds continued to release growth factors after 35 days in culture. In addition, the proliferation of adipose-derived stem cells on PRGF-treated scaffolds was significantly higher than on untreated scaffolds.

Sadoghi *et al.* (2013) assessed the effect of autologous PRP on human rotator cuff (RC) fibroblasts harvested from patients with degenerative RC tears. Cells were cultured in monolayer and treated with PRP with platelet densities of 1, 5 or 10 times that of whole blood. Treatment with PRP at all platelet concentrations increased cell proliferation in comparison with the control. Furthermore, results from the study indicated that increasing the platelet density of the plasma above that of whole blood, had no additional benefit.

A study was conducted in 2014 to assess how platelet density affects the activity of tenocytes *in vitro.* PRP was allowed to gel before extraction of the growth factor rich supernatant. This supernatant was then added to monolayer cultured tenocytes at different concentrations. The results showed that intermediate concentrations (representing $0.5x10^6$ and $1x10^6$ platelets/µl)

induced greatest proliferation and migration, with higher platelet concentrations ($2x10^6$ and $3x10^6$ platelets/µl) being detrimental to both proliferation and migration. *COL1* expression was also higher with intermediate platelet concentration. Higher concentrations reduced *COL1* expression. Additionally, *MMP-2* and *MMP-9* expression positively correlated with platelet concentration, indicating an increase in catabolism which, when combined with reduced ECM deposition, cannot be beneficial to regeneration (Giusti *et al.*, 2014).

Understanding of how leukocyte content affects cellular response to PRP is important for optimising PRP treatment. Krismer *et al.* (2017) published a study in which human ACL cells were grown on collagen patches, and exposed to human non-autologous PRP with and without leukocytes. Addition of 2.5% of both PRP preparations stimulated proliferation and metabolic activity to the same level as 10% FBS. PRP without leukocytes caused an increase in *COL3* expression, although this was not significant. PRP with leukocytes caused a significant upregulation of *MMP-3* suggesting a more catabolic environment when leukocytes are present.

Previous work has also demonstrated the positive effects of PRP on a number of different cell types *in vitro*. PRP has consistently been found to promote proliferation and migration, as well as upregulation of a number of ECM genes. However, there appears to be a limit to the stimulatory effect of platelets, as shown by Giusti *et al.* (2014), after which, cell function may be inhibited. Furthermore, the catabolic phenotype found to be induced by leukocytes would suggest that they should be excluded from PRP intended for regenerative therapy.

1.5.5 Safety of PRP

There is no current literature which suggests that the use of PRP in a clinical setting may be unsafe. As long as the PRP is derived from an autologous blood sample, and is prepared aseptically and without contaminants, there should be no risk of inducing an undesired immune response. Furthermore, concerns that PRP might promote infection have been countered since there is little difference between a clot formed by PRP and a naturally occurring blood clot. In addition, PRP is slightly acidic, with a pH of between 6.5 and 6.7, whereas the pH of a mature blood clot is 7.0-7.2. Based on these findings it has been suggested that PRP may even help to reduce some infections (Marx, 2004).

Finally, the risk of mutagenicity has also been examined. Growth factors are secreted from platelets at physiologically relevant ratios and, once secreted, bind to their corresponding receptors on the surface of cells associated with the wound or lesion which then causes normal signal transduction and gene expression. PRP is not considered to induce tumourigenesis and thus far, there is no documented case of it occurring (Marx, 2004; Sampson *et al.*, 2008).

1.6 Molecular structure of fibrin, collagens and alginates

Upon activation of PRP, an insoluble fibrin matrix is formed. Cells are able to attach and invade this matrix, making it a popular choice of scaffold for tissue engineering strategies. Collagens and alginates have also shown potential as cell scaffolds. The molecular structures of fibrin, collagens and alginates are detailed in this section.

1.6.1 Fibrin

Fibrinogen is a 340 KDa soluble protein which is present in whole blood at concentrations of 2-4 mg/ml, in healthy individuals (Chapin and Hajjar, 2015; Wolberg, 2007). As discussed earlier, this fibrous protein is the main clot-forming component in haemostasis, and as such, has been used for over a decade in natural sealants or glues (Sierra, 1993). Fibrin supports tissue healing and remodelling by providing a scaffold for the synthesis of extracellular matrix (Greiling and Clark, 1997). It has also been found to specifically bind growth factors and proteins implicated in tissue growth and repair (Breen *et al*., 2009). For these reasons, fibrin is an understandable choice of material for the purpose of enhancing the bioactivity of a synthetic scaffold.

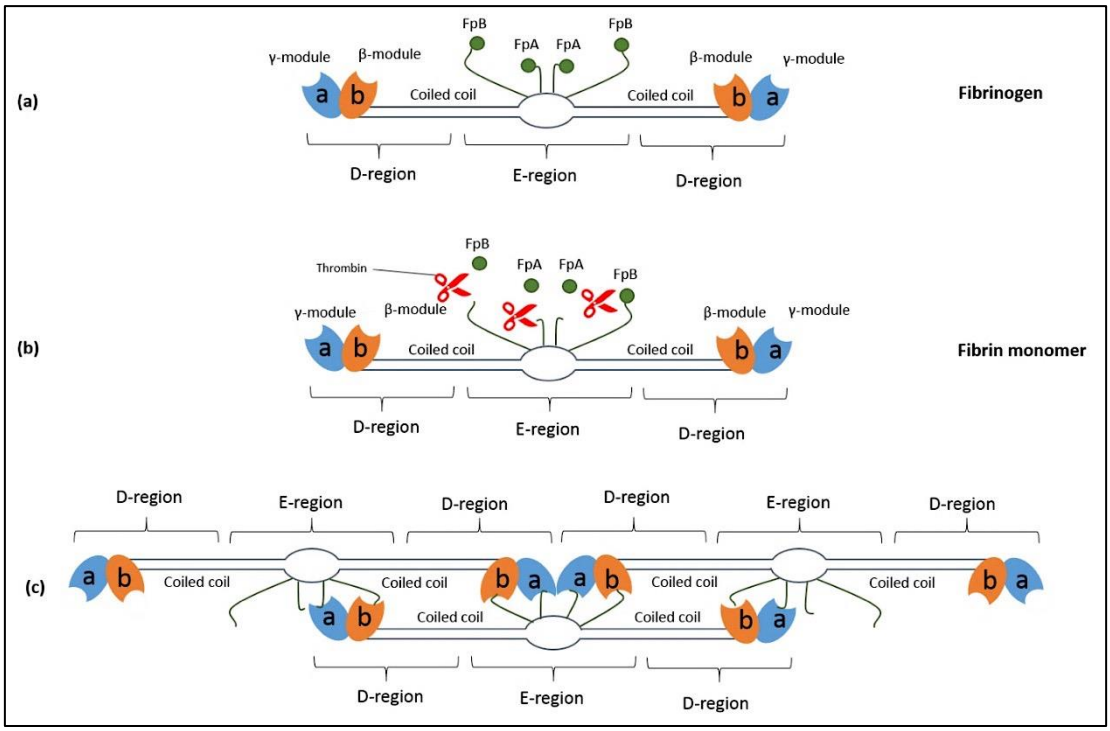

Figure 1.5 The process of fibrin formation by polymerisation of fibrinogen monomers. Thrombin cleaves fibrinopeptides A and B (FpA and FpB) from the Aα and Bβ-chains of the E-region, exposing a binding site for the D-regions of other fibrinogen monomers. The staggering of these monomers creates twisted, double-stranded fibrils. Adapted from (Janmey *et al.*, 2009).

Fibrin is formed by the cleavage of its soluble fibrinogen monomers by the serine protease, thrombin. Fibrinogen molecules are 45 nm protein molecules consisting of two outer D-regions connected to a central E-region by a coiled-coil segment. The molecule is composed of two sets of three polypeptides known as the Aα, Bβ and γ chains. These chains are joined together by five symmetrical disulphide bridges at the E-region. Each Aα-chain contains a fibrinopeptide A (FpA) and each Bβ-chain contains a fibrinopeptide B (FpB) sequence at its N-terminus which, when cleaved by thrombin, exposes a polymerisation site known as E_A. One part of the E_A site is found on the α-chain, and the other is positioned on the β-chain. Each E_A-site combines with a complementary binding-pocket in the D-region of other molecules termed Da (see Figure 1.5). The binding at E_A and Da sites creates a staggered, overlapping pattern at the centre and end of monomers, creating twisted, double stranded fibrils (Mosesson, 2005). Additional branching fibrils results in formation of a dense clot network. A cross-linking site is located at the C-terminal region of each γ-chain where factor XIII/XIIIa (plasma protransglutaminase) catalyses the formation of γ-dimers by forming covalent bonds between lysine and glutamine residues, thus further stabilising the thrombus (Weisel, 2004)

Fibrinolysis is the process by which fibrin is degraded by the proteolytic enzyme, plasmin. This process ensures the balance between haemostasis and thrombosis. Plasmin is formed from its precursor, plasminogen, by tissue-type plasminogen activator (tPA). The presence of fibrin polymers promotes tPA-stimulated plasminogen activation as tPA binds to fibrin, creating a binding site for plasminogen. The addition of plasminogen to this complex forms the ternary structure termed plasmin. Proteolytic cleavage of fibrin by plasmin causes fibrinolysis, thereby leading to clot retraction. Cells known to synthesise tPA include vascular endothelial cells, as well as fibroblasts (Ulfhammer *et al.,* 2005; Saed and Diamond, 2003). A study conducted in 2005 demonstrated that the application of cyclic tensile strain impairs the fibrinolytic system in vascular endothelial cells by suppressing tPA expression, as well as upregulating expression of plasminogen activator inhibitor 1 (PAI-1) (Ulfhammer *et al.,* 2005).

1.6.2 Collagens

Collagens are the most abundant proteins within mammals and so far, 28 members (types I-XXVIII) of the collagen superfamily have been discovered with types I-III making up 80-90 percent of that found in the human body (Lodish *et al.,* 2000). The common feature linking these molecules is the presence of a characteristic triple helical structure which can span the majority of the molecule as it does in collagen I, or can contribute to less than 10% of the structure as found in collagen XII (Ricard-Blum, 2011). The triple helical structure is composed of the repeating motif; glycine-proline-X, where X can be any amino acid. Hydrogen bonds form between the –NH of glycine residues and carbonyl (C=O) groups of

adjacent chains, helping to hold the three chains together. The angle of C-N bonds within the chains causes them to fold into a helix (Lodish *et al*., 2000).

Collagen I is the most abundant of the collagens found in ligament tissue, and thus will be the focus of this section. Fibrils of collagen type I are formed by the packing of triple helices side-by-side to form structures with a diameter of 50-200 nm, and many of these fibrils are packed together to form collagen fibres (see Figure 1.6). As such, these fibres are incredibly strong, making them ideal components for supportive tissues (Kadler *et al*., 1996). Collagen type I has been utilised in a number of regenerative medicine applications including dermal wound healing (Ruszczac, 2003), bone tissue engineering (Rodrigues *et al*. 2003) and ligament regeneration (Laurencin and Freeman, 2005). Since it is such a major component of the ligament ECM, addition of this biopolymer to a synthetic scaffold would create a cellular environment more similar to a natural ligament, and is therefore a logical choice of material for enhancement a synthetic scaffold.

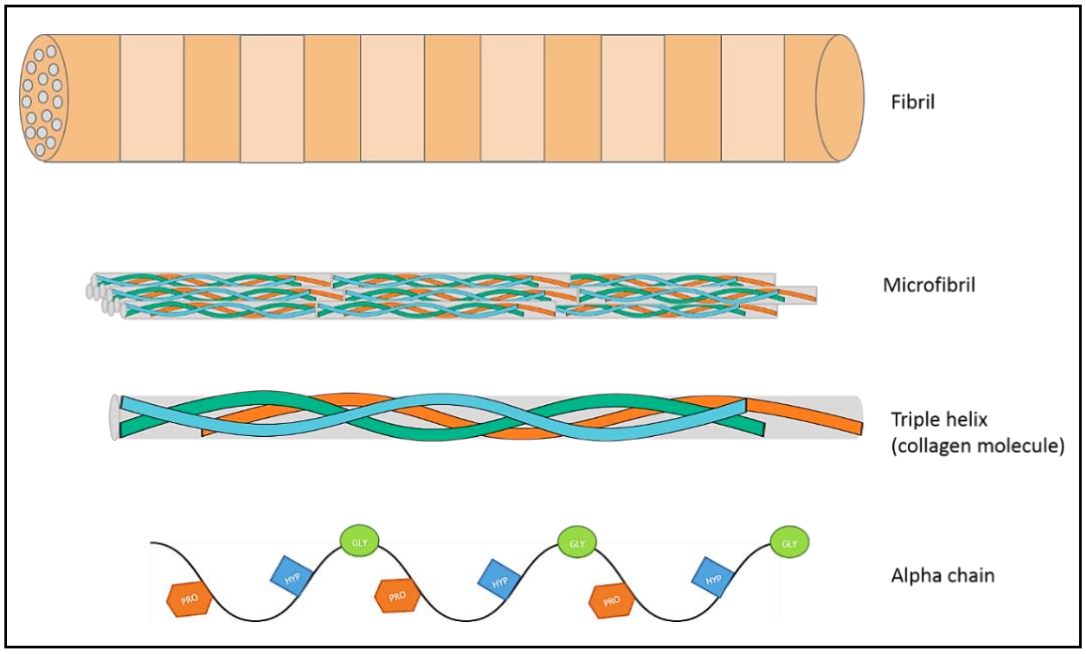

Figure 1.6 The hierarchical structure of collagen type I.
Three alpha chains composed of repeating units of proline, hydroxyproline and glycine wrap around each other to form a triple helix. This triple helix is the basic collagen I molecule, and many of these molecules stack together to form a microfibril. Finally, numerous microfibrils stack together to form a collagen type I fibril. The striped pattern on the collagen fibril represents the characteristic D-banding due to the quarter-staggering of chains during fibrilogenesis (Stamov *et al*., 2015). Adapted from (Canelón and Willis, 2016).

Collagen-I is digested by collagenolytic enzymes belonging to the matrix metalloproteinase (MMP) family of enzymes. Collectively, this family of enzymes is able to digest all components of the ECM. Those found to digest collagen-I fibrils include MMP-1, MMP-8, MMP-13, as well as membrane type 1, 2 and 3 MMPs (Van Doren, 2015). MMPs are responsible for ECM remodelling, but may also be upregulated in chronic wounds; resulting in reduced healing, and in cancer; promoting tumour progression. MMP expression has also been linked to cytoskeletal signalling pathways as a study conducted by Lavagnino *et al*. (2003) demonstrated. This study showed that MMP-1 expression could be inhibited by the application of cyclic strain on tendon cells. Disruption of the cytoskeleton using cytochalasin D abolished this effect, suggesting cytoskeletal involvement in this pathway. Conversely, the application of cyclic strain caused upregulation of MMP-1 in osteoblasts (Sasaki *et al.*, 2006) and periodontal ligament fibroblasts (Kook *et al*., 2011), suggesting that regulation of MMP expression is dependent on multiple factors.

1.6.3 Alginates

Alginates are natural polysaccharides derived from seaweeds, which have been used extensively for cell encapsulation and tissue engineering applications due to their biocompatibility and low toxicity (Lee and Mooney, 2012). Alginates may be altered to control their degradation rates, thereby regulating the release of growth factors or drugs which may be trapped within the gel matrix (Boontheekul and Mooney, 2005). Alginate has also been found to enhance the biostability of fibrin, suggesting that its incorporation into a ligament construct may reduce enzymatic breakdown and subsequent loss of cell substrate (Ma *et al*., 2012).

Alginates are composed of β -D-mannuronic acid (M units) and α-L-guluronic acid (G unit) monomers. Four M or G units make up a 'block,' and many of these blocks compose a polymer chain (see Figure 1.7). The distribution of M and G units varies depending on the source of the alginate. Divalent cations such as Ca^{2+} bind between the G blocks of adjacent polymer chains causing aqueous alginate solutions to become an insoluble Calcium alginate hydrogel (Rowley *et al.*, 1999). Being a polysaccharide, alginate biopolymers do not have the necessary RGD ligands for cell attachment. The gels are often modified by covalently adding RGD-containing ligands (Alsberg *et al.*, 2001), or by incorporating RGD-containing proteins such as collagen to produce a hybrid gel (Cunha *et al.*, 2014).

Alginate may be re-solubilised using an excess of CO_3^{2-} or PO_4^{3-} ions which chelate the Ca^{2+} ions cross-linking the gel, thereby reversing the reaction. This process occurs very slowly within the human body, and since alginases are not produced by mammalian tissues, alginate is relatively stable when implanted *in vivo*. These properties have led to alginates being used for cell encapsulation and drug delivery systems (Tønnesen *et al.*, 2002).

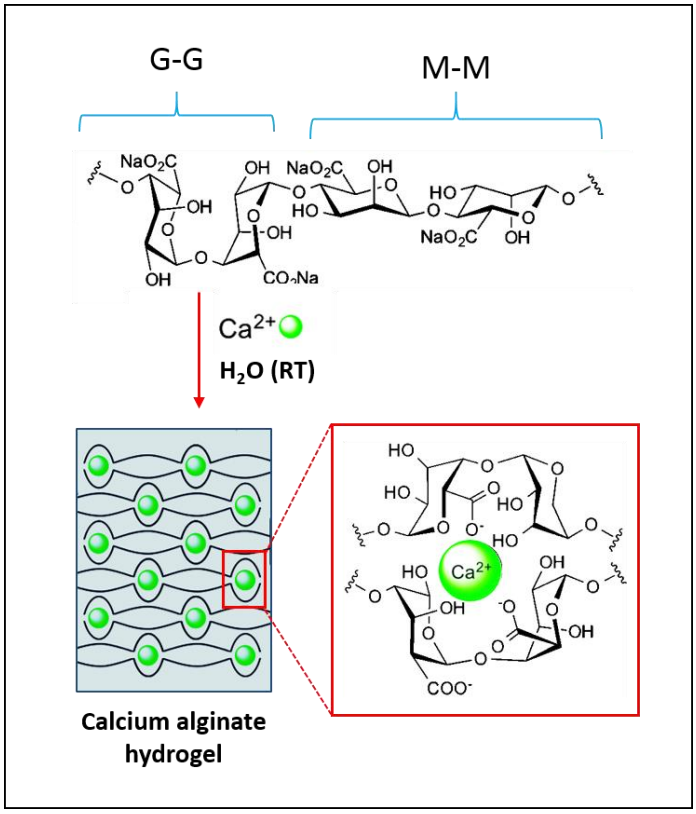

Figure 1.7 Formation of insoluble calcium alginate from M and G monomers in solution. Four M or G units form a block by forming covalent bonds around a suitable ligand, such as Ca^{2+}. These blocks combine to form a polymer chain. Adapted from (Kühbeck *et al.*, 2015).

1.7 Cell selection for ACL regeneration

In vitro investigations into ligament regenerative techniques require the use of a relevant cell type so that some prediction can be made as to how cells would respond *in vivo.* The native ACL is populated by a small number of ACL fibroblasts which are responsible for maintaining the ligament ECM. This is therefore a popular choice of cell type to use when testing an ACL prosthesis or regenerative treatment. However, in a situation where complete ACL rupture has occurred, the damaged ligament is normally removed, meaning that the graft cannot be populated with ACL fibroblasts. A likely source of cells for graft population are the cells which reside in the synovial membrane. These synovial cells, referred to as synovial membrane MSCs by De Bari *et al.* (2001), are multipotent stem cells, which are the most

probable source of cells to populate an ACL prosthesis (Morito *et al*., 2008). MSCs found in the synovium are phenotypically very similar to MSCs derived from other origins. Both cell types express CD44, CD90 and CD105 MSC surface markers, although MSCs derived from the synovium express CD44 (a receptor for hyaluronan) at a greater level (Fox and Warnock, 2011). Synovial cells have also been found to have greater proliferation capacity than other MSC populations (Sakaguchi *et al.*, 2005). Although synovial cells are thought to be the most abundant source of coloniser cells, it is also possible that bone marrow MSCs contribute to colonisation. During surgical graft implantation, tunnels are drilled in the ends of the femur and tibia to create attachment points for the graft (Sauer and Lind, 2017). This procedure would expose bone marrow-derived MSCs, possibly resulting in some attachment of these cells to the implanted material.

De Bari *et al*. (2001) reported very low telomerase activity in human synovial cells from donors aged 18-65. Low telomerase activity is normally associated with telomere shortening and an increased tendency for cells to reach senescence resulting in cell-cycle arrest (Bernadotte *et al.,* 2016). However, despite this, De bari *et al*. observed a linear growth curve up to 30 population doublings. The cells could also be expanded *in vitro* over more than 10 passages, with cells retaining these growth kinetics throughout. Vimentin was highly expressed in these cells, independent of age or passage number, confirming mesenchymal derivation. The authors also demonstrated that synovial cells could be induced into osteogenic, chondrogenic, myogenic and adipogenic differentiation lineages. Furthermore, the cells maintained their multilineage potential regardless of donor age, passage number, or cryopreservation.

A study published by Morito *et al.* (2008) found that synovial MSCs increased in number after ACL injury in humans. Furthermore, in a rabbit model with partial ACL defect, synovial MSCs injected into the knee joint were found to adhere to the injured area more than the uninjured area.

The multipotent nature of synovial cells means that they have the ability to differentiate into a number of different phenotypes to form a number of tissues. Tissues of the mesengenic lineage are mainly involved in support and movement, such as muscle, cartilage, bone, and ligament (Figure 1.8). By providing the right physical and chemical cues, MSCs populating a ligament prosthesis could give rise to differentiated ligament fibroblasts which can subsequently produce the dense collagen network typical of ligament tissue (Caplan, 2007).

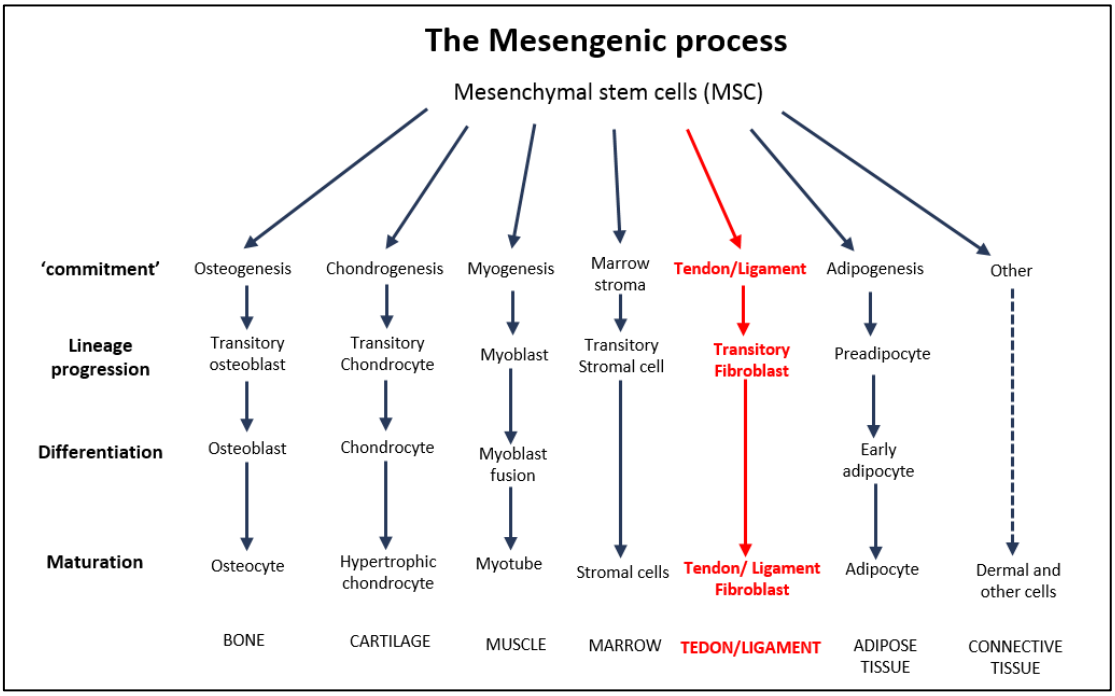

Figure 1.8 The proposed lineages of MSC differentiation.
The possible lineages of MSC differentiation, with the tendon/ligament differentiation pathway highlighted in red. Under the correct conditions, the multipotency of synovial cells would allow differentiation to ligament fibroblasts which populate the ACL mid-substance, as well as chondrocytes which are present at the bone-ligament interface. Adapted from (Caplan, 2007).

1.8 Cell mechanotransduction and extracellular matrix homeostasis

As mentioned previously, fibrin, collagen and alginate have all been successfully used as cell substrates. However, they do not possess the mechanical strength to support the knee joint alone. Furthermore, these materials are far softer than a native ligament, and this could encourage differentiation towards an undesirable lineage, as explained in this section.

Numerous publications, including one by Engler *et al.* (2006), have documented the widely accepted theory that the stiffness of a substrate directs lineage specification in stem cells. As shown in Figure 1.9, mechanical stimuli acting on cells significantly influences gene expression, causing cytoskeletal remodelling as well as affecting proliferation, differentiation, and extracellular matrix (ECM) deposition (Humphrey *et al.*, 2014). Cells attach to and interact mechanically with the ECM via focal adhesion complexes composed of heterodimeric transmembrane receptors called integrins, as well as linker proteins including vinculin, talin and tensin. Integrins bind directly to recognised amino acid motifs such as RGD ligands (arginine-glycine-aspartic acid) found in ECM components including fibronectin, vitronectin,

fibrinogen, osteopontin and bone sialoprotein (Takagi, 2004; Arnaout *et al.*, 2005). These adhesion complexes are attached to actin filaments which comprise the cytoskeleton, causing forces to be transmitted into the cell. This then initiates downstream signalling of a number of signalling molecules including the Rho-family of GTP (Guanosine triphosphate)-ases, Rho-associate protein kinase (ROCK), and myosin light chain kinases, which are all involved in the regulation of cytoskeleton assembly (Spiering *et al.*, 2011; Humphrey *et al.*, 2014) .

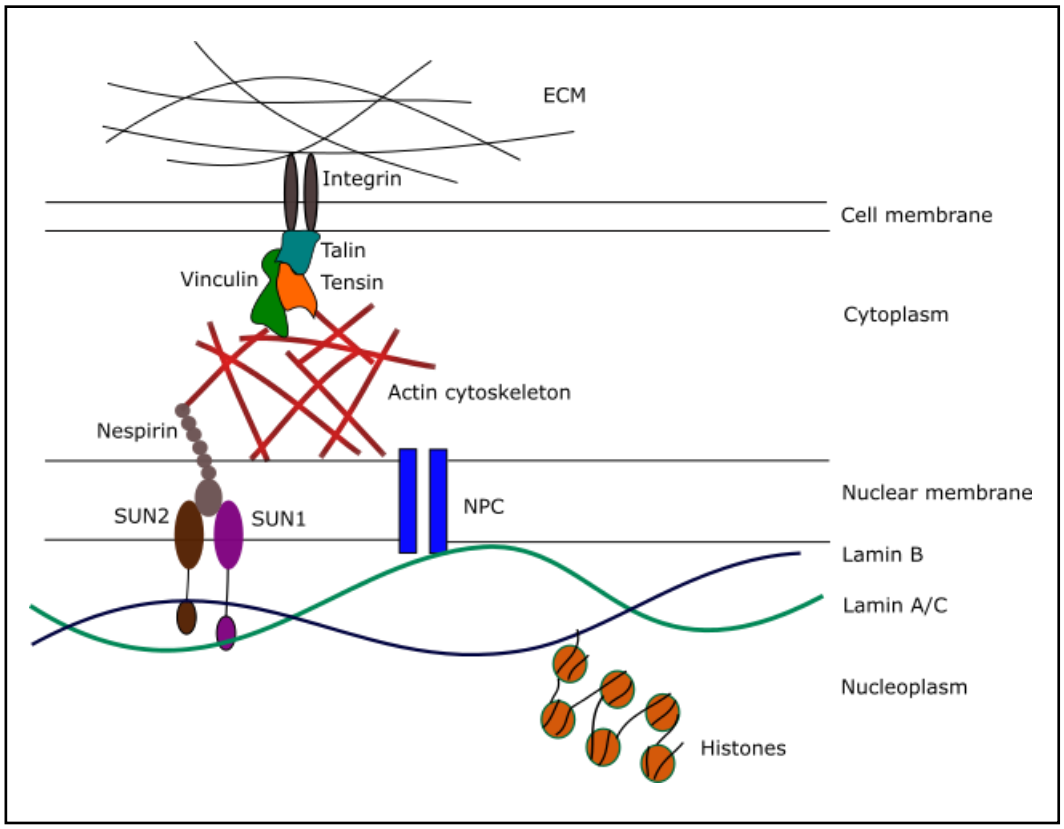

Figure 1.9 Intracellular signalling pathways involved in mechanotransduction.
Mechanical forces acting on the extracellular matrix cause activation of a number of transmembrane receptors which initiate remodelling of the actin cytoskeleton and alterations in gene expression. Adapted from (Feller *et al.*, 2017).

At the nuclear level, mechanotransduction is even less well understood, and any advances are relatively recent. Early observations on the variation in nuclear positioning during different cellular processes, such as proliferation and differentiation, led to the theory that the nucleus is physically connected to the cytoskeleton (Wang et al., 2009; Guilluy and Burridge, 2015). It is now understood that the cytoskeleton and nucleoskeleton are joined by a number of proteins which make up the linker of nucleoskeleton and cytoskeleton (LINC) complex. This structure is composed of Sad1p, UNC-84 (SUN) and Klarsicht/ANC-1/Syne homology (KASH) family members, which are membrane proteins of the inner nuclear membrane and

the outer nuclear membrane respectively (Guilluy and Burridge, 2015). KASH proteins interact with cytoskeletal proteins such as actin, whilst SUN proteins are connected to lamins which are constituents of the nuclear envelope. Lamins A and C have been found to interact with chromatin, thereby being associated with epigenetic modification and regulation of gene expression (Collas *et al*., 2013). A number of pathways have been identified and hypothesised in signalling between cell adhesion sites and the nucleus. There is still requirement for further research before this process can be fully understood.

In light of these discoveries, it is clear that the production of a scaffold with mechanical properties which mimic the extracellular environment of ligaments is crucial for desired cell differentiation. As such, by combining a platelet-rich gel with the Xiros PET ligament, the biopolymer and platelet components provide the necessary biological cues for regeneration, whilst the mechanical cues should encourage differentiation towards the ligament lineage.

1.9 Markers of ligament cell differentiation

A number of genes have been identified as being involved in ligament development and regeneration. However, many of these genes are also expressed in a range of other tissues, including bone, muscle and cartilage (Liu *et al*., 2017). For this reason, as well as the limited understanding of specific transcription factors, definitively identifying differentiation towards the ligament lineage is still a challenge. Characterisation of ligament differentiation is often conducted by quantifying the expression levels of a number of ligament-associated genes, as discussed below.

1.9.1 Collagen type I

Collagen type I is the main ECM-forming component of the ACL, as well as a number of other tissues. Alone, an increase in collagen type I mRNA production is not an indicator of ligament differentiation specifically, but it can signal tissue maturation towards a more differentiated phenotype, in the general sense (Traub and Piez, 1971). Factors found to regulate collagen type I gene expression include both mechanical and chemical cues.

A study published in 2002 assessed how mechanically stretching human ACL fibroblasts affected collagen type I gene expression. The cells were cultured on a silicon membrane and uniaxial strain was applied at 10%, at a frequency of 10 cycles/minute, for 24 hours. Gene expression was measured using qRT-PCR and the authors reported a 1.63-fold increase in collagen type I gene expression as a result of applying strain (Kim *et al.*, 2002).

Raif (2008) published work which investigated the effect of mechanical loading on bovine synovial fibroblasts. Cyclic tensile strain of 4.5% was applied to cells seeded on woven PET scaffolds at a frequency of 1 Hz, for 1 hour. In contrast to the previous study, this resulted in

no change in collagen type I gene expression. However, there were a number of variations between the two studies, including the length of time the cells were exposed to the mechanical stimulus, the percentage strain applied, the substrate on which the cells were seeded, as well as the cell type. All of these factors are likely to contribute to regulation of gene expression.

A more long-term study was conducted into the effects of mechanical cues on the expression of collagen type I in human MSCs. The work by Subramony *et al.* (2013) assessed the effect of both mechanical strain and scaffold fibre alignment on gene expression of cells seeded onto poly(lactide-*co*-glycolide) scaffolds. This ACL model was subjected to 1% strain at a frequency of 1 Hz, for 90 minutes, twice a day. The total rest period between cycles was 10.5 hours, and the straining regime was carried out for a total of 28 days. The data showed a slight increase in collagen type I expression in response to mechanical strain, on aligned matrices only. However, this was not deemed to be statistically significant at any of the time points.

One study, conducted by Karamichos *et al.* (2008), where mechanical stimulus was found to significantly affect collagen type I expression, involved altering the matrix stiffness. A computer controlled tensional loading device was used to apply a static load to collagen gels seeded with human BMSCs and human dermal fibroblasts (HDF), which subsequently altered the matrix stiffness. By applying a pre-strain of 5% to the matrix, collagen type I expression significantly increased in both cell types, although the response was greater in HDFs than BMSCs, with the authors reporting a 13-fold and 3-fold increase in collagen type I gene expression respectively.

Collagen type I synthesis is also regulated by chemical cues, as demonstrated by a study into the effect of growth factors on matrix synthesis in ligament fibroblasts (Marui *et al.,* 1997). The work found that fibroblasts from both the ACL and MCL significantly increased collagen type 1 protein synthesis in response to increasing TGF-β concentration.

Of particular interest to this project is the effect of PRP on collagen type I synthesis, which was investigated by Xie *et al.* (2013) using an *in vivo* canine model of ACL reconstruction. The flexor digitorum longus tendon from the canine limb was harvested and sutured ready for implantation to replace the ACL. Results from the study showed that soaking grafts in PRP before implantation resulted in a 3-fold upregulation of collagen type I gene expression by 6 days post-surgery.

1.9.2 Collagen type III

Collagen type III is also a component of the normal ligament ECM, although it constitutes a much smaller proportion than collagen type I (approximately 10% of the total ECM). Expression of collagen type III alone is not indicative of ligament differentiation, but, as with collagen type I, it can indicate tissue maturation. Furthermore, particularly high collagen type

III content (>20%) of the ECM can indicate abnormal ligament structure, as is found in scar tissue (Williams *et al.,* 1980). As with collagen type I, both mechanical and chemical cues have been found to regulate collagen type III gene expression.

The study by Kim *et al.* (2002) previously described, which cultured human ACL fibroblasts on a silicon membrane, also assessed how collagen type III gene expression was affected by mechanical strain. Cyclic tensile strain was applied at 10%, at a frequency of 10 cycles/minute, for 24 hours. This resulted in a 2.69-fold increase in collagen type III expression, which is much higher than the 1.63-fold increase observed in collagen-I. Results from this study indicate that collagen type III synthesis is much more sensitive to mechanical stimulus than collagen type I.

A study published in 1999 assessed the effect of mechanical strain on collagen type III gene expression in ACL and MCL fibroblasts over 24 hours. Cells were cultured in collagen type I coated plates and mechanical strain was applied at 5% and 7.5% using a Flexercell Strain Unit at a frequency of 1 Hz. The results indicated that collagen type III was upregulated in a time-dependent manner, in MCL fibroblasts only, at a strain of 7.5%. No significant increase in expression was seen with 5% strain, and ACL fibroblasts did not demonstrate upregulation at either strain amplitude. The authors suggested that increased collagen type III expression in MCL but not ACL fibroblasts reflects their differences in healing capacity. Early upregulation of collagen type III in the MCL could lead to formation of bridging scar tissue, which subsequently heals the ligament. In contrast, the lack of upregulation found in ACL fibroblasts may contribute to the poor healing capacity of this ligament (Hsieh *et al.,* 1999).

An *in vivo* study previously discussed (Xie *et al.,* 2013), which assessed the effect of PRP on gene expression in grafts used for ACL reconstruction, also analysed the effect on collagen type III gene expression. The canine model involved soaking the graft in PRP before implantation. Grafts were retrieved at 2, 6, and 12 weeks, and qRT-PCR analysis indicated that PRP treatment induced earlier upregulation of collagen type III in comparison with the control. Furthermore, expression remained higher in the PRP treated graft up until 6 weeks. By the 12th week, collagen type III expression was substantially decreased, and interestingly, this was the point at which collagen type I expression increased.

1.9.3 Tenascin-C

Tenascin-C (TN-C) is an oligomeric glycoprotein which is a component of the ECM of a number of tissues. It is particularly abundant in developing ligaments and tendons, as well as bone and cartilage. As with the other components of the ECM previously discussed, *TN-C* expression is also regulated by mechanical and chemical stimulation (Jones and Jones, 2000).

Chen *et al*. (2008) published their work on the effect of cyclic tensile strain on gene expression in human MSCs grown in monolayer. They found that cells subjected to 10% strain for 48 hours, at a frequency of 1 Hz showed a significant upregulation of *TN-C* gene expression. 3% strain did not induce upregulation, and no change was measured at the shorter strain duration of 8 hours.

In the same year, a study was published on the effect of applying strain to rat BMSCs cultured on elastic silicone membranes. A strain amplitude of 10% was applied at a frequency of 1 Hz, and *TN-C* expression was found to be upregulated by 24 hours (Zhang *et al.,* 2008).

The stimulatory effect of certain growth factors on *TN-C* expression was demonstrated in work published by Chiquet *et al*. (2004) The study found that supplementing chick embryo skin fibroblasts with 3% FBS significantly upregulated *TN-C* expression. In addition, the study found that supplementation with 5 ng/ml of TGFβ or 10 ng/ml PDGF also induced significant *TN-C* upregulation. This same study also demonstrated an increase in *TN-C* expression with mechanical strain.

1.9.4 Scleraxis

Scleraxis (SCX) is a member of the basic helix-loop-helix (bHLH) superfamily of transcription factors, and is encoded by the *SCXA* and *SCXB* genes (Cserjesi *et al.,* 1995). It is highly expressed in both progenitor and terminally differentiated cells of the ligament/tendon lineage (Wang *et al.,* 2011). *SCX* expression has been found to be heavily regulated by physical stimuli, as well as chemical stimuli.

Scott *et al.* (2011) published a study investigating the effect of a 3-dimentional environment on *SCX* gene expression in a murine MSC cell line. Cells grown in 3D collagen constructs subjected to 10% static strain demonstrated a time-dependent upregulation of *SCX* gene expression in comparison with monolayer controls. By applying a cyclic strain regime at a frequency of 0.1 Hz, *SCX* expression was further upregulated.

An earlier study, conducted by Kuo and Tuan. (2008) compared *SCX* gene expression in human BMSCs cultured in 2D and in 3D collagen type I constructs under static tension. Cells cultured in 3D constructs under tension exhibited a 5-fold increase in *SCX* expression on day 1. This expression decreased with time, however if cyclic strain was applied, the level of expression was maintained for the duration of the experiment (7 days).

PRP has also been found to have an effect on *SCX* expression in tenocytes. The cells were cultured with PRP and PPP, and a 2.5-fold upregulation was seen by day 14 with PRP, but not with PPP (Jo *et al.,* 2012).

The sensitivity of these ligament-associated markers to mechanical and chemical cues highlights the need for well optimised culture conditions in order to stimulate ligament lineage specification. Previous work has clearly demonstrated the need to maintain an optimal cyclic strain regime to promote maturation of ligament tissue and deposition of a ligament-like ECM.

1.10 Summary

ACL rupture accounts for a high percentage of sporting injuries, and its poor capacity for spontaneous repair means that surgical intervention is almost always indicated. Currently, the gold standard treatment involves using tissue from the patient's own patellar tendon to form a bone-tendon-bone graft between the femur and tibia. This requires two surgical procedures; the first to harvest autologous tissue to create of the graft, and the second to perform reconstruction of the ACL using the harvested material. This means that two surgical sites are created, and donor site morbidity is often a problem.

A number of attempts have been made to produce an artificial ligament which can perform as well as the native tissue, however these were largely abandoned due to unsatisfactory long term results. The PET woven scaffold developed by Xiros Ltd. has shown significant promise due to its ability to promote tissue ingrowth, thereby regenerating the ligament rather than merely replacing it. However, the relatively slow rate of tissue induction is thought to be responsible for its long term failings, by leaving the material exposed to bone abrasion, which leads to formation of wear debris. By enhancing the bioactivity of this artificial ligament, it may be possible to resolve these shortcomings. A large body of evidence points towards the incorporation of platelet-rich preparations as being a possible method for accomplishing this, by providing a natural fibrin matrix, as well as a physiologically relevant growth factor release system. Other biopolymers, including collagen and alginate, may prove to further enhance the bioactivity of this construct.

The importance of cyclic tensile strain for ligament differentiation and regeneration has been extensively demonstrated *in vitro*. Testing of any synthetic ligament should therefore include application of cyclic tensile strain using parameters representative of those occurring *in vivo*. In addition, the ligament should be seeded with an appropriate cell type. As previously discussed, it is envisaged that an ACL graft will be populated with synovial cells derived from the synovial membrane. The study presented here aimed to optimise a hybrid scaffold that could overcome the insufficiencies associated with the bioactivity of the Xiros Ltd. ligament.

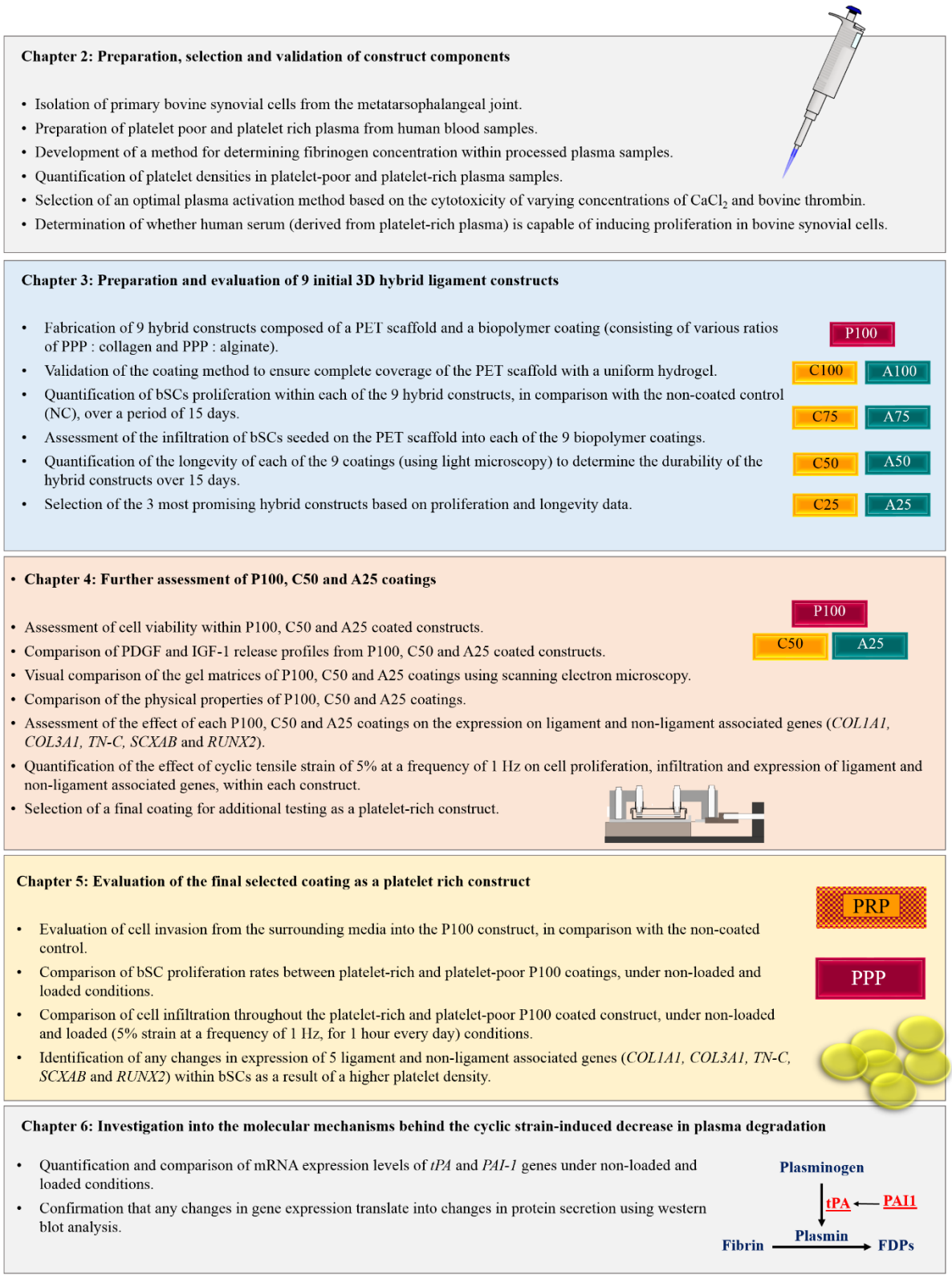

Figure 1.10 Project layout.

Details of the objectives of each chapter.

Chapter 2

Preparation, selection and validation of components required for fabrication of hybrid ligament constructs

Before hybrid ligament constructs could be produced, the components necessary for fabrication had to be selected and validated to ensure they promoted the required response from cells and did not induce cytotoxic effects. This chapter details the processes by which components required to fabricate hybrid ligament constructs were prepared, selected and validated. This includes isolation of the cells used throughout the project, as well as establishing their response to human serum (derived from human plasma) and different concentrations of $CaCl_2$ and thrombin (used to activate gelation of the plasma). A method was developed to quantify fibrinogen concentrations within donor plasma, and from this a single donor was selected for use throughout the project. The platelet densities of platelet-poor and platelet-rich plasma samples were quantified to ensure that they met the criteria to be considered PPP and PRP respectively.

Aim:

To select and validate components required for fabrication of hybrid ligament constructs composed of human blood plasma and the Xiros PET scaffold.

Objectives:

- Isolation of primary bovine synovial cells from the metatarsophalangeal joint.
- Preparation of platelet poor and platelet rich plasma from human blood samples.
- Development of a method for determining fibrinogen concentration within processed plasma samples.
- Quantification of platelet densities in platelet-poor and platelet-rich plasma samples.
- Selection of an optimal plasma activation method based on the cytotoxicity of varying concentrations of $CaCl_2$ and bovine thrombin.
- Determination of whether human serum (derived from platelet-rich plasma) is capable of inducing proliferation in bovine synovial cells.

2.1 Materials and methods

This section describes the methods used to prepare, select and validate components required for fabrication of hybrid ligament constructs. At this stage, focus was given to the plasma component of the construct, by evaluating the response of cells to human serum (derived from plasma), as well as quantifying the fibrinogen concentration and platelet density of plasma samples.

2.1.1 Isolation of synovial cells from the bovine metatarsophalangeal joint

Bovine synovial cells (bSCs) were used throughout this project to evaluate hybrid ligament constructs. Cells were harvested from the synovial tissue of 12-18 month old cattle on the day of slaughter. The skin and hoof were removed and the limb was sprayed with 70% ethanol. Care was taken to ensure the subcutaneous tissue was kept clean. The collateral ligaments surrounding the joint were cut and the joint was opened to reveal the synovial cavity. Sections of synovial membrane were harvested from the joint using sterile surgical forceps and scalpel, and placed in a sterile petri dish with Phosphate buffered saline (PBS, Sigma) containing 10% (v/v) penicillin/streptomycin (Sigma) for 15 minutes. The tissue was washed three times in PBS and cut into smaller pieces using a sterile surgical scalpel.

A 0.25% type IV collagenase solution was prepared in Dulbecco's modified Eagle's medium (DMEM, Sigma) using lyophilised collagenase from *Clostridium histolyticum* (Sigma). The solution was filtered twice using syringe filter units with a membrane pore size of 0.45 µm, followed by 0.2µm (Merck Millipore). The solution was supplemented with 10% (v/v) foetal bovine serum (FBS, Sigma) and the synovial tissue was allowed to digest in the solution for 3 hours at 37˚C degrees. The digested tissue suspension was then passed through a 70 µm nylon cell strainer (BD Falcon) and centrifuged at 200 × g for 5 minutes. The supernatant was removed and the cell pellet was resuspended in DMEM supplemented with 10% (v/v) FBS. Cells from each animal were placed in three 75 cm^2 culture flasks (Corning) and incubated at 37˚C in a humidified atmosphere of 5% CO_2 and 95% air. Once the cells had reached approximately 80% confluency, they were washed three times with PBS to remove any non-adherent cells and debris before being treated with 3 ml of 1X Trypsin/EDTA (Sigma) for 5 minutes to detach them from the flask. DMEM containing 10% FBS was added to inactivate the trypsin, and the cell suspension was centrifuged for 5 minutes at 200 × g to pellet the cells. The supernatant was discarded and the cell pellet was resuspended in fresh culture media, before being transferred to 75 cm^2 culture flasks at an approximate density of 3000 cells/cm^2. These cells were designated passage 1 (P1). At this density cells generally reached 80% confluency within one week, at which point they were passaged again. Once cells had reached

passage 2, they were trypsinised and resuspended in freezing media (50% FBS, 40% DMEM, 10% DMSO). The cell suspension was aliquoted into 2 ml Nunc Cryotube vials (Thermo Scientific) which were placed in a Mr. Frosty™ freezing container (Nalgene) with isopropanol and frozen at -80˚C until required

Bovine synovial cells were seeded at passage 3 in all studies and were maintained in DMEM without antibiotics in a humidified atmosphere incubator containing 5% (v/v) CO_2 and 95% (v/v) air at 37˚C. The media was supplemented with FBS at varying concentrations, depending on the study. Media was replaced every 3 days.

2.1.2 Preparation and characterisation of human plasma fractions

All blood used in this work was collected from healthy individuals based in the department of Oral Biology, University of Leeds. Ethical approval was obtained from the Dental Research Ethical Committee (DREC, reference number: 260215/EMR/156). The blood was collected into 4.5 ml vacutainer tubes containing 3.2% sodium citrate, by a trained phlebotomist. All blood was processed on the day of venepuncture.

2.1.2.1 Separation of platelet-rich and platelet-poor plasma

Each 4.5 ml blood sample was centrifuged at 200 × g for 15 minutes with the break and accelerator deactivated. The plasma was carefully extracted from the top of each tube, leaving the buffy coat and lower erythrocyte layer behind. The plasma was centrifuged at 2000 × g to pellet the platelets. Four fifths of the total plasma volume was removed from the top of the sample and passed through a 0.45 micron syringe filter. This was retained as platelet-poor plasma (PPP). The remaining one fifth of the volume was used to resuspend the pelleted platelets and was retained as platelet-rich plasma (PRP). This method is represented in Figure 2.1. 5 ml aliquots of PPP and PRP were placed in sterile vials and stored at -20˚C until use.

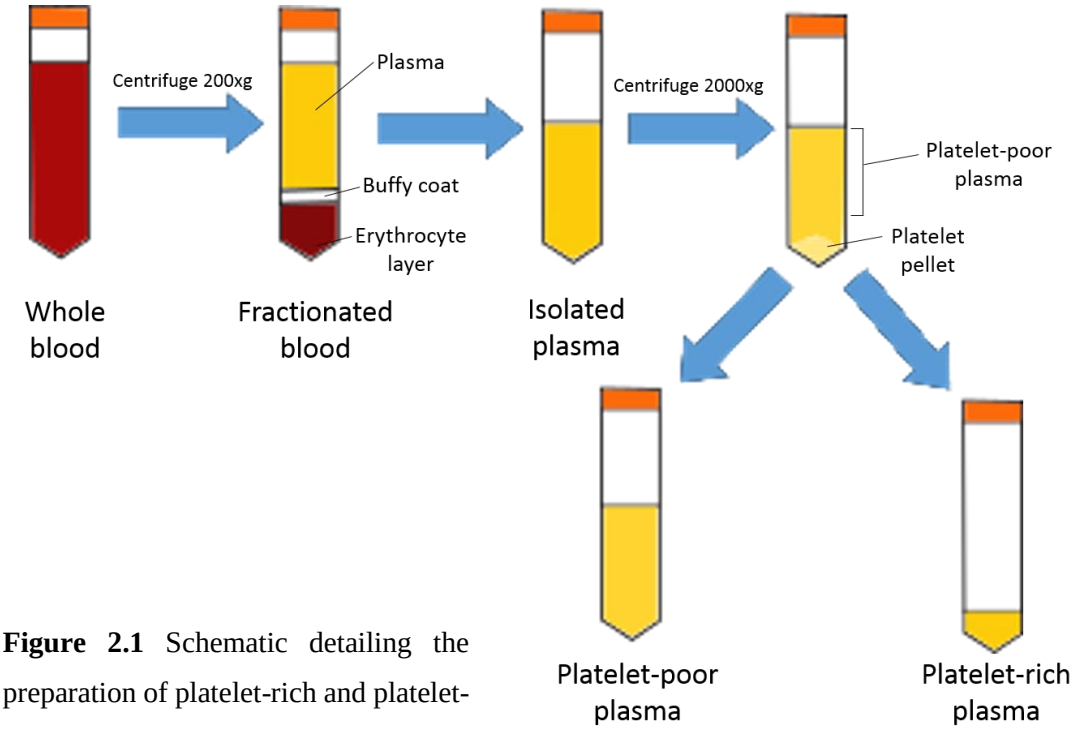

Figure 2.1 Schematic detailing the preparation of platelet-rich and platelet-poor plasma fractions.

2.1.2.2 Quantification of platelet count

Platelet counts were determined in PPP and PRP samples using a Neubauer haemocytometer. Samples were diluted 1 in 100 in PBS before addition of 1 volume of Trypan blue (Sigma). 10 µl was loaded into the haemocytometer and the platelets were allowed to settle at room temperature for 5 minutes prior to counting. The number of platelets in 4 of the 1/16 mm^2 squares of the haemocytometer grid were averaged. The following equation was then applied to determine the number of platelets present in 1 µl.

$$n = \big((a \times 16) \times 10) \times d\big)$$

Where n is the platelet density per µl of plasma, a is the average platelet count in 1/16 mm^2 and d is the dilution factor (ie. 200).

2.1.2.3 Quantification of plasma fibrinogen concentration

Fibrinogen concentration was measured using an in-house method developed during the course of this study, based on the clottable protein method developed by Ratnoff and Menzie (1951). The principle behind this assay is that by initiating the polymerisation of fibrinogen to fibrin, thereby forming a clot, the only protein remaining once the clot is washed is the

matrix-forming protein, fibrin. This fibrin can be dissolved in urea and the protein concentration can be measured using photometric analysis.

Cryocheck™ normal reference plasma with a fibrinogen concentration of 2.96 mg/ml was purchased from Precision BioLogic. To generate the standard curve, the reference plasma was diluted using distilled water, to produce 4 fibrinogen standards from 2.96 - 1.18 mg/ml. 500 µl of each standard and sample were activated with 50 µl of 100 U/ml bovine thrombin (Sigma-Aldrich), and incubated at 37˚C for 30 minutes. The clots were transferred to a clean dish and washed with distilled water. The clots were placed in tubes with a screw-top lid, to limit evaporation, and 500 µl of 5 mM urea was added. The tubes were incubated at 90˚C in a heat block for approximately 1 hour, until the clots had completely dissolved. 200 µl of each solution was placed into wells of a 0.32 cm^2 flat bottom 96 well-plate, and the absorbance was measured at 280 nm, using a Varioskan Flash plate reader (Thermo Scientific). The standard curve was created by graphing the generated absorbance value against the protein concentration (using Microsoft Excel software), and the equation of the line was used to convert the absorbance of the sample plasma to an absolute fibrinogen concentration.

2.1.3 Cytotoxicity of plasma activation agents

Calcium chloride ($CaCl_2$) and thrombin are the most commonly used chemicals for initiation of plasma gelation, as both are involved in the coagulation cascade which converts fibrinogen to fibrin. To select which chemical to use in this system, and at what concentration, the cytotoxicity of each substance was measured at a range of concentrations.

A CytoTox 96® Non-Radioactive Cytotoxicity Assay kit (Promega) was used to determine any potential cytotoxic effects on synovial cells resulting from the use of $CaCl_2$ and thrombin in the activation of plasma. The assay detects lactate dehydrogenase (LDH) released into media due to increased membrane permeability by an enzyme-coupled reaction which converts a tetrazolium salt, present in the CytoTox 96® reagent, into a red formazan product, which can be detected using colorimetric methods.

A 1 M solution of $CaCl_2$ was made by dissolving $CaCl_2$ powder (Sigma) in PBS. The solution was then sterile filtered using a syringe filter unit with a membrane pore size of 0.45 µm. Lyophilised thrombin, from bovine plasma (54 NIH units/mg) was purchased from Sigma-Aldrich. This was suspended in 540 µl of PBS to produce a thrombin solution with a final concentration of 100 units/ml. The solution was sterile filtered using a syringe filter unit with a pore size of 0.45 µm.

$3x10^4$ bovine synovial cells, at passage 3, were seeded in 0.32 cm^2 wells of a flat bottom 96-well plate in a total volume of 100 µl of DMEM with 10% FBS, and cultured at 37˚C in a humidified atmosphere of 5% CO_2 and 95% air until confluent. The prepared thrombin solution was added to wells, in combination with PBS, to produce concentrations ranging from 5-40 units/ml. The $CaCl_2$ solution was added to separate wells, in combination with PBS, to produce concentrations ranging from 5.75-46 mM. The total volume of each well after addition of thrombin/$CaCl_2$ and PBS was 164 µl (See table 1). Negative control wells were set up by the addition of 64 µl of PBS only. A total of 3 replicates were set up per treatment group. Three wells were reserved as positive controls, to which nothing was added at this stage. The plate was then incubated for 24 hours at 37˚C in a humidified atmosphere of 5% CO_2 and 95% air.

Table 1 Components of the test solutions for cytotoxic testing.

Final concentration of test compound	Volume of test compound	Volume of PBS (µl)
0 (Negative control)	0	64
5.75 mM $CaCl_2$	0.94 µl 1M $CaCl_2$	63.06
11.5 mM $CaCl_2$	1.88 µl 1M $CaCl_2$	62.12
23 mM $CaCl_2$	3.77 µl 1M $CaCl_2$	60.23
46 mM $CaCl_2$	7.54 µl 1M $CaCl_2$	56.46
5 U/ml Thrombin	8 µl Thrombin	56
10 U/ml Thrombin	16 µl Thrombin	48
20 U/ml Thrombin	32 µl Thrombin	32
40 U/ml Thrombin	64 µl Thrombin	0
0 (Positive control)	0	0

After the incubation period, 64 µl of 10 X cell lysis solution (Promega) was added to positive control wells and incubated for 45 minutes at 37˚C in a humidified atmosphere of 5% CO_2 and 95% air. This caused maximum LDH release, representing 100% cell death. 50 µl of media was taken from all wells and placed in wells of a fresh 96-well plate. Control wells containing DMEM supplemented with 10% (v/v) FBS only, were used to determine background absorbance levels.

50 µl of CytoTox 96^{TM} reagent (Promega) was added to all wells, and the plate was incubated in the dark for 30 minutes, at room temperature. 50 µl of stop solution (Promega) was then added to each well and the absorbance was measured at 490 nm within an hour of adding the stop solution, using a Varioskan Flash plate reader (Thermo Scientific). Following subtraction of blanks, absorbance values were compared to the positive control (representing 100% cell death) to estimate cell viability in each treatment group.

2.1.4 Effect of human serum on bovine synovial cell proliferation

It was necessary to determine whether human serum is able to induce proliferation in bovine synovial cells, as human blood plasma was to be used to create the hybrid ligament constructs and provide growth factors to supplement the cells. To accomplish this, cells were cultured in monolayer and media was supplemented with either 0.5% or 10% foetal bovine serum (FBS) or 0.5% of 10% serum derived from human PRP.

2.1.4.1 Preparation of human serum

PRP was thawed at 37˚C before activation with 23 mM $CaCl_2$ to induce gelation. The activated PRP was incubated at 37˚C for 30 minutes, until complete gelation had occurred. The gel was centrifuged at 2500 × g for 5 minutes to help to separate the solid and liquid components. The liquid was extracted and placed in a clean tube. This was designated human serum.

2.1.4.2 Culture of bovine synovial cells with human serum

Cells were trypsinised and resuspended in DMEM supplemented with 0.5% (v/v) FBS. 3.8 cm^2 wells of a 12-well plate were seeded at a density of 2500 cells/cm^2 in a total volume of 2 ml and left to attach to the well overnight. After attachment, the wells were washed twice with PBS. 3 wells were incubated with 500 µl of RLT buffer (Qiagen) to lyse the cells and release the DNA. These lysates were frozen at -20˚C for later quantification and represent the initial DNA quantity.

The remaining wells were covered with 1 ml of DMEM supplemented with either 0.5% FBS, 10% FBS, 0.5% human serum or 10% human serum. 3 wells were used per treatment group.

bSCs were cultured for a total of 7 days before digesting with 500 µl of RLT buffer and harvesting the lysate. Cell proliferation was assessed by measuring the DNA content.

2.1.4.3 DNA content assay

A Quant-iT™ PicoGreen® dsDNA Assay Kit (Invitrogen) was used to quantify DNA in the prepared lysates as per the manufacturer's instructions. Briefly, five dsDNA standards were made up in 1 x Tris-EDTA (TE) buffer (Invitrogen) from 50-0 ng/ml. 100 µl of each dsDNA standard was placed in 0.32 cm^2 wells of a flat bottom 96-well plate. Sample lysate was added to wells at a 1 in 100 dilution, in 1 x TE buffer to give a total volume of 100 µl per well. 100 µl of 1 in 200 PicoGreen solution (Invitrogen) in 1 x TE buffer was added to each well and the plate was incubated for 5 minutes at room temperature, in the dark. The samples were excited at 480nm and the fluorescence emission intensity of each well was measured at 520 nm using a Varioskan Flash plate reader (Thermo Scientific).

2.1.5 Statistical analysis

Graphs were generated and statistical significance was calculated using GraphPad 7 Prism software. Significance was determined using a one-way ANOVA for multiple comparisons. Comparisons between 2 groups were conducted using a t-test. A P-value of ≤ 0.05 was considered to be statistically significantly different. These statistical analysis methods were used throughout the entirety of the project.

2.2 Results

This section presents the findings from the studies described in the previous section (2.1). These findings enabled the development of methods used to fabricate hybrid ligament constructs detailed in chapter 3, by evaluating components of the proposed constructs. From these results it was possible to characterise the plasma which would be used throughout the project, select a plasma activation method and determine the effect of human serum on bovine cell proliferation.

2.2.1 Development of a method for quantifying plasma fibrinogen concentration

A number of methods have been developed to measure the fibrinogen concentration of blood. The most commonly used method is the Clauss method which determines the fibrinogen concentration based on the time taken for clot formation in the presence of a high concentration of thrombin (Clauss, 1957). However, it is difficult and inaccurate to determine clot formation by eye. In a clinical setting this method has been developed for use with automatic coagulation analysers which are able to accurately detect the point of coagulation by monitoring changes in viscosity or optical density (Miesbach *et al*., 2010).

Since it was not possible to access an automatic analyser, it was necessary to optimise an alternative method. Using the 'modified clottable protein' assay described in section 2.1.2.3, consistently high linearity (R^2 = >0.9) was observed when plotting fibrinogen concentration against absorbance (Figure 2.2). As a result, this method was utilised for all sample plasma.

It was not feasible to use all donor samples as this would require an unmanageable number of samples. In addition, it was predicted that donor variation could obscure any potential trends in the data. For these reasons it was decided that one donor would be used throughout the project. The mean fibrinogen concentration of the 5 donors was 2.87 mg/ml, and the donor closest to this value was donor 2, with a concentration of 2.89 ±0.07 mg/ml. Donor 2 was therefore selected for further studies (See Figure 2.3 for full results).

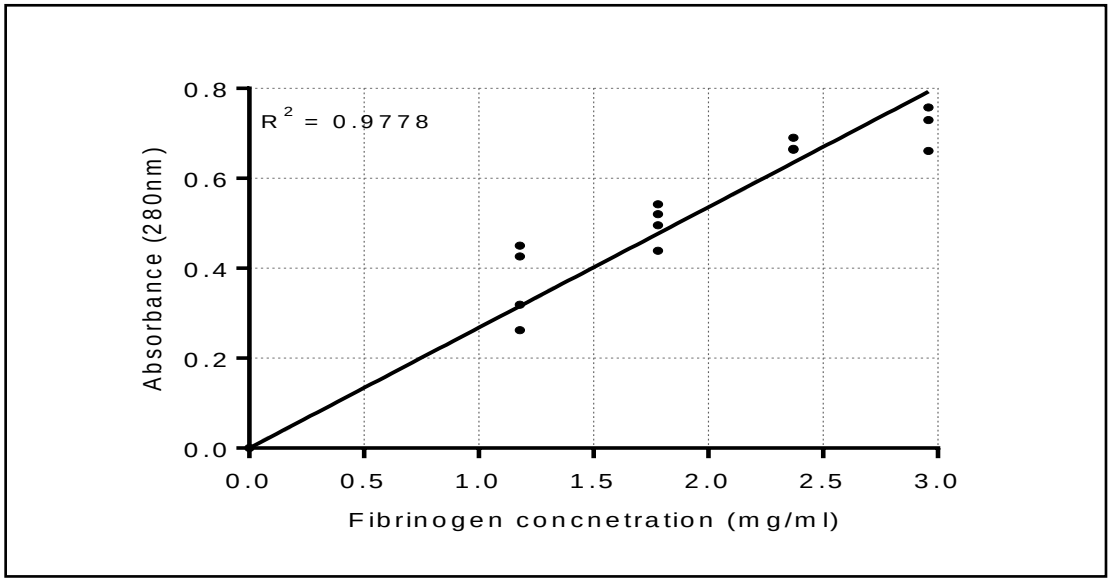

Figure 2.2 Standard curve of fibrinogen concentration generated using the clottable protein assay.

The graph demonstrates high linearity ($R^2 = 0.9778$). Dilutions of normal reference plasma of known fibrinogen concentration were used to generate the graph.

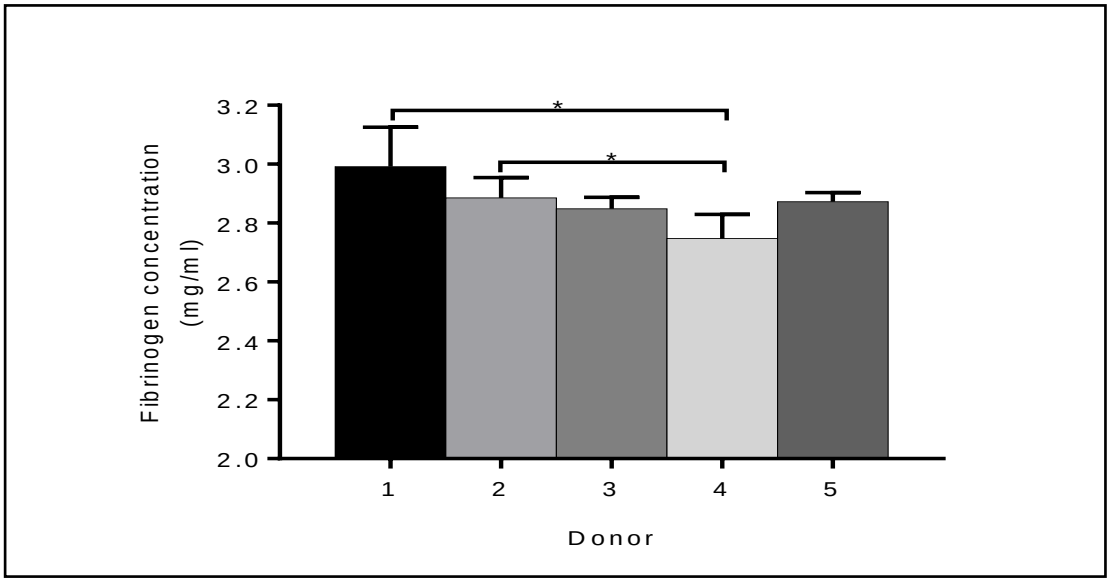

Figure 2.3 Fibrinogen concentration of plasma from donors 1 to 5.

Bars represent the mean ± standard deviation (n=3). Significance was determined using a one-way AVOVA. * indicates significance of $p \leq 0.05$.

2.2.2 Isolation of PPP and PRP by centrifugation

In order to confirm whether the plasma extraction method detailed in section 2.1.2 had yielded preparations which could be considered PPP and PRP, platelet counts were performed on samples using a haemocytometer, as detailed in section 2.1.2.2. PPP and PRP samples had a mean platelet count of $4.5x10^4$ ±3.5 and $200x10^4$ ±91 platelets/µl respectively (Figure 2.4). On average, platelet counts were 44 times higher in PRP than PPP. Statistical analysis determined these values to be significantly different. Furthermore, PPP contained approximately 10 times fewer platelets than whole blood, whilst PRP contained approximately 4 times the platelet density of whole blood. These values are within the ranges used to describe PPP and PRP (Marx, 2004).

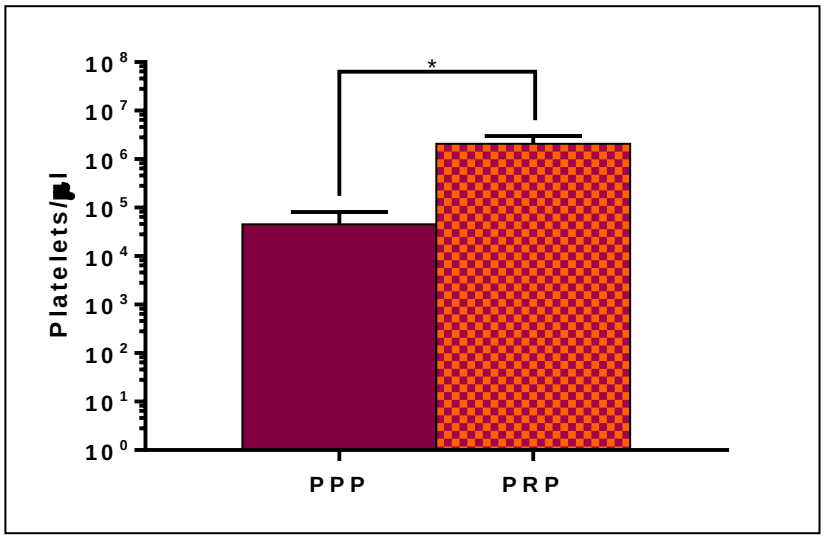

Figure 2.4 Platelet counts in PPP and PRP.
Platelet count measured in platelet-poor and platelet-rich samples using a haemocytometer. Bars represent the mean ± standard deviation (n=3). Statistical significance was determined using a t-test. * indicates significance of $p \leq 0.05$.

2.2.3 Selection of 23 mM $CaCl_2$ as the plasma activation method

As previously explained in chapter 1, the aim of this project was to produce hybrid ligament constructs, composed of a polyester scaffold and a platelet-rich gel. Since blood was collected into tubes containing an anticoagulant, addition of an activation agent was required to initiate coagulation of the plasma to form the fibrin gel component of the construct. $CaCl_2$ and bovine thrombin were the two activation factors selected as candidates for use in construct fabrication. The cytotoxicity of $CaCl_2$ and bovine thrombin was measured using an LDH assay (according to section 2.1.3) to determine which protocol would be most appropriate for initiating gelation of blood plasma without causing significant cytotoxic effects.

According to Figure 2.5 A, there was no significant difference between a $CaCl_2$ concentration of 5.75, 11.2 or 23 mM in terms of cytotoxicity, as measured by LDH release. All of these concentrations produced similar levels of LDH release to PBS (10%). In contrast, a concentration of 46 mM $CaCl_2$ produced a significantly higher level of LDH release (22%) in comparison with PBS ($p \leq 0.01$) and 23mM $CaCl_2$ ($p \leq 0.05$).

Figure 2.5 B shows the relative cytotoxicity of various bovine thrombin concentrations. The profile is similar to $CaCl_2$, with 5, 10 and 20 U/ml thrombin producing similar levels of LDH release (approximately 6-10%). Addition of 40 U/ml thrombin resulted in a significantly greater LDH release than all other tested concentrations (15%).

Although bovine thrombin was found to be slightly less cytotoxic than $CaCl_2$ at the concentrations used within this *in-vitro* assay, the use of bovine thrombin in a clinical setting presents the risk of causing an undesirable immune response, which could necessitate modification of the protocol for clinical application (Ortel *et al.*, 2001). In addition, $CaCl_2$ is much cheaper than bovine thrombin, and since it was no more harmful to cells than PBS when at a concentration of 23 mM, it was selected for use at this concentration, to activate plasma in all future experiments.

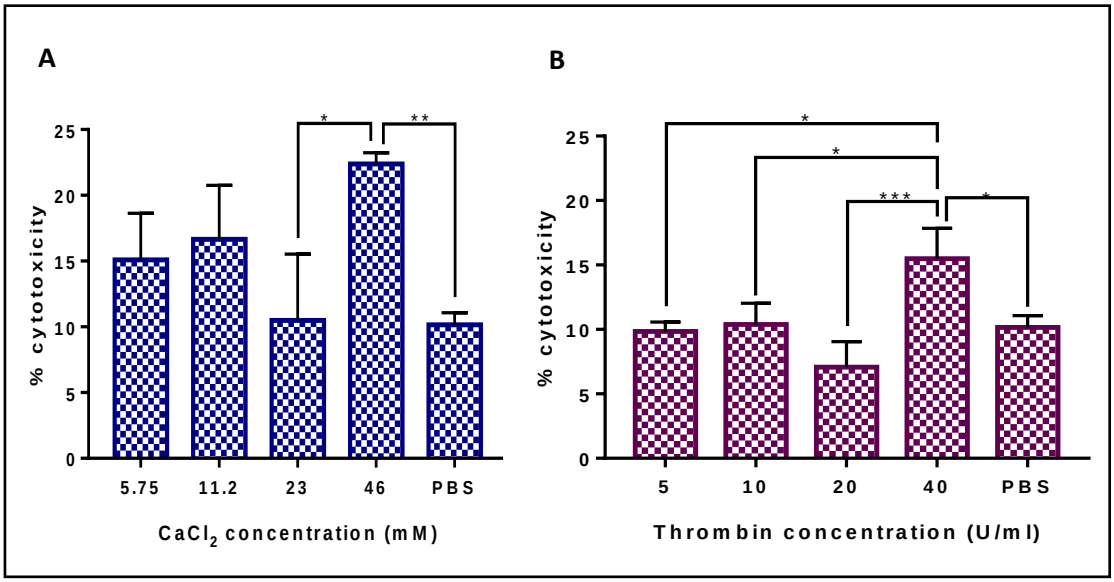

Figure 2.5 LDH release from bSCs due to plasma activation agents.

Cytotoxicity of varying concentrations of $CaCl_2$ (A) and bovine thrombin (B) on bSCs. Bars represent the mean ± standard deviation (n=3). Significance was determined using a one-way AVOVA. * = $p \leq 0.05$, ** = $p \leq 0.01$, *** = $p \leq 0.001$.

2.2.4 Human serum induces a lower proliferation response in bSCs than bovine serum

A proliferation assay was performed on bSCs cultured in monolayer to compare the response to supplementation with human serum (HS) and FBS. This was necessary as all blood used in this project was of human origin. HS was produced from PRP using the method described in section 2.1.2.1. Figure 2.6 shows the proliferation of bSCs over 7 days when supplemented with varying concentrations of FBS and HS in DMEM. The results show a significant increase in proliferation with increasing serum percentage, with both HS and FBS. Supplementation with 10% FBS induced approximately twice the proliferation rate of 10% HS ($p \leq 0.0001$). Although less effective than FBS, the level of stimulation produced by HS was considered sufficient for the purposes of this study.

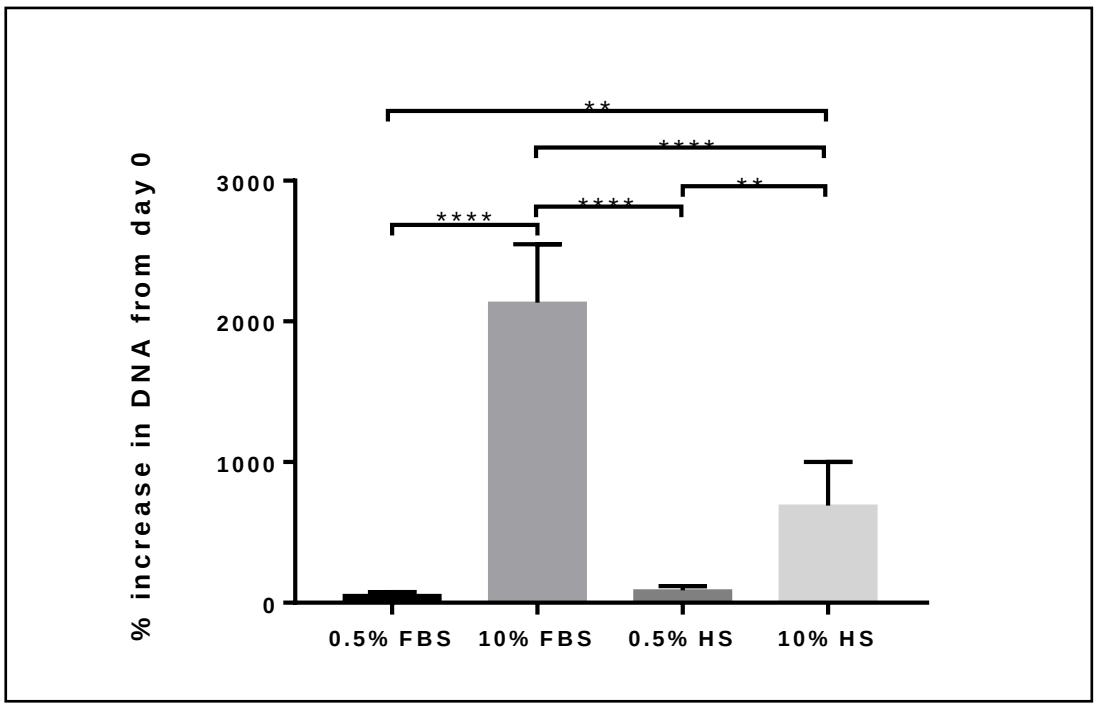

Figure 2.6 Effect of bovine serum (FBS) and human serum (HS) on bSC proliferation. Data is presented as the percentage DNA increase from the day after seeding (day 0) to the 7th day of culture. Bars represent the mean ± standard deviation (n=3). Statistical significance was determine using a one-way ANOVA. ** = $p \leq 0.01$, *** = $p \leq 0.001$, **** = $p \leq 0.0001$.

2.3 Discussion

This section discusses the results presented in this chapter and describes the rationale by which decisions were made on how to fabricate hybrid ligament constructs with a plasma component. This chapter addressed the preparation of platelet-poor and platelet-rich plasma fractions from human blood, as well as their characterisation by the quantification of platelet density and fibrinogen concentration. A suitable method for initiating plasma gelation was identified, and the effect of human serum on bovine synovial cell proliferation was quantified, leading to the conclusion that growth factors released from platelets of human origin could induce proliferation in cells of bovine origin and thus could be relied upon for supplementing cells in later stages of the project.

Cells selected to evaluate the constructs were harvested from the synovial membrane of bovines, rather than from the ligament itself. This was considered an appropriate cell choice from a clinical perspective, since ACL reconstruction generally involves complete removal of the damaged ligament prior to graft fixation. Synovial cells lining the joint capsule are the most likely source of cells for colonization of the graft. Furthermore, synovial cells have multi-lineage potential, which has been found to be conserved *in vitro* (De Bari *et al.*, 2001). Other cell types have been used for studies investigating the potential of tissue engineered ACL constructs, including bone marrow MSCs (Altman *et al*., 2002) and ACL fibroblasts (Cooper *et al.*, 2008). One strategy for using a synthetic ligament construct to replace the ACL could be to seed the construct with patient cells and allow the formation of a more mature ECM before implantation. In this situation it may be preferable to use cells which are more easily isolated than synovial cells or ACL fibroblasts, which require invasive surgery for extraction. Bone marrow MSCs can be aspirated using minimally invasive methods, or can be harvested from the blood using peripheral blood stem cell apheresis (Korbling et al., 1995). Future investigations should consider using bone marrow MSCs, as well as synovial cells, when developing a tissue engineered ACL construct.

As discussed in greater detail in chapter 1, the overall aim of this project was to incorporate a bioactive component into the Xiros PET ligament to attempt to enhance cell proliferation and ECM deposition. The main component of interest for this purpose was blood plasma, which is able to form a gel upon polymerisation of soluble fibrinogen monomers within the plasma. Following the isolation of plasma from human whole blood, it was necessary to quantify the fibrinogen concentration of the samples to ensure that any plasma used in this work reflected normal, healthy plasma, containing a clinically relevant fibrinogen concentration. The assay used to quantify fibrinogen concentration within the donated plasma was developed during the project. Although quantification can be performed more rapidly using automated methods,

the assay developed here allows accurate quantification in situations where such equipment is unavailable. The normal plasma fibrinogen concentration has previously been defined as 1.45-3.48 mg/ml (Oswald *et al.,* 1983), and all plasma donated to this project fell within this normal healthy range, with measured donor fibrinogen concentrations of 2.74-2.99 mg/ml (see Figure 2.3). The donor selected for all subsequent studies had a fibrinogen concentration closest to the mean of the 5 donors, as it was concluded that this would be the sample most representative of the general population. The strength of fibrin gels has been found to be directly proportional to the fibrinogen concentration (Kjaergard and Weis-Fogh, 1994). However, the proposed construct in this work consists of a PET scaffold, which is the force bearing component of the scaffold. The plasma component is not required to support the knee joint, and is merely there to enhance the bioactivity of the scaffold by supplying a biological fibrin matrix, as well as a growth factor release system. Some tissue engineering applications have used concentrated plasma, produced using techniques such as cryoprecipitation, or by addition of other chemicals, to generate fibrinogen concentrations more than 10 times the physiological concentration. However, such methods can be expensive and may alter the structure of the fibrinogen (De la Puente and Ludeña, 2013). For these reasons, the plasma used throughout this project was not concentrated above its physiological level.

Platelet-rich and platelet-poor plasma fractions were separated from the plasma samples using the differential centrifugation method (Dhurat and Sukesh, 2014), whereby whole blood is initially centrifuged to separate the plasma, buffy coat and erythrocyte layer. The plasma layer is then carefully extracted before being centrifuged again, at a higher speed, to pellet the platelets. The majority of the plasma is removed (and stored as platelet-poor plasma) and the platelets are resuspended in the remaining proportion (in this work, a fifth of the total volume was used to resuspend the platelets). The platelet-rich plasma (PRP) fraction produced using this method had a 44-fold higher platelet concentration than the platelet-poor plasma (PPP) fraction, with PPP having a platelet density of less than a third of the lowest normal value for whole blood. PRP fractions had platelet densities approximately 4.4-fold greater than the highest normal value for whole blood (see Figure 2.4). The preparations therefore met the necessary criteria to be described as platelet-poor and platelet-rich plasma (Marx, 2001).

To produce the fibrin matrix to which cells can attach, plasma gelation must be initiated using an activation agent such as calcium or thrombin. The literature reports a range of $CaCl_2$ and thrombin concentrations which have been used in the formation of plasma/fibrin gels. Ye *et al*. (2000) used a combination of 50mM $CaCl_2$ and 20 U/ml of thrombin to produce fibrin gels for cardiovascular tissue engineering. In contrast, Navaei-Nigjeh *et al.* (2013) used just 3 U/ml of thrombin only to activate gels used as constructs for nerve tissue engineering. As fibrin gels have been successfully produced using many different concentrations of $CaCl_2$ and thrombin,

it was decided that these activation factors would be evaluated based on their cytotoxicity. Analysis of LDH release showed little difference in the levels of cytotoxicity induced by $CaCl_2$ and bovine thrombin (Figure 2.5). A study conducted by Rowe *et al*. (2007) evaluated the effect of thrombin concentration on the mechanical properties of the resulting gel. They found that the lower the thrombin concentration, the greater the tensile strength of the gel, suggesting that including additional thrombin in the construct would not result in any mechanical benefit. Furthermore, the same study assessed the rate of proliferation of rat smooth muscle cells in fibrin gels with varying thrombin concentration, and concluded that there was no significant difference in proliferation.

Another important factor when considering the activation method of fibrin gels is how the method affects platelet activation and subsequent growth factor release. A previous study compared the release of growth factors and cytokines from fibrin gels activated with $CaCl_2$ only, and with a mixture of $CaCl_2$ and thrombin. The work found there to be no significant difference in growth factor or cytokine release from gels activated with $CaCl_2$/thrombin or $CaCl_2$ alone (Amable *et al.*, 2013). Again, this indicated that there is no benefit to the addition of exogenous thrombin within the plasma activation system. Since bovine thrombin is more expensive, and has been found to produce adverse effects *in vivo* (Ortel *et al.*, 2001), $CaCl_2$ was selected as the activation agent. A concentration of 23mM $CaCl_2$ induced the lowest LDH release from bSCs (see Figure 2.5), and this was subsequently the concentration selected for construct production.

All blood used in this project was of human origin, due to ease of accessibility. This also ensured minimal time between venepuncture and processing of the blood. To ensure that growth factors originating from human platelets could induce a proliferation response in synovial cells of bovine origin, a cell proliferation assay was conducted, comparing human serum (HS) with FBS. Supplementation with 0.5% FBS or HS was intended to act as a negative control and was expected to induce a low level of proliferation. At this concentration both supplementation with FBS and HS resulted in a DNA increase of less than 2-fold over the 7 day culture period. Supplementation with 10% human serum induced an 800-fold increase in bSCs cultured in monolayer over a period of 7 days (see Figure 2.6). Although this was less than half the rate of proliferation induced by the same percentage of FBS, the stimulatory effect of human serum was considered to be sufficient for the purposes of the project. A study published by Bieback *et al*. (2009) compared the proliferation rates of human BMSCs cultured with FBS and HS. Proliferation rates were comparable between FBS and HS at all passages. However, this may reflect the use of human-derived cells, rather than bovine cells. Alternatively, variations in growth factor concentration between commercially available FBS, and the HS produced in-house may be responsible for the reduced proliferation seen in

response to HS. For a superior comparison of the two, growth factor concentrations could be equalised prior to testing. However this would have required costly growth factor quantification assays, as well as a significant amount of time. No examples could be found in the literature of investigations which compared FBS and HS supplementation of bovine cells.

Sequence alignments were performed on some of the key human and bovine growth factors released from the alpha granules of platelets (full sequence alignment results can be found in the Appendix). The average similarity of all 6 growth factors was 93% with human and bovine VEGF having the lowest sequence similarity (79%), and bFGF having the highest similarity (99%). The high percentage sequence similarity between human and bovine growth factors indicates that growth factors of human origin are very likely to interact with receptors on cells of bovine origin. Nevertheless, it is anticipated that in a clinical setting, any PRP used would be autologous, and would therefore have maximum stimulatory effect.

2.4 Summary

The studies detailed in this chapter have resulted in the successful production of PPP and PRP, and have led to the selection of an appropriate blood donor for use throughout the project, through the development of a method for quantifying donor plasma fibrinogen concentration. Gelation of the PPP for construct fabrication should be activated using 23 mM CaC_2, as indicated by the results from the cytotoxicity assay. Due to the reduced proliferation rate of bSCs supplemented with human serum, it was decided that platelet-poor plasma would be used in the initial stages of construct optimisation, and that the hybrid constructs would be supplemented with FBS. This was to ensure that all cells were exposed to a similar method of supplementation, so that constructs could be evaluated based on their physical composition, rather than any potential variation in bioactivity due to variable growth factor concentrations.

Chapter 3

Preparation and evaluation of 9 initial 3D hybrid ligament constructs

Following the preparation of PPP and selection of an appropriate activation method, 9 hybrid ligament constructs were produced according to the methods detailed in this chapter. This chapter explains the processes by which 3 constructs were eventually selected for further study based on their performance in cell proliferation and coatings longevity studies.

Aim:

This phase of the project aimed to evaluate 9 hybrid ligament constructs coated with various ratios of PPP, collagen and alginate, with a view to selecting the three most promising candidates for further study.

Objectives:

- Fabrication of 9 hybrid constructs composed of a PET scaffold and a biopolymer coating (consisting of various ratios of PPP : collagen and PPP : alginate).

- Validation of the coating method to ensure complete coverage of the PET scaffold with a uniform hydrogel.

- Quantification of bSCs proliferation within each of the 9 hybrid constructs, in comparison with the non-coated control (NC), over a period of 15 days.

- Assessment of the infiltration of bSCs seeded on the PET scaffold into each of the 9 biopolymer coatings.

- Quantification of the longevity of each of the 9 coatings (using light microscopy) to determine the durability of the hybrid constructs over 15 days.

- Selection of the 3 most promising hybrid constructs based on proliferation and longevity data.

3.1 Materials and methods

The methods described in this chapter include details of the construct fabrication process which was used throughout this project. Constructs were composed of a section of Xiros PET scaffold coated with various combinations of PPP, collagen and alginate. This section also includes the methods used to evaluate each of the hybrid constructs based on their ability to induce cell proliferation and infiltration, as well as the overall durability of each hydrogel combination.

3.1.1 Preparation of cell-seeded coated hybrid ligament constructs

The following section details the methods used to fabricate hybrid constructs composed of a synthetic woven scaffold and biopolymer coating. bSCs were seeded directly onto the scaffold before addition of the biopolymer coating.

3.1.1.1 The PET ligament scaffold

Polyethylene terephthalate (PET) scaffolds (Figure 3.1) were kindly supplied by Xiros® Ltd (Leeds, UK). The scaffolds had an identical weave pattern to those used as ligament implants, and were comprised of 9 yarns, each consisting of 96 monofilaments, with a diameter of 20 µm. The scaffolds were supplied pre-sterilized with a total diameter of 5 mm and a length of 100 mm. These were cut to the required length for each study, using a sterile surgical scalpel.

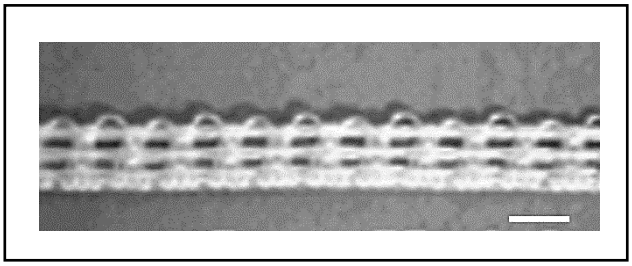

Figure 3.1 Photograph of the polyethylene terephthalate ligament scaffold.
Scale bar = 5 mm.

3.1.1.2 Dynamic seeding of bSCs on the PET ligament scaffold

For maximum attachment and homogenous distribution of bSCs to the ligament scaffolds, an in-house developed seeding device was used (Figure 3.2). 2 ml microtubes were prepared by making a small hole in the lid (approximately 3 mm in diameter) to allow gaseous exchange, before sterilisation by autoclaving. bSCs were trypsinised and suspended in DMEM supplemented with 10% (v/v) FBS to yield a density of 1 x 10^5 cells/ml. The scaffold sections were placed in the tubes and 2 x 10^5 bSCs were added in a total of 2 ml. The lids of the tubes were covered with a gas-permeable Opsite Flexigrid membrane (Smith & Nephew), and the sealed tubes were placed in the outer holes of the cylindrical modules only (to ensure all tubes were subjected to the same range of motion). The tubes were secured by screwing on a stainless steel plate, with holes corresponding to the position of the tubes, to ensure gaseous exchange was not obstructed (Figure 3.3). The modules were then mounted on the seeding apparatus and placed in a humidified atmosphere incubator containing 5% (v/v) CO_2 and 95% (v/v) air at 37˚C and allowed to rotate at 10 RPM for 48 hours, before transferring the scaffolds to a sterile petri dish and covering with 10 ml of DMEM supplemented with 10% (v/v) FBS.

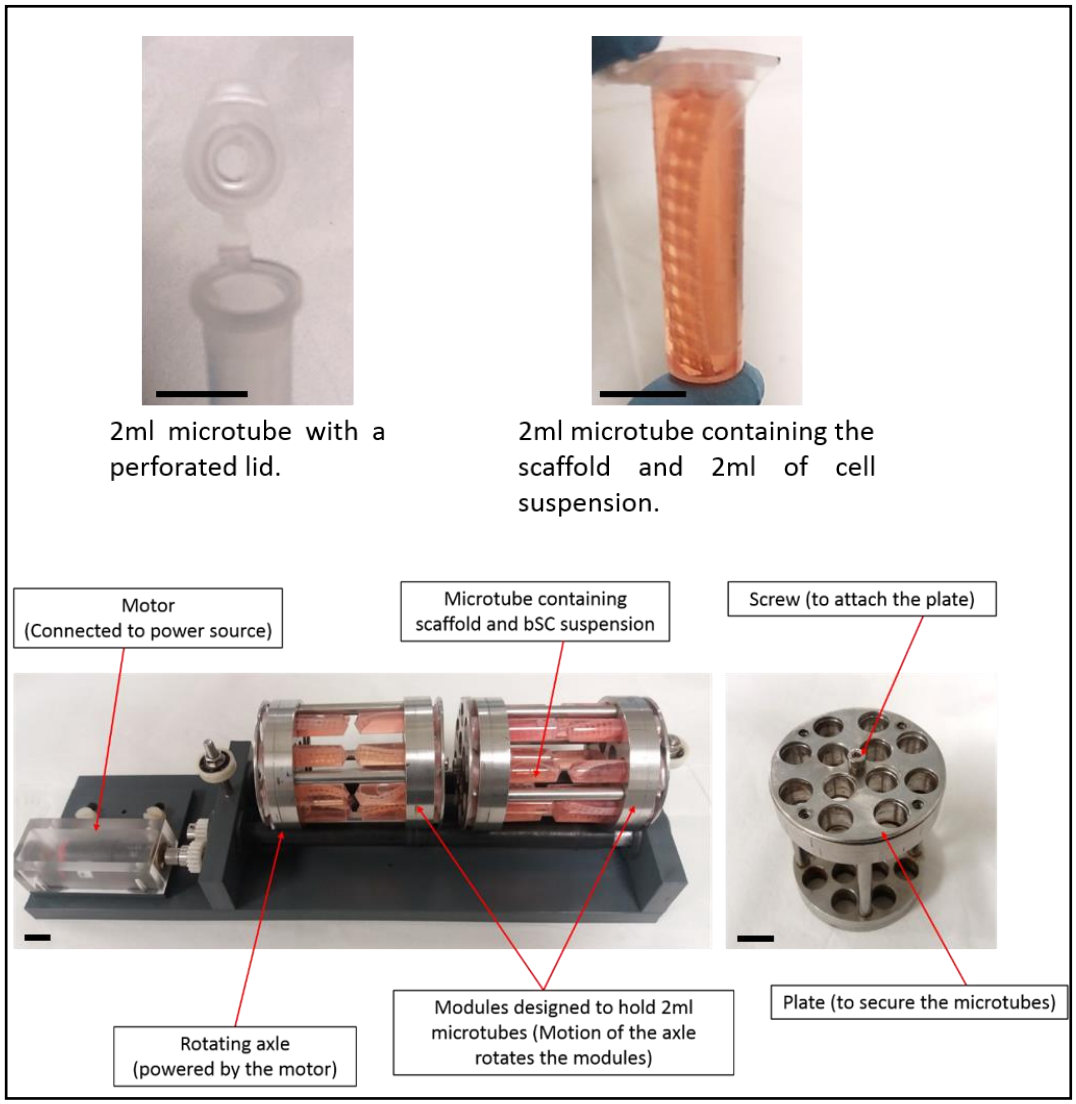

Figure 3.2 Photographs of the dynamic seeding apparatus.

The tubes containing the scaffold and cell suspension were secured in the outer holes of the cylindrical modules only (to ensure all tubes were subjected to the same range of motion) and placed on the axles of the seeding apparatus. The motor rotates the axles resulting in rotation of the modules. Scale bar =1cm.

3.1.1.3 Coating of bSC-seeded PET scaffolds using plasma, collagen and alginate

To determine the most appropriate substrate for enhancing tissue induction, cell-seeded scaffolds were coated with a variety of hydrogel mixtures (Table 2). After 48 hours of dynamic seeding, scaffolds were washed thoroughly in PBS to remove any non-adherent cells, and were coated using the following method.

3.1.1.3.1 Preparation of coating biopolymers

Alginate was prepared from alginic acid, sodium salt (sigma-Aldrich) as a 2% (w/v) solution in PBS. To sterilise, the solution was autoclaved and allowed to cool before use.

Collagen type I (PureCol® EZ Gel) solution was purchased from Sigma-Aldrich. This product is a pre-neutralised 5 mg/ml bovine collagen solution in DMEM-F12 media, which forms a gel upon warming to 37˚C.

Fresh frozen PPP (prepared as described in section 2.1.2) was thawed at 37˚C and activated with 23 mM $CaCl_2$ within 5 minutes of coating.

3.1.1.3.2 Coating procedure

Polymer solutions were combined in the proportions presented in Table 2. Each polymer mixture was pipetted onto the top of seeded scaffolds using a volume of 10 µl per millimetre length of scaffold. The scaffolds were incubated at 37˚C for 1 hour to allow gelation. After the incubation period, scaffolds coated with alginate-based mixes were covered with approximately 1 ml of 100 mM $CaCl_2$ for 1 minute, at room temperature, to initiate alginate gelation. The constructs were washed thoroughly in PBS to remove excess salt.

Table 2 Ratios of the biopolymers comprising each coating type evaluated during this phase of the study.

Coating group	PPP (%)	Collagen (%)	Alginate (%)
P100	100	0	0
C100	0	100	0
C75	25	75	0
C50	50	50	0
C25	75	25	0
A100	0	0	100
A75	25	0	75
A50	50	0	50
A25	75	0	25

3.1.1.4 Maintenance of cell-seeded coated scaffolds *in vitro*

Following complete gelation, cell-seeded coated scaffolds (see table 2) were transferred to 3.8 cm^2 wells of a 12-well plate. The wells were pre-coated with 1% agarose, to prevent cell attachment to the bottom of the well. Non-coated cell seeded scaffolds (NC) were used as controls. The constructs (coated and non-coated) were covered with 1 ml of DMEM supplemented with 10% (v/v) FBS and placed in a humidified atmosphere incubator containing 5% (v/v) CO_2 and 95% (v/v) air at 37˚C. Cell growth and migration was monitored every three days using light microscopy. All media was replaced every three days.

3.1.2 Methods for monitoring growth of bSCs in coated scaffolds

This section details the methods used to monitor proliferation, and infiltration of bSCs within the hybrid ligament constructs. Hybrid constructs were fabricated by dynamically seeding bSCs onto PET woven scaffolds for 48 hours before coating the scaffolds with each biopolymer mix detailed in table 2. For a detailed description of the hybrid construct fabrication process, see section 3.1.1. A total of 9 different hybrid cell-seeded constructs were used to monitor bSC proliferation and infiltration, in comparison with non-coated control scaffolds (NC). Three of each construct were produced and assessed using the following methods.

3.1.2.1 Quantification of cell proliferation within coated scaffolds

A total of 33 scaffolds were dynamically seeded with 2 x 10^5 bSCs, as described in section 3.1.2, to assess cell proliferation. Directly after seeding the PET scaffolds, 3 non-coated cell-seeded scaffolds were washed twice with PBS before transferring them to 1.5 ml microtubes. 500 µl of RLT buffer (Qiagen) was added and the scaffolds were incubated at room temperature for 30 minutes, to lyse the cells. The lysates, representing the 0 hour DNA quantity, were frozen at -20˚C until use.

The remaining 30 cell-seeded scaffolds were coated using the polymer combinations detailed in table 2, using the method described in section 3.1.3. A total of 3 coated constructs were fabricated for each coating type, leaving 3 non-coated constructs as controls. All constructs were cultured in 3.8 cm^2 wells of a 12-well plate, which were pre-coated with 1% agarose to prevent cells from attaching to the bottom of the well. Constructs were covered with 1 ml of DMEM supplemented with 10% (v/v) FBS and cultured using the conditions detailed in section 3.1.4.

After 15 days of culture, the constructs were washed with PBS and transferred to 1.5 ml microtubes. 500 µl of RLT buffer (Qiagen) was added and the constructs were incubated at room temperature for 30 minutes, to digest the gels and lyse the cells. Coatings containing alginate were digested with the same volume of a 1:1 mixture of RLT buffer (Qiagen) and 1 M Na_2CO_3. A pestle was used to help mechanically break the constructs to release the cells. The lysates were stored at -20˚C until use.

All lysates (including those representing 0 hours) were thawed at room temperature on the day of analysis. Lysates were passed through a QIAshredder column (Qiagen) which was centrifuged at 2000 × *g* for 5 minutes, to homogenise the sample and remove any debris. A Quant-iT™ PicoGreen® DNA content assay (Invitrogen) was used to assess cell proliferation within each construct (detailed in section 3.1.3).

3.1.2.2 Assessment of cellular infiltration using confocal microscopy

Hybrid constructs for infiltration analysis were fabricated and cultured to 15 days (As described in section 3.1.1) before being washed three times in PBS and fixed in neutral buffered formalin (NBF) for 20 minutes. The samples were then washed three times in PBS before incubating with 0.1% Triton X-100 in PBS for 20 minutes, at room temperature. To stain for actin, samples were incubated with Alexa Fluor 488 phalloidin (Invitrogen) diluted 1/10 in PBS, for 2 hours at room temperature. Washing was performed three times in PBS before incubating with 1/200 TO-PRO®-3 (Invitrogen) in PBS for 20 minutes. A final PBS wash was performed three times before using a Leica TCS SP2 confocal laser scanning microscope with a 20 X objective lens to image bSCs within the constructs.

3.1.3 Analysis of gel coating longevity

In addition to the suitability of each coating for cell proliferative purposes, it was also considered important to assess the stability of these matrices for supporting long-term tissue induction. Gel stability was monitored by quantifying gel loss, characterised by reduction of intra-fibre filling over time.

This method, developed to assess gel loss, is an image analysis technique to quantify visual loss of gel from each scaffold. 20 mm lengths of scaffold were dynamically seeded with 2 × 10^5 cells (see section 3.1.1.2), and coated with the polymer combinations detailed in table 2, according to the method in section 3.1.3. Non-seeded scaffolds were all coated with the same polymer combinations for comparative purposes. The two intra-fibre voids positioned at each end of the scaffolds were imaged using a Zeiss Axiovert A1 light microscope with in situ

digital camera. Each scaffold was imaged in this way at days 1, 5, 10 and 15. Three constructs were produced and imaged per coating group.

ImageJ software was used to measure the total area of the scaffold intra-fibre void, as well as the areas of gel loss (Figure 3.3), so that a percentage filling could be calculated using the following equation:

$$n = 100 - \left(\left(\frac{a}{t}\right) \times 100\right)$$

Where n is the percentage filling, a is the area of gel loss and t is the total area of the void.

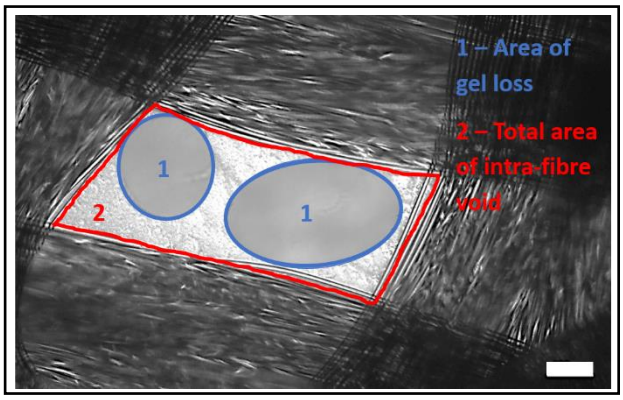

Figure 3.3 Reduction of intra-fibre filling by gel coatings.
The image shows an intra-fibre void of a PET scaffold coated with 100% plasma (P100), imaged using light microscopy. The image is annotated to demonstrate areas of gel loss as well as the total area of the intra-fibre void (scale bar = 200 µm).

3.2 Results

This section presents the findings from methods described in sections 3.1. This includes evaluation of the initial 9 hybrid constructs in terms of cell proliferation and infiltration, and the longevity of each biopolymer coating, such that 3 hybrid constructs could be selected for further analysis in chapter 4, based on these findings.

3.2.1 PPP, collagen and alginate coatings resulted in complete filling of the scaffold intra-fibre spaces

To produce hybrid constructs, each gel used in this work (PPP, collagen and alginate) had to be able to completely coat the polyester scaffold and fill the intra-fibre voids so that maximum cell infiltration could be achieved. To test this, 200 µl of plasma, collagen and alginate solutions were pipetted onto a section of scaffold and polymerisation was activated according to the method described in section 3.1.3. This was the first and only method tested. Photographs of the intra-fibre voids and the edges of the scaffold were taken using light microscopy. The images showed that all three polymers were able to form a gel which completely filled the intra-fibre voids and coated the entire scaffold (Figure 3.4).

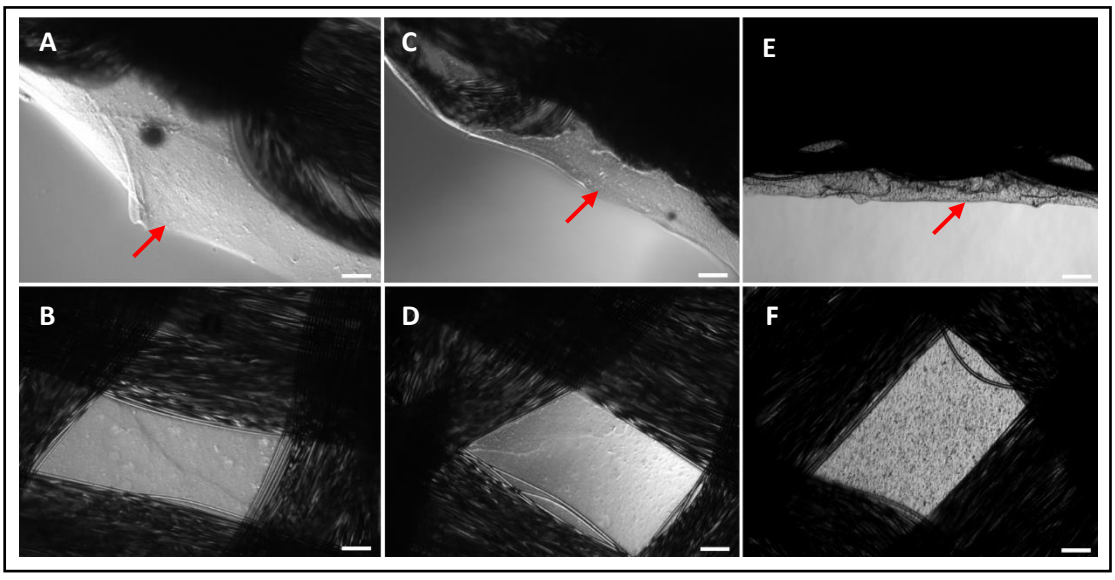

Figure 3.4 PPP, collagen and alginate filling the intra-fibre voids of the PET scaffold. Light microscope images demonstrating scaffold coverage by plasma (A-B), collagen (C-D) and alginate (E-F). A, C and E show coating at the edge of the scaffold (arrows). B, D and F show the filling of intra-fibre voids within the scaffold. Scale bar = 200µm.

3.2.2 The effect of each biopolymer coating on cell proliferation and infiltration

This section details the results generated from experimental work using the 9 different hybrid constructs (P100, C100, C75, C50, C25, A100, A75, A50 and A25), in comparison with the non-coated control (NC). The constructs were fabricated according to the methods detailed in section 3.1. The aim of this phase was to narrow down the candidates brought forward for further study by monitoring cell growth quantitatively (using a cell proliferation assay) and qualitatively (using confocal microscopy). Coatings were also assessed for their durability *in vitro*.

3.2.3 Alginate hinders bSC proliferation in comparison with plasma and collagen coatings

2 cm lengths of the PET scaffold were dynamically seeded with 2 x 10^5 cells before coating with each biopolymer mix to form the 9 different hybrid constructs (P100, C100, C75, C50, C25, A100, A75, A50 and A25), according to the methods in section 3.1. Non-coated seeded scaffolds were used as a control. The DNA content of each construct was measured after 15 days of culture to determine which coatings encouraged or hindered bSC proliferation.

Figure 3.5 shows the increase in cell number in each construct over 15 days. Graph A compares each single polymer coating (P100, C100, A100), with the non-coated control scaffold. An 81% increase in cell number was measured on non-coated scaffolds. By coating the scaffold with plasma to form the P100 construct, proliferation increased to 120% (not significant). By coating the scaffold with collagen to produce the C100 construct, proliferation was significantly increased to 146% ($p \leq 0.01$) in comparison with the non-coated control. In contrast, by coating the scaffold with alginate to form the A100 construct, proliferation significantly decreased to 42% ($p \leq 0.05$). Both plasma and collagen coatings had a positive effect on proliferation (although only significant in C100), whereas the alginate coating had a significantly negative effect.

Graph B shows how combining plasma and collagen at different ratios affects cell proliferation. By coating the PET scaffold with a 75:25 mixture of collagen/plasma (C75), the proliferation rate decreased to 63%, which is significantly lower than either plasma ($p \leq 0.01$) or collagen ($p \leq 0.0001$) alone, as well as being significantly lower than the non-coated control scaffold ($p \leq 0.05$). Coating the scaffold with a 50:50 mixture of collagen/plasma (C50) resulted in a 112% increase in cell number by 15 days. This was not significantly different from the non-coated control but was significantly lower than C100 ($p \leq 0.05$). By coating the scaffold with a 25:75 mixture of collagen/plasma (C25), the increase in cell number by 15

days was 122%. This was not significantly different to the non-coated control, nor the P100 or C100 coatings.

Graph C shows how combining plasma and alginate at different ratios alters the proliferation of bSCs. By combining alginate/plasma at a 75:25 ratio (A75), the total DNA content increased by just 20% over 15 days. This was significantly lower than the non-coated control ($p \leq 0.001$). Coating with a 50:50 mixture of alginate/plasma (A50) resulted in no significant difference in proliferation in comparison with A100 or A75 coatings. A100, A75 and A50 coatings all produced significantly lower rates of cell proliferation than the non-coated control ($p \leq 0.01$, $p \leq 0.001$ and $p \leq 0.01$ respectively). By combining alginate/plasma at a 25:75 ratio (A25), the cell proliferation value was the highest of any of the alginate-based constructs (75%). This value was not significantly different to the non-coated control. However, this was significantly lower than the P100 coating ($p \leq 0.01$).

The only coating which promoted a significant increase in proliferation in comparison with the non-coated control was C100 (composed of collagen only). The only alginate-based construct which performed similarly to the non-coated control, in terms of proliferation, is the A25 construct (composed of 25% alginate and 75% PPP). All other alginate-containing coatings resulted in significant decreases in cell proliferation in comparison with the non-coated control scaffold.

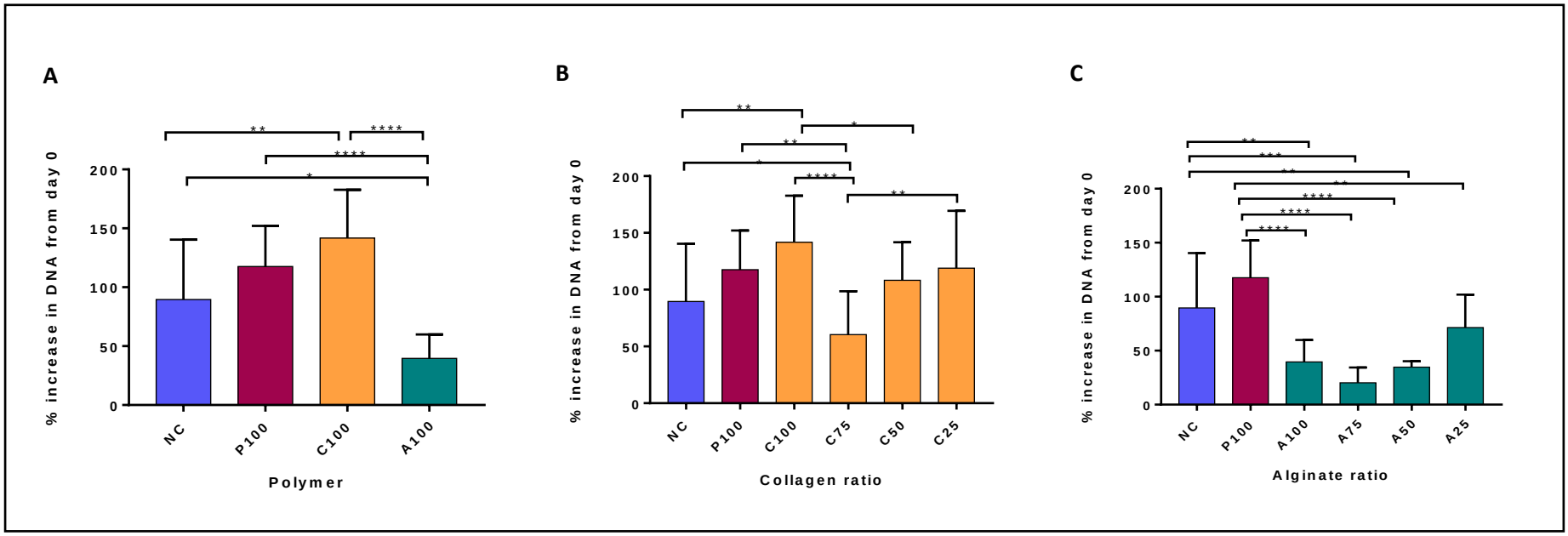

Figure 3.5 Cell proliferation within all 9 hybrid constructs over 15 days.

Comparison of the proliferation rate of bSCs in plasma, collagen or alginate coated constructs (A), varying ratios of collagen and plasma (B), and varying ratios of alginate and plasma. Data is presented as the percentage DNA increase from the day that seeding was completed (day 0), to the 15th day in culture. Bars represent the mean percentage DNA increase ± standard deviation (n=3). Statistical significance was determined using a one-way AVOVA. (P, C and A denote PPP, collagen and alginate respectively. The number signifies the proportion of the gel composed of that biopolymer in percentage. The remaining proportion is PPP (eg. C75 = 75% collagen, 25% plasma). NC = non-coated. * = $p \leq 0.05$, ** = $p \leq 0.01$, *** = $p \leq 0.001$, **** = $p \leq 0.0001$.

3.2.4 PPP and collagen promote cell infiltration throughout the hybrid construct

2 cm lengths of PET scaffold were dynamically seeded with 2 x10^5 cells before coating with each biopolymer mix to form the 9 different hybrid constructs (P100, C100, C75, C50, C25, A100, A75, A50 and A25), according to the methods in section 3.1. Non-coated seeded scaffolds were used as a control. The constructs were cultured to either 5 days or 15 days before being analysed using confocal microscopy to assess cell infiltration throughout each construct.

Confocal microscopy images of bSCs, cultured for 5 days within each construct, are shown in Figure 3.6. At this time point, all plasma/collagen based constructs (P100, C100, C75, C50, C25) promoted cell infiltration throughout the constructs, causing all intra-fibre voids to be completely filled with cells. In contrast, cells on non-coated scaffolds were confined to the PET fibres of the scaffold, preventing infiltration into the intra-fibre voids by 5 days. The voids can be seen as black rectangles within the images. These rectangular voids are also visible in the alginate based constructs (A100, A75, A50, A25), at day 5. Although not visible using confocal microscopy, these voids were filled with gel. This indicates that cells were unable to migrate through the alginate-based gels as readily as they were through the plasma/collagen based gels. Some migration into the voids is visible (red arrows), and appears to increase with decreasing alginate concentration in the gel (A25 shows greatest cell infiltration while A100 shows almost no cells infiltrating into the voids from the PET fibres).

Confocal microscopy images of constructs cultured for 15 days are shown in Figure 3.7. In contrast to the cell coverage seen at day 5, the intra-fibre voids (black rectangular areas) of the plasma/collagen based constructs (P100, C100, C75, C50, and C25) were clearly visible by day 15. This indicates that the gel which originally filled these voids was lost between day 5 and 15 of culture. Furthermore, the edges of the voids were brightly stained, possibly indicating that many cells retracted back to the edges of the voids as the gel was lost. Alginate-based constructs (A100, A75, A50 and A25) did not show visible signs of gel loss by day 15. Cell migration through A100, A75 and A50 constructs remained low at this time point. However, a number of cells were visible within voids of the A25 construct. Non-coated scaffolds showed some cells bridging the corners of the voids by 15 days, but the spaces remained largely unfilled.

These results indicate that PPP/collagen coatings greatly promote cell infiltration throughout the constructs, whereas alginate significantly impairs migration, apparently in a concentration dependent manner. The results also indicated that PPP/collagen gels have a relatively low durability, resulting in cells either retracting back to the edges of the intra-fibre voids, or being lost from the construct along with the gel. In contrast, gels containing alginate appeared to

remain on the scaffold, continuing to fill the intra-fibre voids throughout the 15 day culture period.

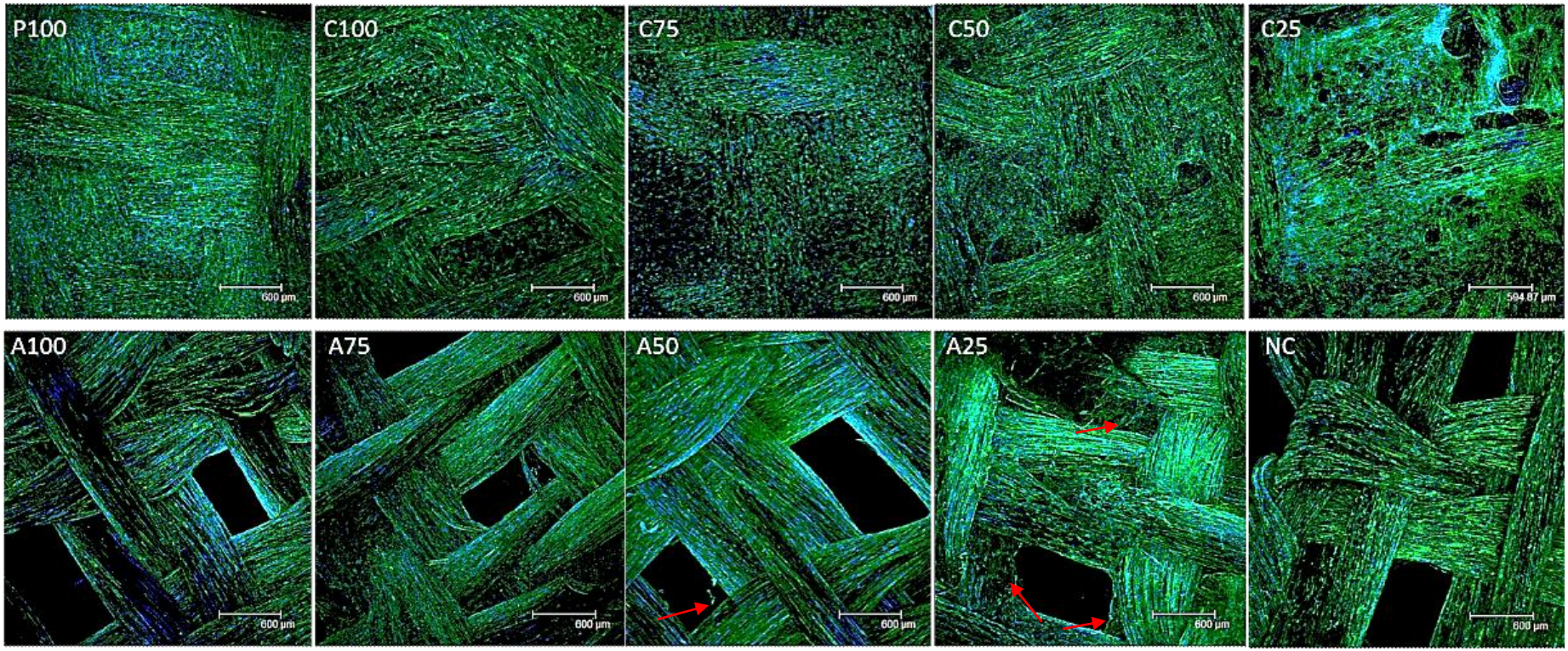

Figure 3.6 Confocal microscope images of cell seeded constructs after 5 days in culture.

Confocal microscopy of all constructs (P100, C100, C75, C50, C25, A100, A75, A50 and A25), plus the non-coated control, after 5 days in culture. Actin is stained with Alexa Fluor 488 phalloidin (green) and nuclei are stained with To-pro-3 (blue). C, A and P denote collagen, alginate and PPP respectively. The number signifies the proportion of the gel composed of that biopolymer in percentage. The remaining proportion is PPP (eg. C75 = 75% collagen, 25% PPP). NC = non-coated. Red arrows indicate areas of cell infiltration in alginate-based constructs. Scale bar = 600 µm

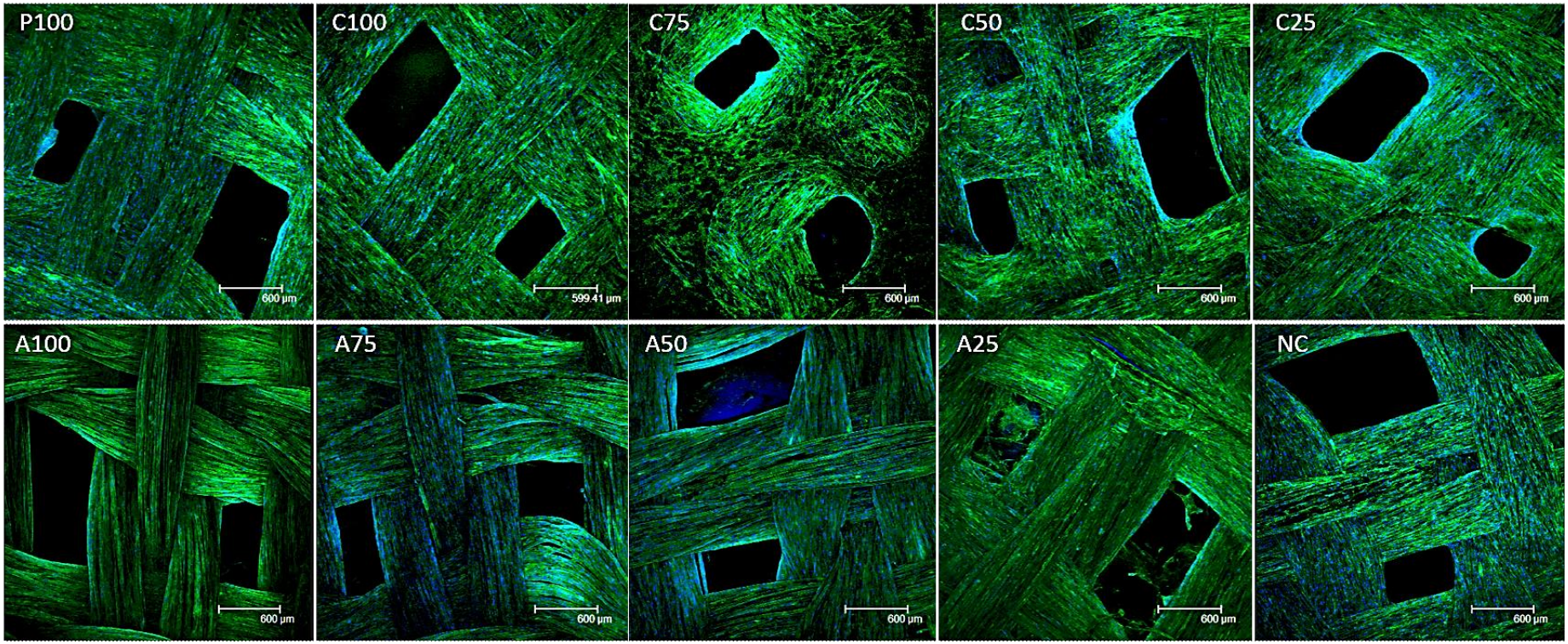

Figure 3.7 Confocal microscope images of cell seeded constructs after 15 days in culture.

Confocal microscopy of all constructs (P100, C100, C75, C50, C25, A100, A75, A50 and A25), plus the non-coated control, after 15 days in culture. Actin is stained with Alexa Fluor 488 phalloidin (green) and nuclei are stained with To-pro-3 (blue). Mag. 5x. C, A and P denote collagen, alginate and PPP respectively. The number signifies the proportion of the gel composed of that biopolymer in percentage. The remaining proportion is PPP (eg. C75 = 75% collagen, 25% PPP). NC = non-coated. Scale bar = 600 µm.

3.2.5 Alginate enhances the longevity of biopolymer coatings

It was evident that PPP and collagen gel coatings were being lost over time by observing the constructs using light microscopy. To determine the rate of gel loss of each polymer an assay was developed which used light microscopy to photograph and measure the reduction in filling of the intra-fibre voids of the PET scaffold. Light microscopy was used to measure the percentage filling of intra-fibre voids over 15 days in all hybrid constructs (P100, C100, C75, C50, C25, A100, A75, A50 and A25), according to the method described in section 3.1.3. ImageJ software was used to measure the percentage area of the intra-fibre voids filled with gel.

Figure 4.9 (A) shows the reduction of intra-fibre void filling by PPP/collagen coatings (C100, C75, C50, C25 and P100). C100 was the least stable of the gels, with just 55% of intra-fibre filling remaining by 15 days. Constructs coated with PPP only (P100) were the second least stable, with 78% of void filling remaining by 15 days. Interestingly, by combining PPP and collagen at different ratios to form C25, C50 and C75, the gel stability increased slightly with increasing collagen content, such that the percentage void filling was 82%, 86% and 87% respectively.

Figure 4.9 (B) shows the reduction of intra-fibre void filling by PPP/alginate coatings. All gels containing alginate showed a negligible loss of intra-fibre filling, even the A25 construct, of which alginate makes up just 25%. A100, A75, A50 and A25 gels maintained intra-void filling of 100%, 97%, 99% and 99% respectively. By combining PPP with alginate, the stability of the gel was significantly enhanced in comparison with PPP alone, which had a void filling of 78% by 15 days.

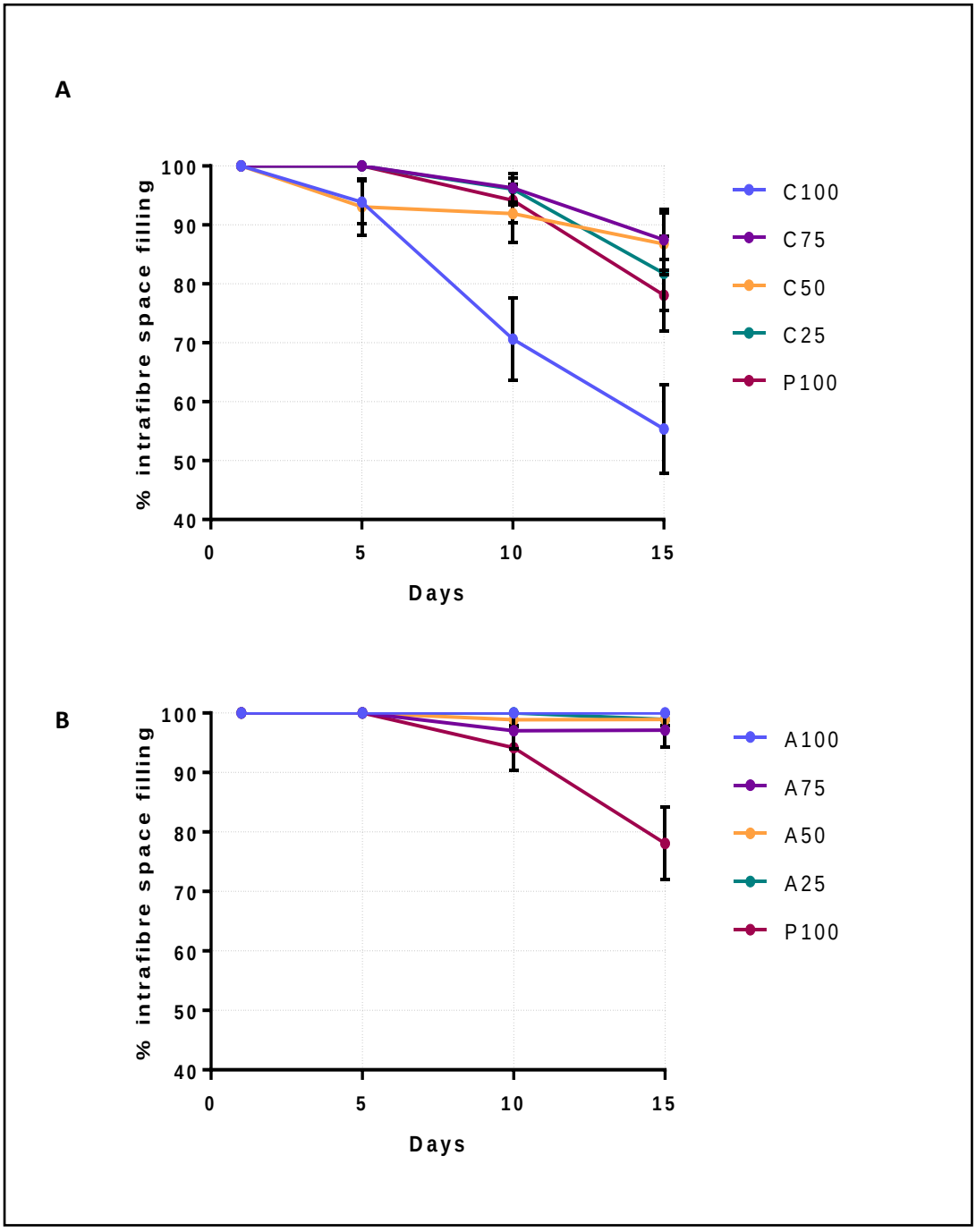

Figure 3.8 Gel loss profiles for all 9 coatings over 15 days.

Reduction in intra-fibre void filling over 15 days using cell seeded constructs coated with collagen/PPP coatings (C100, C75, C50, C25, P100) (A) and alginate/PPP coatings (A100, A75, A50, A25, P100) (B). P, C and A denote PPP, collagen and alginate respectively. The number indicates the proportion of the coating composed of that biopolymer in percentage. The remaining proportion is PPP (eg. C75 = 75% collagen, 25% PPP). Values represent the mean ± standard deviation (n=3).

3.2.6 P100, C50 and A25 coatings were selected for further study

As mentioned at the start of this chapter, the studies conducted here were designed to select 3 hybrid constructs for further investigation based on the performance of all 9 constructs in terms of gel longevity and cell proliferation. Results from sections 3.2.2.1 and 3.2.3 were combined such that cell proliferation and coating longevity values were displayed on one graph (see figure 3.8). Using this graph, 3 coatings were brought forward for further investigation.

It was decided that P100 would be brought forward for further testing as this is also representative of platelet rich plasma, which is a popular choice of material for enhancing graft performance. In addition, the best performing candidates from the collagen and alginate coatings were selected. Although C100 supported a high proliferation rate, this coating was the least stable of all. C75 was the most durable of the collagen-based coatings, but induced a significantly lower proliferation rate than the non-coated control ($p \leq 0.05$). C25 and C50 induced similar levels of proliferation (122% and 112% increase in DNA content respectively). These constructs also had similar stabilities (82% and 86% intra-fibre void filling by 15 days respectively). Based on the slightly improved stability (not significant), C50 was selected as the most promising collagen-based coating.

Selection of the most promising alginate-based coating was much simpler than the collagen coating. This is because all alginate coatings had very similar durabilities, with a negligible visible loss of gel by 15 days. In contrast, cell proliferation rate did vary between alginate constructs. The A25 construct induced the greatest proliferation rate (75% increase in DNA content by 15 days), and evidence of superior cell infiltration within this construct, demonstrated by confocal microscopy (section 3.2.2.2), led to A25 being selected as the most promising alginate-based coating.

P100, C50 and A25 coated hybrid constructs were therefore brought forward for further in the next phase of this project, in which the application of cyclic tensile strain to these constructs was also introduced.

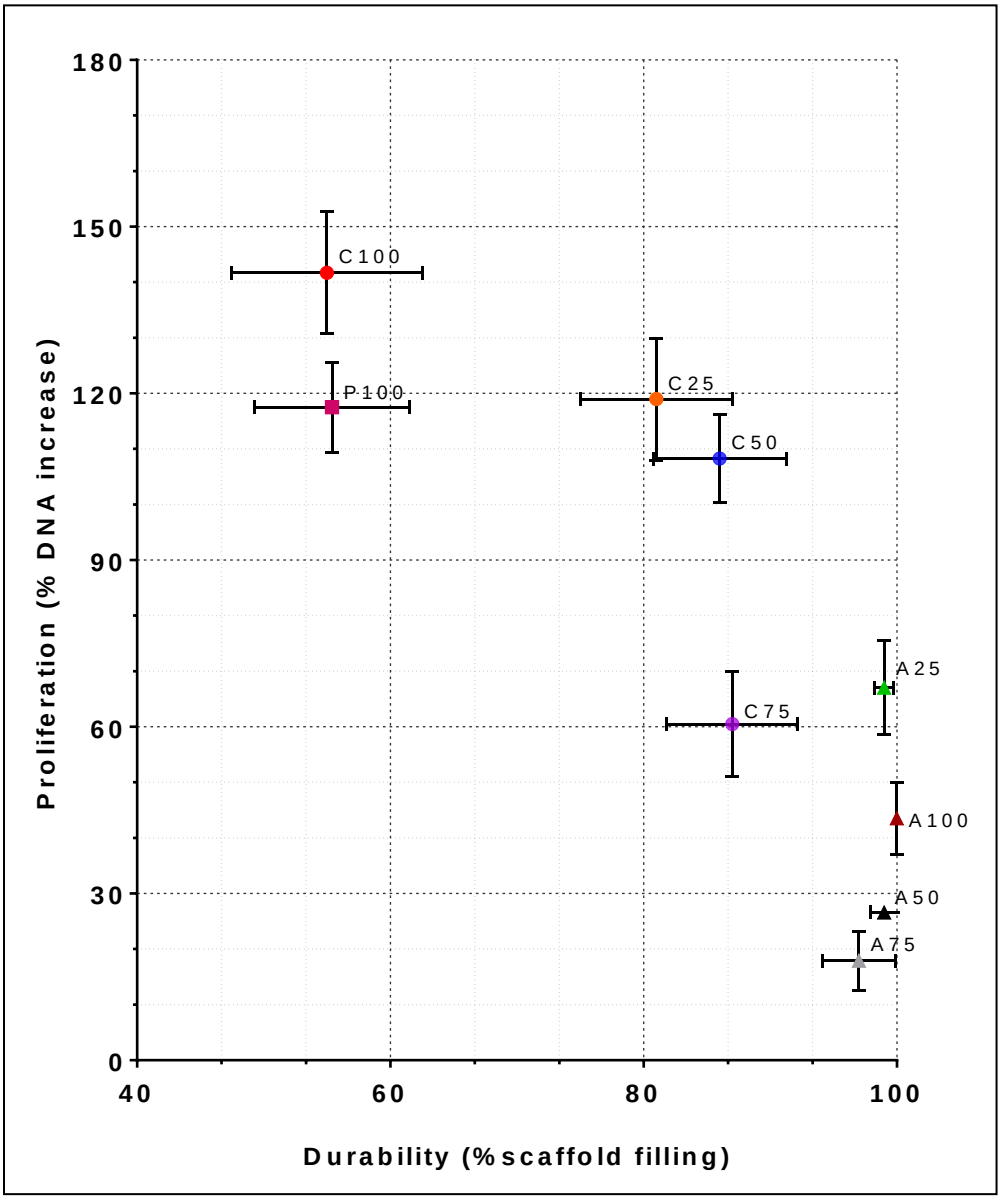

Figure 3.9 Proliferation versus durability of all 9 hybrid coatings.

Proliferation (y axis) and durability (x axis) data combined for comparisons of the overall performance of each coating (the closer the point is to the top right hand corner of the graph, the more desirable the properties of that coating). Data points represent the mean ± standard deviation.

3.3 Discussion

A total of 9 formulations of hybrid construct coated with varying ratios of PPP, collagen and alginate were compared with the non-coted Xiros PET scaffold, during this phase of the construct selection process. The coating procedures developed to fabricate each construct were found to create a uniform polymer coating which filled all intra-fibre spaces within the PET scaffold. PPP, collagen and alginate were all found to form a satisfactory coating over the scaffold (see Figure 3.4). This phase of the project was designed to narrow down the candidates by assessing cell proliferation and infiltration within each construct, and by comparing the durability of each coating so that the 3 most promising candidates could be brought forward for further assessment.

In order to enhance tissue induction on the Xiros ligament, cell proliferation should be increased, so that the cells quickly fill the construct before starting to synthesise an ECM which will eventually surround and protect the scaffold from abrasive forces. Proliferation of bSCs in each of the 9 constructs was assessed after 15 days in culture. By coating the scaffold with combinations of PPP and collagen, the rate of proliferation remained similar to the non-coated control. In contrast, coating the scaffold with coatings containing alginate significantly reduced cell proliferation in all but the A25 coating (see Figure 3.5). The concentration of alginate gels has been previously demonstrated to have a significant effect on cell proliferation when used as a cell substrate (Barralet *et al*., 2005). The proliferation rate of rat bone marrow cells was found to negatively correlate with alginate concentration, such that cells seeded on 3% alginate gels proliferated significantly faster (600% increase in cell number by day 12) than those on 10% alginate gels (cell number decreased over 12 days). The alginate coatings used in this project were made from 2% alginate, which would suggest that these gels should induce an even greater proliferation response. However, in the current study, cells were covered with alginate after seeding of the PET scaffold, whereas in the study by Barralet *et al*. (2005), cells were seeded on top of the alginate gels. It is likely that by encapsulating the cells with alginate in this way, proliferation is greatly reduced. This may be reflective of reduced access to nutrients from the media.

A study by Banerjee *et al.* (2009) also investigated the proliferation rate of cells encapsulated in alginate gels of different concentration. Again, they found that lower alginate concentration promoted greater neural stem cell proliferation. However, the alginate concentrations used in this study were much lower than the Barralet *et al.* (2005) study, with concentrations ranging from 0.25% to 1%. Encapsulation in the 0.25% gel resulted in a 1750% increase in cell number over 7 days, whereas the 1% gel induced a cellular increase of just 250%. By coating the Xiros PET ligament with a 2% alginate gel (A100 coated construct) in the current project, the cell

number increased by just 42% over 15 days. It is possible that using a lower percentage alginate gel may improve cell proliferation. Indeed, by replacing 75% of the coting with plasma, to form the A25 coated construct, cell proliferation was increased. Assuming the plasma and alginate solution were able to mix such that there was a homogenous distribution of each biopolymer throughout the scaffold, this would have resulted in an alginate matrix with a quarter of the density of the A100 coating.

By combining a 5 mg/ml collagen type I solution with plasma to produce the C50 (50% collagen, 50% plasma) and C25 (25% collagen, 75% plasma) coatings, cell proliferation in these constructs remained similar to the 100% plasma (P100) and 100% collagen (C100) coated constructs. This is consistent with work by Cummings *et al*. (2004), which found there to be no significant difference in the proliferation rate of rat smooth muscle aortic cells cultured in matrices composed of collagen, fibrin or a 50:50 ratio of collagen-fibrin. The only collagen-based coating which did demonstrate a reduction in proliferation in comparison with the C100 and P100 coatings was the C75 coating (75% collagen, 25% plasma). Repetition of this study may be necessary to confirm this result, although Rowe *et al*. (2006) also compared the proliferation of smooth muscle cells seeded in collagen/fibrin gels of varying ratios. Their study found that gels composed of 0.5 mg/ml collagen type I and 0.5 mg/ml fibrin induced significantly greater proliferation than all other gel ratios tested. Although this cannot be directly compared with ratios used in the present study, it does indicate that collagen and fibrin polymers may interact in a way which does not produce a readily predictable trend. The authors concluded that more understanding was required on how collagen and fibrin fibres interact with each other, and cellular components, to reveal the link between structure and function of these gels.

Confocal microscopy was used to assess cell infiltration within each of the 9 coated constructs. The presence of alginate within the coatings appeared to hinder movement of cells into the gel filling the intra-fibre voids (see figure 3.7). With the lowest alginate proportion, A25 constructs allowed some cellular movement, with bSCs visibly filling the intra-fibre voids by day 15 of culture. The inhibitory effect of alginate on fibroblast motility has previously been demonstrated (Doyle *et al.*, 1996). Fibroblasts cultured in alginate beads demonstrated significantly reduced motility with all alginate concentrations tested. Interestingly, keratinocyte motility was not inhibited by alginate.

In contrast, bSCs infiltrated quickly through PPP/collagen coatings, achieving total void filling within 5 days (see Figure 3.6). The ability of cells to readily migrate through collagen (Vernon and Sage, 1999) and fibrin (Brown *et al*., 1993) gels has previously been reported. However, due to a loss of collagen and PPP coatings over time, the voids became exposed and

cells would have either retracted back to the edges of the voids by the end of the 15 days, or would have been lost along with the coating. To establish whether coating loss results in the loss of cells from the construct, the DNA content of the media surrounding each construct could be measured.

The biopolymer coatings used in this study were found to bridge the intra-fibre voids of the PET scaffold, thereby allowing cells to fill the scaffold more quickly than when the coating was absent (this was particularly true of PPP/collagen coatings). Although a hybrid construct may be able to initially improve cell infiltration, if the coating is lost before cells have had sufficient time to synthesise an extracellular matrix, then there will likely be no improvement in the rate of tissue induction. The inclusion of alginate significantly improved the durability of the coating, with no visual loss of intra-fibre filling over 15 days in all alginate constructs (see Figure 3.8 B). No significant improvements in construct durability was measured by combining PPP with collagen (Figure 3.8 A).

By comparing the degradation of bSC seeded and non-seeded constructs, it was clear that the cells were responsible for the significant gel loss seen in PPP and collagen coated constructs (data not shown). Since alginate is of plant origin, it is unsurprising that mammalian cells do not express enzymes capable of digesting this hydrogel (Andersen *et al.,* 2014). Fibroblasts are, however, able to secrete enzymes capable of digesting both fibrin and collagen. Fibroblasts express matrix metalloprotease-1 (MMP-1), which is a collagenase that breaks down collagen type-I (Raif, 2008). They also express tissue-type plasminogen activator (tPA), which converts the serine protease, plasminogen, to its active form, plasmin, which in turn breaks down fibrin (Saed and Diamond, 2003). Fibrin breakdown has been successfully inhibited in culture by addition of ϵ-aminocaproic acid to the media (Grassl *et al*., 2002), and this is something that could be considered for future *in vitro* work. Similarly, the addition of tissue inhibitor of metalloproteases (TIMPs) in culture media may enhance the longevity of collagen within coatings (Ellis *et al*., 1994).

Alginate gels have been used extensively in cell encapsulation research, in which the aim is to immobilize cells within the matrix (Blombäck *et al.,* 1994). It is perhaps unsurprising that addition of a material so effective in trapping cells will substantially inhibit their infiltration and ability to proliferate. Nevertheless, by combining plasma with alginate, the longevity of the construct coating was significantly enhanced, and an intact coating is crucial for maintaining complete filling of the construct with cells. Without a coating, the cells will eventually fill the voids of the scaffold, by gradually bridging around the edges of the voids, but this has been found to take over 5 weeks (Raif and Seedhom, 2005). If cells are able to fill the entire construct within the first few days of invasion, it may promote the deposition of

a more uniform ECM throughout the whole construct, and promote differentiation at an earlier time point, since cells will reach confluency before committing to a differentiation lineage (Ruijtenberg and Van den Heuvel, 2016).

3.4 Summary

Based on their performance in this phase of the study, one collagen-based coating and one alginate-based coating were selected for further testing, alongside 100% PPP. C50, composed of a 50:50 ratio of collagen to PPP was selected from the collagen-based constructs. C50 and C25 showed similar levels of performance in both the proliferation and durability tests. Due to C50's marginally superior durability (not significant), this coating was brought forward for further testing.

Selection of the most promising alginate-based coating was much simpler. There was very little variation in durability between these constructs, and all of them outperformed collagen and PPP constructs in this context. By considering proliferation and cell infiltration only, A25 was clearly the better candidate (see section 3.2.4), and was therefore selected for further investigation, along with C50 and P100 coatings, in Chapter 4.

Chapter 4

Further assessment of P100, C50 and A25 coatings

Following the selection of the 3 coatings brought forward for further study, additional tests were conducted with a view to selecting a final coating which could be assessed as a platelet-rich construct. The effect of each coating on cell viability and expression of ligament and non-ligament associated genes was assessed, as well as the release of growth factors and physical characterisation of each coating. The 3 coated constructs were also subjected to cyclic tensile strain of 5% at a frequency of 1 Hz, for 1 hour per day and the effect of this on cell proliferation and gene expression was quantified.

Aim:

To carry out further tests on P100, C50 and A25 coated constructs in order to select a single, most promising coating for enhancement of the Xiros PET scaffold and subsequent tests as a platelet-rich construct.

Objectives:

- Assessment of cell viability within P100, C50 and A25 coated constructs.
- Comparison of PDGF and IGF-1 release profiles from P100, C50 and A25 coated constructs.
- Visual comparison of the gel matrices of P100, C50 and A25 coatings using scanning electron microscopy.
- Comparison of the physical properties of P100, C50 and A25 coatings.
- Assessment of the effect of each P100, C50 and A25 coatings on the expression on ligament and non-ligament associated genes (*COL1A1*, *COL3A1*, *TN-C*, *SCXAB* and *RUNX2*).
- Quantification of the effect of cyclic tensile strain of 5% at a frequency of 1 Hz on cell proliferation, infiltration and expression of ligament and non-ligament associated genes, within each construct.
- Selection of a final coating for additional testing as a platelet-rich construct.

4.1 Materials and methods

This section describes the methods used to assess each of the three coated constructs (P100, C50 and A25) in order to select a final construct for assessment as a platelet-rich construct. As such, all investigations detailed here were carried out using platelet-poor plasma (PPP), rather than platelet-rich plasma (PRP), and all constructs were supplemented with FBS, similarly to the previous chapter. As previously stated, this was to ensure that cellular responses to coatings could be evaluated based on their physical composition and were not obscured by any variations in growth factor supply.

4.1.1 Assessment of cell viability within P100, C50 and A25 coated constructs

To assess the effect of each coating (P100, C50 and A25) on cell viability, a LIVE/DEAD assay was performed. 20 mm scaffolds were dynamically seeded for 48 hours with 2×10^5 bSCs according to the method described in section 3.1.2. Cell-seeded scaffolds were coated (see section 3.1.1.3) using P100 (100% PPP), C50 (50% collagen) and A25 (25% alginate) formulations only (Table 2). Three hybrid constructs were fabricated per coating group, and three non-coated cell-seeded scaffolds were used as controls. All constructs were transferred to 3.8 cm^2 wells of a 12-well plate, which were pre-coated with 1% agarose to prevent cells from attaching to the bottom of the plate. The constructs were covered with 1 ml of DMEM supplemented with 10% (v/v) FBS and placed in a humidified atmosphere incubator containing 5% (v/v) CO_2 and 95% (v/v) air at 37˚C. Constructs were cultured for 15 days according to the method in section 3.1.4.

A LIVE/DEAD™ Viability/Cytotoxicity Kit, for mammalian cells (Invitrogen) was used to assess the viability of bSCs in each of the three hybrid constructs in comparison with the non-coated construct. Upon completion of the 15 day culture period, coated and non-coated constructs were washed three times in PBS before being incubated in 1 ml of a solution of 2 µM calcein-AM (Invitrogen) and 4 µM ethidium homodimer-1 (Invitrogen), for 30 minutes. The constructs were imaged on the day of staining using a Leica TCS SP2 confocal laser scanning microscope. Z stacks were generated for qualitative comparisons between constructs using a 20 X objective lens.

4.1.2 Analysis of PDGF-AB and IGF-1 release from platelet-rich coatings

To determine the growth factor release profile for the hybrid constructs, an enzyme-linked immunosorbent assay was used (ELISA). Platelet-rich coatings were used in this study as the growth factors which were to be quantified are contained within platelets and are released

upon activation. The use of platelet-poor plasma may result in the release of growth factors below detectable levels. Non-seeded PET scaffolds were coated and PDGF-AB and IGF-1 concentrations were measured in the media at 1, 2, 4, 8, 16, 72, 120, and 216 hours.

4.1.2.1 Preparation of non-seeded platelet-rich coated scaffolds

PRP, PPP, collagen and alginate were combined as shown in Table 3 to produce platelet-rich constructs of P100 (50% PRP, 50% PPP), C50 (50% collagen, 50% PRP) and A25 (25% alginate, 25% PPP, 50% PRP). PRP was added to each coating mixture such that it comprised 50% of the total volume. 200 µl of each mixture was pipetted onto 20 mm lengths of PET scaffold, which had not been seeded with cells. The mixtures were prepared and activated according to the methods previously described in section 3.1.3.1. Three coated scaffolds were used for each coating group.

Table 3 Ratios of components used to create platelet-rich coatings for the quantification of growth factor release.

Coating	PRP (%)	PPP (%)	Collagen (%)	Alginate (%)
P100	50	50	0	0
C50	50	0	50	0
A25	50	25	0	25

The coating solutions were allowed to polymerise at 37˚C for 1 hour. Immediately following this, the constructs were covered with 1ml of serum-free DMEM and incubated at room temperature for 2 minutes. The total media volume was then harvested and frozen at -80˚C. This first harvest is descried as the 1 hour harvest. The constructs were covered with 1ml of fresh serum-free DMEM, and harvesting was repeated in the same way for all time points.

4.1.2.2 Detection of PDGF-AB and IGF-1 using an enzyme-linked immunosorbent assay

The concentration of IGF-1 and PDGF-AB released into the media surrounding the hybrid constructs was measured using a sandwich Enzyme-linked immunosorbent assay (ELISA) purchased from R&D Systems as a DuoSet ELISA kit.

4.1.2.2.1 ELISA assay principle

This assay uses a 96-well microplate pre-coated with a capture antibody specific to the molecule of interest. After blocking (with either a protein-rich solution or a detergent) and washing to prevent non-specific binding, the plate is incubated with the samples and standards, allowing the analyte to be 'captured' by binding to the antibody coating the plate. A detection antibody is then added, which binds to any analytes bound to the capture antibody. Streptavidin-horseradish peroxidase (Strep-HRP) is used to bind to the detection antibody. This conjugated enzyme catalyses a blue colour change upon addition of tetramethylbenzidine (TMB). The colour change is proportional to the amount of bound analyte. Sulphuric acid is then added to stop the reaction and the colour change is quantified by determining the absorbance of each well measured at 450 nm.

4.1.2.2.2 ELISA experimental procedure

Non-treated 96-well microplates were coated with 100 µl of 4 µg/ml IGF-1 or PDGF-AB capture antibody in PBS. The plate was incubated at room temperature overnight before being washed 3 times with 0.05% Tween 20 in PBS. Any remaining liquid was removed by inverting the plate and gently tapping on a paper towel. IGF-1 plates were blocked with 200 µl of 5% Tween 20 in PBS, and PDGF-AB plates were blocked with the same volume of 5% bovine serum albumin (BSA) in PBS. The plate was incubated with the blocking solution for 1 hour at room temperature before washing the plate as previously described. Six IGF-1/PDGF-AB standards were added to plates in triplicate using the recombinant growth factor provided in the kit. The six standards were prepared in serum-free DMEM and were generated by performing a 2-fold serial dilution with IGF-1 and PDGF-AB top standards of 2000 pg/ml and 1000 pg/ml respectively. Serum-free DMEM was used to produce blank wells. Samples were diluted at a 1:1 ratio in PBS and were also run in triplicate. 100 µl of standards and samples were added to wells and the plate was incubated for 2 hours at room temperature. The plate was washed as previously described before adding the detection antibody. IGF-1 detection antibody was diluted to a concentration of 150 ng/ml with 5% Tween 20 in PBS. PDGF-AB detection antibody was diluted to a concentration of 50 ng/ml with 5% BSA in PBS. 100 µl of the corresponding detection antibody was added to wells and incubated for 2 hours at room temperature. The plate was washed again as previously described before adding 100 µl of Strep-HRP. Before use, Strep-HRP was diluted to the working concentration specified on the

vial label using 5% Tween 20 or 5% BSA in PBS for the IGF-1 or PDGF-AB assays respectively. The plate was incubated for 20 minutes at room temperature before being washed as previously described. 100 µl of TMB was then added and was left to incubate at room temperature until a clearly visible gradient could be seen from the highest to the lowest standard. This generally required approximately 5 minutes. 50 µl of sulphuric acid stop solution was then added to stop the reaction. The absorbance was immediately measured at 450 nm using a Varioskan Flash plate reader (Thermo Fisher Scientific).

A standard curve was generated by plotting the concentration of each standard against its measured absorbance using Microsoft Excel software. The equation of the line was used to convert the absorbance of each sample to a concentration. The concentrations calculated for each time point were plotted as cumulative data, such that it represented the total growth factor release over time. The values were normalised to the platelet count using the following equation:

$$n = m - \left(\left(\frac{pv}{r + pv}\right) \times m\right)$$

Where n is the normalised growth factor concentration, m is the measured growth factor concentration in ng/ml, p is the platelet concentration in PPP (platelets/µl), v is the volume of PPP in the construct and r is the number of platelets in 100 µl of PRP (ie. $2x10^8$).

4.1.3 Physical characterisation of biopolymer coatings

This section describes methods used to characterise the physical structure and properties of the P100 (100% PPP), C50 (50% collagen) and A25 (25% alginate) biopolymers. For scanning electron microscopy, gels were analysed as coatings on the PET scaffold. For rheological assessment, gels were formed into disks and were not combined with scaffolds.

4.1.3.1 Analysis of coatings using Scanning electron microscopy (SEM)

20 mm scaffolds (without cells) were coated as described in section 3.1.3. Samples were prepared for scanning electron microscopy analysis by fixing in 10% NBF for 20 minutes, followed by dehydration in increasing ethanol concentrations from 30% to 100% (30, 50, 70, 90, 100% (v/v)), for 30 minutes each. The samples were then desiccated in a vacuum desiccator overnight before mounting on metal stubs using adhesive carbon discs. The samples were sputter coated with gold for 30 seconds at 40 mA, in an argon atmosphere. The structure of the gels was observed using a Hitachi S-3400N scanning electron microscope.

4.1.3.2 Rheological characterisation of coating biopolymers

Rheology was used to investigate the mechanical properties of the biopolymers. PPP, collagen and alginate are all hydrogels as they consist of polymer matrices which hold water. Rheology is commonly employed for the measurement of fluids and hydrogels, and was therefore utilised for characterisation of the coatings used in this project.

Rheology studies the flow and deformation of matter. The material of interest is sandwiched between two metal plates and the top plate oscillates with variable force. The shear stress applied is defined as the force per unit surface area of the sample. A position sensor in the lower plate senses displacement of the material and records the shear strain, which is defined as the deformation per unit height. The machine calculates the change in strain over time to give the shear rate. Using the sheer rate and the sheer stress applied by the rheometer, the viscosity of the material can be calculated. These relationships are shown in the following equations:

$$\tau = \frac{F}{A}$$

Where τ is the shear stress (Pa), F is the force (N) and A is the shear area (m^2).

$$\gamma = \frac{s}{h}$$

Where γ is the shear strain, s is the deflection path (m), and h is the shear gap (m).

$$\dot{\gamma} = \frac{v}{h}$$

Where $\dot{\gamma}$ is the shear rate (s^{-1}), v is the velocity (ms^{-1}), and h is the gap (m).

$$\mu = \frac{\tau}{\dot{\gamma}}$$

Where μ is the viscosity (P), τ is the shear stress (Pa), and $\dot{\gamma}$ is the shear rate (s^{-1}).

By plotting the input stress along with the resultant strain, the phase angle (δ) can be calculated (Figure 4.1). Purely elastic materials with solid-like behaviour, which do not displace under

stress, will have stress and strain curves which are exactly in phase and therefore have a phase angle of zero. Purely viscous materials with liquid-like behaviour, which do displace under stress, have stress and strain curves which are out of phase by ¼ of a cycle and therefore have a phase angle of 90˚.

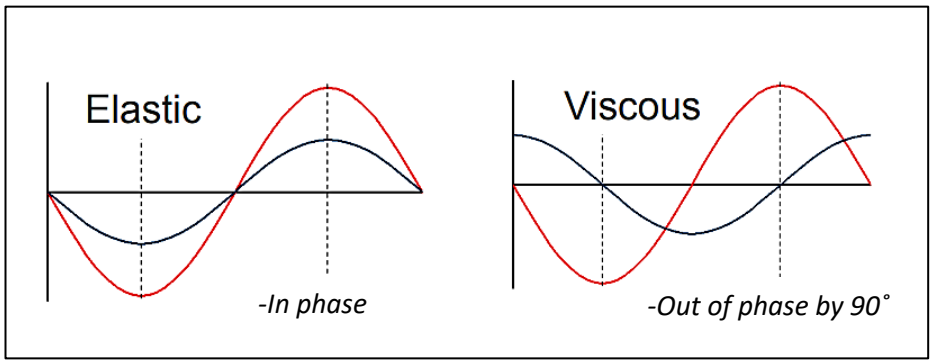

Figure 4.1 Example stress and strain profiles for elastic and viscous materials.
The image shows stress and strain curves which are in phase, representing a purely elastic material, and out of phase by 90˚, representing a purely viscous material.

In rheology studies, the stress and strain are used to calculate what is known as the complex modulus *G**. The higher the *G**, the greater the stiffness of the material. The complex modulus *G** can be split into storage (elastic) modulus *G'* which represents the ability of the material to store energy, and the loss (viscous) modulus *G''* which represents the ability of the material to dissipate energy in the form of heat loss. These values are calculated using the equations below:

$$Storage\ modulus\ G'(Pa) = \frac{stress}{strain} \times Sin\ \text{(phase angle)}$$

$$Loss\ modulus\ G''(Pa) = \frac{stress}{strain} \times Cos\ \text{(phase angle)}$$

In general, materials with a G'>G'' and a phase angle of <45˚ behave like solids. Materials with a G'<G'' and a phase angle of >45˚ behave as liquids. Rheology was used in this study to determine any differences in the mechanical properties of hydrogels P100 (100% PPP), C50 (50% collagen) and A25 (25% alginate).

Samples were tested post-gelation on an Anton Parr MACR 302 rheometer in the form of discs with a diameter of 60 mm and a depth of approximately 3 mm. The plates of the rheometer were pre-heated to 37˚C before addition of the sample, to represent the temperature during culture. The test geometry (measuring cone CP50-1 with a diameter of 50 mm and an angle of 1˚) was lowered to form a gap of 0.4 mm, and the excess sample was trimmed accordingly.

The first test carried out on the samples was an amplitude sweep to determine the linear viscoelastic region (LVER). This involved applying an increasing shear strain to the sample and plotting the resulting strain along with the Storage G' and Loss G'' moduli. The limit of the LVER is the point at which the material starts to break down, and this can be determined by noting the point at which the G' profile loses its linearity. G' represents how much energy is being stored by the material as stress is being applied. Once enough stress is applied to break the suspension of the material, G' starts to decrease. The longer the LVER the more stable the material.

The second test carried out was a frequency sweep. This involved applying shear stress to the sample such that the strain was kept at a constant, pre-set value. This value fell within the LVER for all samples. The angular frequency (ω) of the geometry was increased and G' and G'' were plotted against angular frequency. This test is used to categorise materials into one of three general behaviours based on their frequency sweep profile. In general a viscoelastic solid is characterised by an increasing G'' but a fairly constant G', with increasing frequency. Viscoelastic liquids display an increasing G' with increasing frequency, with a constant G''. Gel-like materials display little change in either G' or G'' with increasing frequency.

4.1.4 Application of cyclic tensile strain to bSC-seeded hybrid constructs

In order to determine how the hybrid constructs would respond to the forces associated with joint movement, the constructs were placed in a bioreactor, which was developed in house to mimic the tensile strain acting on the ACL during locomotion (Raif *et al.*, 2007). The bioreactor and its setup are described in greater detail in section 4.1.4.2.

4.1.4.1 Fabrication of P100, C50 and A25 coated constructs for use with the cyclic strain bioreactor

For use with the cyclic strain bioreactor, PET scaffolds were cut to 350 mm before seeding to ensure the constructs were long enough to easily span the distance between the clamps. Scaffolds were dynamically seeded with 3 x 10^5 bSCs (at passage 3) for 48 hours (see section 3.1.1.2) and coated with P100 (100% PPP), C50 (50% collagen) and A25 (25% alginate) biopolymer combinations, as described in section 3.1.3. The day after coating, the hybrid

constructs were attached to the stainless steel clamps, which are responsible for transferring cyclic tensile strain to the constructs. Three of each hybrid cell-seeded construct were attached to clamps, as well as three cell-seeded non-coated control scaffolds. Loading began 3 days after clamping (see section 4.1.4.2) to allow the cells to settle and spread throughout the construct. The same number of coated and non-coated cell-seeded constructs were maintained under non-loaded conditions (with no forces applied) in 9.5 cm^2 wells of a 6-well plate, pre-coated with 1% agarose. Both non-loaded (not clamped) and loaded (clamped) constructs were covered with 3.5 ml of DMEM supplemented with 10% (v/v) FBS, which was replaced every 3 days.

4.1.4.2 Bioreactor setup and construct loading

Cyclic tensile strain was applied to constructs using unique apparatus, designed and manufactured in house, as described elsewhere (Raif *et al*., 2007). Briefly, the apparatus is composed of a camshaft powered by an external motor, via a flexible drive shaft. This allows application of uniform cyclic tensile strain to a maximum of 8 test stations within the range of 0.5%-5% at a frequency of 1 Hz.

The constructs were held between two stainless steel clamps (see Figure 4.2; B) contained in a glass chambered culture well (Lab-Tek), which was filled with 3.5 ml of DMEM supplemented with 10% (v/v) FBS. The plastic lid of the chamber was modified by cutting 2 rectangular holes so that the clamps protruded out of the chamber (see Figure 4.2; C). The space surrounding each clamp is sealed using a wide rectangular stainless steel ring positioned on top of the lid, and a subsequent rectangular rubber ring placed on top of the first ring (see Figure 4.2; A and C). This 2 ring system was designed to reduce the risk of contamination. The chamber is held in a metal carriage which has a viewing window in its base to enable observation of the constructs by inverted light microscopy, throughout the culture period. The carriage is composed of 2 parts so that it can extend and contract in order to apply the forces to the construct (see Figure 4.2; D). The construct was secured in the carriage via 2 clamp holders which attach to the ends of each clamp. The test station is then bolted onto the apparatus such that one clamp is secured to the base plate, whilst the other is left free to move (see Figure 4.2; E). The free clamp is attached to a loading rod which is associated with the camshaft via a cam follower. A loading spring surrounds the rod, which is compressed between one of the bearing blocks and a ring firmly attached to the rod (see Figure 4.3). By varying the compression of the spring, the percentage strain on the constructs can be altered. The relationship between spring compression and construct strain was previously measured using a displacement transducer (Raif *et al.,* 2007).

The chambers housing the scaffolds were filled with 3.5 ml of media. Cyclic tensile strain was applied to constructs every day for 1 hour, with a percentage strain of 5%, at a frequency of 1 Hz. All tensile strain experiments included an equal number of non-loaded controls for each construct type. Non-loaded controls were placed in 9.5 cm^2 wells of a 6-well plate, which were pre-coated with 2% agarose to prevent cell attachment. These constructs remained unloaded throughout the duration of the experiment and were covered with 3.5 ml of media.

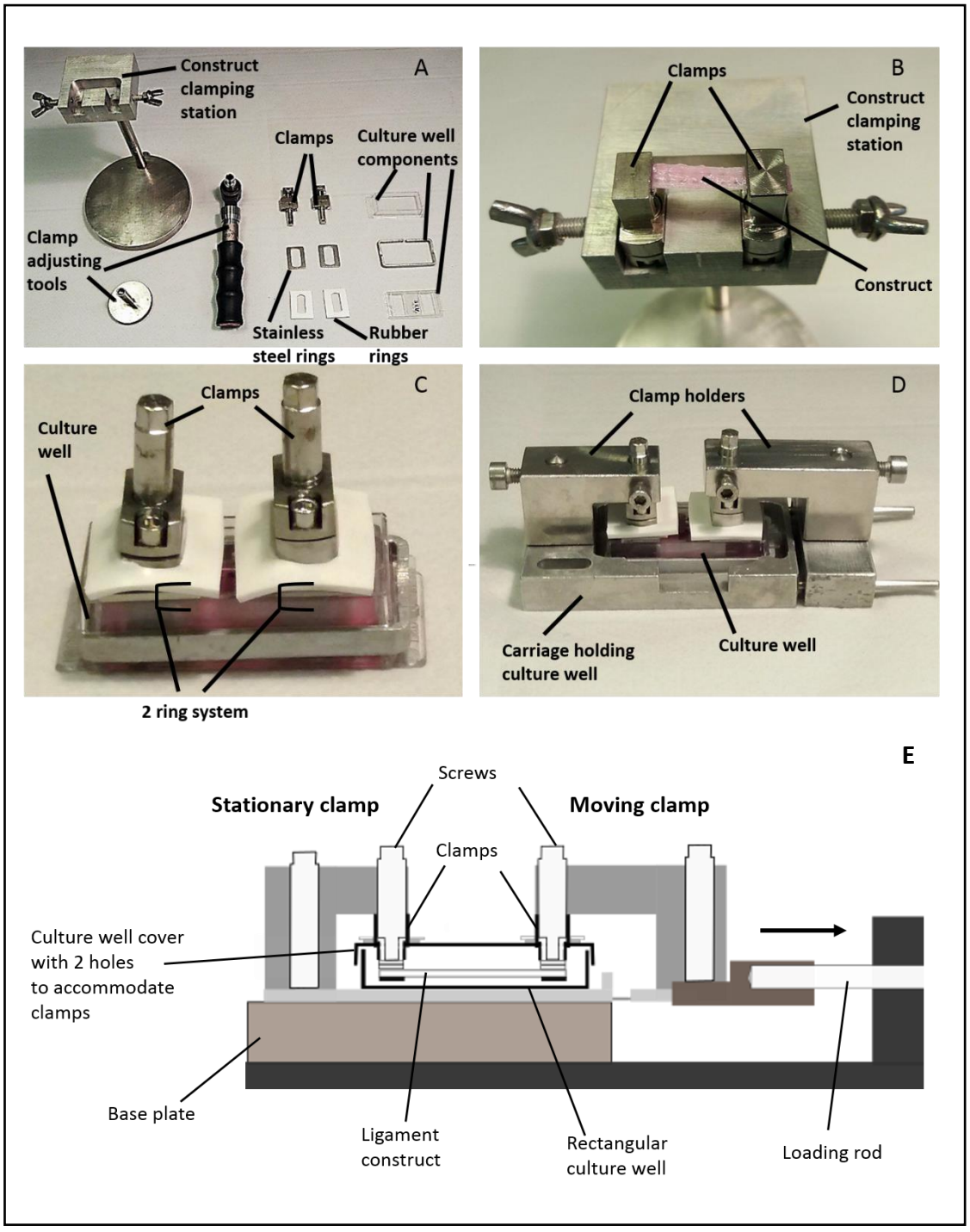

Figure 4.2 The assembly of the components used to build a cyclic tensile strain test station.

A) The individual components and tools required to assemble the culture well.
B) A clamped construct being assembled in the clamping station.
C) An assembled culture well with the clamps protruding.
D) The culture well enclosed in a carriage with clamp holders attached.
E) Schematic diagram showing a vertical cross-section through a test station.

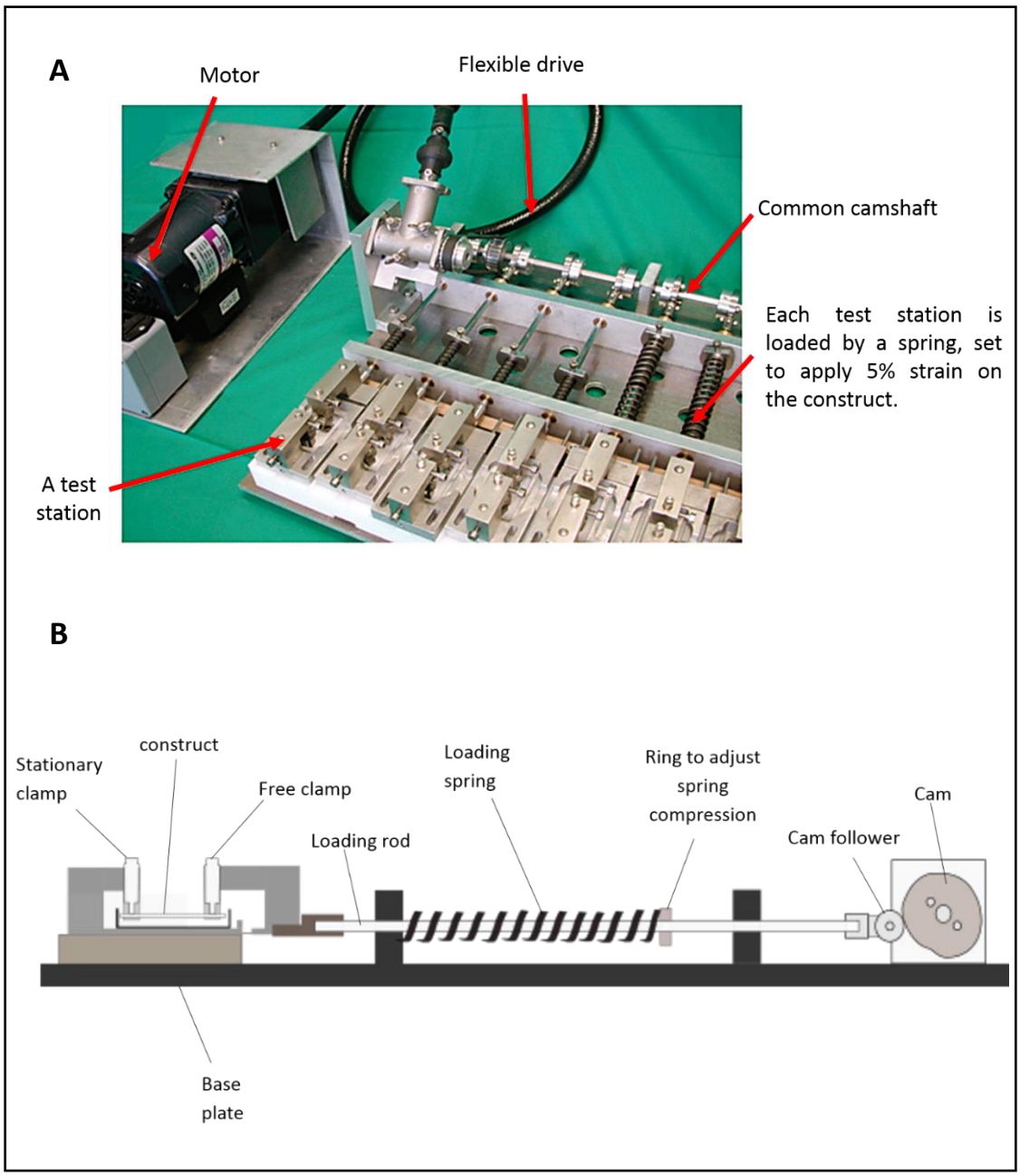

Figure 4.3 The cyclic strain apparatus.

A) A photograph of the apparatus showing 6 of the 8 test stations which are mounted onto the base plate. The motor is connected to the cam shaft via a flexible drive. Taken from (Raif *et al*., 2007) with modifications.

B) Schematic diagram of a complete test station and the loading mechanism.

4.1.5 Gene expression analysis

The expression of ligament and non-ligament associated genes was measured to determine whether the constructs induce a ligamentous phenotype in the cells. Quantitative reverse transcription polymerase chain reaction (qRT-PCR) was used to analyse this.

4.1.5.1 Isolation of mRNA using the RNeasy mini kit (Qiagen)

At the end of their culture period, loaded constructs were cut from their clamps and non-loaded constructs were removed from their culture wells. The samples were blotted with Whatman filter paper to remove excess liquid and 1 cm sections were transferred to a 1.5 ml microtube for gene expression analysis. The remaining portion of the construct was fixed in 10% NBF for subsequent confocal microscopy analysis (as described in section 3.1.2.2). mRNA was extracted using the RNeasy mini kit (Qiagen) as per the manufacturer's instructions. The RLT buffer provided in the kit lyses tissues and inactivates RNases to preserve the extracted RNA. Following treatment with buffer RLT, the lysates were passed through a QIAshredder column (Qiagen) which was centrifuged at 2000 × *g* for 5 minutes, to homogenise the lysate and filter out any debris. 10 µl of the lysate was retained for DNA quantification, which was carried out using a Quant-iT™ PicoGreen® dsDNA assay according to the method in section 3.1.2.1. The remaining 490 µl of lysate was transferred to an RNeasy spin column which contains a silica membrane to which RNA readily binds. Treatment of the lysate with 70% ethanol precipitates the RNA to improve membrane binding. In addition, the lysates were treated with DNase (Qiagen) to enhance the purity, followed by sequential washing with the provided buffers to yield high quality, uncontaminated RNA. The yield and purity of the resulting RNA product was measured using a NanoDrop-100 spectrophotometer (NanoDrop Technologies Inc.). The prepared RNA was stored at -20˚C for later use in quantitative analysis of expression levels for the genes of interest.

4.1.5.2 Synthesis of single-stranded cDNA by reverse transcription

cDNA was synthesised from the RNA prepared in section 4.1.5.1 by reverse transcription using the High Capacity RNA-to-cDNA Kit (Applied Biosystems). 10 µl of 2 x RT buffer (Applied Biosystems) and 1 µl of 20 x RT Enzyme Mix (Applied Biosystems) were added to 0.1 ml PCR tubes. Sample RNA was added so that the tubes contained equal amounts of total RNA (which ranged between 12 and 70 ng, depending on the experiment). Volumes ranged between 0.4 and 9 µl depending on the initial RNA yield of each sample within an experiment. Nuclease-free H_2O was added to bring the total volume of each tube to 20 µl.

The tubes were sealed and centrifuged briefly to spin down the contents before being placed in a thermal cycler (Techne) which incubated the samples at 37˚C for 60 minutes followed by 5 minutes at 95˚C. The samples were cooled to 4˚C and then stored at -20˚C for subsequent use in Quantitative Real Time PCR.

4.1.5.3 Quantitative Real Time PCR (qRT-PCR)

Quantitative real time PCR was conducted on mRNA samples according to the method developed by Heid *et al.* (1996). Bovine TaqMan® Gene Expression Assays for the genes of interest (see Table 4) were purchased from Applied Biosystems. Each assay contains the specific forward and reverse primers, a TaqMan® probe labelled with a fluorescent dye on the 5' end, and a minor groove binder and non-fluorescent quencher on the 3' end. Most of the assays were pre-designed and available from the Advanced Biosystems catalogue. However, assays for *RUNX2* and *SCXAB* were not available and had to be generated using the TaqMan® custom design tool. This required the input of target sequences obtained from the National Centre for Biotechnology Information (NCBI) online database. By uploading the sequences for these genes to the TaqMan® custom assay pipeline, bioinformatics analysis was applied to generate custom primer sequences which were then purchased as a complete TaqMan® assay.

Table 4 Details of TaqMan assays used to quantify the expression of ligament and non-ligament associated genes.

Gene	Assay ID (Applied Biosystems)	Gene Location	Amplicon length
GAPDH	Bt03210913_g1	Chr.5: 10852909 - 10857192	66 bp
HPRT1	Bt03225308_g1	Chr. X: 18223033-18254237	111 bp
COL3A1	Bt03249924_m1	Chr.2: 7760252 - 7799885	140 bp
TNC	Bt03253343_m1	Chr.8: 109490395 - 109562936	62 bp
COL1A1	Bt03225338_gH	Chr.19: 37326070 - 37342835	148 bp
RUNX2	ARMFWWV (custom)	Chr. 23:19419184-19425316	91 bp
SCXAB	ARNKRGT (custom)	Chr. 14: 483723-480389	57 bp

TaqMan® Gene Expression Master Mix was purchased from Applied Biosystems. This product is designed for optimum performance when used in conjunction with TaqMan® Gene Expression Assays. The Master Mix contains all of the components for the qRT-PCR reaction, excluding the template and primers. It contains AmpliTaq Gold® DNA Polymerase, dNTPs, as well as Uracil-DNA Glycosylase, which prevents amplification of carry-over PCR products.

Reactions for qRT-PCR were prepared in white 96-well PCR plates and components were added to wells as described in Table 5 before covering the plate with an adhesive PCR plate seal. The plate was centrifuged briefly to spin down the contents before placing in a Light Cycler 480-II (Roche) which performed quantitative Real time PCR on the samples over 45 amplification cycles.

Table 5 Volumes of components used in qRT-PCR reactions.

Component	Volume (µl)
TaqMan Gene Expression Master Mix	10
TaqMan Gene Expression Assay (20X)	1
Nuclease-free water	8
cDNA template	1
Total	20

4.1.5.4 House-keeping gene screen

GAPDH and *HPRT1* (Table 4) genes were initially screened to search for a house-keeping gene which showed consistent expression levels across all treatment groups. Expression levels of target genes can then be normalised to the house-keeping gene. Expression levels of house-keeping genes were plotted as 2^{-Ct}, where C_t is the number of amplification cycles required to reach a threshold, and a one-way ANOVA statistical test was applied to identify any significant differences in expression between treatment groups.

4.1.5.5 Calculation of the expression of target genes

Gene expression data was calculated using the ΔC_t and $\Delta\Delta C_t$ methods, where ΔC_t represents the absolute mRNA expression level relative to the house-keeping gene, and $\Delta\Delta C_t$ represents the fold change in mRNA expression relative to the experimental control (Shmittgen and Livak, 2008). This was either hybrid coated constructs versus non-coated constructs, or loaded constructs versus their corresponding non-loaded construct. *GAPDH* was selected as the house-keeping gene (based on results presented in section 4.2.5.1). ΔC_t and $\Delta\Delta C_t$ were calculated using the following equations:

$$2^{-\Delta Ct} = 2^{-(X_{TG} - X_{HK})}$$

$$2^{-\Delta\Delta Ct} = 2^{-[(T_{TG} - T_{HK}) - (C_{TG} - C_{HK})]}$$

Where T represents a treated construct (ie. coated or loaded), C represents a control construct (ie. non-coated or non-loaded), x_{TG} is the C_t value generated from a target gene, and x_{HK} is the C_t value generated from the house-keeping gene (ie. *GAPDH*).

4.2 Results

This section presents experimental data from additional studies conducted on P100 (100% PPP), C50 (50% collagen, 50% PPP) and A25 (25% alginate, 75% PPP) coated constructs, according to the methods described in section 4.1. These coatings were evaluated based on their ability to support cell viability, as well as expression of ligament and non-ligament associated genes. The coatings were also characterised by comparing PDGF and IGF-1 release profiles, and physically characterised using scanning electron microscopy and rheology. Finally, these coated constructs were subjected to cyclic tensile strain of 5% at a frequency of 1 Hz, and the effect of this on cell proliferation, infiltration and gene expression was analysed. The aim of this phase of the project was to select a final coated construct for additional testing as a platelet-rich construct.

4.2.1 P100, C50 and A25 coated constructs support similar levels of cell viability

The viability of cells within each construct was assessed using live/dead staining. Confocal microscopy was used to image cells seeded on constructs (P100, C50 and A25) after incubation with live/dead stain (according to the method in section 4.1). Constructs were cultured for a total of 15 days before staining, and imaging took place on the day of staining. Confocal analysis demonstrated a high level of viability in bSCs cultured within all constructs, with only limited dead cells visible in the images (Figure 4.4).

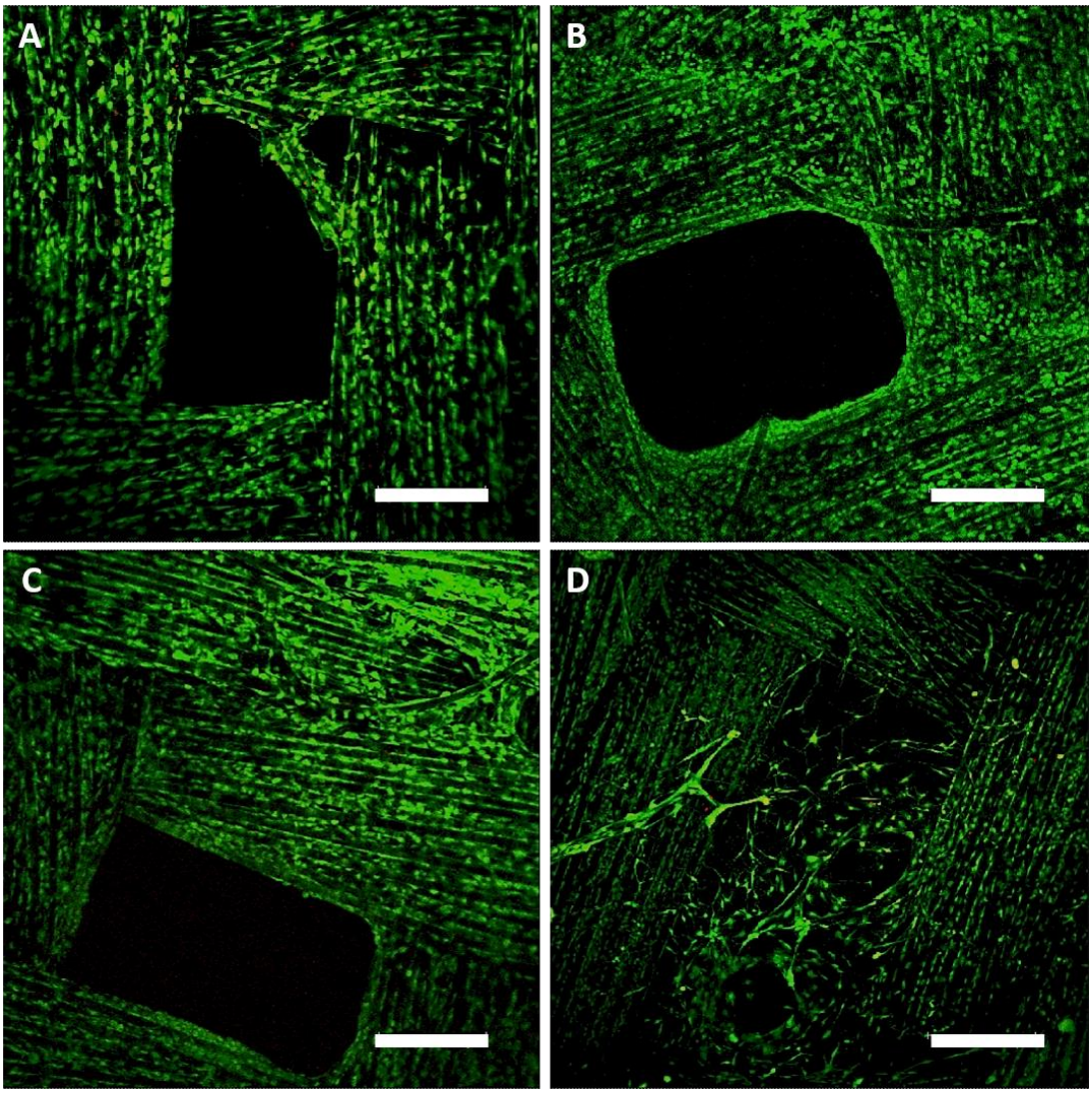

Figure 4.4 Cell viability staining within P100, C50 and A25 coated constructs.
Confocal images of NC (A), P100 (B), C50 (C) and A25 (D) stained with Live/dead stain after 15 days of culture. Live: Calcein-AM (green). Dead: Ethidium homodimer-1 (red). Only limited dead cells are visible in the images. Scale bar = 300μm.

4.2.2 Almost total PDGF-AB and IGF-1 release occurred within 3 days of platelet activation, from all platelet-rich coatings

It was anticipated that platelets within the coatings of hybrid constructs would release growth factors which would enhance cell proliferation, thereby improving integration of the construct if implanted *in vivo*. To establish the growth factor release profile for PDGF and IGF-1 from each construct (P100, C50 and A25), non-seeded coated constructs were produced by incorporating platelet-rich plasma (PRP), and PDGF-AB and IGF-1 concentrations were measured in the media in ng/ml using an ELISA. Each coating contained 50% PRP and volumes were equalised using PPP (see section 4.1.2 for a full description of the method). Values were compared to the concentrations of PDGF and IGF-1 in media containing 10% FBS as this is a commonly used supplementation method for *in vitro* cell culture.

Figure 4.5 A shows the release profile of PDGF-AB from each of the constructs (P100, C50 and A25) over 9 days. The results are presented as the cumulative concentration of PDGF-AB (in ng/ml) in the media at each time point. By day 9 (216 hours), coated constructs released 38-60 fold more PDGF-AB into the media than the amount from FBS supplementation alone. The P100 coating released the most PDGF-AB by day 9 (2 ng/ml), with the C50 and A25 coatings releasing 1.3 and 1.5 ng/ml respectively.

Figure 4.5 B shows the release of IGF-1 from each construct over 9 days. The results are presented as the cumulative concentration of IGF-1 (in ng/ml) in the media at each time point. By 9 days (216 hours), hybrid constructs released 9-22 fold more IGF-1 into the media than the amount from FBS supplementation. In contrast to PDGF release, the A25 coating released the most IGF-1 by day 9 (10.3 ng/ml). C50 and P100 constructs released 4.4 and 6.7 ng/ml respectively, by day 9.

All hybrid constructs tested (P100, C50 and A25) released 94-96% of their PDGF and IGF-1 by day 3. Although the total growth factor release varied significantly between coatings ($p \leq 0.0001$), the profile of release was similar, with very little PDGF or IGF-1 being released between days 3 and 9. Release of IGF-1 was slightly more gradual than PDGF, with 78-88% of total release occurring within 16 hours post activation. 90-93% of PDGF was released within 16 hours.

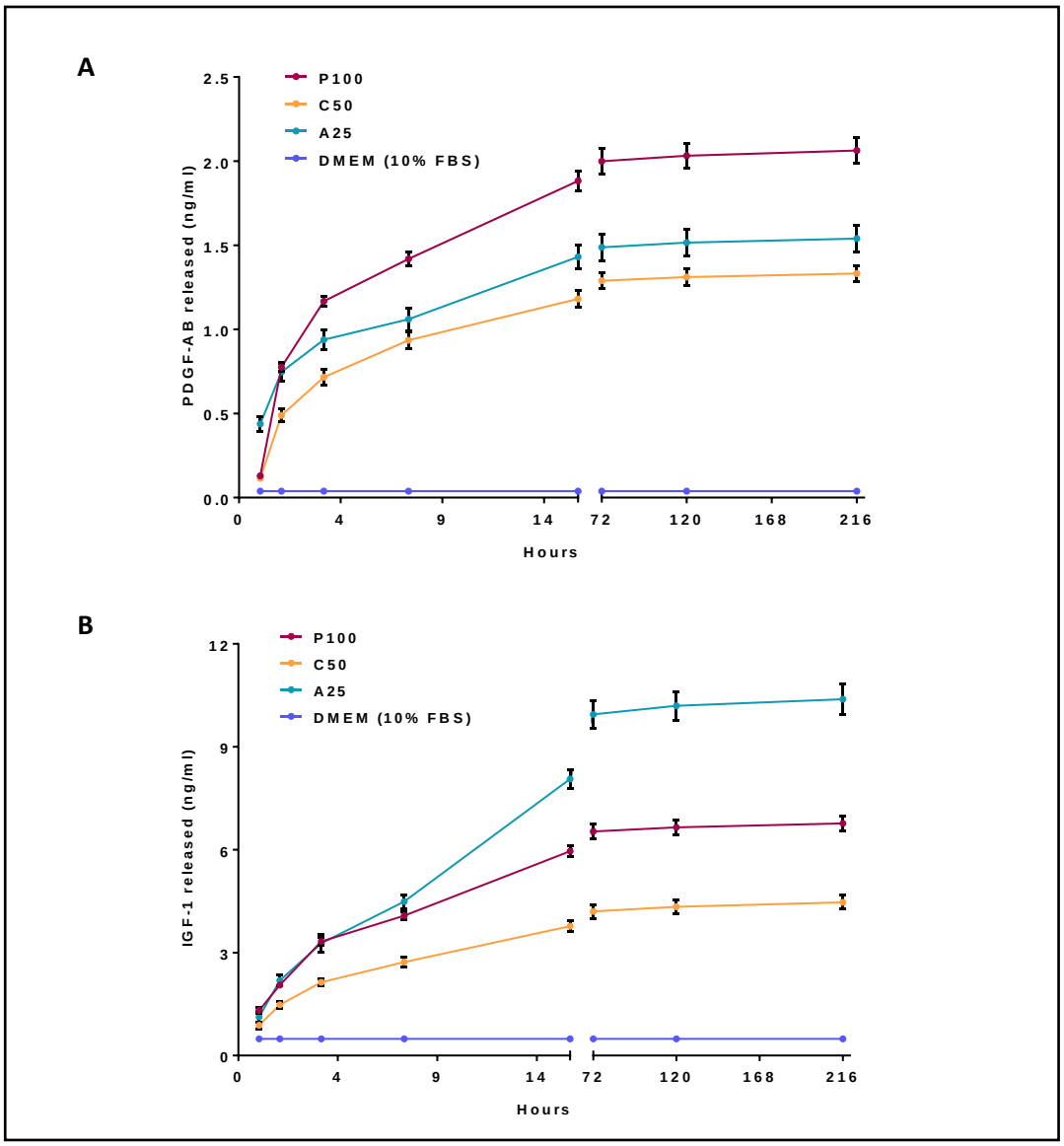

Figure 4.5 Growth factor release profiles from platelet-rich coated constructs.
Release of PDGF-AB (A) and IGF-1 (B) from non cell-seeded platelet rich constructs over 9 days. Data points represent the mean growth factor concentration (µg/ml) ± standard deviation (n=3). Values were normalised to platelet content to account for variations in platelet density in each construct, using the following equation:

$$n = m - \left(\left(\frac{pv}{r + pv} \right) \times m \right)$$

Where n is the normalised growth factor concentration, m is the measured growth factor concentration in ng/ml, p is the platelet density in PPP (ie. 4.5×10^4 platelets/µl), v is the volume of PPP in the construct and r is the number of platelets in 100 µl of PRP (ie. 2×10^8). Statistical analysis was conducted using a one-way ANOVA, which revealed significant differences in the total PDGF and IGF-1 release between all coated constructs ($p \leq 0.0001$).

4.2.3 Variation in matrix density between coatings

SEM was used to visualise the matrix of each of the biopolymer coatings. Non cell-seeded hybrid constructs were used and these were prepared for imaging by dehydrating with increasing ethanol concentrations before desiccating and sputter coating according to the method detailed in section 4.1.3.1. Images were captured using a back-scattered electron detector.

Images of the P100 coating showed an open fibrous network with fibril diameters varying from approximately 0.25-0.5 µm (Figure 4.6 A and B). The fibrils composing the C50 coating appeared to be smaller (0.1-0.2 µm) than those composing the P100 coating and the matrix was denser. However, pores are still clearly visible within this matrix. In addition, platelets can be clearly seen embedded within the fibres of the C50 coating (Figure 4.6 C and D). Platelets are 2-3 µm in diameter, and this is consistent with the structures visible in the images (indicated by red arrows). In contrast to the P100 and C50 coatings, A25 had a highly dense matrix and appeared to have a much lower porosity than the other constructs (not quantified). Furthermore, platelets can be clearly seen on the surface of the A25 construct, protruding from the matrix (Figure 4.6 E and F).

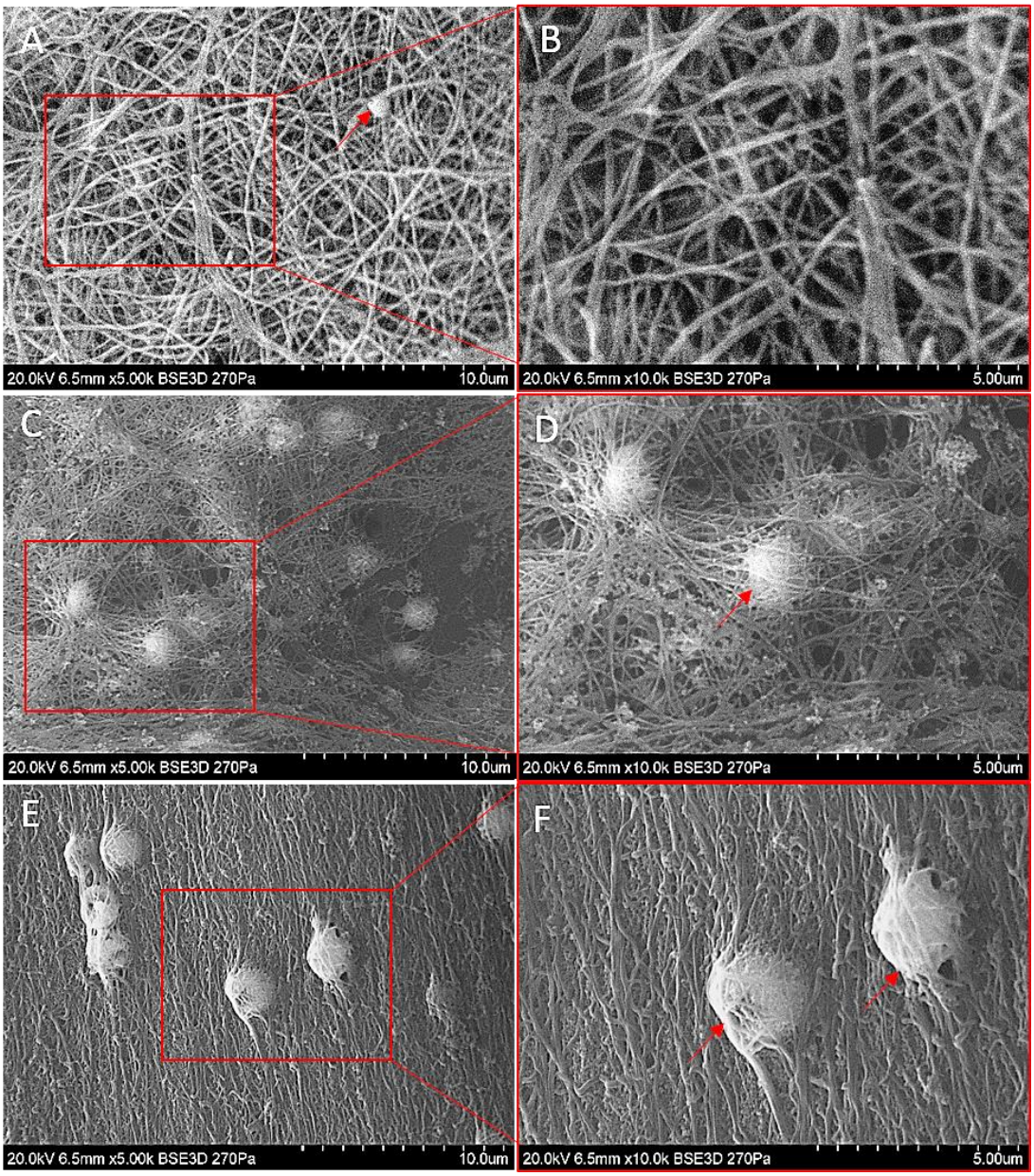

Figure 4.6 Scanning electron microscopy images of coated constructs.

SEM images of non-seeded P100 (A-B), C50 (C-D) and A25 (E-F) coatings. Images were taken at 5,000x (A, C and E) and 10,000x (B, D and F) magnification. Platelets are clearly visible in the constructs (red arrows). Note the more open structure of P100 and C50 in comparison with A25.

4.2.4 Variation in mechanical stability between coatings

An amplitude sweep was carried out to determine the linear viscoelastic region (LVER) of each gel. This is the point at which the storage modulus (G') starts to decrease, due to breakdown of the material's structure. The A25 gel had the longest LVER and so was the most stable gel in response to shear strain. With the shortest LVER, the C50 gel was the least stable gel. In addition, A25 had the highest G', indicating that it is the stiffest of the gels. P100 is the softest of the gels, indicated by its relatively low G' (Figure 4.7).

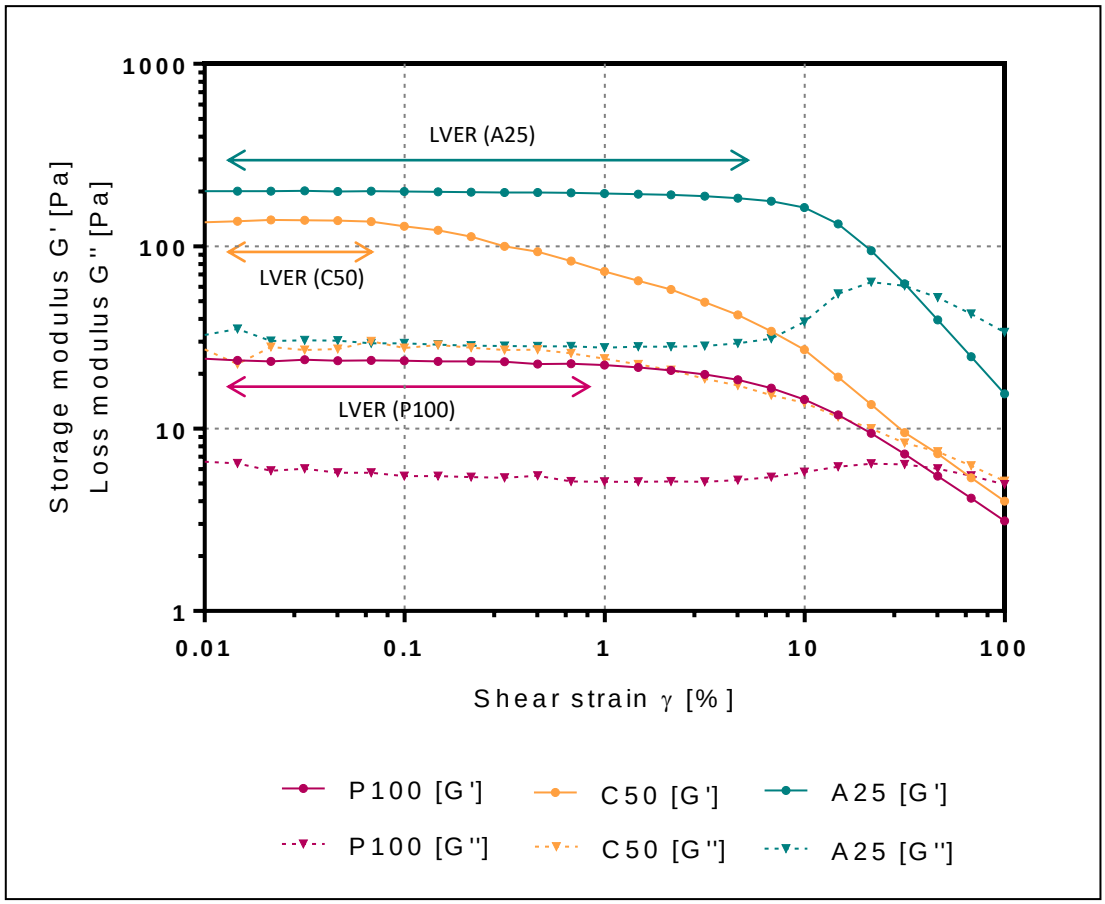

Figure 4.7 Amplitude sweep results from each biopolymer using a rheology.
Amplitude sweeps were conducted on P100, C50 and A25 gels formed into circular discs with a diameter of 60mm and a depth of approximately 3mm. The graph shows the measured G' (solid line) and G'' (dotted line) values with increasing shear strain (γ). Arrows show the LVER for each gel.

A frequency sweep was conducted on each gel within the parameters of the LVER to obtain an understanding of their structural properties. Figure 4.8 shows the results from the frequency sweep, with no change in G' or G'' with changing frequency. This is indicative of a gel-like structure, as was expected with these materials.

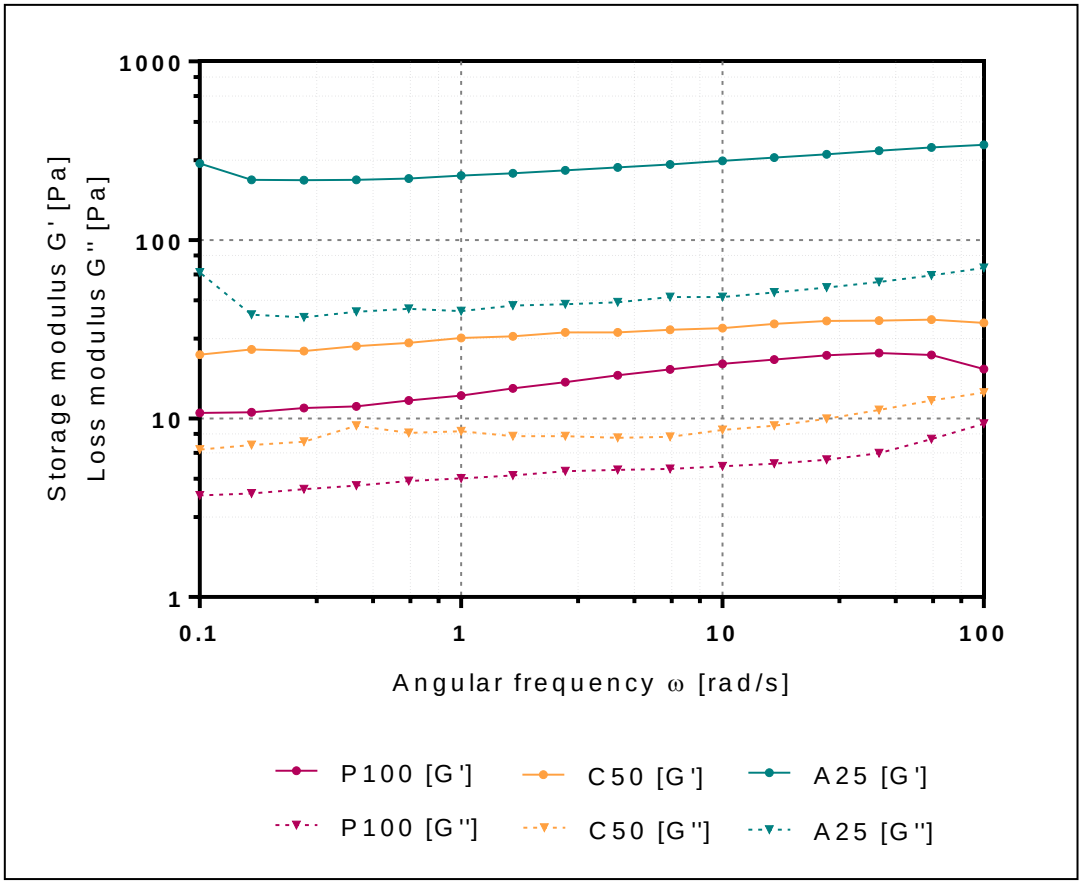

Figure 4.8 Frequency sweep results from each biopolymer using rheology.
Frequency sweeps were conducted on P100, C50 and A25 gels within the parameters of their LVER. The graph shows the measured G' (solid line) and G'' (dotted line) values with increasing angular frequency (ω) and a constant strain of 0.7%.

4.2.5 The effect of P100, C50 and A25 biopolymer coatings on gene expression

RT-qPCR was used to assess the effect of each coating on the expression of ligament and non-ligament associated genes by bSCs. Expression levels for each gene of interest were normalised to a pre-selected house-keeping gene.

4.2.5.1 Selection of *GAPDH* as the house-keeping gene for relative quantification of gene expression

HPRT1 and *GAPDH* were screened in the search for a house-keeping gene which showed consistent expression levels across all treatment groups. The expression level of a suitable house-keeping gene should not vary significantly between constructs, or between loaded and non-loaded conditions.

Results for the house-keeping gene screens were plotted as 2^{-Ct}, where the C_t is the number of amplification cycles required to reach a threshold (Figure 4.17). Expression of *HPRT1* did not remain consistent across each treatment group, with significant differences being measured between different constructs, and between non-loaded and loaded conditions. *GAPDH* showed no significant difference in expression level between constructs, or between non-loaded and loaded conditions. GAPDH was therefore selected as the house-keeping gene to be used for normalisation in all qRT-PCR experiments.

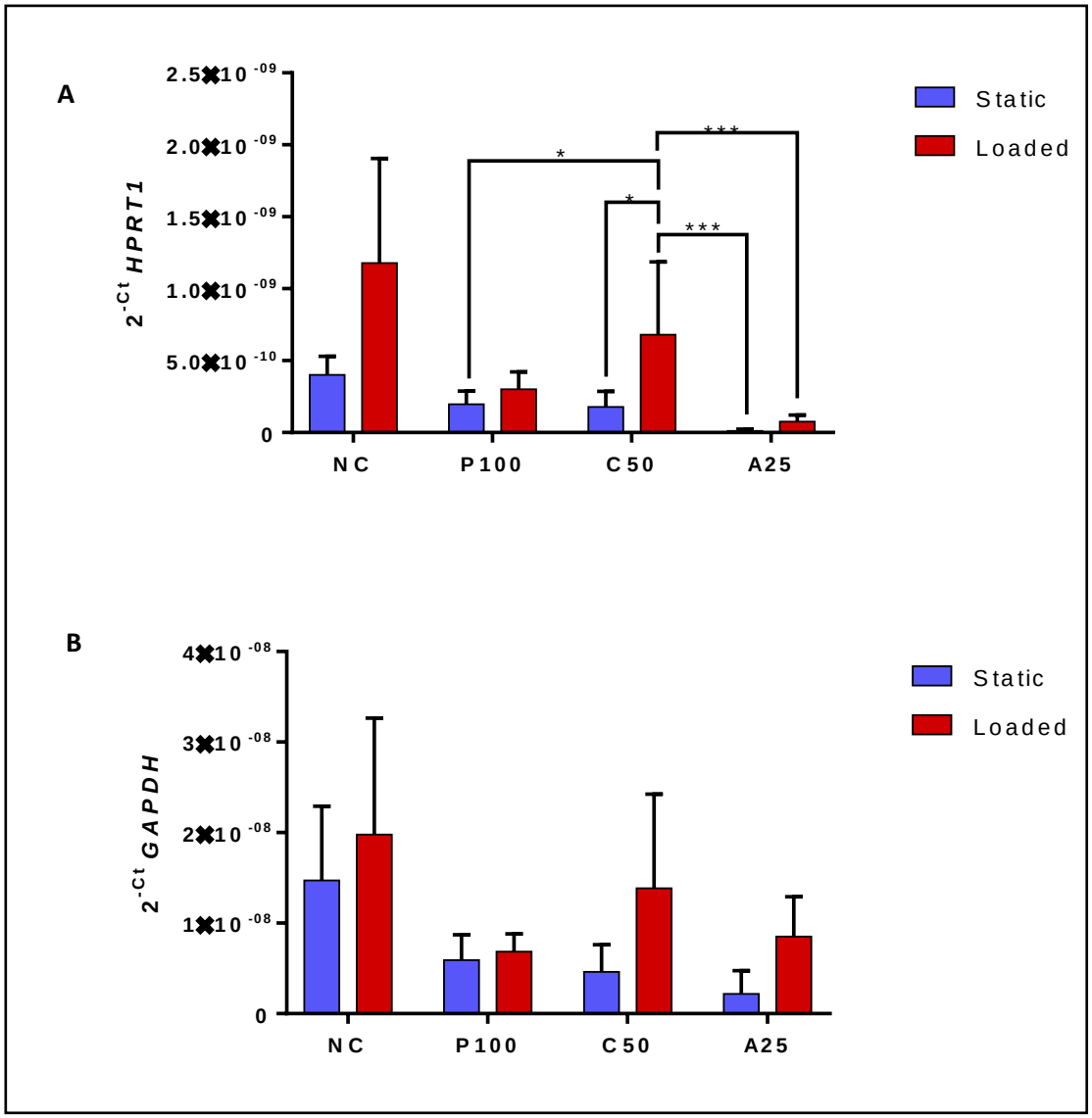

Figure 4.9 Results of the house-keeping gene screens conducted on *HPRT1* and *GAPDH*. Expression of *HPRT1* (A) and *GAPDH* (B) in bSCs within non-coated, P100, C50 and A25 coated constructs under non-loaded (blue) and loaded (red) conditions, represented as 2^{-Ct}. Bars represent the mean ± standard deviation (n=3). Statistical significance was determined using a one-way ANOVA. * = $p \leq 0.05$, *** = $p \leq 0.001$.

4.2.5.2 The effect of P100, C50 and A25 coatings on the expression of ligament and non-ligament associated genes in bSCs

To assess of the effect of each coating on bSC gene expression mRNA was isolated from non-loaded constructs (no forces applied) after 3 and 15 days of culture, as described in section 4.1.5.1. Results were analysed using the ΔΔ Ct method (described in section 4.1.5.5) and are presented as a fold change in expression level relative to the non-coated scaffold (NC), and normalised to the expression level of *GAPDH* for each construct. The data presented in this section was generated from bSCs isolated from 2 bovines (donor 1 and 2). All conditions and experimental methods were kept consistent between donors.

COL1A1

No significant difference in *COL1A1* expression was measured after 3 days in both donors, across all coated constructs, in comparison with the non-coated control (Figure 4.10). However, although not significant, the presence of the gel coatings tended to slightly reduce levels of expression measured at the early time point, in both donors.

By 15 days, the P100 coating induced a 2-fold upregulation of *COL1A1* expression in donor 2 cells ($p \leq 0.05$), but this was not evident in donor 1.

COL3A1

After 3 days in culture, all coatings caused a slight decrease in the level of *COL3A1* expression measured in donor 1 cells, although this was only significant in A25 constructs ($p \leq 0.05$). By 15 days, expression levels resulting from P100 and C50 coatings were similar to the non-coated control.

None of the coatings caused significant changes in *COL3A1* expression in donor 2 cells by 3 days or 15 days in comparison with the non-coated control. Donor 2 cells within the A25 coated construct had significantly lower *COL3A1* expression levels than those within P100 ($p \leq 0.01$) and C50 ($p \leq 0.05$) coated constructs by 15 days (Figure 4.11).

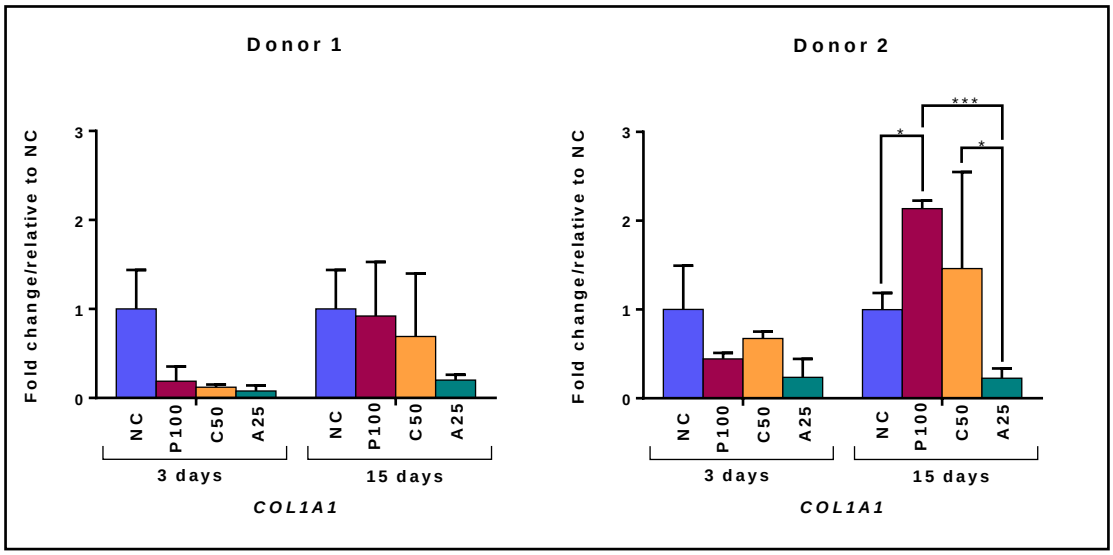

Figure 4.10 Effect of each coating on *COL1A1* mRNA expression.
The effect of P100, C50 and A25 coated constructs on *COL1A1* expression in bSCs from two different donors. Data is presented for 3 days and 15 days of non-loaded culture with DMEM containing 10% FBS. Bars represent the mean of the fold change relative to non-coated (NC) ± relative standard deviation (n=3). Values are normalised to *GAPDH* expression. Statistical significance was determined using a one-way ANOVA. * = $p \leq 0.05$, *** = $p \leq 0.001$.

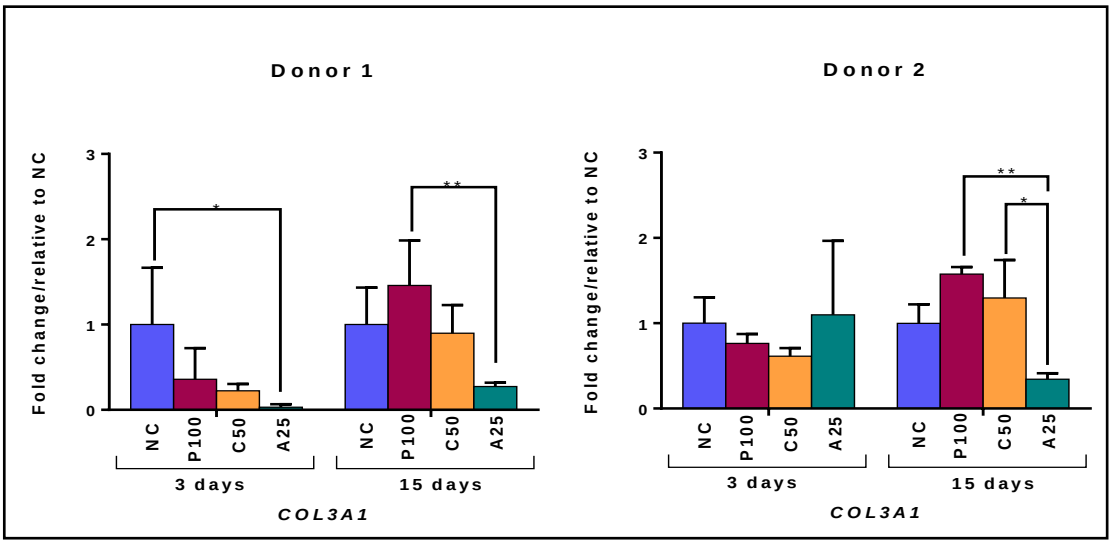

Figure 4.11 Effect of each coating on *COL3A1* mRNA expression.
The effect of P100, C50 and A25 coated constructs on COL3A1 expression in bSCs from two different donors. Data is presented for 3 days and 15 days of non-loaded culture with DMEM containing 10% FBS. Bars represent the mean of the fold change relative to non-coated (NC) ± relative standard deviation (n=3). Values are normalised to *GAPDH* expression. Statistical significance was determined using a one-way ANOVA. * = $p \leq 0.05$, ** = $p \leq 0.01$.

TN-C

Changes in *TN-C* expression in response to each coating, in comparison with the non-coated scaffold, are presented in figure 4.12. Downregulation of *TN-C* in P100 ($p \leq 0.01$) and C50 ($p \leq 0.001$) coated constructs (in comparison with the non-coated control) could be seen in donor 1 cells at 3 days, but this was not reproduced in donor 2 cells which showed no significant change in expression as a result of any of the coatings at day 3.

P100 coated constructs caused a 2-fold upregulation ($p \leq 0.05$) of *TN-C* expression by 15 days in donor 2, but this was not found in donor 1. *TN-C* expression of donor 1 cells within the C50 coated construct remained significantly lower ($p \leq 0.01$) than the non-coated control at 15 days. By 15 days, donor 2 cells within A25 coated constructs expressed significantly less *TN-C* than both P100 ($p \leq 0.0001$) and C50 ($p \leq 0.05$) coated constructs.

SCXAB

The effect of each coating on SCXAB expression is presented in Figure 4.13. Changes seen are inconsistent across donors. Early upregulation at 3 days was seen in donor 2, in C50 coated constructs (4.5-fold, $p \leq 0.01$). In donor 1 cells, P100 induced a 1.7-fold increase ($p \leq 0.01$) in expression at this time point, and the C50 coating induced a slight decrease (not significant) in *SCXAB* expression.

No significant change in expression (in comparison with the non-coated control) was induced by any of the coatings at 15 days, in both donors (Figure 4.13).

RUNX2

Figure 4.14 Shows the effect of each coating on expression of *RUNX2*, which was used to rule out osteogenic differentiation, as this gene is a key transcription factor in osteogenesis. No significant increase in *RUNX2* expression was induced by coated constructs in comparison with the non-coated scaffold at either 3 or 15 days in both donors. In donor 2 cells, P100 and C50 coatings induced a significant 2-fold downregulation ($p \leq 0.05$) of *RUNX2* at 3 days, which then returned to a similar level to the non-coated control by 15 days. A25 constructs induced a significant 2-fold downregulation ($p \leq 0.01$) by 15 days in donor 2 cells.

A summary of the results from the investigation into the effect of each coating on gene expression can be found in table 6.

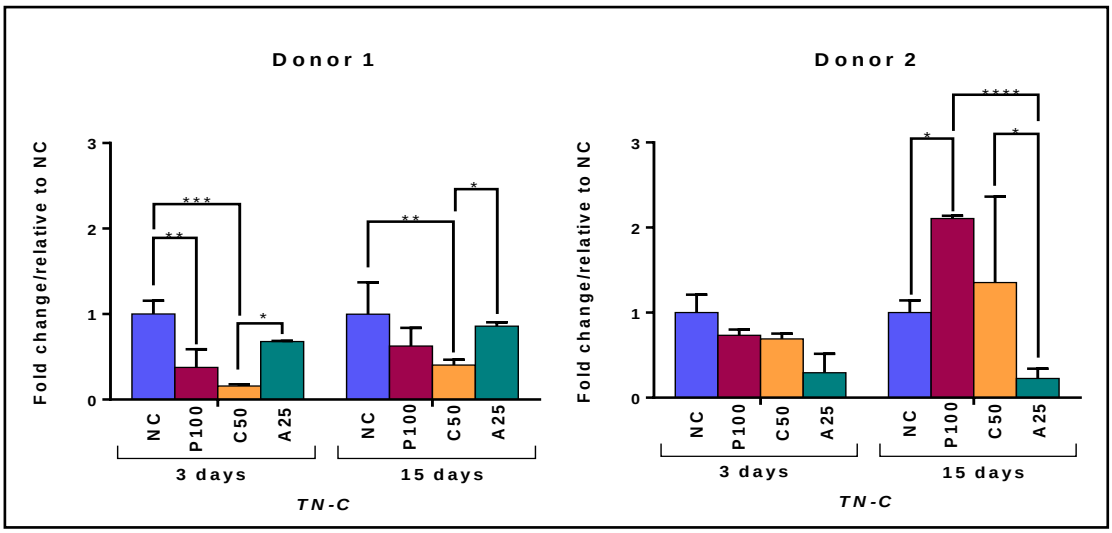

Figure 4.12 Effect of each coating on *TN-C* mRNA expression.

The effect of P100, C50 and A25 coated constructs on *TN-C* expression in bSCs from two different donors. Data is presented for 3 days and 15 days of non-loaded culture with DMEM containing 10% FBS. Bars represent the mean of the fold change relative to NC ± relative standard deviation (n=3). Values are normalised to *GAPDH* expression. Statistical significance was determined using a one-way ANOVA. * = $p \leq 0.05$, ** = $p \leq 0.01$, *** = $p \leq 0.001$, **** = $p \leq 0.0001$.

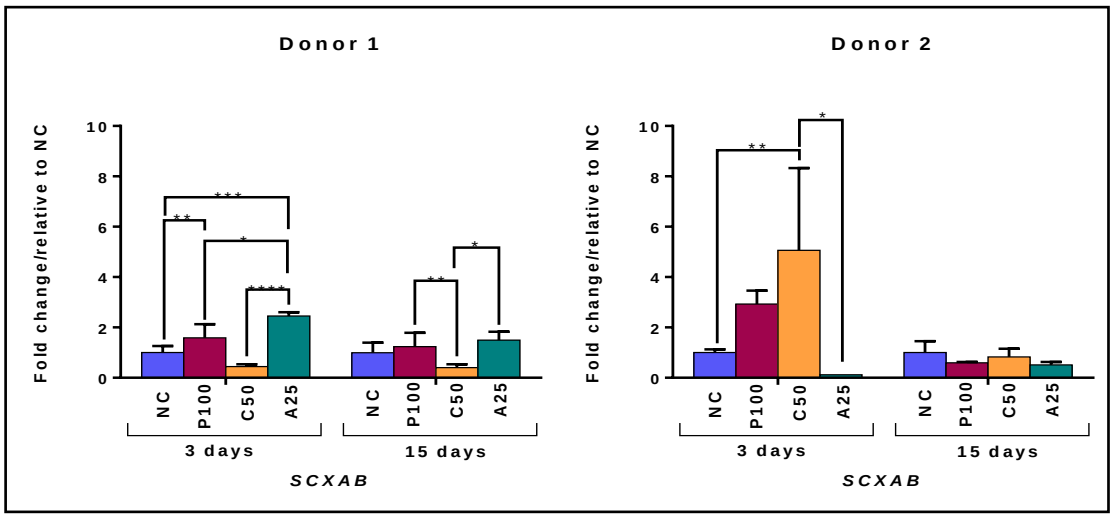

Figure 4.13 Effect of each coating on *SCXAB* mRNA expression.

The effect of P100, C50 and A25 coated constructs on *SCXAB* expression in bSCs from two different donors. Data is presented for 3 days and 15 days of non-loaded culture with DMEM containing 10% FBS. Bars represent the mean of the fold change relative to NC ± relative standard deviation (n=3). Values are normalised to *GAPDH* expression. Statistical significance was determined using a one-way ANOVA. * = $p \leq 0.05$, ** = $p \leq 0.01$, *** = $p \leq 0.001$, **** = $p \leq 0.0001$.

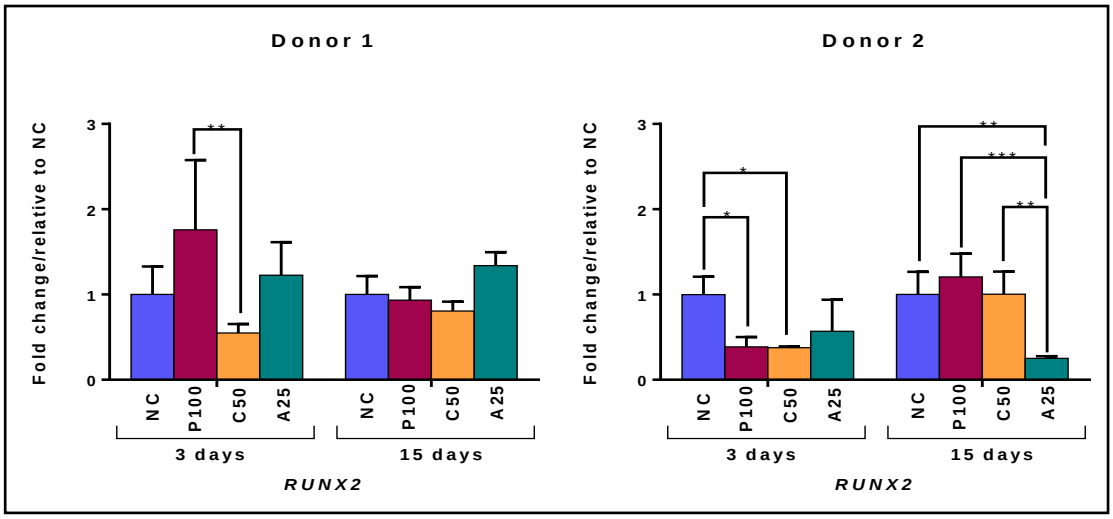

Figure 4.14 Effect of each coating on *RUNX2* mRNA expression.

The effect of P100, C50 and A25 coated constructs on *RUNX2* expression in bSCs from two different donors. Data is presented for 3 days and 15 days of non-loaded culture with DMEM containing 10% FBS. Bars represent the mean of the fold change relative to NC ± relative standard deviation (n=3). Values are normalised to *GAPDH* expression. Statistical significance was determined using a one-way ANOVA. * = $p \leq 0.05$, ** = $p \leq 0.01$, *** = $p \leq 0.001$.

Table 6 Summary of cellular gene expression changes in response to biopolymer coatings.

		P100		C50		A25	
	Gene	Donor 1	Donor 2	Donor 1	Donor 2	Donor 1	Donor 2
3 days	*COL1A1*	NS	NS	NS	NS	NS	NS
	COL3A1	NS	NS	NS	NS	33 (p≤0.05)	NS
	TN-C	2 (p≤0.01)	NS	6 (p≤0.001)	NS	NS	NS
	SCXAB	1.7 (p≤0.01)	NS	NS	4.5 (p≤0.01)	2.5 (p≤0.001)	NS
	RUNX2	NS	2 (p≤0.05)	NS	2 (p≤0.05)	NS	NS
15 days	*COL1A1*	NS	2 (p≤0.05)	NS	NS	NS	NS
	COL3A1	NS	NC	NS	NS	NS	NS
	TN-C	NS	2 (p≤0.05)	2 (p≤0.01)	NS	NS	NS
	SCXAB	NS	NS	NS	NS	NS	NS
	RUNX2	NS	NS	NS	NS	NS	2 (p≤0.01)

Table 6 summarises the changes in *COL1A1*, *COL3A1*, *TN-C*, *SCXAB* and *RUNX2* gene expression resulting from each coating (P100, C50 and A25), after 3 and 15 days, in cells from donors 1 and 2. Values indicate the fold change in gene expression relative to non-coated scaffolds (green and red cells indicate upregulation and downregulation respectively). Statistical significance is presented in brackets. NS indicates no statistically significant difference.

4.2.6 Cellular response to the application of cyclic tensile strain within P100, C50 and A25 coated constructs

As discussed in detail in chapter 1, the application of cyclic strain to ligament progenitor cells has been found to enhance cell proliferation and differentiation towards the ligament lineage. To evaluate the response of synovial cells to mechanical cyclic tensile strain bSCs were cultured in constructs in non-loaded and loaded conditions for 15 days. Loaded constructs were subjected to cyclic tensile strain of 5% at a frequency of 1 Hz, for 1 hour every day as described in section 4.1.4. Loaded constructs were maintained in culture attached to stainless steel clamps. To ensure the clamps had no significant effect on cell behaviour, some preliminary studies were conducted, as detailed in section 4.2.6.1.

4.2.6.1 Clamping constructs in the bioreactor chambers had no significant effect on cell proliferation or gene expression

To determine any effects of clamping on cell proliferation and gene expression, cell seeded non-coated scaffolds were attached to clamps but were not subjected to mechanical load. These clamped scaffolds were compared to cell seeded non-coated scaffolds which were left unclamped and cultured in wells of a 6-well plate.

The increase in DNA content of non-loaded (non-clamped) and non-loaded (clamped) constructs was measured after 15 days in culture. The results from this comparison are presented in Figure 4.15. Statistical analysis indicated that there was no statistically significant difference in DNA increase between clamped and non-clamped constructs after 15 days.

To identify any effect of clamping on gene expression, mRNA was isolated from non-loaded (non-clamped) and non-loaded (clamped) non-coated scaffolds after 15 days of culture (according to the method in section 4.1.5.1). The expression levels of each gene are presented in Figure 4.16, under both non-clamped and clamped conditions. Although clamped scaffolds had a slightly lower average expression of each gene, statistical analysis showed no significant difference in expression between non-clamped and clamped constructs for all 5 genes analysed.

Since clamping caused no significant difference in proliferation rate nor gene expression, it was decided that non-loaded constructs would be cultured in well plates as this would increase the number of samples that could be cultured at any one time.

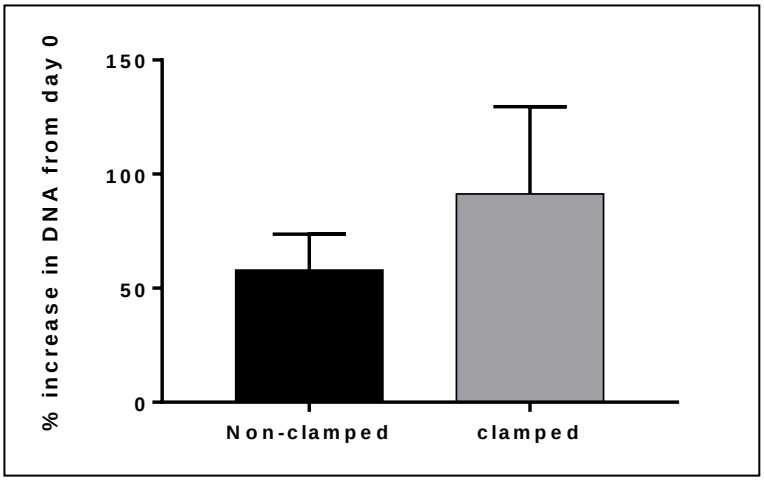

Figure 4.15 A comparison of cell proliferation on non-clamped and clamped scaffolds. Data is presented as the percentage increase in DNA from day 0 to day 15, harvested from non-clamped and clamped (non-coated) scaffolds seeded with bSCs and cultured under non-loaded conditions (with no forces applied). Bars represent the mean ± standard deviation (n=3). Statistical significance was determined using a t-test. No statistically significant difference in proliferation was determined between cells on non-clamped and clamped scaffolds.

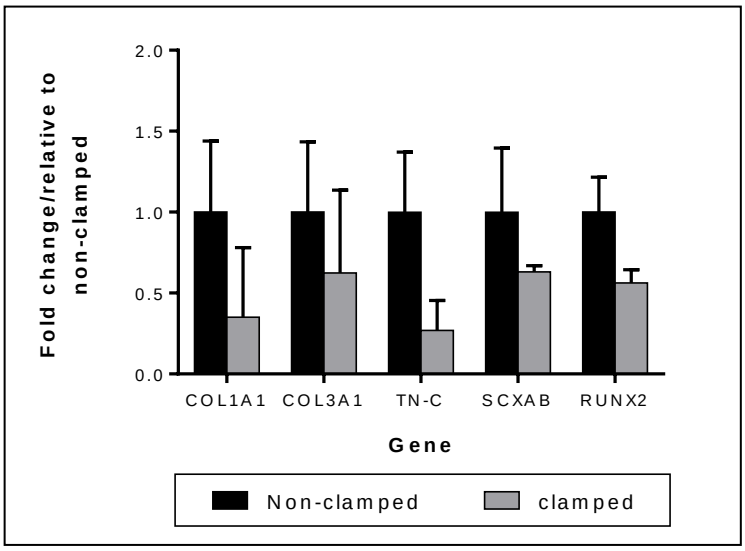

Figure 4.16 A comparison of gene expression in cells on non-clamped and clamped scaffolds. Data is presented for the expression levels of *COL1A1, COL3A1, TN-C, SCXAB* and *RUNX2* in bSCs cultured on non-clamped and clamped (non-coated) scaffolds under non-loaded conditions (with no forces applied). Bars represent the mean of the fold change relative to non-clamped ± standard deviation (n=3). Values are normalised to the GAPDH expression level for each condition. Statistical significance was determined using a t-test. No statistically significant difference in expression was identified between cells cultured on non-clamped and clamped scaffolds for any of the 5 genes analysed.

4.2.6.2 Cyclic tensile strain significantly increased cell proliferation

The effect of cyclic tensile strain on bSC proliferation within P100 (100% PPP), C50 (50% collagen, 50% PPP) and A25 (25% alginate, 75% PPP) coated constructs (as well as the non-coated control) was assessed using 2 donors. The results are presented in Figure 4.17 as the percentage increase in DNA over 15 days, relative to the DNA content directly after cell-seeding. Values are presented for non-loaded constructs (cultured in wells with no forces applied) as well as constructs to which 1 hour daily sessions of cyclic tensile strain (5% strain at a frequency of 1 Hz) had been applied, using the cyclic strain bioreactor previously described in section 4.1.4.2.

By applying strain to non-coated (NC) scaffolds, DNA content significantly increased 2.3-fold ($p \leq 0.001$) and 1.5-fold ($p \leq 0.05$) for donor 1 and 2 respectively, by 15 days. The application of cyclic tensile strain to P100 coated constructs resulted in a significant 1.7-fold ($p \leq 0.01$) and 2.3-fold ($p \leq 0.0001$) DNA increase in donor 1 and donor 2 cell-seeded constructs respectively. By applying cyclic strain to the C50 coated construct, the DNA content increased significantly by 2.2-fold ($p \leq 0.001$) and 2.3-fold ($p \leq 0.0001$) in donor 1 and donor 2 cell-seeded constructs respectively. Applying cyclic strain to A25 coated constructs caused a significant increase in proliferation in donor 2 (3-fold, $p \leq 0.0001$), but this was not replicated in donor 1, which had a slightly lower DNA content than the non-loaded construct by 15 days.

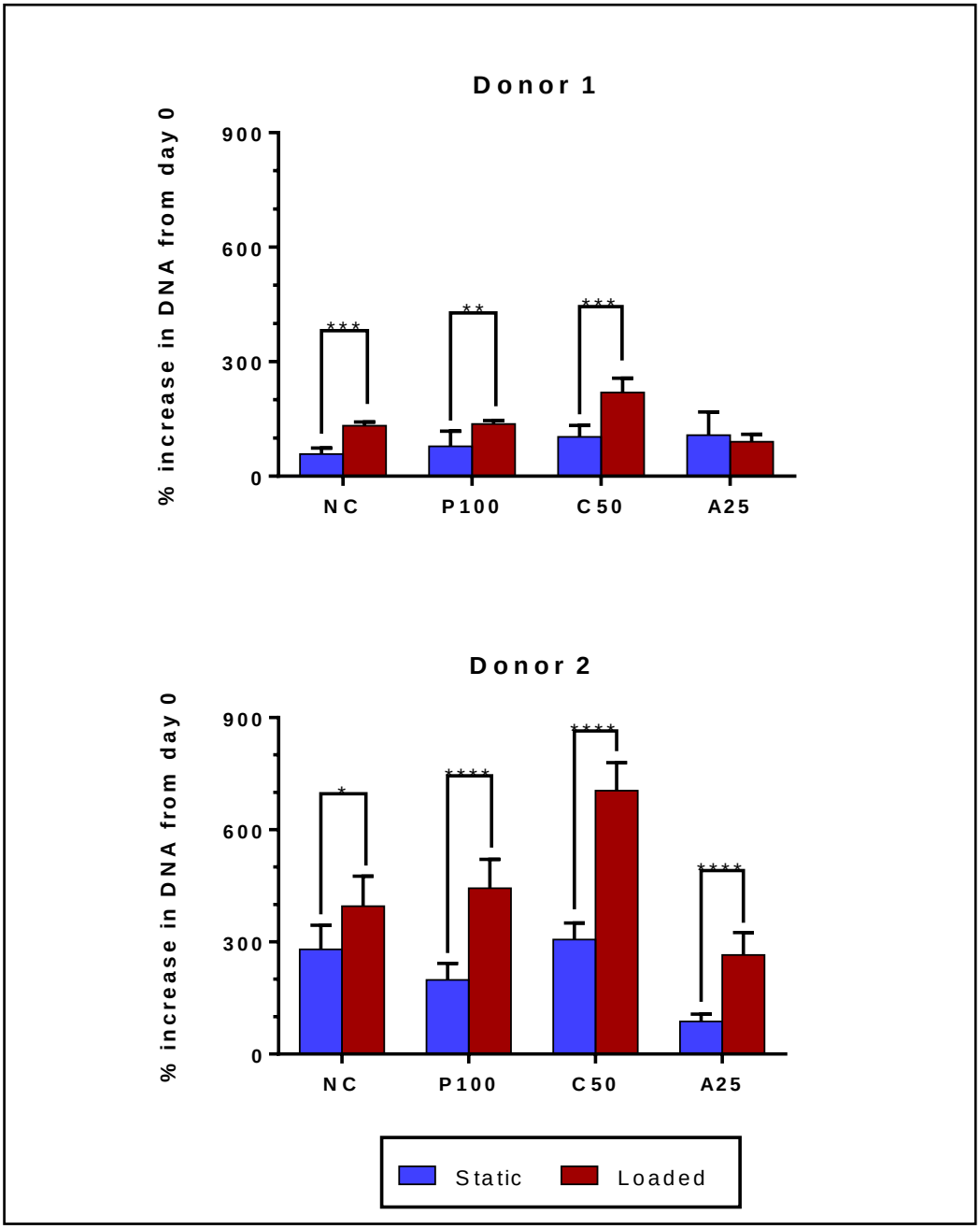

Figure 4.17 A comparison of cell proliferation within loaded and non-loaded constructs over 15 days.

The effect of cyclic tensile strain on proliferation of bSCs from two different donors cultured in non-coated (NC), P100, C50 and A25 coated constructs. Data is presented as the percentage DNA increase from the day that seeding was completed (day 0), to the 15th day in culture with DMEM supplemented with 10% FBS. Bars represent the mean ± standard deviation. Statistical significance was determined using a t-test. * = $p \leq 0.05$, ** = $p \leq 0.01$, *** = $p \leq 0.001$, **** = $p \leq 0.0001$.

4.2.6.3 Cyclic tensile strain enhances the longevity of the P100 coating

Confocal microscopy was used to examine constructs under non-loaded and loaded conditions, after the 15 day culture period (Figure 4.18). Constructs were stained with Alexa Fluor 488 phalloidin (green) and TO-PRO-3 (blue) which stain the cytoskeleton and nucleus respectively, according to the method detailed in section 3.1.2.2.

After applying cyclic tensile strain to non-coated constructs for 15 days, the cell population appeared to be denser, with larger areas of cells bridging the PET fibres, in comparison with non-loaded scaffolds. A higher cell density was also apparent in A25 coated constructs when subjected to cyclic tensile strain. However, areas of gel breakage were visible in loaded A25 coating. No obvious differences were observed between non-loaded and loaded C50 coated constructs by 15 days, with intra-fibre voids being exposed by this time point regardless of loading.

In contrast, the application of cyclic tensile strain for 15 days resulted in a visible difference in the longevity of the P100 coated construct. Under non-loaded conditions, much of the intra-fibre voids were exposed due to gel loss. However, under loaded conditions, the voids remained filled, with cells continuing to span the total area of the voids.

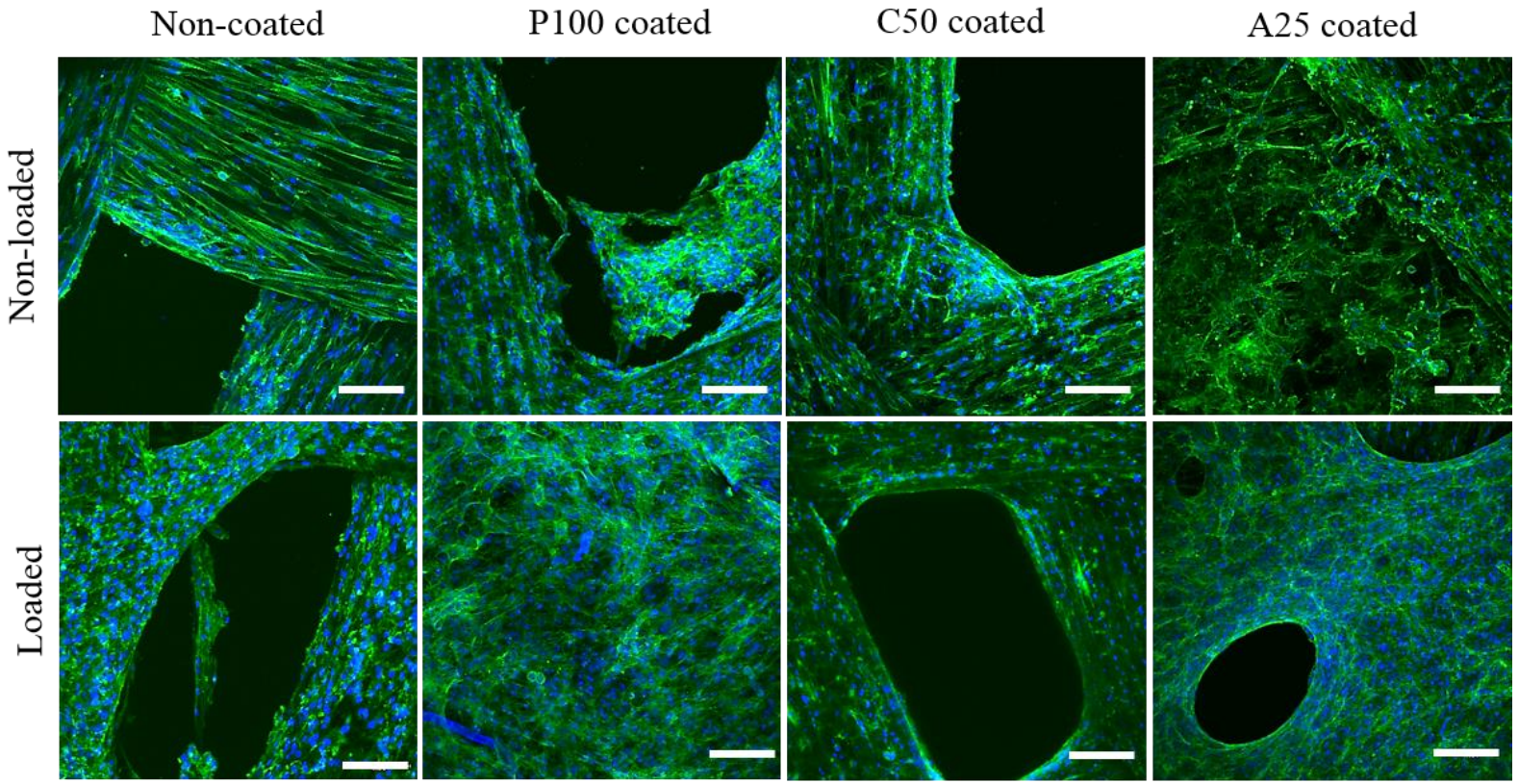

Figure 4.18 Confocal microscope images of each construct taken after 15 days under non-loaded and loaded conditions.

Confocal microscope images of non-coated, P100, C50 and A25 coated constructs were taken after 15 days under non-loaded (top row) and loaded (bottom row) conditions. Constructs were stained for actin (green) with Alexa Fluor 488 phalloidin and nuclei (blue) with To-pro-3 and imaged using a 20 X objective lens. Scale bar = 100µm.

4.2.6.4 The effect of cyclic tensile strain on the expression of ligament and non-ligament associated genes within bSCs in P100, C50 and A25 coated constructs

qRT-PCR was used to assess how the application of cyclic tensile strain (5% at a frequency of 1 Hz, for 1 hour every day) effects expression of ligament and non-ligament associated genes in bSCs cultured within each construct (NC, P100, C50, A25). mRNA was isolated from constructs after 3 and 15 days of culture, as described in section 4.1.5.1. Results were analysed using the Δ Ct and ΔΔ Ct methods (described in section 4.1.5.5) and are presented as both the absolute mRNA expression level under non-loaded and loaded conditions (normalised to *GAPDH*), and as a fold change in expression level relative to the non-loaded control for each construct. The data presented in this section was generated from bSCs isolated from 2 bovines (donor 1 and 2).

COL1A1

The effect of cyclic tensile strain on *COL1A1* expression in bSCs is shown in Figure 4.19. Cyclic strain caused significant upregulation of *COL1A1* expression by 3 days in donor 1 cells grown in P100 and C50 coated constructs (17-fold ($p \leq 0.0001$) and 6-fold ($p \leq 0.01$) increase respectively). This was not replicated in donor 2, which showed no change in expression at 3 days in any construct.

At 15 days, donor 1 cells in NC, P100 and C50 coated constructs showed a slight increase in *COL1A1* expression, in response to strain (2.1-fold to 3.7-fold), but this was not significant. A moderate increase in *COL1A1* expression (2.3-fold to 3.8 fold) was measured in donor 2 cells at 15 days in NC, C50 and A25 coated constructs. However, this was only significant in cells on the NC scaffold ($p \leq 0.01$).

COL3A1

The effect of cyclic tensile strain on *COL3A1* expression in bSCs is shown in Figure 4.20. Cyclic strain induced a significant 10-fold increase ($p \leq 0.0001$) in *COL3A1* in donor 1 cells, in P100 constructs. Approximately 3-fold increases in expression were measured in C50 and A25 constructs at the same time point, but this was not significant. No significant change in expression was measured in donor 2 cells in any construct by 3 days.

By day 15 significant upregulation of *COL3A1* was measured in both donors, in NC and C50 constructs. Donor 1 demonstrated a 7-fold ($p \leq 0.01$) and 6-fold ($p \leq 0.01$) upregulation in NC and C50 constructs respectively, whilst donor 2 demonstrated a 4-fold ($p \leq 0.001$) and 3-fold ($p \leq 0.05$) upregulation.

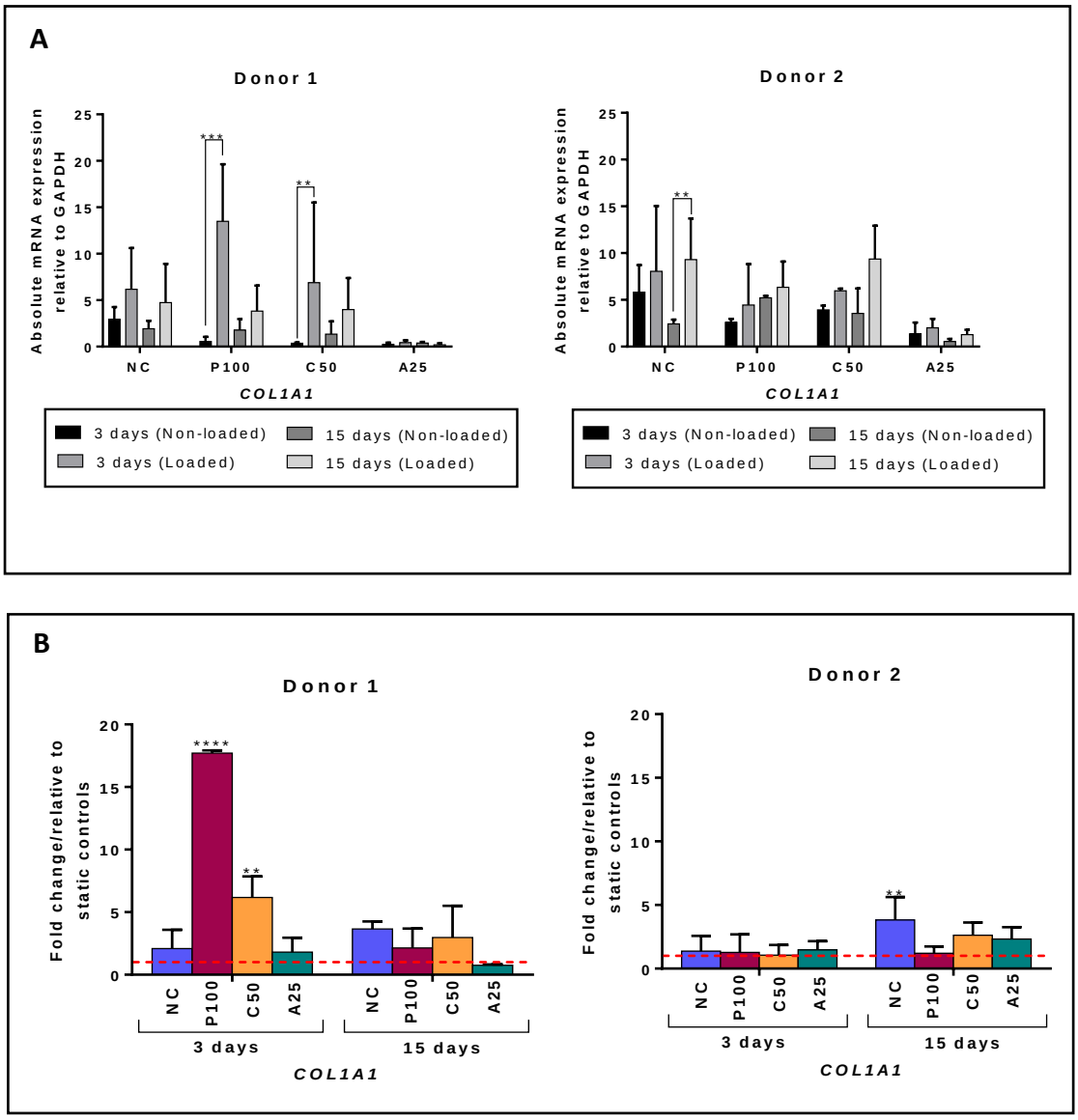

Figure 4.19 Effect of cyclic tensile strain on *COL1A1* mRNA expression of bSCs in P100, C50 and A25 coated constructs.

The figure demonstrates the effect of applying cyclic tensile strain of 5% at a frequency of 1 Hz (for 1 hour every day) on *COL1A1* expression of bSCs within each construct (NC, P100, C50 and A25). Data is presented for 3 days and 15 days of culture with DMEM supplemented with 10% FBS, for two donors. Values are normalised to *GAPDH* expression. Statistical significance was determined using a one-way ANOVA. ** = $p \leq 0.01$, **** = $p \leq 0.0001$.

A) Bars represent the mean absolute mRNA expression (Δ Ct) of non-loaded and loaded constructs ± relative standard deviation (n=3).

B) Bars represent the mean of the fold change (ΔΔ Ct) relative to corresponding non-loaded controls (indicated by the dotted line) ± relative standard deviation (n=3).

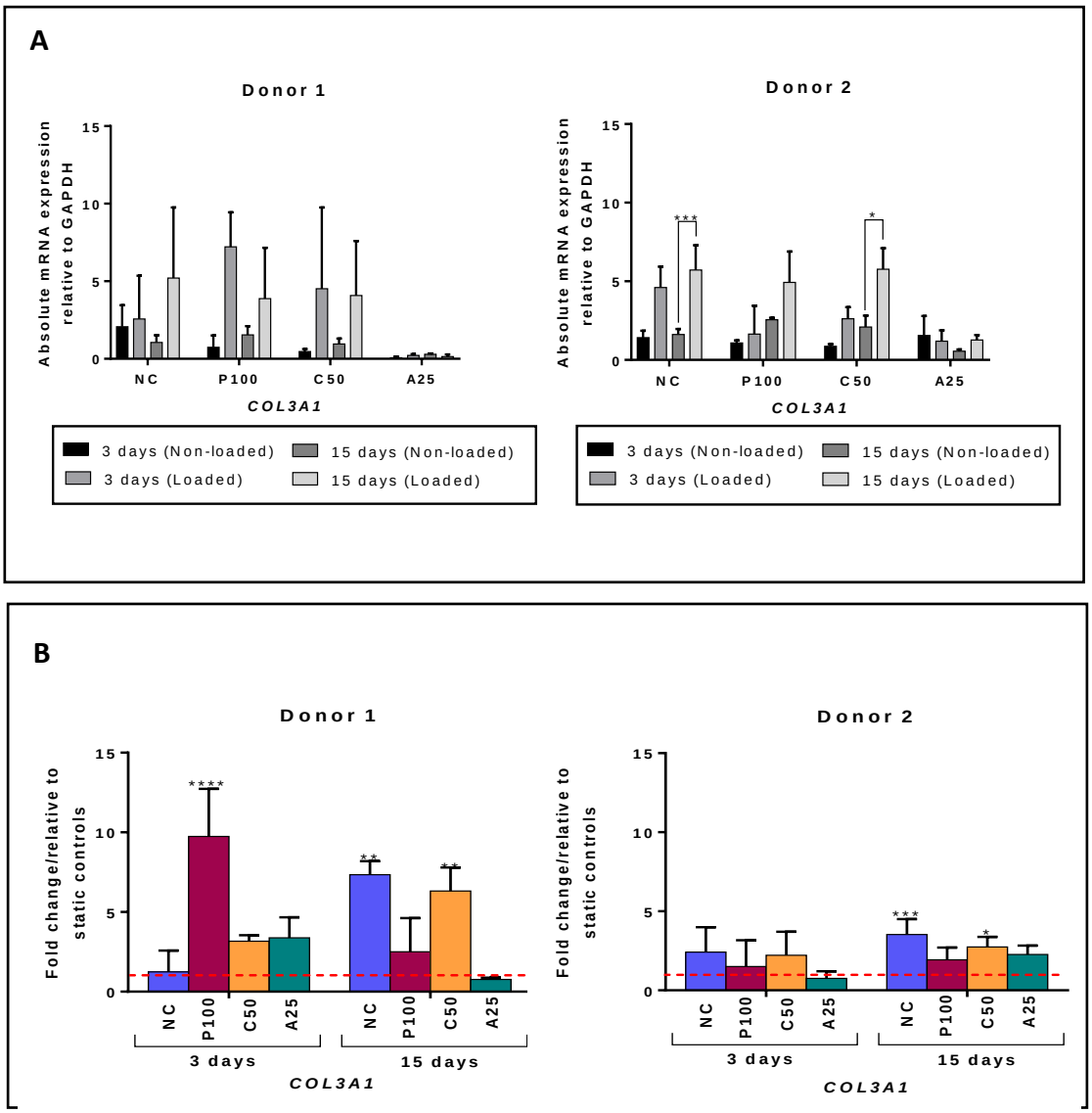

Figure 4.20 Effect of cyclic tensile strain on *COL3A1* mRNA expression of bSCs in P100, C50 and A25 coated constructs.

The figure demonstrates the effect of applying cyclic tensile strain of 5% and frequency of 1 Hz (for 1 hour every day) on *COL3A1* expression of bSCs within each construct (NC, P100, C50 and A25). Data is presented for 3 days and 15 days of culture with DMEM supplemented with 10% FBS, for two donors. Values are normalised to *GAPDH* expression. Statistical significance was determined using a one-way ANOVA. ** = $p \leq 0.01$, *** = $p \leq 0.001$, **** = $p \leq 0.0001$.

A) Bars represent the mean absolute mRNA expression (Δ Ct) of non-loaded and loaded constructs ± relative standard deviation (n=3).

B) Bars represent the mean of the fold change (ΔΔ Ct) relative to corresponding non-loaded controls (indicated by the dotted line) ± relative standard deviation (n=3).

TN-C

The effect of cyclic tensile strain on *TN-C* expression in bSCs is shown in Figure 4.21. Donor 1 cells showed a significant 2.7-fold increase (($p \leq 0.01$) in *TN-C* expression in C50 coated constructs at 3 days. No other significant changes in expression were measured as a result of cyclic strain after 3 days.

By 15 days, significant increases in *TN-C* expression were measured in NC (3.6-fold, $p \leq 0.001$) and C50 (2.5-fold, $p \leq 0.05$) constructs. A slight increase in expression was also measured in A25 (2.2-fold) constructs, in donor 2 cells, although this was not significant.

SCXAB

Figure 4.22 shows the effect of cyclic tensile strain on *SCXAB* expression in bSCs. Significant upregulation was seen at 3 days in donor 1 cells in NC (5.8-fold, $p \leq 0.001$) and C50 (6.7-fold, $p \leq 0.0001$) constructs. With regard to donor 2 cells, loading induced a significant 6-fold ($p \leq 0.0001$) increase in *SCXAB* expression in A25 coated constructs, at 3days.

By 15 days, no significant difference in *SCXAB* expression was measured in either donor as a result of applying cyclic tensile strain to any of the constructs.

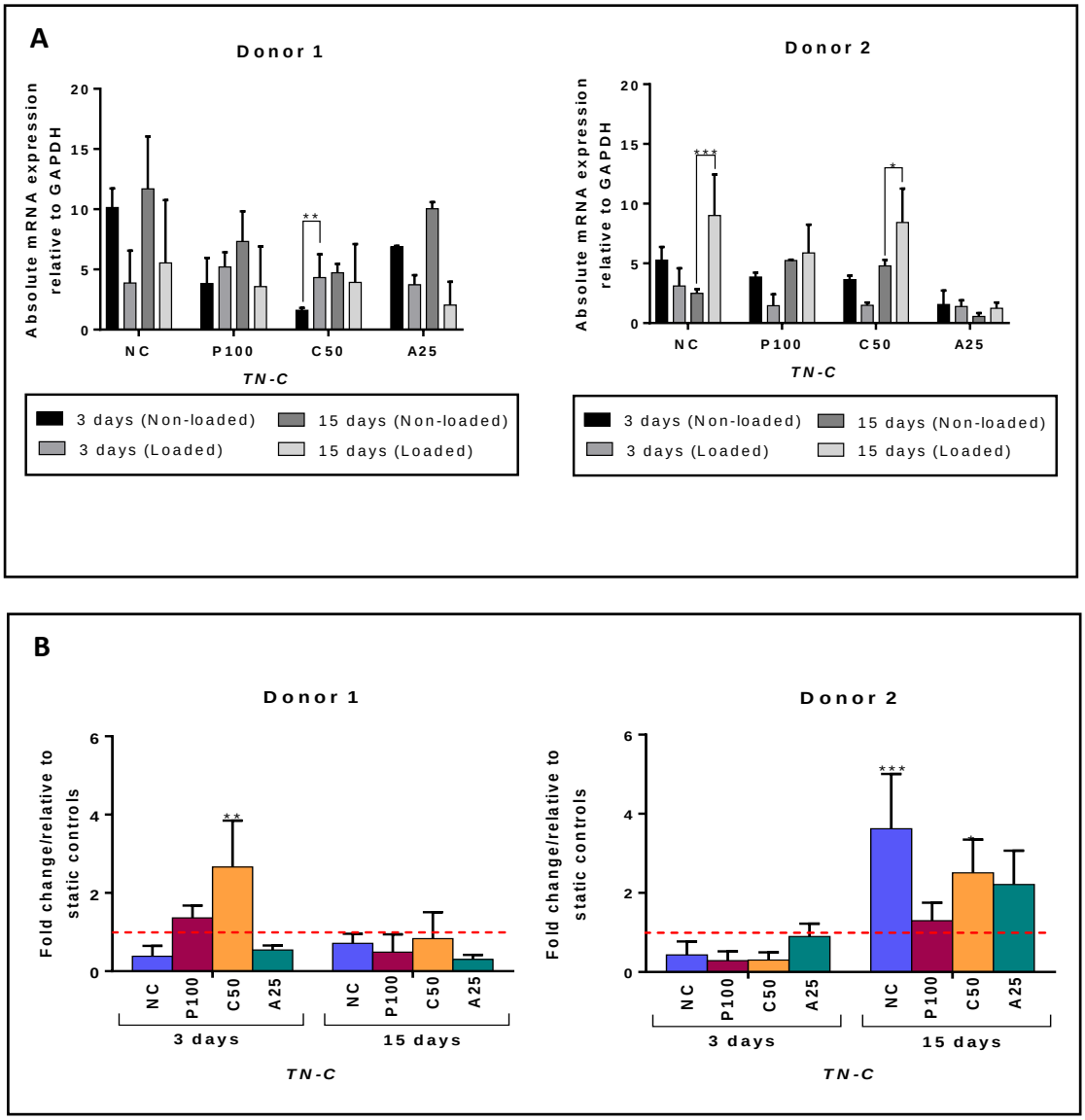

Figure 4.21 Effect of cyclic tensile strain on *TN-C* mRNA expression of bSCs in P100, C50 and A25 coated constructs.

The figure demonstrates the effect of applying cyclic tensile strain of 5% and frequency of 1 Hz (for 1 hour every day) on *TN-C* expression of bSCs within each construct (NC, P100, C50 and A25). Data is presented for 3 days and 15 days of culture with DMEM supplemented with 10% FBS, for two donors. Values are normalised to *GAPDH* expression. Statistical significance was determined using a one-way ANOVA. ** = $p \leq 0.01$, *** = $p \leq 0.001$.

A) Bars represent the mean absolute mRNA expression (Δ Ct) of non-loaded and loaded constructs ± relative standard deviation (n=3).

B) Bars represent the mean of the fold change (ΔΔ Ct) relative to corresponding non-loaded controls (indicated by the dotted line) ± relative standard deviation (n=3).

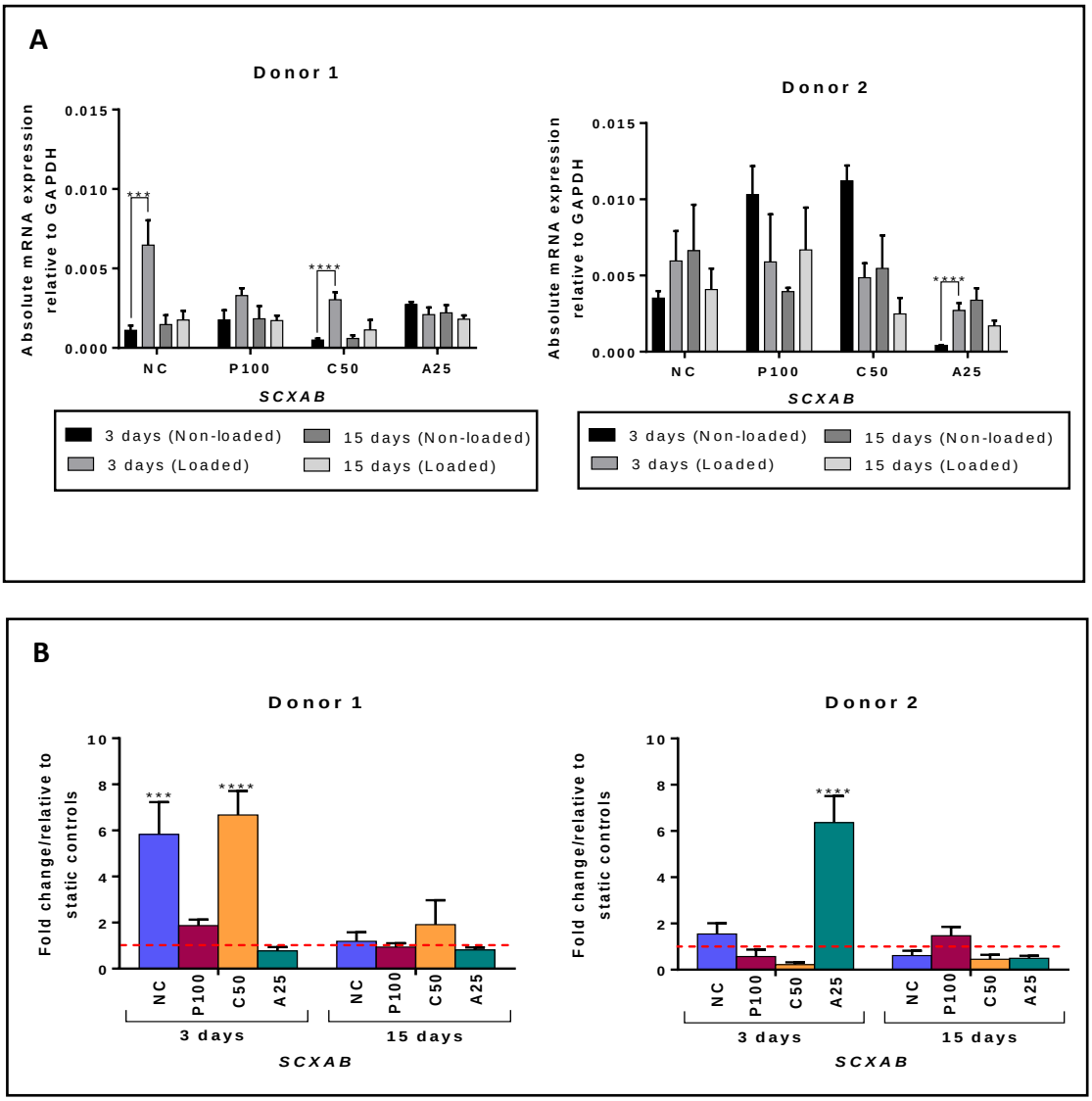

Figure 4.22 Effect of cyclic tensile strain on *SCXAB* mRNA expression of bSCs in P100, C50 and A25 coated constructs.

The figure demonstrates the effect of applying cyclic tensile strain of 5% and frequency of 1 Hz (for 1 hour every day) on *SCXAB* expression of bSCs within each construct (NC, P100, C50 and A25). Data is presented for 3 days and 15 days of culture with DMEM supplemented with 10% FBS, for two donors. Values are normalised to *GAPDH* expression. Statistical significance was determined using a one-way ANOVA. *** = $p \leq 0.001$, **** = $p \leq 0.0001$.

A) Bars represent the mean absolute mRNA expression (Δ Ct) of non-loaded and loaded constructs ± relative standard deviation (n=3).

B) Bars represent the mean of the fold change (ΔΔ Ct) relative to corresponding non-loaded controls (indicated by the dotted line) ± relative standard deviation (n=3).

RUNX2

The effect of cyclic tensile strain on *RUNX2* expression in bSCs is shown in Figure 4.23. A significant 2-fold ($p \leq 0.05$) decrease in *RUNX2* expression was measured in donor 1 cells in P100 coated constructs as a result of applying cyclic tensile strain for 3 days. Conversely, cyclic tensile strain induced a significant 2-fold ($p \leq 0.001$) increase in expression in cells within the C50 coated construct. Regarding donor 2 cells, a slight increase in expression was measured in P100 coated constructs subjected to cyclic tensile strain (1.8-fold, $p \leq 0.05$). No other significant differences in expression of *RUNX2* were identified as a result of applying cyclic tensile strain.

By 15 days, *RUNX2* expression was significantly reduced in donor 1 cells as a result of applying cyclic tensile strain to all coated constructs (approximately 2-fold, $p \leq 0.05$). Donor 2 cells in all constructs demonstrated no change in expression level by 15 days, in comparison with non-loaded constructs.

A summary of the results presented in this section can be found in table 7.

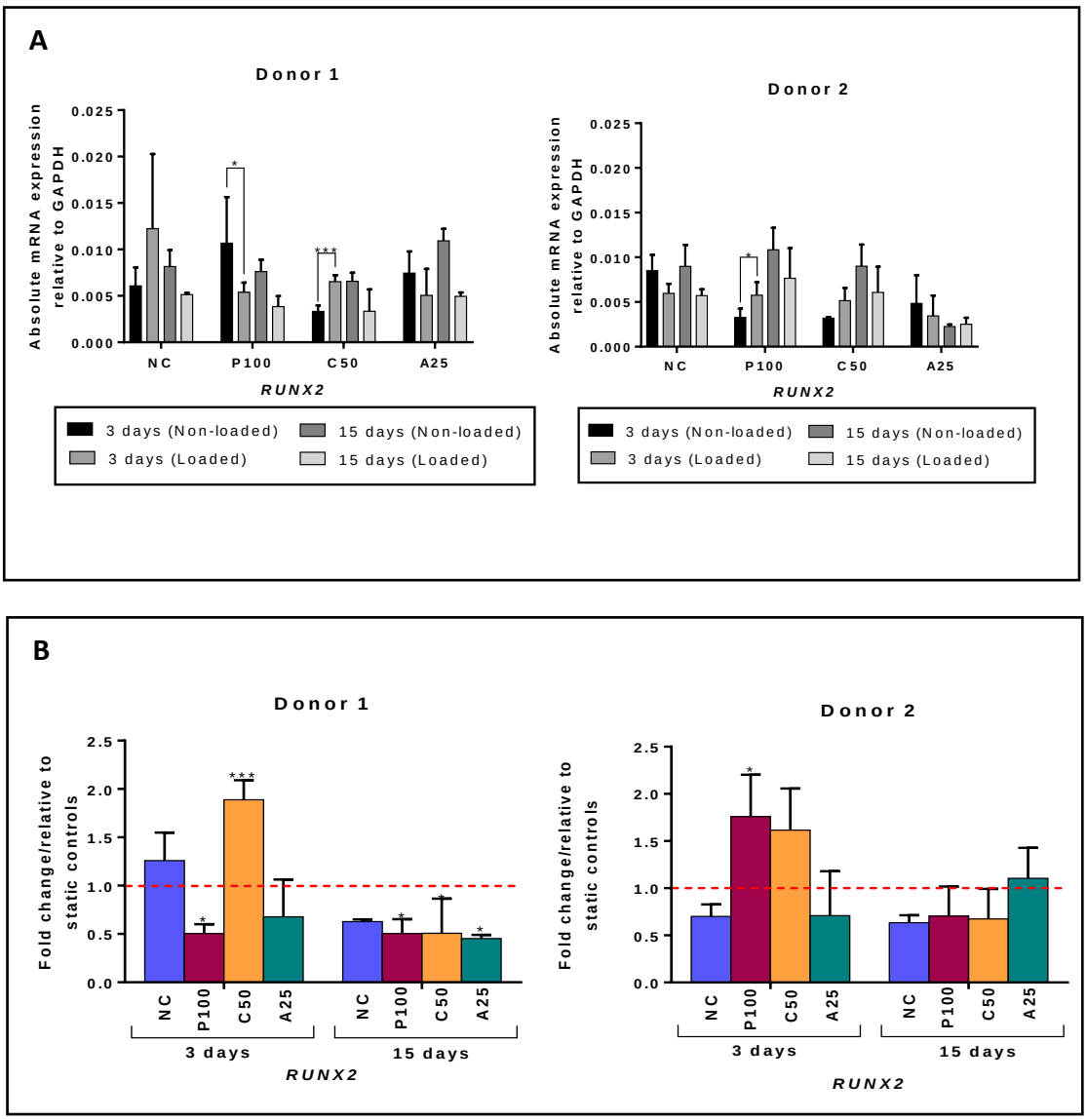

Figure 4.23 Effect of cyclic tensile strain on *RUNX2* mRNA expression of bSCs in P100, C50 and A25 coated constructs.

The figure demonstrates the effect of applying cyclic tensile strain of 5% and frequency of 1 Hz (for 1 hour every day) on *RUNX2* expression of bSCs within each construct (NC, P100, C50 and A25). Data is presented for 3 days and 15 days of culture with DMEM supplemented with 10% FBS, for two donors. Values are normalised to *GAPDH* expression. Statistical significance was determined using a one-way ANOVA. * = $p \leq 0.05$, *** = $p \leq 0.001$.

A) Bars represent the mean absolute mRNA expression (Δ Ct) of non-loaded and loaded constructs ± relative standard deviation (n=3).

B) Bars represent the mean of the fold change (ΔΔ Ct) relative to corresponding non-loaded controls (indicated by the dotted line) ± relative standard deviation (n=3).

Table 7 Summary of cellular gene expression changes in response to cyclic tensile strain.

		NC		P100		C50		A25	
	Gene	Donor 1	Donor 2	Donor 1	Donor 2	Donor 1	Donor 2	Donor 1	Donor 2
3 days	*COL1A1*	NS	NS	17 (p≤0.0001)	NS	6 (p≤0.01)	NS	NS	NS
	COL3A1	NS	NS	10 (p≤0.0001)	NS	NS	NS	NS	NS
	TN-C	NS	NS	NS	NS	2.7 (p≤0.01)	NS	NS	NS
	SCXAB	5.8 (p≤0.001)	NS	NS	NS	6.7 (p≤0.0001)	NS	NS	6 (p≤0.0001)
	RUNX2	NS	NS	2 (p≤0.05)	1.8 (p≤0.05)	2 (p≤0.001)	NS	NS	NS
15 days	*COL1A1*	NS	3.8 (p≤0.05)	NS	NS	NS	NS	NS	NS
	COL3A1	7 (p≤0.01)	4 (p≤0.001)	NS	NS	6 (p≤0.01)	3 (p≤0.05)	NS	NS
	TN-C	NS	3.6 (p≤0.001)	NS	2.5 (p≤0.05)	NS	NS	NS	NS
	SCXAB	NS	NS	NS	NS	NS	NS	NS	NS
	RUNX2	NS	NS	2 (p≤0.05)	NS	2 (p≤0.05)	NS	2 (p≤0.05)	NS

Table 7 summarises the changes in *COL1A1*, *COL3A1*, *TN-C*, *SCXAB* and *RUNX2* gene expression resulting from the application of cyclic tensile strain to each construct (NC, P100, C50 and A25), after 3 and 15 days, in cells from donors 1 and 2. Values indicate the fold change in gene expression relative to non-loaded controls (green and red cells indicate upregulation and downregulation respectively). Statistical significance is presented in brackets. NS indicates no statistically significant difference.

4.3 Discussion

This section discusses the results presented in section 4.2 in which further tests were carried out on P100, C50 and A25 coated constructs only, with non-coated scaffolds serving as the control. These tests included cell viability analysis and gene expression analysis. The PDGF and IGF-1 release profiles from each construct were also characterised, and physical assessments of the coatings were conducted using SEM and rheology. Finally, these constructs were also subjected to cyclic tensile strain (5% at a frequency of 1 Hz) to determine how the forces experienced by the ACL in *vivo* would affect cell proliferation, infiltration and gene expression of cells within these constructs.

4.3.1 Cell viability within coated constructs

It is essential that a tissue engineered construct supports good cell viability so that the constructs can be highly populated with functional cells that will eventually synthesise matrix proteins crucial for maturation of the graft. Live/dead staining was used to assess the viability of bSCs in each of the constructs evaluated in this phase of the project (P100, C50 and A25 coated constructs). Good viability was seen in bSCs within all constructs at day 15 of culture, with very limited numbers of dead cells identified in any of the fields imaged (see Figure 4.4). Even the A25 coating, which induced relatively poor proliferation and inhibited cell infiltration (see sections 3.2.2.1 and 3.2.2.2, Chapter 3), demonstrated cell viability similar to the non-coated control. This is consistent with work conducted by Zhou and Xu, (2011), in which human umbilical cord mesenchymal stem cells were encapsulated in beads composed of either alginate only, or a mixture of alginate and fibrin. Live/dead staining showed very high viability of cells within both bead types, up to 21 days. Furthermore, cells were found to migrate out of the alginate/fibrin beads within 4 days, whereas cells within alginate beads remained encapsulated until the final 21 day time point. This is consistent with the improvement in cell infiltration which was demonstrated by increasing the plasma proportion of the coating, and reducing the alginate proportion, which was reported in Chapter 3. This indicates that cells remain viable even in environments where proliferation and migration is limited. A high level of cell viability has also previously been demonstrated with endothelial cell and MSCs co-cultured in collagen/fibrin gels (Rao *et al*., 2012). The study reported a viability of almost 100% by day 7.

The LIVE/DEAD^{TM} viability/cytotoxicity kits have been found to have limitations. As the dead stain (ethidium homodimer-1) only fluoresces when bound to DNA, any dead cells which have lost their DNA through enzymatic degradation would not be detected as a dead cell. This limitation was previously described by Zhou *et al.* (2011), who found that the presence of DNase I in serum used to supplement cells, led to DNA breakdown within dead cells and a

subsequent underestimation of dead cell percentage when compared to the results of a trypan blue assay. However the live/dead assay was the only viability assay that was found to be compatible with this 3D system. Most other viability/cytotoxicity assays rely on colorimetric methods (such as the commercially available LDH or MTS assays), which gels can interfere with as a result of their optical properties. Cell infiltration, proliferation, and live/dead staining were all taken into account when forming an understanding of how bSCs tolerate the environment of each construct.

4.3.2 PDGF-AB and IGF-1 release from coatings

The poor regenerative capacity of the ACL is often attributed to its limited blood supply. Normally, when a tissue is damaged, the rupturing of blood vessels causes blood to flow to the injured area, and cell signalling coordinates formation of a blood clot. Within the clot are cells, as well as platelets, which mediate healing through release of cytokines and growth factors (Velnar *et al*., 2009). By producing coated constructs containing platelets, it was anticipated that growth factors would be released at physiologically relevant ratios, and that this would stimulate a normal healing process. Two growth factors in particular, PDGF and IGF-1, are of high importance in regulation of tissue healing (Molloy *et al.,* 2003). Previous work has also identified PDGF-AB (the PDGF isoform detected in this study) and IGF-1 as two of the most abundant growth factors released from platelets, with concentrations being measured at thousands of times greater than less abundant growth factors, such as FGF (Durante *et al.,* 2013). Detection of more abundant molecules reduces the chance of samples containing concentrations of target molecules below the detection limit of the assay. To investigate the release of PDGF and IGF-1 from coated constructs, platelet-rich coatings were applied to the PET scaffolds. This was to ensure detectable levels of growth factor release. All other studies described in this chapter used platelet-poor coatings to evaluate the cellular responses to the gel matrices of the coatings.

All coatings showed a similar duration of PDGF-AB and IGF-1 release, with total release occurring 3 days after activation (see Figure 4.5). The media content of both growth factors surpassed the concentration resulting from supplementation with 10% FBS, within the first hour of release. The final concentration of each growth factor was between 13 and 30 times greater than the concentration of FBS supplemented media.

PDGF is an essential mediator of cell proliferation and migration, however, these two processes are mutually exclusive, and one is favoured over the other depending on the PDGF concentration to which a cell is exposed. A study conducted by De Donatis *et al.* (2008) exposed NIH3T3 fibroblasts to varying concentrations of PDGF, and found that significant proliferation was only induced with concentrations >5 ng/ml. In contrast, the cell migratory

response was induced by PDGF concentrations of just 1 ng/ml, and became negligible at higher concentrations. Even in the platelet rich system used in the present study, the maximum PDGF concentration measured was just 1.7 ng/ml (see Figure 4.5 A); well below the 5 ng/ml reportedly necessary for inducing proliferation. However, bSCs were found to both migrate and proliferate, possibly suggesting that not all cells are defined by these thresholds. Moreover, platelets release a number of other growth factors which stimulate proliferation and migration, including bFGF and EGF, which likely contribute to this effect. For a more comprehensive understanding of growth factor release from the coatings, a greater number of growth factors could be quantified. Commercially available antibody arrays are able to detect more than 40 target molecules within a sample. However, these products are expensive and not as quantitative as an ELISA, which was the detection method used in this study. With the large number of samples and time points used in this investigation, the use of arrays would not have been feasible.

IGF-1 is involved in normal growth and healing, and tissues which lack this growth factor have been found to have significantly impaired healing (Steenfos *et al.*, 1989). The primary function of IGF-1 is to promote cell proliferation and migration at the inflammatory stage of tissue healing, and to stimulate synthesis of ECM components during the remodelling phase (Molloy *et al.*, 2003).

All coatings showed significant differences in total IGF-1 release ($p \leq 0.0001$), with C50, P100 and A25 coatings releasing a total of 6.7, 4.5 and 10.3 ng/ml respectively over 9 days (see Figure 4.5 B). The constructs used to measure growth factor release were non-seeded, to prevent cellular sequestration of growth factors. This means that collagen and fibrin matrices would not have been subjected to enzymatic breakdown caused by cellular activity, potentially slowing the diffusion of IGF-1 into the media. Alginate, however, will dissolve in media by the process of ion-exchange. DMEM contains Na^+ ions, which readily displace Ca^{2+} ions forming the calcium alginate gel. This would lead to gradual dissolution of the A25 construct coating, subsequently releasing growth factors captured within the matrix (Bajpai and Sharma, 2004). The high IGF-1 release from the A25 coating, relative to the C50 and P100 coatings, could be due to variations in matrix stability. If growth factor release positively correlates with coating loss, it is expected that the presence of cells within P100 and C50 coated constructs would increase growth factor release into the media.

The findings presented in this section demonstrate that platelet-rich constructs were able to release PDGF-AB and IGF-1 over a period of 3 days, which is consistent with work conducted by Kobayashi *et al*., (2016) which found that platelet-rich fibrin gels released very little PDGF-AB or IGF-1 after 3 days. The concentrations of growth factors released from the

coatings were significantly greater than those achieved by supplementation with 10% FBS. Although negligible PDGF and IGF-1 was found to be released after 3 days, it is possible that some remained trapped within the coating matrices. To determine whether this is the case, the coatings would need to be digested following completion of the study, and growth factor quantification of the digested coating could then be carried out.

4.3.3 Structural and mechanical characterisation of coatings

Coatings were also physically characterised to understand how their structure may influence the behaviour of cells. Platelets were visible in many of the images generate by scanning electron microscopy (SEM), and it was noted that platelets in PPP/collagen gels were embedded within the matrix, whereas in the A25 coated construct, platelets could be seen protruding onto the surface of the gel. The gel structure of the P100 coating was the most open of the three, but was composed of the thickest fibrils (0.25-0.5 μm). By combining PPP and collagen at a 1:1 ratio, the matrix became denser, and the fibril diameters decreased (0.1-0.2 μm) (see Figure 4.6). This is consistent with work carried out on collagen-fibrin co-gels by Lai *et al.* (2012), in which the diameter of fibrin fibrils was found to decrease with an increase in collagen content. The total matrix-forming protein concentration within PPP was 2.9 mg/ml, whereas combining collagen (5 mg/ml) and PPP at a 50:50 ratio to produce the C50 coating would result in a total protein concentration of 3.9 mg/ml. An increase in matrix density is therefore expected, due to this increase in total matrix-forming protein. It is worth noting that preparing hydrogels for SEM analysis by vacuum desiccation can introduce drying artefacts which may result in some alteration of the gel structure.

The A25 gel structure was much more closed than P100 or C50 (see Figure 4.6), which may explain the inhibition of cell infiltration previously described in Chapter 3 (section 3.2.2.2) resulting from incorporation of alginate into coatings. The platelets on the surface of the A25 construct may have migrated from within the construct or, alternatively, their position may be the result of an inability to infiltrate into the construct. The active migratory response of platelets was proven in 1973 (Lowenhaupt *et al.,* 1973), with collagen being the first described platelet chemotactic agent (Lowenhaupt, 1982). Other chemotactic agents to which platelets respond have since been discovered, including formyl peptides (cleavage products of mitochondrial and bacterial proteins) (Czapiga *et al.,* 2005) and stromal cell-derived factor-1α (SDF-1α) (Kraemer e*t al*., 2010). It is possible that the position of platelets on the outside of A25 constructs is the result of a chemotactic response, although further work would be required to confirm this.

Rheology was also used to physically characterise each gel. Oscillatory amplitude sweeps were conducted at 1Hz and showed that all samples had parallel G’ and G’’ moduli, with G’

remaining higher in the linear viscoelastic region (LVER), indicating that each gel was in a solid-like state. Each sample varied in their maximum shear strain, with the A25 gel being able to withstand the greatest strain, and the C50 withstanding the lowest (see Figure 4.7).

As discussed previously, the A25 coating was found to be the most durable of the three, in response to cellular activity. The amplitude sweeps also demonstrated this gel to be the stiffest of the three, indicated by its comparatively high G' modulus. By incorporating just 25% alginate into the PPP gel, the G' was increased approximately 10-fold (in comparison with gels composed of PPP only). The amplitude sweep conducted on the gels also indicated that the A25 coating had the longest linear viscoelastic region (LVER), and was able to tolerate strain of up to 10% before damaging the structure. P100 was the softest gel, and addition of 50% collagen caused a 6-fold increase in the G'. However, this addition of collagen caused a shortening of the LVER, indicating that the gel structure started to break when subjected to a strain of just 0.06%. This was substantially less than P100, which was able to tolerate a shear strain of up to 1%. These observations are consistent with the work of Lai *et al.* (2012) who found that the macroscopic stiffness of their collagen-fibrin co-gels increased with increasing collagen content, and in turn, a reduction in extensibility was observed. This is indicative of some form of interaction between collagen and fibrin fibrils, however understanding of these interactions is limited.

A well-defined characteristic of collagen and plasma gels, which could not be identified in this study, was their ability to undergo strain hardening. Work by Weigandt and colleagues showed that gels formed from low concentrations of fibrinogen (~3mg/ml), start to harden at a strain of around 3%. In essence, the application of strain to these gels has been found to causes them to harden. This presents as an increased G' modulus with increasing strain (Weigandt *et al.,* 2009). However, the P100 gel was found to have a maximum shear strain of just 1%, which is inconsistent with rheological measurements of other fibrin gels, published in the literature.

Frequency sweeps were conducted in the linear viscoelastic region (the region in which the gel structure was still intact) to further characterise the samples. All gels had parallel storage (G') and loss (G'') moduli, with G' remaining higher than G'' within this region, indicating that the stored energy of the gels (G') remained higher than the dissipated energy (G''). This is typical of solid-like viscoelastic hydrogels (Okamoto *et al.,* 2017).

4.3.4 Effect of coatings on gene expression

Gene expression analysis was conducted on bSCs cultured within each of the constructs in an attempt to acquire an understanding of their differentiation pathway. The effect of P100, C50

and A25 coatings on the expression of five target genes (*COL1A1, COL3A1, TN-C, SCXAB and RUNX2*), were analysed using qRT-PCR (the data is presented in section 4.2.6.2). It is well known that matrix stiffness directs lineage specification in cells (Humphrey *et al.,* 2014), and since physical characterisation showed notable differences in the matrix density and stiffness of each gel, it was necessary to establish how cells responded to these differences. This section discusses the transcriptional response of bSCs to the coated constructs under non-loaded conditions only, and does not address changes resulting from applying tensile strain. Two donors were used to explore variations in gene expression to account for genetic variation.

Collagen type I is a key component of the ligament extracellular matrix (ECM), and any increase in expression would suggest a possible increase in tissue induction. The trend in Figure 4.10 suggests that *COL1A1* expression decreased slightly at the early time point (3 days) as a result of all coatings, although this was not statistically significant in either donor. Expression recovered by 15 days in P100 and C50 coated constructs, and even increased beyond the non-coated control, in cells from the second donor within P100 coated constructs. This increase was not evident in A25 constructs, which maintained a consistently low *COL1A1* expression in comparison with the control (although this was not significant). A possible explanation for this time dependent change in expression could lie with the degradation profiles of each gel. Minimal P100 and C50 coating loss was seen by day 3 of culture, resulting in more cells adhering to the gel fibrils. By 15 days, much of the gel was lost, forcing more cells to interact with the PET fibres of the scaffold. The change in *COL1A1* expression in these constructs may be a response to the changing substrate stiffness. A study by Xu *et al*. (2017) demonstrated that MSCs increase collagen type I expression with increasing matrix stiffness, by culturing the cells on polyacrylamide gels of varying stiffness. Cummings *et al*., (2004) measured the Young's modulus of fibrin and fibrin/collagen mixed gels and found that fibrin gels of 2 mg/ml (plasma used in this project had a fibrinogen concentration of 2.89 mg/ml) had a Young's modulus of 28 KPa. Their 50:50 fibrin/collagen gels with a total protein concentration of 4 mg/ml (the C50 coating gel has a calculated total protein concentration of 3.9 mg/ml) had a stiffness of 116 KPa. The Xiros PET ligament is said to have stiffness similar to the ACL (Fujikawa *et al.*, 200), which has a Young's modulus of 980 MPa, which is more than 8000 times greater than either of the gels. Based on this evidence, it is possible that the initially low *COL1A1* expression measured at 3 days (in cells within P100 and C50 coated constructs) is the result of interaction of cells with the P100 and C50 coatings. By 15 days, due to substantial loss of these coatings, it is likely that most cells would be interacting with the stiffer PET fibres of the scaffold, leading to slightly raised expression levels. Owing to the

enhanced stability of the A25 gel, cells would remain in contact with the gel matrix for the duration of the culture period, maintaining a low *COL1A1* expression.

In the ACL, Collagen type III is much less abundant than type I, but is still an important component of the ligament ECM. In response to the hybrid construct, bSCs showed little alteration in expression of *COL3A1* (see Figure 4.11). Like *COL1A1*, slight early downregulation was detected which tended to recover by 15 days (not significant in either donor). Again, this trend was only detected in P100 and C50 constructs, suggesting that this may be the result of gel degradation and subsequent alteration in substrate stiffness. *COL3A1* expression has previously been found to be affected by substrate stiffness, with substrates with a higher Yong's modulus inducing greater expression (Karamichos *et al.*, 2007).

Tenascin-C is a large glycoprotein component of the extracellular matrix. Its expression is mainly confined to tissues which are subjected to high tensile forces, such as ligaments, as well as tendons and muscle tissues (Chiquet *et al.*, 2009). It is not surprising then that under non-loaded conditions, no consistent upregulation was detected in response to the hybrid scaffolds (see Figure 4.12). Slight increases in expression in P100 and C50 constructs (in donor 2 cells) over time may, again, be attributed to changes in the mechanical cues experienced by cells as the gels degrade.

Scleraxis is a transcription factor involved in the regulation of tendon and ligament development. It is highly expressed in both progenitor and terminally differentiated cells of the ligament lineage (Wang *et al.*, 2011). Slight changes in *SCXAB* expression were detected but these were inconsistent across donors and may have been the result of donor variation (see Figure 4.13). Greater understanding of how these coatings influence gene expression might be achieved by using a greater number of donors.

RUNX2 encodes a transcription factor which determines the osteoblastic lineage in mesenchymal stem cells (Komori, 2008). As such, *RUNX2* expression is expected to be low in cells differentiating towards the ligament lineage. As there is no definitive marker for ligament differentiation, expression levels of *RUNX2* were used to rule out osteogenic differentiation. No significant upregulation of *RUNX2* was observed in hybrid constructs, which suggests that the properties of the gels did not induce an osteogenic response (see Figure 4.14). Some early reductions in expression could be the result of cells interacting with the gels, which have a much lower stiffness than the PET scaffold. *RUNX2* expression has been linked to matrix stiffness (Hwang *et al.*, 2014).

4.3.5 Effect of cyclic tensile strain on cell proliferation and infiltration

Cell-seeded constructs were then subjected to cyclic tensile strain of 5%, at a frequency of 1 Hz, for 1 hour every day, to mimic the mechanical forces to which the constructs would be subjected *in vivo*. A frequency of 1 Hz approximately represents walking speed, and a strain amplitude of 5% is reflective of the maximum strain likely to be applied to the graft during normal activities (Beynnon *et al*., 1995). Cyclic tensile strain was applied to all coated constructs (P100, C50 and A25), as well as the non-coated control scaffold, to assess its effect on bSC proliferation, infiltration and gene expression. Selection of these parameters was based on previous work by Raif *et al.* (2005), which found these conditions to be optimal for maximum stimulation of bSCs.

By applying cyclic tensile strain, bSC proliferation was consistently increased by an average of 2-fold across all constructs, by conclusion of the experiment at day 15 (see Figure 4.17). This demonstrates a significant stimulatory effect and consistent force transmission to cells within each construct. *In vivo,* transmission of the forces to coloniser cells within the graft is crucial for stimulating ECM remodelling and tissue induction (Humphrey *et al.*, 2014).

Again, some variation in response between donors was detected. For example, a 3-fold increase in proliferation was detected in donor 2 cells in response to applying strain to A25 coated constructs. However, no change was detected in donor 1, possibly indicating some discrepancies in force transmission through the A25 coating, or differences in the response of cells from different donors. The proliferation rate of cells from donor 1 were consistently lower than donor 2, with donor 1 DNA increases as little as a third of the value measured with donor 2, despite both donor's cells being seeded at the same density. Phinney *et al*. (1999) have also reported significant variations in proliferation, as well as gene expression of cells from different donors. They found that growth rates of human bone marrow MSCs varied 12-fold between donors, and that the expression of alkaline phosphatase, bone sialoprotein and parathyroid hormone receptor varied substantially between donors. They also found no correlation with age nor gender. This highlights the difficulty of establishing consistent trends using cells from different donors.

To evaluate the effect of cyclic strain on cell infiltration, confocal microscopy was used to visualise bSCs after 15 days, under non-loaded and loaded conditions (see Figure 4.18). A greater number of cells could be seen in all loaded constructs, but this was most evident in non-coated scaffolds, which showed large areas of cell bridging between PET fibres when strain was applied. Both P100 and C50 coated constructs showed almost total loss of void filling by 15 days, under non-loaded conditions, with cells no longer being able to fill the entire scaffold. When cyclic strain was applied, this coating loss appeared to be substantially

reduced in the P100 coated construct, with cells continuing to completely fill the voids up to 15 days. The hindered dissolution of fibrin when exposed to mechanical stress has previously been described by Varjú *et al.* (2011). This effect was not evident in C50 constructs, which still showed considerable gel loss by 15 days under loaded conditions. Investigation into the mechanism behind this construct preservation is discussed in Chapter 6.

Cells cultured within the in A25 coated constructs appeared to be more uniformly dispersed when loaded, with greater infiltration of cells into the voids. This may be linked with the higher PPP content remaining at 15 days as a result of mechanical strain. Indeed, Shikanov *et al*. (2009) have previously demonstrated the independent degradation of fibrin from fibrin-alginate interpenetrating networks. Without application of strain to A25 coated constructs, it is expected that the fibrin component will degrade, leaving only the alginate. If this is the case, it could explain the difference in uniformity of cells cultured in non-loaded and loaded A25 coated constructs. The overall durability of A25 coatings remained high in both non-loaded and loaded constructs, although some areas of gel breakage were evident in loaded A25 coated constructs, suggesting that this gel may fatigue with prolonged cyclic strain. As previously described in Chapter 1 (section 1.6.3), alginate is composed of a number of M and G monomers. A study which investigated the relationship between the proportions of M and G monomers composing alginate found that gels with a high M content were more elastic than those with a high G content (Mancini *et al*., 1999). Information on the composition of the alginate used in this project was not supplied upon purchase. Perhaps the use of an alginate with a high M content could be considered for future studies. This may prevent areas of gel breakage upon application of strain, or may have an effect of cell behaviour.

4.3.6 Effect of cyclic tensile strain on gene expression

Mechanical cues are also crucial for differentiation of cells towards the desired lineage, and significant alterations in gene expression, particularly of ECM genes have previously been demonstrated with the application of mechanical strain to cell-seeded substrates (Li *et al.*, 2012; Humphrey *et al.*, 2014). The genetic response of bSCs to cyclic tensile strain (5% at a frequency of 1 Hz, for 1 hour every day) was assessed in each coated construct (P100, C50 and A25), as well as the non-coated control, using qRT-PCR. Five target genes were analysed (*COL1A1, COL3A1, TN-C, SCXAB and RUNX2*), and expression levels were measured after 3 and 15 days of applying cyclic tensile strain, using cells from 2 donors.

The effect of cyclic strain on *COL1A1* expression differed substantially between donors (see Figure 4.19). Cyclic tensile strain of 5% at a frequency of 1 Hz induced a significant early upregulation in bSCs from donor 1, in both P100 and C50 constructs (17-fold and 6-fold increase respectively). However, since the expression level is relative to the corresponding

non-loaded construct, in which expression was found to be substantially reduced, this may explain the high fold change. It is likely that by applying strain, the mechanical properties of the gels themselves was altered, by forcing out liquid as the fibrils were pulled tight (Brown *et al*., 2009). As previously discussed in this chapter, fibrin and collagen have been shown to undergo strain hardening, whereby the storage modulus increases upon application of strain. This could offer some explanation for the early difference in expression. If the stiffness of the substrate is increased, it is possible that cells will respond by increasing transcription of a number of mechanosensitive genes, including COL1A1 (Xu *et al*., 2017). Donor 2 did not demonstrate this early upregulation, which is consistent with other studies which demonstrate that *COL1A1* tends to be upregulated at later time points. Subramony *et al.* (2014) applied strain of 1% at a frequency of 1 Hz to poly(lactide-*co*-glycolide) (PLGA) scaffolds seeded with MSCs, for 90 minutes, twice daily. They found that loading the cell-seeded scaffolds caused greater expression of collagen type I by day 7, but no difference was measured between loaded and unloaded scaffolds at earlier time points.

In general, applying cyclic tensile strain did cause an increase (between 2 and 4-fold) in the average *COL1A1* expression measured after 15 days. However, this was not consistent in all constructs with all donors. It is likely that the presence of the gels caused some interference in force transmission to the cells, and may also have provided mechanical cues which do not promote collagen synthesis. Conducting this study with a greater number of replicates and additional donors could reveal a more conclusive trend of *COL1A1* upregulation with the application of cyclic tensile strain, but this cannot be confirmed in the study presented here.

Expression of *COL3A1* in response to mechanical strain showed a similar trend to *COL1A1,* in that upregulation generally occurred at the later time point (see Figure 4.20). This trend was, again, particularly evident in donor 2, and less so in donor 1. As with *COL1A1* expression, significant upregulation was seen early on in donor 1 (3-10-fold), in response to cyclic tensile strain of 5% at 1 Hz. As explained in the context of *COL1A1* expression, the fold-change in expression is relative to corresponding non-loaded constructs, and so the high fold-change measured in donor 1 cells in response to cyclic tensile strain is a reflection of the low level of expression measured in non-loaded constructs. By applying cyclic tensile strain to constructs, the mechanical properties of the gel coatings would likely have been altered (by pulling the fibrils tight and forcing out liquid). A sudden increase in stiffness of coated constructs could be responsible for discrepancies in trends between coated and non-coated constructs, particularly in donor 1 at day 3. Non-coated scaffolds showed the expected time dependent increase in *COL3A1* expression with cyclic tensile strain, in both donors, which has previously been demonstrated (Subramony *et al.,* 2014).

A number of studies have implicated mechanical stress in the regulation of TN-C expression both *in-vitro* (Chiquet-Ehrismann *et al.,* 1994) and *in-vivo* (Jarvinen *et al.,* 1999). Previous work looking at *TN-C* expression in response to mechanical strain has indicated that upregulation tends to occur at around 2 weeks (Subramony

et al., 2013). Furthermore, this same study found that upregulation could only be induced in scaffolds composed of aligned fibres. In the present study, late upregulation was only induced in bSCs from donor 2 upon application of strain and was not evident in donor 1 (see Figure 4.21). This may be the result of variation between donors. Interestingly, Chiquet-Ehrismann *et al.* (1986) found that culturing fibroblasts in the presence of foetal bovine serum induced expression of *TN-C.* As both non-loaded and loaded constructs were cultured in the presence of FBS in this phase of the project, this could have dampened other potential changes in *TN-C* expression resulting from strain application. Another factor which has been found to affect *TN-C* expression is the presence of MMPs (Jones *et al*., 2000). As cyclic tensile strain has been found to upregulate MMP-3 expression in bovine synovial cells (Raif, 2008), this suggests another mode by which *TN-C* expression might be indirectly modulated by strain.

Changes in *SCXAB* expression were also inconsistent across donors. Application of cyclic tensile strain tended to cause an early upregulation of *SCXAB* which returned to basal level by 15 days (see Figure 4.22). However, this did not occur in every construct type. This was particularly evident in donor 1, although this is inconsistent with previous work by Subramony *et al.* (2013) which showed *SCX* upregulation to occur later. This was also found to be dependent on fibre alignment. SEM analysis was only conducted on cells which had not been subjected to strain. Kang *et al.* (2009) and Brown *et al*. (2009) have demonstrated that application of strain to fibrin gels promotes fibre alignment. Assuming *SCX* expression is dependent on fibre alignment, and that cyclic strain does promote fibre alignment, this would suggest that strain would cause an upregulation in *SCX* expression within the system presented in this project. As this was not the case, further investigations into the factors which affect *SCX* expression should be carried out.

Some early upregulation of *RUNX2* was seen as a result of loading P100 and C50 constructs, but this may be a response to the shift in the construct's mechanical properties, as previously discussed in this chapter (see Figure 4.23). An increase in substrate stiffness has been found to increase *RUNX2* expression (Hwang *et al*., 2014). Expression then decreased to below the level of non-loaded constructs by day 15, which suggests that cells were not induced into osteogenic differentiation by the application of cyclic tensile strain. This is consistent with work by Shi *et al*. 2010, which found that applying cyclic mechanical tension at a frequency of 0.5 Hz with a strain amplitude of 3%, to MSCs, inhibited *RUNX2* expression.

4.3.7 Rationale for the selection of the final coating

Following the studies detailed in this chapter, a final coating was selected from the 3 coatings tested in this phase of the study (P100, C50 and A25). The coating selected was considered to hold greatest promise in enhancing the Xiros PET ligament. The only coatings which had sufficient stability to support long-term cell infiltration throughout the construct were A25 and P100. Although the C50 coating maintained high levels of proliferation, the poor stability of the gel meant that cells which had infiltrated into the intra-fibre voids of the scaffold were either forced to return to the edges of the voids, or were lost from the construct along with the coating. While the A25 coating was, by far, the most stable construct under non-loaded conditions, the application of cyclic tensile strain revealed the P100 coating to be the better candidate. Furthermore, in terms of cell proliferation and infiltration, the P100 coated construct consistently outperformed the A25 coated construct. By looking at the transcriptional response of bSCs, it was evident that cells within A25 coated constructs tended to express lower levels of mRNA for ECM genes such as *COL1A1* and *COL3A1* than cells within the other constructs (see Figures 4.19 A and 4.20 A) . Furthermore, significant transcriptional responses to strain were identified far less frequently in A25 coated constructs in comparison with other constructs (see Table 7). These supressed expression levels could be the result of an elongated cell growth phase due to the lower proliferation rate identified in A25 constructs. Indeed, before differentiation and ECM synthesis can take place, cells must reach confluency (Ruijtenberg and Van den Heuvel, 2016). For the reasons discussed here, the P100 coating was brought forward for the final phase of testing.

4.3.8 Summary

During this phase of the project, 3 platelet-poor coated constructs (P100, C50 and A25) were compared with the non-coated Xiros PET scaffold by monitoring cell viability and expression of ligament and non-ligament associated genes in bSCs cultured within these constructs. The growth factor release profiles indicated that PDGF and IGF-1 are only released from each platelet-rich coating for approximately 3 days, after which, no additional release takes place. This should be taken into consideration when designing experiments in which platelets will be relied upon as the growth factor source for cells. Physical characterisation of each coating using SEM and rheology demonstrated variations in matrix density and mechanical properties between gels. The application of cyclic tensile strain (5% at a frequency of 1 Hz, for 1 hour every day) to each construct produced an increase in cell proliferation in almost all cases (the only exception being donor 1 cells cultured in A25 coated constructs), indicating the importance of applying regular forces to a graft following surgical reconstruction of the ACL. Confocal imaging of P100 coated constructs following 15 consecutive days of cyclic tensile

strain application revealed a vast improvement in coating longevity in comparison with non-loaded constructs, such that the gel supported complete cellular filling of the whole construct for the duration of the culture period. This finding led to selection of the P100 coating as the final test coating for subsequent investigation as a platelet-rich construct in Chapter 5.

Chapter 5

Evaluation of the final selected coating as a platelet rich construct

After selection of the P100 (100% PPP) coating as the most promising coating for enhancing cell proliferation and infiltration throughout the Xiros PET ligament, further tests were carried out to establish whether a platelet-rich P100 coating would induce greater cell proliferation or infiltration than the platelet-poor construct. Additionally, the expression of ligament and non-ligament associated genes was quantified to indicate whether a higher platelet density had any effect on differentiation. Cyclic tensile strain was also applied (5% strain at a frequency of 1 Hz, for 1 hour every day) to platelet-rich and platelet-poor coated constructs to investigate the combined effect of platelet-rich plasma and strain on cell proliferation, infiltration and gene expression.

Aim:

To conduct additional tests on a platelet-rich P100 coated construct to determine whether coating the Xiros PET scaffold enhances cell proliferation, infiltration and differentiation towards a ligamentous phenotype.

Objectives:

- Evaluation of cell invasion from the surrounding media into the P100 construct, in comparison with the non-coated control.

- Comparison of bSC proliferation rates between platelet-rich and platelet-poor P100 coatings, under non-loaded and loaded conditions.

- Comparison of cell infiltration throughout the platelet-rich and platelet-poor P100 coated construct, under non-loaded and loaded (5% strain at a frequency of 1 Hz, for 1 hour every day) conditions.

- Identification of any changes in expression of 5 ligament and non-ligament associated genes (*COL1A1, COL3A1, TN-C, SCXAB* and *RUNX2*) within bSCs as a result of a higher platelet density.

5.1 Materials and methods

This section describes the methods used to evaluate the platelet-rich P100 construct in terms of its ability to support cell proliferation and infiltration, as well as differentiation towards a ligamentous phenotype. Invasion of cells into the coated construct was assessed to determine whether cells would be able to attach to and invade the construct if implanted *in vivo*. Cyclic tensile strain (5% strain at a frequency of 1 Hz, for 1 hour every day) was also applied to constructs in this phase of the project using the bioreactor previously described in Chapter 4. It was anticipated that this would provide insight into how the constructs would respond to the forces experienced by the ACL *in vivo*.

5.1.1 Assessment of bSC invasion into the final coated construct

All previous methods leading to optimisation of the final construct involved using constructs produced by seeding the PET scaffold prior to coating. Although this ensures a consistent initial cell number for direct comparisons, in a clinical setting, the host's cells would need to invade the construct upon implantation. An assay was therefore designed to assess invasion of cells into the final coated construct (P100), in comparison with the non-coated scaffold.

5.1.1.1 Invasion assay setup

To compare cell invasion into coated and non-coated scaffold, non-seeded PET scaffolds were cut to 20 mm and coated with PRP (prepared from human blood using the method described in section 2.1.2), using the coating method detailed in section 3.1.3. The constructs were placed in 3.8 cm^2 wells of a 12-well plate, which were pre-coated with 1% agarose (to prevent cells from attaching to the bottom of the well) before being covered with a 1 ml cell suspension in DMEM containing 1 $x10^5$ bSCs, supplemented with 10% (v/v) FBS. Non-coated scaffolds were used in parallel as a comparison.

To determine a percentage infiltration from the total number of cells seeded, 3 wells of a 12-well plate (which had not been treated with agarose) were seeded with 1 ml of the same cell suspension. These wells were incubated overnight in a humidified atmosphere incubator containing 5% (v/v) CO_2 and 95% (v/v) air at 37˚C to allow cells to attach to the wells as a monolayer. These wells were then washed three times with PBS and cells were lysed with 500 µl of RLT buffer (Qiagen) for 30 minutes, to liberate the DNA. The total cell monolayer lysates were transferred to 1.5 ml microtubes before being frozen at -20˚C until the end of the experiment.

5.1.1.2 Light microscopy imaging of bSC invasion into the coated construct

After 72 hours in culture, the coated and non-coated constructs were imaged using a Zeiss Axiovert light microscope with in situ digital camera for qualitative analysis, using a 10 X objective lens.

5.1.1.3 Quantification of cell invasion into coated and non-coated constructs

Directly after imaging, all coated and non-coated constructs were washed three times in PBS and transferred to microtubes. The constructs were treated with 500 µl of RLT buffer (Qiagen) for 30 minutes, at room temperature, to digest the constructs. All lysates, including the total cell monolayer lysates, were passed through a QIAshredder column at 2000 *x g* for 5 minutes. A Quant-iT™ PicoGreen® DNA content assay (Invitrogen) was performed to compare invasion of cells into coated and non-coated scaffolds (detailed in section 3.2.1).

5.1.2 Monitoring cellular responses within platelet-poor and platelet-rich P100 coated constructs

Platelet-poor and platelet-rich coated P100 constructs were evaluated by assessing bSC proliferation, infiltration and gene expression for a maximum culture period of 4 days. This was due to the limited period of growth factor release identified in a previous growth factor release study (section 4.2.2), which indicated that total PDGF and IGF-1 release occurred by around 3 days after platelet activation. In this phase of the study, coated constructs were not supplemented with FBS, and so, since cells within coated constructs would be entirely reliant on growth factors released from platelets present in the coatings, all of the following investigations detailed in this chapter involve a maximum culture period of 4 days. The studies compare platelet-poor P100 and platelet-rich P100 coatings, and non-coated scaffolds were tested in parallel as positive and negative controls, by supplementing with either 10% FBS or 0.5% FBS respectively. Cyclic tensile strain was applied to all 4 of these constructs (PPP, PRP, 10% FBS and 0.5% FBS) for a total of 3 sessions (1 hour each day) before assessing the cellular responses.

5.1.2.1 Application of cyclic tensile strain to platelet-poor and platelet-rich P100 coated constructs

350 mm PET scaffolds were dynamically seeded (see section 3.1.2) with 3 x 10^5 bSCs and coated (see section 3.1.3) with platelet-rich and platelet-poor plasma (production of platelet-rich and platelet-poor plasma is detailed in section 2.1.2). Due to a limited period of growth factor release from the platelets, coating and clamping were performed on the same day.

Loading (see section 4.1.4.2) began on the following day, and the experiment was terminated after 3 consecutive days of loading (with 5% strain at a frequency of 1 Hz, for 1 hour every day). PRP and PPP coated constructs were cultured with serum-free media. Non-coated control scaffolds were cultured with media supplemented with either 10% or 0.5% (v/v) FBS. The same number of coated and non-coated cell-seeded constructs were maintained under non-loaded conditions in 9.5 cm^2 wells of a 6-well plate, pre-coated with 1% agarose (to prevent cells attaching to the bottom of the well). The length of the study was sufficiently short to eliminate the need for media replacement. This was to ensure maximum retention of growth factors (released from platelets) within the media.

5.1.2.2 Preparation of samples for assessment of cellular responses

At the end of their culture period, loaded constructs were cut from their clamps and non-loaded constructs were removed from their culture wells. The samples were blotted with Whatman filter paper to remove excess liquid and 1 cm sections were transferred to 1.5 ml microtubes for quantitative proliferation and gene expression analysis. The remaining portion of the construct was fixed in 10% NBF for subsequent confocal microscopy analysis (as described in section 3.1.2.2). Following treatment of the quantitative samples with 500 µl of buffer RLT (Qiagen) for 30 minutes at room temperature, the lysates were passed through a QIAshredder column (Qiagen) which was centrifuged at 2000 × *g* for 5 minutes, to homogenise the lysate and filter out any debris. 10 µl of the lysate was retained for DNA quantification, which was carried out using a Quant-iT™ PicoGreen® dsDNA assay according to the method in section 3.2.1. Results from this assay were used to quantify cell proliferation. The remaining 490 µl of lysate was used for mRNA isolation and subsequent gene expression analysis, which was carried out according to the method in section 4.1.5. The expression of *COL1A1, COL3A1, TN-C, SCXAB* and *RUNX2* were quantified using cells within non-loaded and loaded constructs, relative to *GAPDH*.

5.2 Results

This section presents the findings from investigations described in section 5.1, in which further investigations were carried out to evaluate the final P100 coated construct. The effect of the coating on cell invasion was assessed in comparison with the non-coated scaffold. The effect of platelet-rich and platelet poor coatings were compared to establish how different platelet densities affect cell proliferation, infiltration and expression of ligament and non-ligament associated genes within the final coated construct.

5.2.1 Assessment of cell invasion into the final P100 construct

If the P100 coated construct were to be used in a clinical setting, the host's cells would be required to innvade the construct upon implantation. The attachment and invasion of bSCs to the newly developed P100 coated construct was compared with the original non-coated PET scaffold. P100 coated constructs and non-coated scaffolds (20 mm in length) were incubated with 1 ml of a cell suspensions (containing 1×10^5 cells) for 72 hours before analysis, as described in section 5.1.1. Quantitative comparison was made by DNA quantification, and light microscopy was used for qualitative evaluation.

5.2.1.1 The P100 coating does not significantly hinder cell invasion into the construct

Figure 5.1 shows cell invasion into the non-coated (NC) scaffold and P100 construct, as the percentage DNA within each construct relative to the total DNA present in the initial cell suspension. 6.7% and 5.7% of cells invaded the non-coated scaffold and the P100 coated construct respectively. Although slightly more cells were able to attach to the non-coated scaffold, there was no statistically significant difference measured between non-coated and P100 coated constructs, indicating that the P100 coating does not hinder bSC attachment and invasion.

5.2.1.2 The P100 coating promotes a more uniform distribution of cells throughout the construct

Figure 5.2 shows light microscope images taken after the cells were allowed to attach and invade into the non-coated (NC) and P100 coated constructs for 72 hours. Non-coated scaffolds showed a number of areas where cells had aggregated upon attachment (indicated by red arrows in Figure 5.2). In contrast, cells were uniformly distributed throughout the P100 coating.

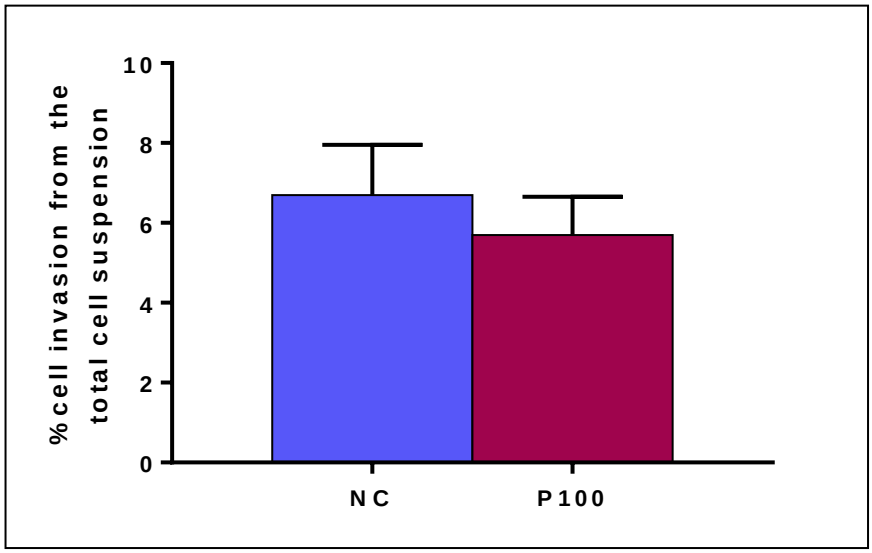

Figure 5.1 Percentage cell invasion into NC and P100 coated constructs.
Invasion of bSCs into non-coated and P100 coated constructs was measured by quantifying DNA content after 72 hours incubation with a cell suspension. Data is presented as the percentage DNA within each construct relative to the total DNA from the initial cell suspension. Bars represent the mean ± standard deviation (n=3). Statistical significance was determined using a t-test (no statistically significant difference was found).

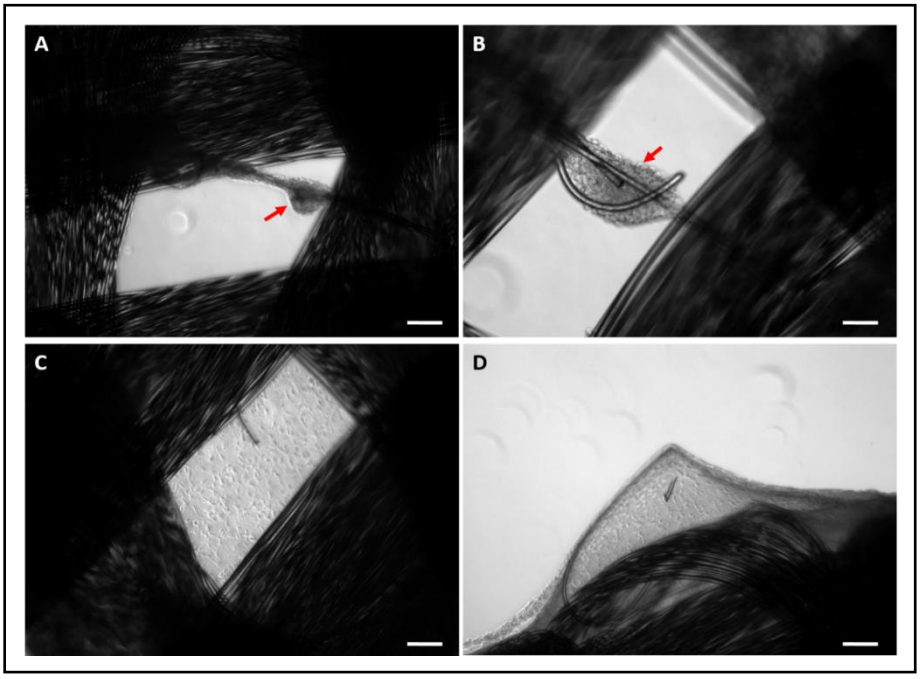

Figure 5.2 Visual assessment of cell invasion into the non-coated and P100 coated construct.
Light microscopy images of cell invasion into non-coated (A-B) and P100 coated (C-D) constructs, taken after 72 hours in culture with a suspension of bSCs. Arrows indicate areas of aggregated cells on the non-coated scaffold. Scale bar =200µm (10 × objective lens).

5.2.2 The effect of platelet density on the expression of ligament and non-ligament associated genes

In this phase of the project, platelet-poor and platelet-rich P100 (PPP and PRP respectively) coated constructs were compared by providing them with serum-free media only. Two non-coated controls were used, supplemented with either 0.5% or 10% FBS. A full description of the experimental setup is provided in section 5.1.2 Due to the limited duration of growth factor release (established in section 4.2.2), constructs were cultured for a total of 4 days before ending the experiment. Gene expression in bSCs was initially quantified to compare the effect of PPP and PRP coatings on the expression of ligament and non-ligament associated genes (*COL1A1*, *COL3A1*, *TN-C*, *SCXAB* and *RUNX2*. qRT-PCR was used to measure the effect of each treatment group (0.5% FBS, 10% FBS, PPP and PRP) on gene expression in bSCs from 2 bovines (donor 1 and 2). mRNA was extracted after 4 days in culture, from non-loaded constructs only. Expression levels of each target gene were normalised to *GAPDH*, and analysed using the ΔΔ Ct method (described in section 4.1.5.5). Results are presented as a fold change in expression level relative to the non-coated (0.5% FBS) scaffold. All conditions and experimental methods were kept consistent between donors.

COL1A1

Figure 5.3 shows the effect of each supplementation method (0.5% FBS, 10% FBS, PPP and PRP) on *COL1A1* expression in bSCs. Non-coated scaffolds supplemented with 0.5% FBS induced the highest *COL1A1* expression in donor 1 cells, with 10% FBS, PPP and PRP constructs inducing a 7-fold ($p \leq 0.05$), 6-fold ($p \leq 0.05$) and 3.6-fold (not significant) reduction in expression respectively.

Results from donor 2 cells however, showed a 3.5-fold upregulation in *COL1A1* in response to supplementation with 10% FBS ($p \leq 0.05$). Addition of PPP induced a slight increase (1.8-fold) but this was not significant. The addition of PRP resulted in a similar level of expression (1.03-fold) to supplementation with 0.5% FBS.

COL3A1

Figure 5.4 shows the effect of each supplementation method (0.5% FBS, 10% FBS, PPP and PRP) on *COL3A1* expression in bSCs. No significant change in *COL3A1* expression was induced by coating scaffolds with PPP or PRP in donor 1 cells. Supplementation with 10% FBS caused a 6-fold (non-significant) decrease in expression in comparison with supplementation with 0.5% FBS.

Conversely, in donor 2, supplementation with either 10% FBS or PRP induced significant upregulation (4.3-fold ($p \leq 0.01$) and 3.7-fold ($p \leq 0.05$) respectively). Supplementation with PPP also induced an increase (3-fold) in donor 2, although this was not found to be statistically significant.

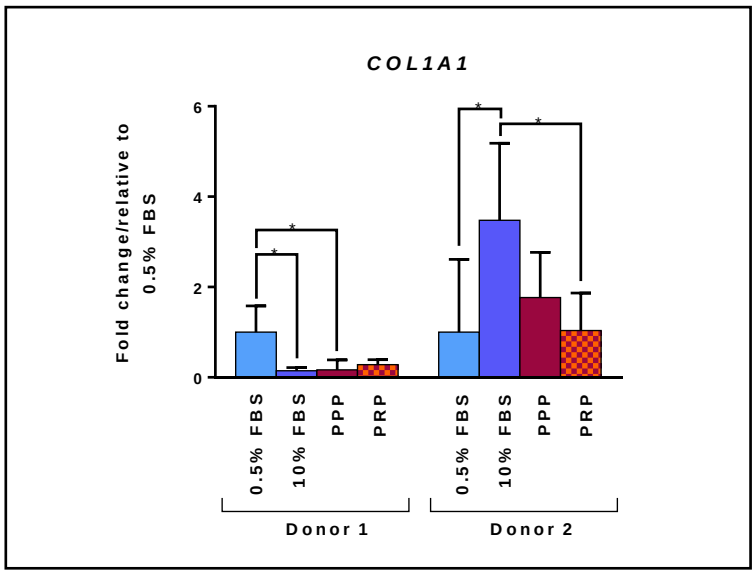

Figure 5.3 Effect of platelet density on *COL1A1* mRNA expression in bSCs.
The effect of each supplementation method (0.5% FBS, 10% FBS, PPP and PRP) on *COL1A1* expression in bSCs from two different donors cultured in non-loaded constructs for 4 days. Bars represent the mean of the fold change relative to the non-coated (0.5% FBS) scaffold ± relative standard deviation (n=3). Values are normalised to *GAPDH* expression. Statistical significance was determined using a one-way ANOVA. * = $p \leq 0.05$.

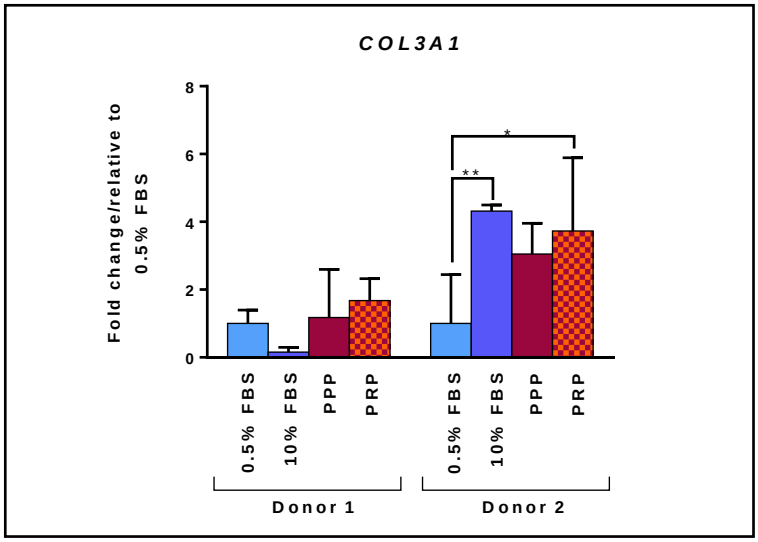

Figure 5.4 Effect of platelet density on *COL3A1* mRNA expression in bSCs.
The effect of each supplementation method (0.5% FBS, 10% FBS, PPP and PRP) on *COL3A1* expression in bSCs from two different donors cultured in non-loaded constructs for 4 days. Bars represent the mean of the fold change relative to the non-coated (0.5% FBS) scaffold ± relative standard deviation (n=3). Values are normalised to *GAPDH* expression. Statistical significance was determined using a one-way ANOVA. * = $p \leq 0.05$, ** = $p \leq 0.01$.

TN-C

Figure 5.4 shows the effect of each supplementation method (0.5% FBS, 10% FBS, PPP and PRP) on *TN-C* expression. Supplementation with 10% FBS, PPP or PRP resulted in significant downregulation (5-fold ($p \leq 0.05$), 9-fold ($p \leq 0.05$) and 4-fold ($p \leq 0.05$) respectively) of *TN-C* expression in donor 1 cells.

In donor 2 cells, 10% FBS induced a 6-fold ($p \leq 0.0001$) upregulation. PPP induced a slight increase (2.5-fold) in comparison with 0.5% FBS, but this was not found to be significant. PRP caused no significant change in *TN-C* expression in donor 2 cells in comparison with 0.5% FBS. Both PPP and PRP coated scaffolds induced significantly lower *TN-C* expression than 10% FBS ($p \leq 0.0001$).

SCXAB

Figure 5.6 shows the effect of each supplementation method (0.5% FBS, 10% FBS, PPP and PRP) on *SCX* expression. Regarding donor 1, coating scaffolds with PPP or PRP resulted in a significant 14-fold decrease ($p \leq 0.0001$) in expression, in comparison with the control (0.5% FBS). Supplementation with 10% FBS resulted in a 1.9-fold increase in *SCXAB* expression, although this was not statistically significant.

In donor 2 cells, supplementation with 10% FBS induced significantly higher *SCXAB* expression than all other supplementation methods with a 6-fold ($p \leq 0.0001$) increase relative to 0.5% FBS. PPP and PRP coatings induced no significant difference in comparison with the control (0.5% FBS).

RUNX2

Figure 5.7 shows the effect of each supplementation method (0.5% FBS, 10% FBS, PPP and PRP) on *RUNX2* expression. Supplementation with 10% FBS, PPP or PRP caused a significant downregulation of expression (7-fold ($p \leq 0.01$) 7-fold ($p \leq 0.01$) and 5-fold ($p \leq 0.01$) respectively), in donor 1 cells.

A slight increase in expression was measured in donor 2 cells supplemented with 10% FBS, PPP or PRP (1.9-fold, 2.3-fold and 2.1-fold respectively). However, this was only significant in PPP coated constructs ($p \leq 0.05$).

A summary of the results presented in this section can be found in table 8.

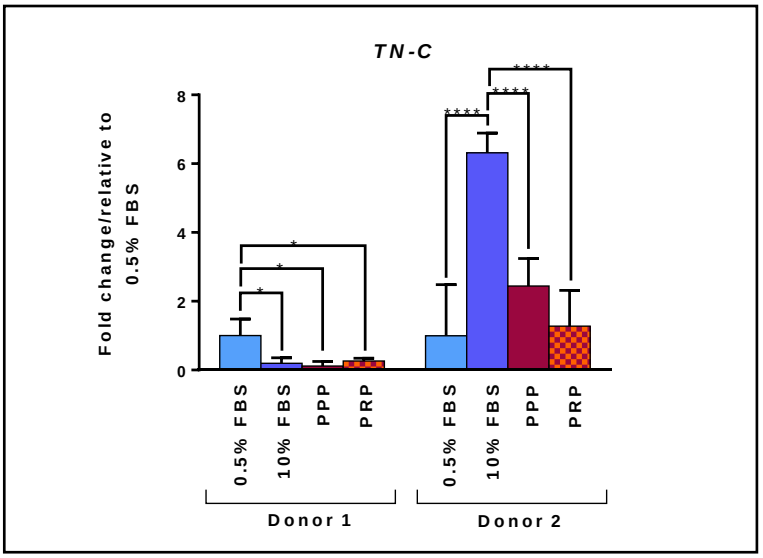

Figure 5.5 Effect of platelet density on *TN-C* mRNA expression in bSCs.

The effect of each supplementation method (0.5% FBS, 10% FBS, PPP and PRP) on *TN-C* expression in bSCs from two different donors cultured in non-loaded constructs for 4 days. Bars represent the mean of the fold change relative to the non-coated (0.5% FBS) scaffold ± relative standard deviation (n=3). Values are normalised to *GAPDH* expression. Statistical significance was determined using a one-way ANOVA. * = $p \leq 0.05$, **** = $p \leq 0.0001$.

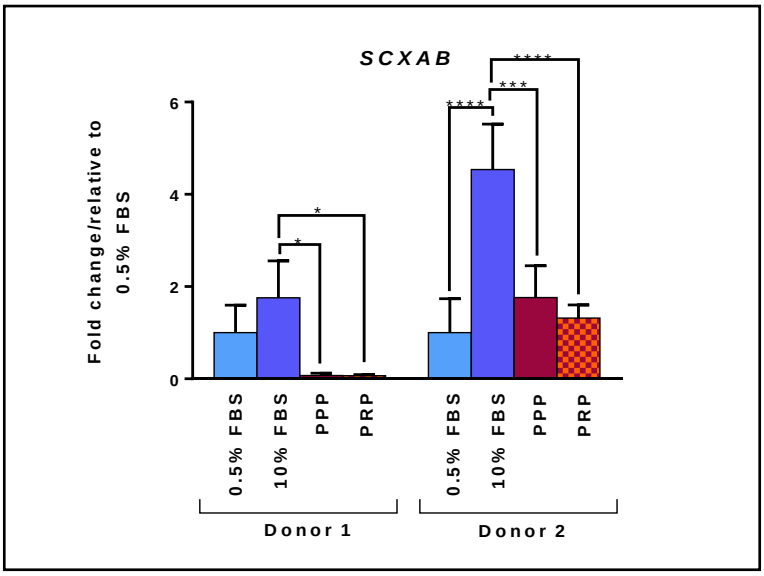

Figure 5.6 Effect of platelet density on *SCXAB* mRNA expression in bSCs.

The effect of each supplementation method (0.5% FBS, 10% FBS, PPP and PRP) on *SCXAB* expression in bSCs from two different donors cultured in non-loaded constructs for 4 days. Bars represent the mean of the fold change relative to the non-coated (0.5% FBS) scaffold ± relative standard deviation (n=3). Values are normalised to *GAPDH* expression. Statistical significance was determined using a one-way ANOVA. * = $p \leq 0.05$, *** = $p \leq 0.001$, **** = $p \leq 0.0001$.

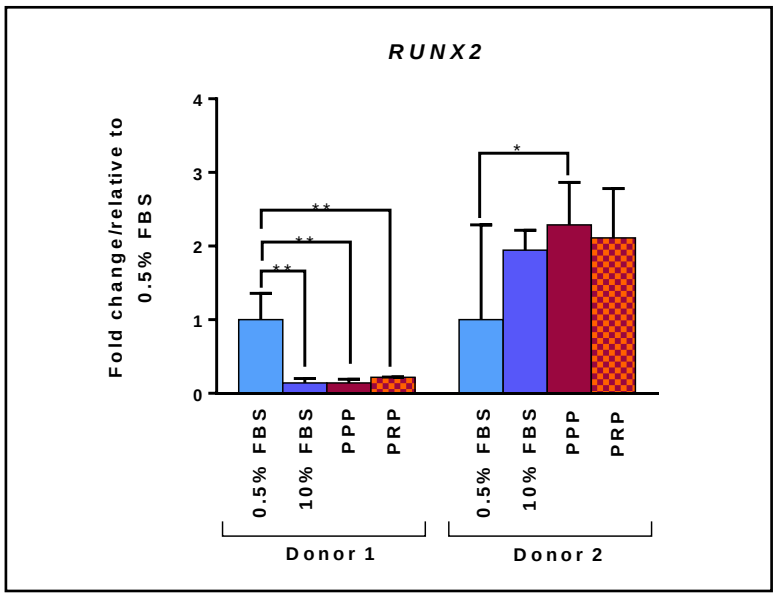

Figure 5.7 Effect of platelet density on *RUNX2* mRNA expression in bSCs.
The effect of each supplementation method (0.5% FBS, 10% FBS, PPP and PRP) on *RUNX2* expression in bSCs from two different donors cultured in non-loaded constructs for 4 days. Bars represent the mean of the fold change relative to the non-coated (0.5% FBS) scaffold ± relative standard deviation (n=3). Values are normalised to *GAPDH* expression. Statistical significance was determined using a one-way ANOVA. * = $p \leq 0.05$, *** = $p \leq 0.001$, **** = $p \leq 0.0001$.

Table 8 Summary of cellular gene expression changes in response to PPP and PRP coatings.

	10% FBS		PPP		PRP	
Gene	Donor 1	Donor 2	Donor 1	Donor 2	Donor 1	Donor 2
COL1A1	7 (p≤0.05)	3.5 (p≤0.05)	6 (p≤0.05)	NS	NS	NS
COL3A1	NS	4.3 (p≤0.01)	NS	NS	NS	3.7 (p≤0.05)
TN-C	5 (p≤0.05)	6 (p≤0.0001)	9 (p≤0.05)	NS	4 (p≤0.01)	NS
SCXAB	NS	6 (p≤0.0001)	NS	NS	NS	NS
RUNX2	7 (p≤0.01)	NS	7 (p≤0.01)	2.3 (p≤0.05)	5 (p≤0.01)	NS

Table 8 summarises the changes in *COL1A1*, *COL3A1*, *TN-C*, *SCXAB* and *RUNX2* gene expression resulting from each supplementation group (10% FBS, PPP and PRP), after 4 days of culture, in cells from donors 1 and 2. Values indicate the fold change in gene expression relative to scaffolds supplemented with 0.5% FBS (green and red cells indicate upregulation and downregulation respectively). Statistical significance is presented in brackets. NS indicates no statistically significant difference.

5.2.3 The effect of cyclic tensile strain on cell behaviour within PPP and PRP coated constructs

Cyclic tensile strain (5% at a frequency of 1 Hz, for 1 hour every day) was applied to PPP and PRP coated constructs, as well as non-coated scaffolds supplemented with DMEM containing 0.5% or 10% FBS (a full description of the experimental setup is provided in section 5.1.2). Due to the limited duration of growth factor release (established in section 4.2.2), constructs were cultured for a total of 4 days before ending the experiment. Cell proliferation, infiltration and gene expression was assessed within each construct in response to the cyclic strain regime.

5.2.3.1 PRP did not significantly enhance proliferation in comparison with PPP

Figure 5.8 shows the percentage DNA increase induced by each supplementation method (0.5% FBS, 10% FBS, PPP and PRP), over a total of 4 days in culture under either non-loaded or loaded conditions. Loaded constructs underwent 3 loading sessions in total (for 1 hour per day). Non-loaded and loaded constructs exhibited the same general trend, with non-coated (0.5% FBS) scaffolds inducing the lowest proliferation rate (45% and 0.2% DNA increase in non-loaded and loaded constructs respectively), followed by non-coated (10% FBS) scaffolds which induced 53% and 162% increases in DNA content in non-loaded and loaded constructs respectively. PPP coated constructs induced 99% and 200% increases in DNA content under non-loaded and loaded conditions respectively. Finally, PRP coated constructs induced the highest rate of proliferation with increases in DNA content of 157% and 253% under non-loaded and loaded conditions respectively.

Apart from non-coated (0.5% FBS) scaffolds, all other constructs showed increased proliferation when subjected to cyclic tensile strain. Loading induced an increase in DNA content in non-coated (10% FBS) PPP and PRP coated constructs of 3-fold, 2-fold and 1.6-fold respectively. This increase was found to be statistically significant in non-coated (10% FBS) and PPP constructs only ($p = \leq 0.05$) (not indicated in Figure 5.8).

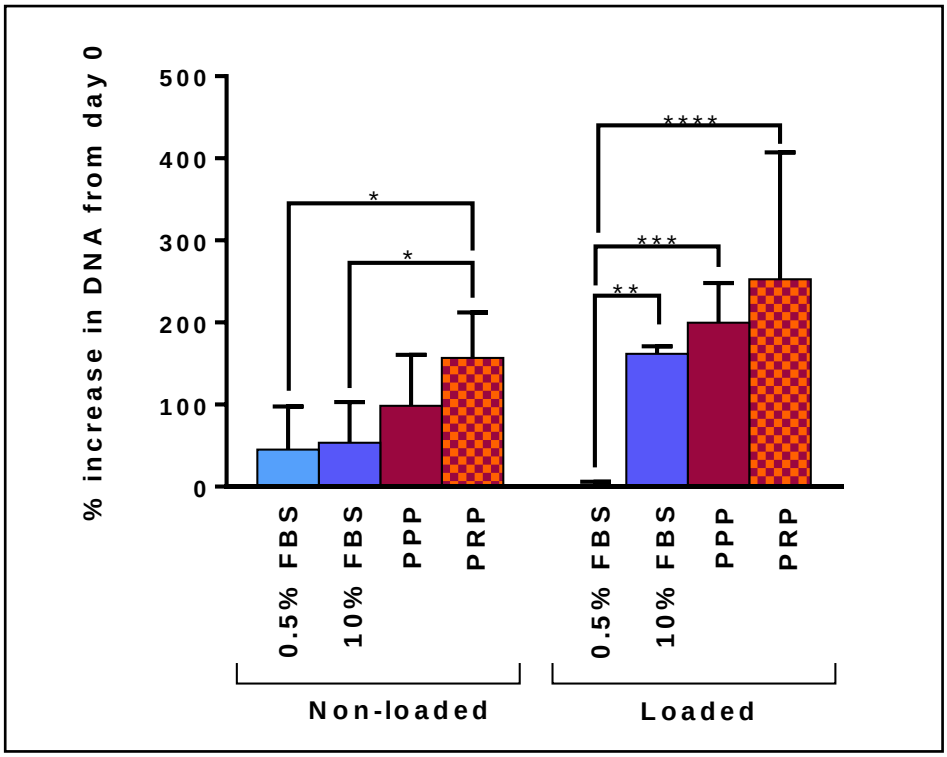

Figure 5.8 Effect of platelet density on cell proliferation under non-loaded and loaded conditions.

Effect of each supplementation method (0.5% FBS, 10% FBS, PPP and PRP) on proliferation of bSCs. Data is presented as the percentage increase in DNA from the day that seeding was completed (day 0) to the 4th day of culture. Bars represent the mean ± standard deviation (n=3). Statistical significance was determined using a two-way ANOVA. * = $p \leq 0.05$, ** = $p \leq 0.01$, *** = $p \leq 0.001$, **** = $p \leq 0.0001$. Additional comparisons between non-loaded and loaded constructs were conducted using a t-test. This indicated that loading produced a significant difference in non-coated (10% FBS) and PPP coated constructs only ($p = \leq 0.05$).

5.2.3.2 Both PPP and PRP coatings promoted cell infiltration throughout the construct

Confocal microscopy was used to examine bSC infiltration throughout scaffolds exposed to each supplementation method (0.5% FBS, 10% FBS, PPP and PRP), under non-loaded and loaded conditions. Cells were cultured in constructs for a total of 4 days before imaging (Figure 5.9). Constructs were stained with Alexa Fluor 488 phalloidin (green) and TO-PRO-3 (blue) which stain the cytoskeleton and nucleus respectively.

More cellular bridging was evident between PET fibres when non-coated scaffolds (both 10% and 0.5% FBS supplemented) underwent cyclic loading. Constructs coated with PPP or PRP induced complete cellular bridging throughout the intra-fibre voids, in both non-loaded and loaded conditions, with no obvious difference between coatings.

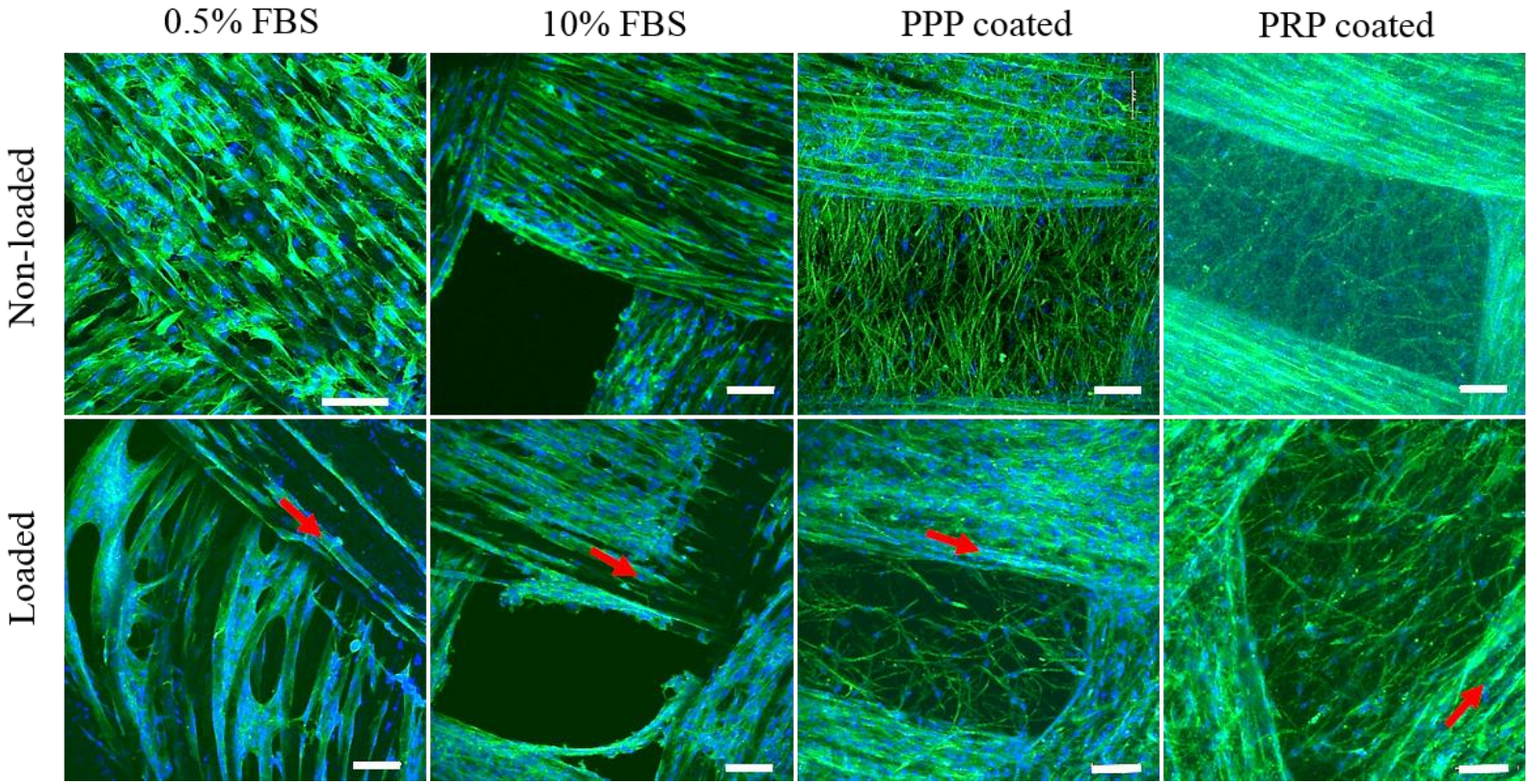

Figure 5.9 Confocal microscope images of constructs (0.5% FBS, 10% FBS, PPP and PRP) under non-loaded and loaded conditions.

Images of scaffolds supplemented with 0.5% FBS, 10% FBS, PPP and PRP after 4 days under non-loaded (top row) and loaded (bottom row) conditions. Constructs were stained for actin (green) with Alexa Fluor 488 phalloidin and nuclei (blue) with To-pro-3 and imaged using a 20 × objective lens. Scale bar = 100 µm. Red arrows indicate the direction of strain.

5.2.3.3 The effect of cyclic tensile strain on the expression on ligament and non-ligament associated genes within bSCs in PPP and PRP coated constructs

Cyclic tensile strain was applied to constructs subjected to each supplementation method (0.5% FBS, 10% FBS, PPP and PRP) using the regime previously described (5% strain at a frequency of 1 Hz, for 1 hour per day). PPP and PRP constructs destined for loading were clamped and coated on the same day. Loading commenced on the following day for a total of 3 sessions, and mRNA was extracted on the 4th day of culture. qRT-PCR was used to assess how the application of cyclic tensile strain affects expression of ligament and non-ligament associated genes in bSCs exposed to each supplementation method. Results were analysed using the Δ Ct and ΔΔ Ct methods (described in section 4.1.5.5) and are presented as both the absolute mRNA expression level under non-loaded and loaded conditions, and as a fold change in expression level relative to the non-loaded control for each supplementation group. The data presented in this section was generated from bSCs isolated from 2 bovines (donors 1 and 2).

COL1A1

The effect of applying 3 sessions of cyclic tensile strain (total culture period of 4 days) on each construct (0.5% FBS, 10% FBS, PPP and PRP) is presented in Figure 5.10. A slight increase in *COL1A1* expression was measured in 10% FBS and PPP treated constructs seeded with donor 1 cells (2.1-fold and 2.5-fold respectively), although this was not found to be statistically significant.

Cyclic tensile strain induced a significant 2.9-fold ($p = \leq 0.05$) upregulation of *COL1A1* expression in donor 2 cells on 0.5% FBS scaffolds. Slight increases were also measured in PPP and PRP treated constructs seeded with donor 2 cells (2-fold and 2.2-fold respectively). However, these were not statistically significant.

COL3A1

The effect of cyclic tensile strain on *COL3A1* expression is presented in Figure 5.11, for each supplementation method (0.5% FBS, 10% FBS, PPP and PRP). A significant 5-fold ($p = \leq 0.001$) upregulation was measured in donor 1 cells on non-coated (NC) scaffolds supplemented with 10% FBS. No significant changes in expression were measured in response to the application of strain in donor 1 cells on any of the other constructs, although loading caused a slight decrease (2-fold) in expression in PRP coated constructs.

No significant changes in *COL3A1* expression were measured as a response to cyclic tensile strain in donor 2 cells within any of the constructs.

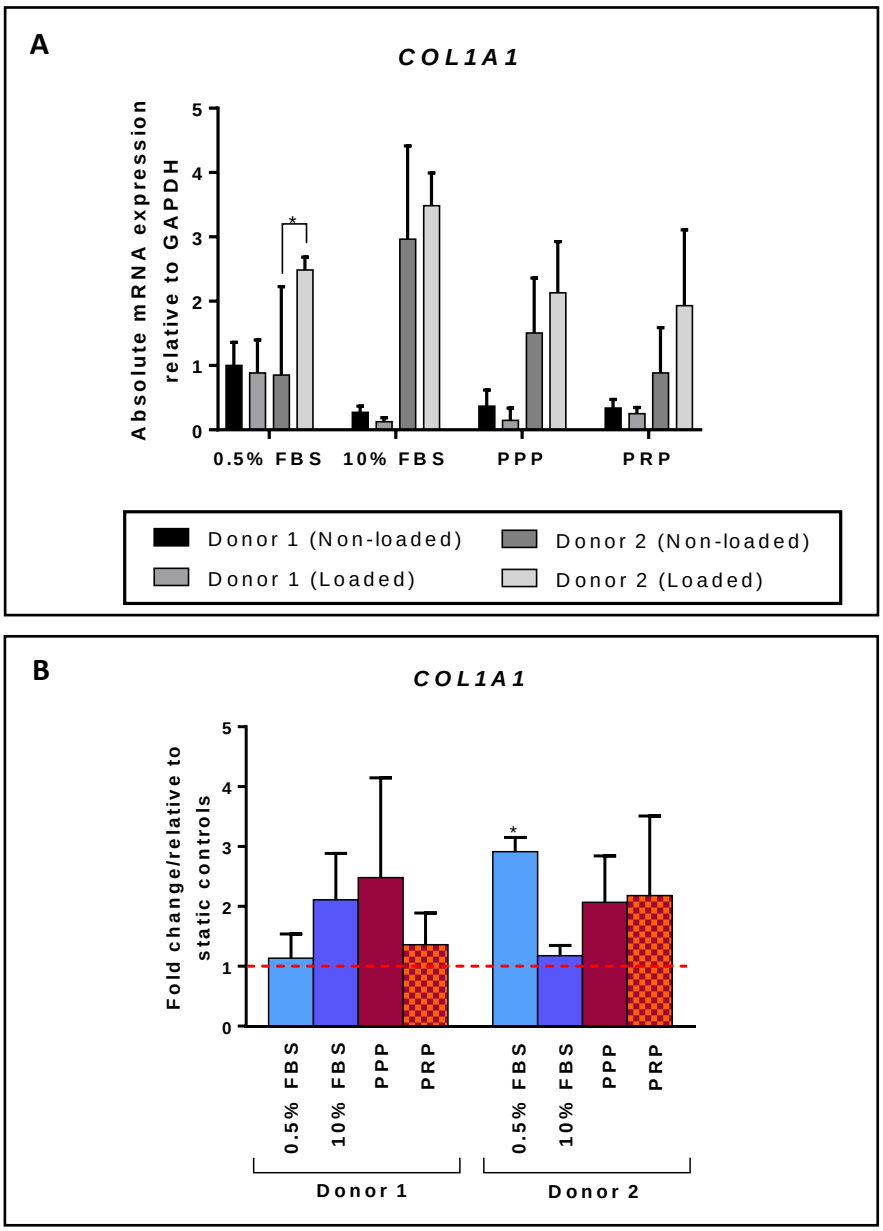

Figure 5.10 Effect of cyclic tensile strain on *COL1A1* expression of bSCs in PPP and PRP coated constructs.

The figure demonstrates the effect of applying cyclic tensile strain of 5% at a frequency of 1 Hz on *COL1A1* expression of cells within each construct (0.5% FBS, 10% FBS, PPP and PRP). All constructs were cultured for a total of 4 days and loaded constructs were subjected to 3 strain sessions (for 1 hour per day). Data is presented for donors 1 and 2. Values are normalised to *GAPDH* expression. Statistical significance was determined using a one-way ANOVA. * = $p \leq 0.05$.

A) Bars represent the mean absolute mRNA expression (Δ Ct) of non-loaded and loaded constructs ± relative standard deviation (n=3).

B) Bars represent the mean of the fold change (ΔΔ Ct) relative to corresponding non-loaded controls (indicated by the dotted line) ± relative standard deviation (n=3).

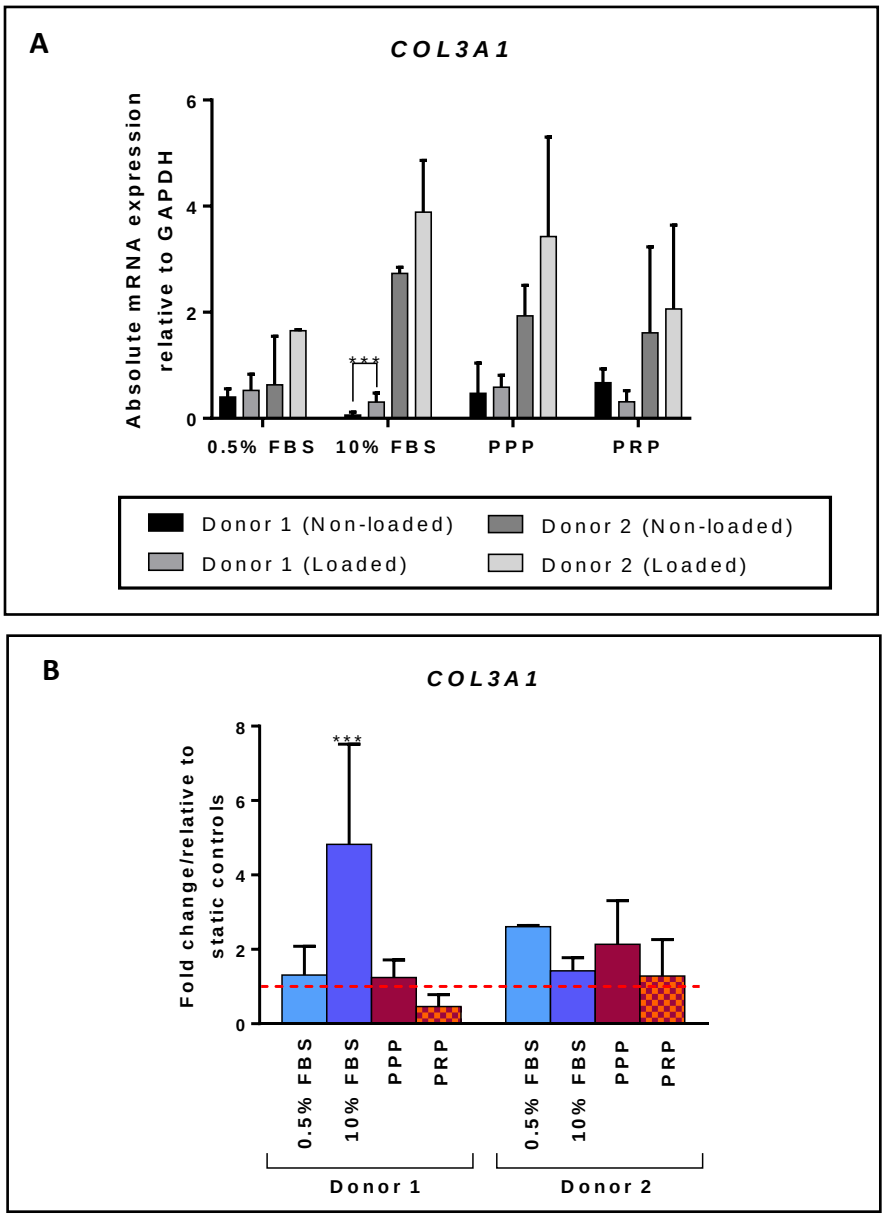

Figure 5.11 Effect of cyclic tensile strain on *COL3A1* expression of bSCs in PPP and PRP coated constructs.

The figure demonstrates the effect of applying cyclic tensile strain of 5% at a frequency of 1 Hz on *COL3A1* expression of cells within each construct (0.5% FBS, 10% FBS, PPP and PRP). All constructs were cultured for a total of 4 days and loaded constructs were subjected to 3 strain sessions (for 1 hour per day). Data is presented for donors 1 and 2. Values are normalised to *GAPDH* expression. Statistical significance was determined using a one-way ANOVA. *** = $p \leq 0.001$.

A) Bars represent the mean absolute mRNA expression (Δ Ct) of non-loaded and loaded constructs ± relative standard deviation (n=3).

B) Bars represent the mean of the fold change (ΔΔ Ct) relative to corresponding non-loaded controls (indicated by the dotted line) ± relative standard deviation (n=3).

TN-C

Figure 5.12 shows the effect of cyclic tensile strain on *TN-C* expression in bSCs exposed to each supplementation method (0.5% FBS, 10% FBS, PPP and PRP). A slight increase in expression (1.9-fold) was seen in donor 1 cells in PPP constructs upon application of strain, although this was not found to be significant. Loading all other constructs showed no significant change in expression, although a slight (2.5-fold) decrease in mRNA was measured in cells from non-coated (0.5% FBS) and PRP treated scaffolds.

Applying strain resulted in a significant 2.8-fold ($p \leq 0.001$) upregulation of *TN-C* expression in donor 2 cells on 0.5% FBS supplemented scaffolds only. 10% FBS, PPP and PRP treated scaffolds showed a similar level of expression to their non-loaded control.

SCXAB

The effect of cyclic tensile strain on *SCXAB* expression in bSCs exposed to each supplementation method (0.5% FBS, 10% FBS, PPP and PRP) is presented in Figure 5.13. Donor 1 showed a significant 23-fold ($p \leq 0.0001$) and 14-fold ($p \leq 0.001$) upregulation of expression in PPP and PRP coated constructs respectively, as a result of applying cyclic tensile strain. No change in expression was identified in either non-coated control scaffold as a result of applying strain.

Cyclic tensile strain also induced significant *SCXAB* upregulation in donor 2 cells in PPP and PRP coated constructs with 9-fold ($p \leq 0.05$) and 10-fold ($p \leq 0.01$) increases in expression being measured respectively. Application of cyclic strain to non-coated scaffolds supplemented with 0.5% FBS also induced a 12.5-fold ($p \leq 0.01$) increase in expression in donor 2 cells.

RUNX2

Figure 5.14 shows the effect of cyclic tensile strain on *RUNX2* expression in bSCs exposed to each supplementation method (0.5% FBS, 10% FBS, PPP and PRP). Donor 1 cells on scaffolds supplemented with 0.5% FBS demonstrated a significant 3.8-fold ($p \leq 0.05$) downregulation of *RUNX2* expression in response to cyclic strain.

No change in RUNX2 expression was identified in response to cyclic tensile strain in donor 2 cell within any of the constructs.

A summary of the results presented in this section can be found in table 9.

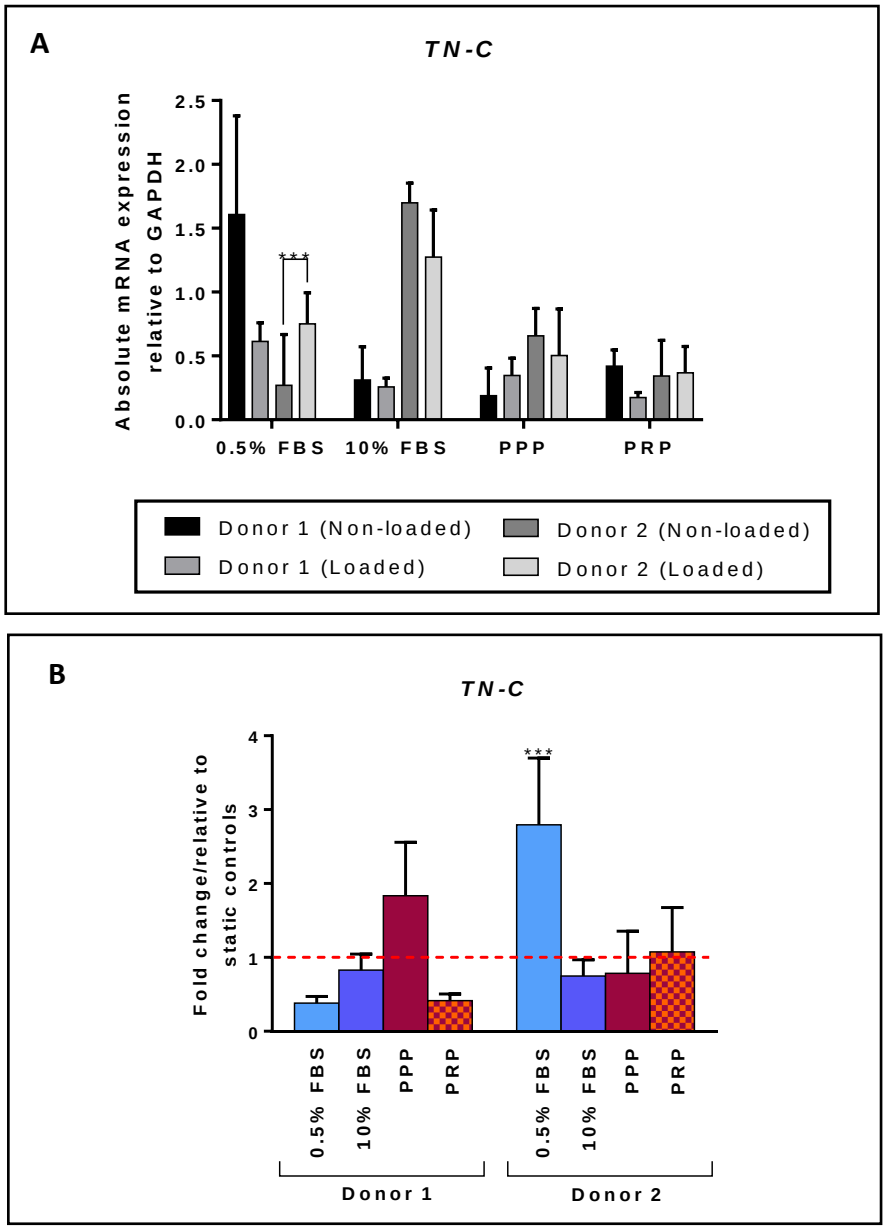

Figure 5.12 Effect of cyclic tensile strain on *TN-C* expression of bSCs in PPP and PRP coated constructs.

The figure demonstrates the effect of applying cyclic tensile strain of 5% at a frequency of 1 Hz on *TN-C* expression of cells within each construct (0.5% FBS, 10% FBS, PPP and PRP). All constructs were cultured for a total of 4 days and loaded constructs were subjected to 3 strain sessions (for 1 hour per day). Data is presented for donors 1 and 2. Values are normalised to *GAPDH* expression. Statistical significance was determined using a one-way ANOVA. *** = $p \leq 0.001$.

A) Bars represent the mean absolute mRNA expression (Δ Ct) of non-loaded and loaded constructs ± relative standard deviation (n=3).

B) Bars represent the mean of the fold change (ΔΔ Ct) relative to corresponding non-loaded controls (indicated by the dotted line) ± relative standard deviation (n=3).

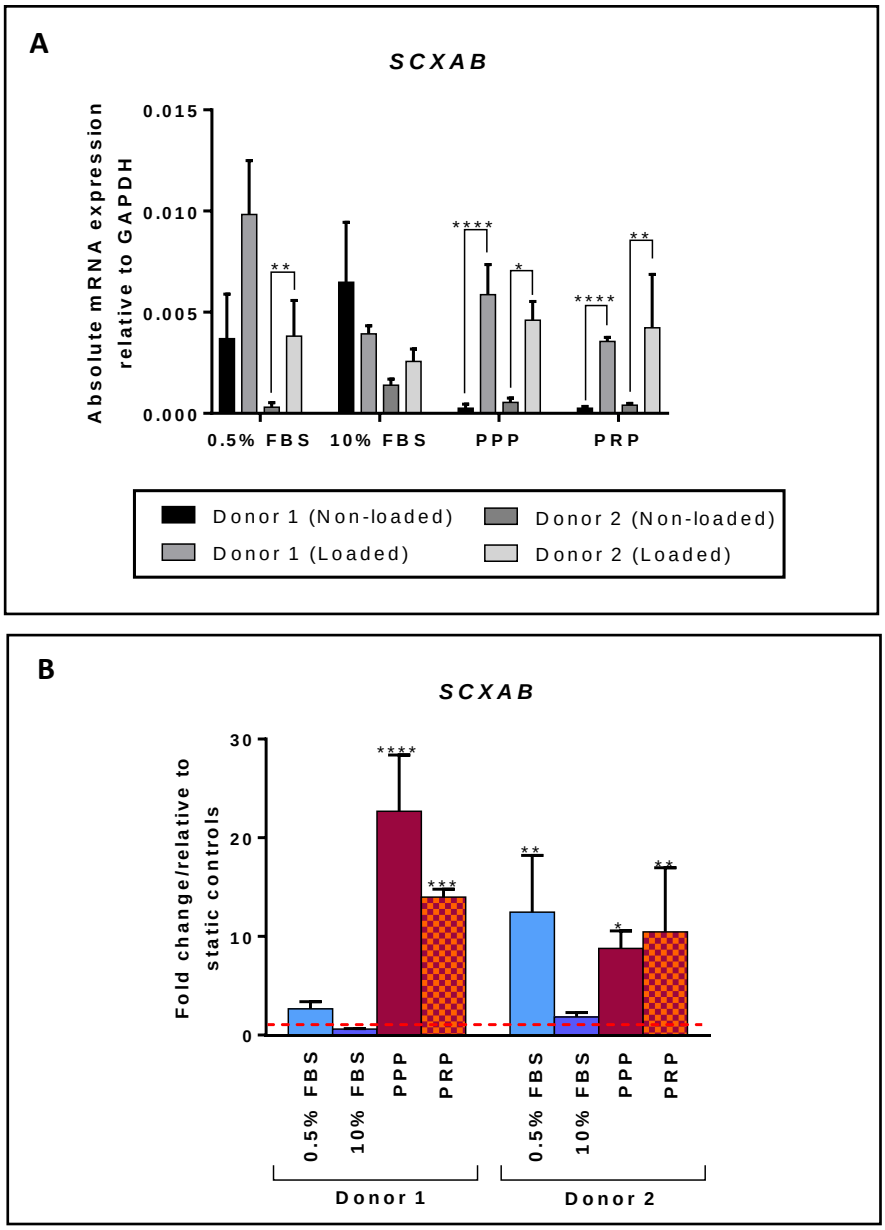

Figure 5.13 Effect of cyclic tensile strain on *SCXAB* expression of bSCs in PPP and PRP coated constructs.

The figure demonstrates the effect of applying cyclic tensile strain of 5% at a frequency of 1 Hz on *SCXAB* expression of cells within each construct (0.5% FBS, 10% FBS, PPP and PRP). All constructs were cultured for a total of 4 days and loaded constructs were subjected to 3 strain sessions (for 1 hour per day). Data is presented for donors 1 and 2. Values are normalised to *GAPDH* expression. Statistical significance was determined using a one-way ANOVA. * = $p \leq 0.05$, ** = $p \leq 0.01$, *** = $p \leq 0.001$, **** = $p \leq 0.0001$.

A) Bars represent the mean absolute mRNA expression (Δ Ct) of non-loaded and loaded constructs ± relative standard deviation (n=3).

B) Bars represent the mean of the fold change (ΔΔ Ct) relative to corresponding non-loaded controls (indicated by the dotted line) ± relative standard deviation (n=3).

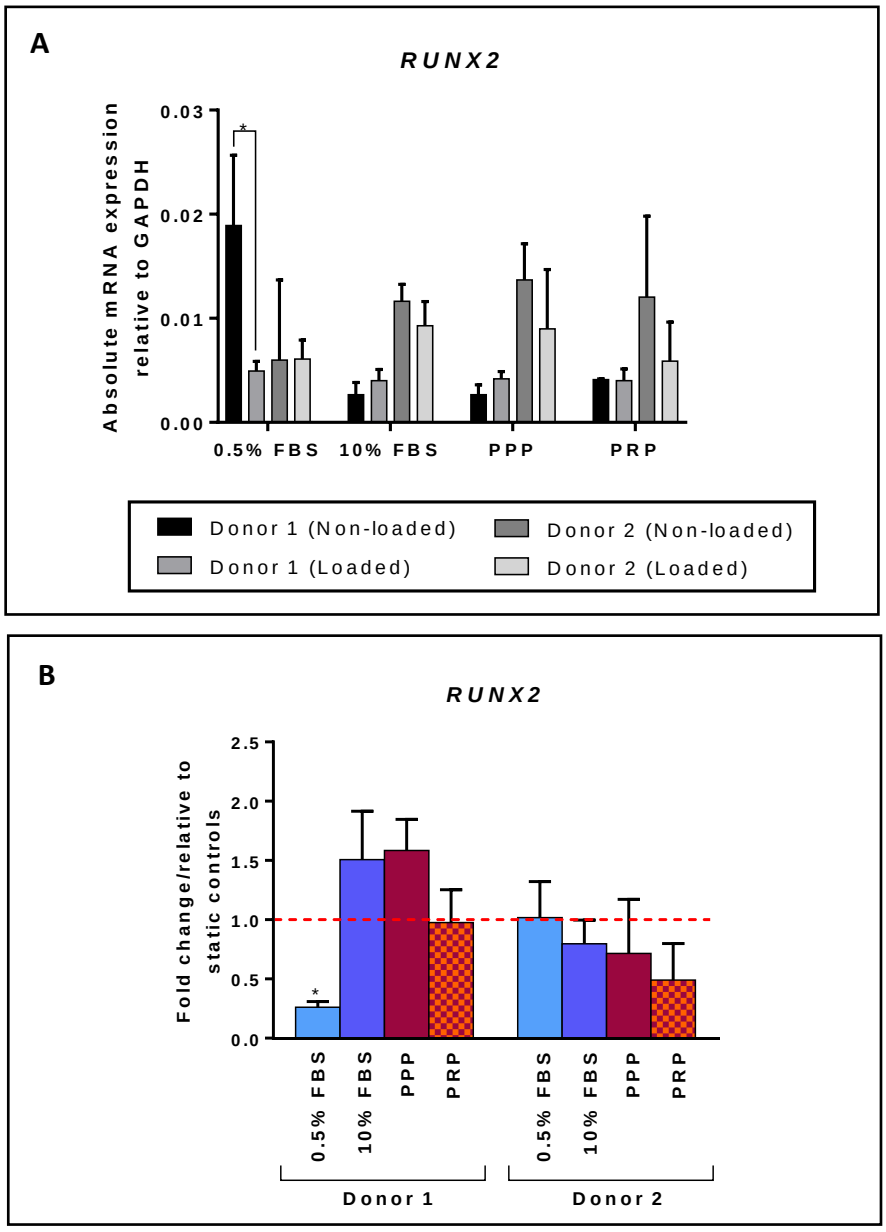

Figure 5.14 Effect of cyclic tensile strain on *RUNX2* expression of bSCs in PPP and PRP coated constructs.

The figure demonstrates the effect of applying cyclic tensile strain of 5% at a frequency of 1 Hz on *RUNX2* expression of cells within each construct (0.5% FBS, 10% FBS, PPP and PRP). All constructs were cultured for a total of 4 days and loaded constructs were subjected to 3 strain sessions (for 1 hour per day). Data is presented for donors 1 and 2. Values are normalised to *GAPDH* expression. Statistical significance was determined using a one-way ANOVA. * = $p \leq 0.05$.

A) Bars represent the mean absolute mRNA expression (Δ Ct) of non-loaded and loaded constructs ± relative standard deviation (n=3).

B) Bars represent the mean of the fold change (ΔΔ Ct) relative to corresponding non-loaded controls (indicated by the dotted line) ± relative standard deviation (n=3).

Table 9 Summary of cellular gene expression changes in response to cyclic tensile strain within PPP and PRP coated constructs.

	0.5% FBA		10% FBS		PPP		PRP	
Gene	Donor 1	Donor 2	Donor 1	Donor 2	Donor 1	Donor 2	Donor 1	Donor 2
COL1A1	NS	2.9 (p≤0.05)	NS	NS	NS	NS	NS	NS
COL3A1	NS	NS	5 (p≤0.001)	NS	NS	NS	NS	NS
TN-C	NS	2.8 (p≤0.001)	NS	NS	NS	NS	NS	NS
SCXAB	NS	12.5 (p≤0.01)	NS	NS	23 (p≤0.0001)	9 (p≤0.05)	14 (p≤0.001)	10 (p≤0.001)
RUNX2	3.8 (p≤0.05)	NS	NS	NS	NS	NS	NS	NS

Table 9 summarises the changes in *COL1A1, COL3A1, TN-C, SCXAB* and *RUNX2* gene expression resulting from the application of 3 sessions of cyclic tensile strain to scaffolds supplemented with 0.5% FBS, 10% FBS PPP and PRP, in cells from donors 1 and 2. Values indicate the fold change in gene expression relative to non-loaded controls (green and red cells indicate upregulation and downregulation respectively). Statistical significance is presented in brackets. NS indicates no statistically significant difference.

5.3 Discussion

This chapter details investigations conducted on the P100 coating, which was selected for further testing as a result of the findings from the previous chapter (Chapter 4). This section discusses the results presented in sections 5.2, in which platelet-rich and platelet-poor P100 coatings were applied to the Xiros PET scaffold to determine whether a higher platelet density had any effect on cell proliferation, infiltration or gene expression within the constructs. Cyclic tensile strain was also applied to these constructs (5% strain at a frequency of 1 Hz, for 1 hour every day) to mimic the forces experienced by the ACL during walking. This gave an understanding of how bSCs respond to these forces within platelet-rich and platelet-poor coated constructs.

5.3.1 Invasion of cells into the final P100 construct

There are two potential approaches to the use of the coated construct in a clinical setting. One possibility is that the construct could be seeded with autogenic or allogenic cells and cultured *in vitro* to produce a more mature graft with a pre-existing extracellular matrix. Implantation of such a graft would result in necrosis of the resident cells and repopulation with the host's cells (Corsetti *et al.*, 1996). Alternatively, the construct could be implanted as an acellular graft, which would subsequently be invaded by the host's cells. All studies presented here involved seeding the scaffold prior to coating to ensure an equal initial cell density, for accurate comparison of cell proliferation, infiltration and gene expression. To investigate how the plasma coating affects cell invasion, acellular (non-seeded) constructs were incubated in a suspension of bSCs. Invasion into coated and non-coated scaffolds was compared.

The plasma coating was not found to significantly hinder cell infiltration into the construct, as determined by a DNA content assay. The total number of cells which had managed to infiltrate the construct in 72 hours was only approximately 6% of the total number of cells in suspension (see Figure 5.1). However, this was a motionless system, meaning that cells were able to settle to the bottom of the culture well. *In vivo*, it is anticipated that cells will migrate from the synovial membrane to colonise the construct, leading to a greater invasion of cells. This study was conducted purely to confirm that cells could readily invade the P100 coated construct. This result is expected since cellular invasion into fibrin clots is a normal event in the wound healing process, whereby fibroblast from the stroma migrate into the clot and contribute to formation of granulation tissue (Greiling and Clark, 1997).

Light microscopy analysis showed cells on non-coated scaffolds to aggregate, forming large masses of cells interspersed along the scaffold. In contrast, within P100 coated scaffolds, cells infiltrating the constructs were evenly distributed throughout its volume. This demonstrates

that not only does the plasma gel not inhibit cell invasion, but it actually promotes uniform distribution of cells (see Figure 5.2). Yan *et al*. (2001) have previously reported the presence of cell aggregation upon static seeding of cells onto PET matrices. In a clinical context it is unclear whether cells would be likely to aggregate upon attachment to the Xiros PET ligament *in vivo*, as the more sophisticated signalling environment might prevent cells from aggregating as they do *in vitro*. If cellular aggregation on the Xiros ligament does occur *in vivo*, this could contribute to the lack of tissue ingrowth into the Xiros ligament reported by Schroven *et al*. (1994), due to the non-uniform dispersion of cells throughout the scaffold. The presence of the P100 coating on the Xiros ligament might then also promote the uniform distribution of cells when implanted *in vivo*. However, relevant *in vivo* studies would be required to confirm this.

5.3.2 Effect of platelet density on gene expression

PPP and PRP coated constructs were fabricated to assess whether the difference in platelet density had any effect on gene expression. In this study, coated constructs were compared with non-coated constructs supplemented with 0.5% and 10% FBS. 0.5% FBS represents minimal growth factor stimulation, and was intended to act as a negative control. 10% FBS is regularly used to supplement cells in culture and so this was used as a positive control. It has previously been demonstrated that high platelet densities induce differentiation towards tendon/ligament phenotypes to a greater extent than lower densities (Jo *et al.*, 2012). To assess whether platelet density had any effect on gene expression in the system presented in this project, qRT-PCR was used to measure expression levels of the five target genes after 4 days of culture under non-loaded conditions. Gene expression was assessed in PPP and PRP coated scaffolds, as well as the control scaffolds, supplemented with either 0.5% or 10% FBS. Cells from 2 donors were used to assess the expression of each gene.

Donors showed very different trends in *COL1A1* expression at this 4 day time point (see Figure 5.3). In donor 1, 0.5% FBS induced the highest expression level, with all other supplementation methods substantially reducing expression. In contrast, higher FBS concentration resulted in a significant upregulation of *COL1A1* in donor 2, with PPP and PRP causing no significant change in expression. As discussed in the previous chapter in the context of the A25 construct, cells undergo a proliferation phase to initially populate a graft before transitioning to a differentiation phase (Ruijtenberg and Van den Heuvel, 2016). By coating the scaffold with a gel, the volume of the construct is suddenly increased. As seen by confocal microscopy, this induces cells to migrate into the gel (see Figure 5.9), and further proliferation would then be required to achieve confluency. As coated constructs were also found to induce higher proliferation rates than non-coated constructs (see Figure 5.8), it is

possible that cell activity was focussed more towards proliferation than differentiation. Moreover, bSCs from donor 1 were found to proliferate more slowly than those from donor 2 (see Figure 4.17, Chapter 4). Since both donor's cells were seeded at the same density, it is likely that cells from donor 1 achieved an even lower confluency. If most cells are proliferating rather than differentiating, this may explain the particularly low expression levels seen in donor 1, in all constructs. In addition, matrix stiffness is also likely to play a part in the expression levels. The relatively low levels of *COL1A1* expression in cells cultured in PPP and PRP coated constructs may reflect the relatively low stiffness of the gel substrate in comparison with the PET fibres (Xu *et al*., 2017). There was no evidence that platelet density effected *COL1A1* expression at the densities used in this study.

PPP and PRP constructs did induce an increase in *COL3A1* mRNA in donor 2 cells, in comparison with bSCs supplemented with 0.5% FBS only, but this was only significant in PRP treated scaffolds. No difference in expression was identified between PPP and PRP in either donor. Consistent with the findings presented here, previous work by Schnabel *et al*. (2006) found no significant difference in collagen type III expression between tendon explants cultured in PPP or PRP. No change in expression was measured in donor 1 cells within PPP or PRP coated constructs, which, as discussed in relation to *COL1A1* expression, is possibly due to a greater focus on proliferation at this early stage (see Figure 5.4). There is no evidence to suggest that a higher platelet density effects the expression of *COL3A1* in bSCs within coated constructs.

TN-C expression showed similar trends to the other ECM genes (*COL1A1* and *COL3A1*), with donor 1 showing very low expression levels (see Figure 5.5). In bSCs from donor 2, 10% FBS induced a 6-fold increase in *TN-C* expression, which is consistent with a previous study which found that FBS increases *TN-C* expression (Chiquet-Ehrismann *et al*., 1986), although this was not identified in donor 1. No increase in *TN-C* expression was found relative to cells cultured on scaffolds supplemented with 0.5% FBS. This supports the theory that by coating the scaffold with a gel, genes associated with differentiation are initially supressed to allow cells to focus on migration and proliferation.

Donor variation existed in levels of *SCXAB* expression, which is likely due to the difference in proliferation rate, as well as the variation in matrix stiffness, as discussed previously in Chapter 4. Highest expression was seen again in cells treated with 10% FBS, with consistently lower expression levels in coated constructs (see Figure 5.6). Interestingly, a study comparing the effect of autologous human serum and FBS on proliferation and differentiation in human MSCs found that FBS induced greater differentiation, whilst autologous serum promoted greater proliferation (Shahdadfar *et al.*, 2005). Whether this could offer any additional insight

into why FBS induced greater expression of all target genes (in donor 2 only) than growth factors released from human platelet gels remains unclear. It is likely that the effect of serum differs greatly depending on whether it is autogenic, allogenic, or xenogenic. In addition, the reduced stiffness of the gel in comparison with the PET fibres, would likely have caused an initial reduction in *SCXAB* expression, as matrix stiffness has been found to modulate scleraxis expression (Sharma and Snedeker, 2010). The reduced matrix stiffness to which cells are exposed, as a result of the gel coatings, is likely to promote differentiation towards an alternative lineage. Again, platelet density was not found to have an effect on *SCX* expression.

Donor 1 showed a significant downregulation of *RUNX2* when supplemented with 10% FBS or PPP/PRP gels (see Figure 5.7). This could be the result of a substantial proliferation response, as described previously, rather than a differentiation response. These three treatment groups had the reverse effect on donor 2 cells, possibly indicating a general increase in cell function in comparison with the 0.5% FBS control, although PRP has previously been found to promote osteogenesis in osteosarcoma cells lines (Kanno *et al*., 2005). Neither the PPP nor PRP coating induced greater *RUNX2* expression than supplementation with 10% FBS, suggesting that the gels do not promote differentiation towards the osteogenic lineage over and above any effect attributed to 10% FBS.

By supplementing cell-seeded scaffolds with 10% FBS, PPP or PRP, donor 2 cells showed an increased expression of ECM genes (*COL1A1*, *COL3A1* and *TN-C*). Highest levels of expression were measured in cells on 10% FBS scaffolds. This could be due to a higher cell confluency on non-coated scaffolds owing to the smaller total volume. In contrast, by supplementing donor 1 cell-seeded scaffolds with 10% FBS, PPP or PRP, expression of all ECM genes either decreased or remained at the same level as the control (0.5% FBS). Differences between donors could be due to the slower proliferation rate of donor 1 cells, resulting in lower confluency and fewer differentiating cells than donor 2. Results did not indicate that platelet-rich constructs induced greater ECM gene expression than platelet-poor.

In both donors, *SCX* expression was highest in cells on scaffolds supplemented with 10% FBS. The lower expression measured in cells within PPP and PRP-coated constructs may be due to the lower matrix stiffness experienced by cells in contact with the gels. Donors 1 and 2 show opposite trends in *RUNX2* expression, with each supplementation method (10% FBS, PPP and PRP) causing a downregulation in donor 1 cells, but an upregulation in donor 2 cells. There was no evidence to suggest that PPP or PRP promoted differentiation towards a ligament-like phenotype.

5.3.3 Effect of cyclic tensile strain on cell proliferation and infiltration in platelet-rich coated constructs

Analysis of proliferation and cell spreading was conducted in platelet-rich and platelet-poor constructs, under both non-loaded and loaded conditions. Since growth factor release from the construct did not occur beyond 3 days post activation (see section 4.2.2, Chapter 4), it was decided that all experiments investigating cellular response to platelets would be confined to a total duration of 4 days. This was to avoid complications resulting from media changes. By changing the media, growth factors released from platelets would be removed. By extending the duration of culture much beyond 4 days, in the absence of media changing, essential nutrients may be depleted, and toxic metabolic waste products could build up (Cruz *et al.*, 1999). No examples of long-term culture of cells in platelet-rich gels, without additional supplementation, were identified in the literature. To maximise the number of strain sessions that could be conducted during this period, scaffolds were coated and clamped on the same day, and loading began the following day. Constructs were subjected to a total of 3 strain sessions.

Although not statistically significant, the platelet-rich coating induced slightly higher bSC proliferation than the platelet-poor construct (see Figure 5.8). There is much disparity in the literature regarding the benefits of PRP over PPP. A number of studies have found PRP to induce greater proliferation than PPP (Kakudo *et al.*, 2008; Jo *et al.*, 2012), whilst others have concluded comparable, if not slightly superior stimulatory effects from PPP (Creeper *et al.*, 2009; Amrichová *et al.*, 2014). A study conducted by Rughetti *et al.* (2008) investigated the effect of different platelet densities on the proliferation of human endothelial cells. They concluded that the stimulation of proliferation peaks at 1.25×10^3 platelets/µl, which is lower than the platelet densities of both the PPP (4.5×10^4) and PRP (2×10^6) used in this project. For a greater understanding of how platelet density effects bSC proliferation within the P100 coated construct, it may be more appropriate to use plasma which is entirely free of platelets. Platelets could then be added to produce coatings with a range of relevant platelet densities. This would also mean that during the early construct optimisation phases, in which constructs were supplemented with FBS, platelet-free coatings could be used, removing any effects as a result of growth factors released from platelets.

Numerous biological variables, as well as differences in production and administration methods between studies make it extremely difficult to draw parallels between results. Furthermore, PRP has been found to initially inhibit proliferation (Creeper *et al.*, 2009), suggesting that substantial variation will exist between studies of different duration.

Upon application of cyclic strain, proliferation increased in all treatment groups except for the scaffold supplemented with 0.5% FBS. It is likely that the handling of scaffolds during the clamping process caused some disruption to the cells, and may have resulted in loss of some cells. Due to the limited proliferation in such low serum conditions, the cell number may not have recovered within this short culture period, leading to an apparent reduction in cell number. One way to overcome this may be to clamp all scaffolds prior to the addition of coatings and allowing cell numbers to recover before addition of PPP or PRP coatings. However, coating the scaffolds with liquid plasma whilst suspended from the clamps of the bioreactor may prove challenging. Alternatively, non-loaded scaffolds could be subjected to the same clamping process, but not subjected to cyclic strain. This would be the ideal scenario, but is subject to the number of clamps available for use.

Scaffolds supplemented with 10% serum, PPP and PRP demonstrated 3, 2 and 1.6-fold increases in proliferation respectively, in comparison with non-loaded controls. Although the 10% FBS treatment group was more responsive to mechanical strain, both PPP and PRP constructs induced a higher overall proliferation rate in loaded construct. The slightly lower response to mechanical stimulation seen in coated constructs may be the result of a reduction in force transmission through the gel matrices, or could indicate that cells reached the maximum level of stimulation under these conditions. Yang *et al.* (2004) investigated the effect of cyclic tensile strain on tendon cell proliferation under serum-free conditions, and found that cells subjected to one session of 8% strain for 4 hours resulted in a significant increase in cell number by just 24 hours. It is possible that supplementation with serum or PRP may mask the effect of cyclic strain on cell proliferation. Indeed, Raif and Seedhom (2005) found that bovine synovial cells supplemented with just 0.5% FBS, seeded onto the same Xiros PET scaffold used in this study, and subjected to a similar strain regime as the one used in this project (1 hour session of cyclic tensile strain of 4.5%, at a frequency of 1 Hz) proliferated at a significantly greater rate than those on non-loaded scaffolds.

To assess cellular invasion, constructs were stained with Alexa Fluor-conjugated phalloidin and TO-PRO-3 and imaged using confocal microscopy (see Figure 5.9). Images showed a particularly greater cell number on loaded constructs supplemented with 10% FBS, in comparison with the non-loaded control. This is consistent with the findings from the quantitative analysis of proliferation (Figure 5.8). Cells in PPP and PRP constructs could be seen infiltrating the scaffold voids, with a spindle-like morphology characteristic of those seen in 3D culture (Bell *et al.,* 1979). It was also noted that, without application of strain, cells tended to be randomly orientated. However, in constructs subjected to cyclic strain, cells aligned with the direction of the force being applied. Aligned cells have been found to synthesise a more organised ECM, characteristic of normal ligament tissue (Wang *et al.,*

2003). This observation was not evident in experiments of longer duration, presumably due to the high cell density and subsequent difficulty in determining the orientation of any individual cells. The shorter culture period of this experiment meant that cellular confluency was much lower at the time of examination, allowing clear distinction of individual cells.

5.3.4 Effect of cyclic tensile strain on gene expression in platelet-rich coated constructs

The effect of cyclic tensile strain on gene expression in PPP and PRP coated constructs was also assessed and compared with the two control scaffolds (supplemented with 0.5% or 10% FBS). As previously mentioned, the total duration of the experiment was 4 days, determined by completion of growth factor release (section 4.2.2, Chapter 4). A total of 3 strain sessions were conducted during this time, and gene expression was measured in cells from 2 donors.

Although there were differences in response between donors, and in many cases the effects were not statistically significant, the application of cyclic tensile strain generally increased *COL1A1* mRNA levels (see Figure 5.10). Between 2-fold and 3-fold increases were measured as a result of applying cyclic tensile strain in donor 1 (10% FBS and PPP constructs only) and donor 2 (0.5% FBS, PPP and PRP constructs only). This trend was most consistent in PPP constructs, although it was not determined to be significant. Studies assessing the effect of cyclic strain on the expression of ECM genes have generally found upregulation to occur at time points beyond 4 days (Subramony *et al.*, 2014). This could offer an explanation as to why significant differences were not seen at this time point. In contrast, a study conducted by Screen *et al*. (2005) found that cyclic strain of 5% at 1 Hz significantly increased collagen synthesis in isolated tendon fascicles. However, tendon fascicles are mature tissue which will be populated with terminally differentiated tenocytes which are already focussed on synthesising matrix proteins (Schulze-Tanzil *et al.*, 2004). It is therefore likely that if changes in *COL1A1* were to occur as a result of applying cyclic tensile strain, they would do so at a later time point.

Some slight increases in *COL3A1* mRNA were measured in response to cyclic tensile strain within some of the treatment groups in donor 1 (10% FBS constructs only) and donor 2 (0.5% FBS and PPP constructs only). Again, there was much variation between donors and differences did not always reach significance. This study also suggests that platelet density has no effect on *COL1A1* expression at the densities used in this project (see Figure 5.11). The limited response to mechanical strain is likely due to the relatively short duration of the experiment, leading to low levels of differentiation. Previous work has reported that cyclic tensile strain does not significantly increase collagen type III expression in human MSCs until day 14 (Subramony *et al*., 2014).

Like other genes encoding components of the ECM (*COL1A1* and *COL3A1*), changes in *TN-C* under cyclic tensile strain of 5% at 1 Hz were not consistent across donors (see Figure 5.12). Variations in expression between donors and constructs likely result from differences in cell growth rate leading to discrepancies in confluency and subsequent differentiation status. Some evidence of upregulation was measured in donor 1 cells in PPP constructs (2-fold) and donor 2 cells on scaffolds supplemented with 0.5% FBS (3-fold). As with other ECM genes it is likely that the short duration of the experiment meant that many cells did not reach the differentiation phase and did not start to express ECM genes. Subramony *et al*. (2014) also investigated the effect of strain on *TN-C* expression, and identified a time dependent increase in expression. The difference in expression between cells on their loaded and non-loaded scaffolds did not reach significance until day 14, which supports the lack of upregulation at this much shorter time pint.

The upregulation of *TN-C* expression by FBS supplementation, described by Chiquet-Ehrismann (1986), could also contribute to the absence of transcriptional change in *TN-C* as a result of strain. The use of 10% FBS may induce maximum *TN-C* upregulation, thereby preventing any additional effects from the application of strain. Donor 2 cells on non-loaded scaffolds, supplemented with 10% FBS, had a 6-fold higher expression level than cells supplemented with 0.5% FBS. This might support the claim that FBS promotes *TN-C* expression, but it is unclear whether this diminishes changes that might result from the application of strain. Using the same donor, applying strain to scaffolds supplemented with 0.5% FBS did significantly increase expression of *TN-C*, giving further evidence to support the theory that serum is masking potential changes in *TN-C* expression resulting from loading.

Application of cyclic strain to both PPP and PRP coated constructs consistently resulted in a statistically significant upregulation (10-23-fold) of *SCXAB* (see Figure 5.13). This gene encodes a transcription factor which is highly expressed in tendon/ligament progenitor cells as well as terminally differentiated cells (Wang *et al.*, 2011). This suggests that applying cyclic tensile strain of 5% at a frequency of 1 Hz to PPP and PRP coated hybrid constructs may promote differentiation towards a ligament-like phenotype. Interestingly, the study by Subramony *et al*. (2014) did not find that cyclic tensile strain increased Scleraxis expression. Although their earlier study (Subramony *et al*., 2013) did identify a significant increase in scleraxis expression in scaffolds composed of aligned fibres, by 14 days.

Applying strain to all constructs induced no significant change in expression of *RUNX2* (see Figure 5.14). There was no evidence to suggest that the cyclic tensile strain regime induced differentiation towards an osteogenic lineage. As mentioned in Chapter 4, cyclic tensile strain has previously been demonstrated to inhibit *RUNX2* expression (Shi *et al*., 2010).

Overall, applying cyclic tensile strain of 5% at a frequency of 1 Hz to platelet-poor and platelet-rich P100 coated constructs for 3 days pointed towards an increase in expression of some ECM components, but in most cases any differences between non-loaded and loaded expression did not reach significance. This limited genetic response to applied cyclic tensile strain could be due to the short duration of the experiment, which may not have allowed time for cells to start expressing ECM genes. Alternatively, this lack of strain-induced expression could be the result of over-supplementation of cells with serum which subsequently masks any effects induced by cyclic strain. Indeed, donor 2 cells supplemented with just 0.5% FBS showed significant increases in *COL1A1*, *TN-C* and *SCXAB* expression when seeded on scaffolds subjected to strain. Cyclic tensile strain did promote *SCX* expression in PPP and PRP coated constructs, possibly indicating the early stages of tendon/ligament differentiation. Analysis of *RUNX2* expression indicated that application of cyclic tensile strain did not promote osteogenic differentiation.

5.4 Summary

The investigations detailed in this chapter aimed to identify any benefits of using a platelet-rich coating over a platelet-poor coating on the Xiros PET ligament. Results indicated no benefits with regard to cell proliferation nor infiltration, and there was nothing to suggest that PRP promoted greater expression of ECM genes, or differentiation towards a ligament phenotype, which is consistent with the conclusions of a review by Foster *et al.* (2009). As far as these studies can conclude, there is no benefit in concentrating platelets to the density used within these investigations (ie. 2×10^6 platelets/µl) with a view to producing a plasma gel that will enhance cell proliferation or ligament differentiation. However, these cellular functions may be enhanced with lower platelet densities (perhaps those resembling normal plasma), or higher densities, although further investigations would be required to determine this.

Chapter 6

Investigation into the molecular mechanisms behind the cyclic strain-induced decrease in plasma degradation

Following application of cyclic tensile strain to each construct in Chapter 4, it was evident that the longevity of the P100 coating was increased as a result of the application of these forces. This was apparent by observing the constructs using confocal microscopy under non-loaded and loaded conditions after 15 days. P100 coated constructs which were not subjected to loading had lost much of their coating by 15 days, and this meant that the intra-fibre voids of the scaffold were exposed. Since no gel was filling these voids, cells were unable to remain within these areas. In contrast, P100 coated constructs which were subjected to stain had reduced gel loss and this meant that the coating continued to fill the voids of the scaffold up to the 15 day time point. As such, cells continued to infiltrate the voids so that the entire construct was filled with cells (see Figure 4.18). It was hypothesised that this reduction in plasma loss was the result of decreased breakdown of fibrin (the matrix forming component of plasma). Fibrin is digested by plasmin (see Figure 6.1), a serine protease which is secreted in its inactive form (plasminogen). Plasminogen is converted to plasmin by tissue-type plasminogen activator 1 (tPA). tPA is inhibited by plasminogen activator inhibitor 1 (PAI-1) and previous studies have identified an upregulation of tPA in combination with a downregulation of PAI-1 in fibroblasts exposed to cyclic tensile strain (Ulfhammer *et al*., 2005). As a result, the expression levels of tPA and PAI-1 were analysed using qRT-PCR and western blot to determine whether the observed change in P100 coating longevity with cyclic strain could be linked to changes in the expression of these proteins.

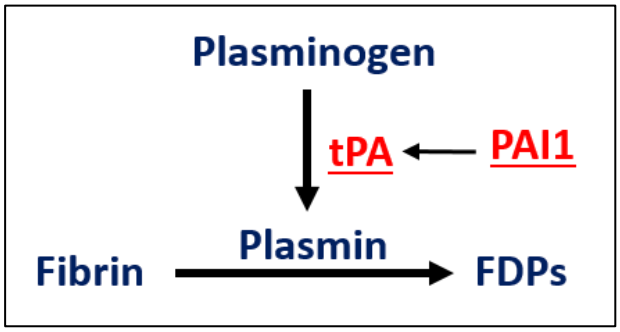

Figure 6.1 The mechanism of fibrinolysis.
Fibrin is broken down to fibrin degradation products (FDPs) by the activity of plasmin, a serine protease. Plasmin is secreted by the liver in its inactive form, plasminogen, which is activated by tissue-type plasminogen activator (tPA). tPA is inhibited by plasminogen activator inhibitor 1 (PAI-1).

Aim:

To determine whether improvement in the P100 coating longevity as a result of applying cyclic tensile strain could be attributed to changes in the expression levels of tissue-type plasminogen activator (tPA) and/or its inhibitor, plasminogen activator inhibitor 1 (PAI-1).

Objectives:

- Quantification and comparison of mRNA expression levels of *tPA* and *PAI-1* genes under non-loaded and loaded conditions.

- Confirmation that any changes in gene expression translate into changes in protein secretion using western blot analysis.

6.1 Materials and methods

This section describes the methods used to evaluate *tPA* and *PAI-1* gene expression using qRT-PCR and describes the process of selecting an appropriate antibody for western blot analysis of secreted PAI-1 protein. Gene expression was assessed using mRNA extracted from all constructs to which cyclic tensile strain was applied. This includes P100, C50, A25 coated and non-coated constructs subjected to 3 and 15 days of cyclic tensile strain (5% strain at a frequency of 1 Hz, for 1 hour every day) as detailed in Chapter 4, as well as the constructs assessed in Chapter 5 (0.5% FBS, 10% FBS, PPP coated and PRP coated) which were subjected to 3 days of cyclic strain.

6.1.1 Comparison of *tPA* and PAI-*1* gene expression under non-loaded and loaded conditions

To compare the expression of *tPA* and *PAI-1* genes under non-loaded and loaded conditions, TaqMan assays were purchased from Applied Biosystems (see Table 10). The cDNA samples used to assess *tPA* and *PAI-1* expression were the same as those used to assess the expression of ligament and non-ligament associated genes in sections 4.2.2 (Chapter 4) and 5.2.2 (Chapter 5). These samples were generated from P100, C50, A25 and non-coated constructs subjected to 3 and 15 days of cyclic tensile strain (5% strain at a frequency of 1 Hz, for 1 hour every day) as detailed in Chapter 4, as well as the constructs assessed in Chapter 5 (0.5% FBS, 10% FBS, PPP coated and PRP coated) which were subjected to 3 days of cyclic strain. mRNA was isolated from these constructs, cDNA was synthesised, and quantitative real-time PCR was carried out according to the methods described in sections 4.1.3.1-4.1.3.3. The expression of *tPA* and *PAI-1* genes were quantified using cells from 2 donors cultured in both non-loaded and loaded constructs. *GAPDH* expression was measured in parallel and used to normalise the values of target genes.

Table 10 Details of TaqMan assays used to quantify the expression of *tPA* and *PAI-1*.

Gene	Assay ID (Applied Biosystems)	Gene Location	Amplicon length
tPA	Bt03237442_m1	Chr.27: 39268525 - 39292539	57 bp
PAI-1	Bt03212915_m1	Chr.25: 37725011 - 37733316	59 bp

6.1.2 Analysis of PAI-1 protein secretion using western blot

To analyse the secretion of plasminogen activator inhibitor-1 from synovial cells at protein level, a western blot was carried out to semi-quantitatively measure the PAI-1 content of media from loaded and non-loaded constructs. Western blot involves loading a protein sample into a polyacrylamide gel in the presence of SDS which imparts a constant charge to mass ratio on the proteins present. The gel acts as a molecular sieve and, on applying a current the individual proteins therefore migrate through the gel at a speed relative to their molecular size. Standard proteins of known molecular weight are also run in order to calibrate the gel and thus allow the size of the sample proteins to be estimated.

The separated protein bands are then electrophoretically transferred to a nitrocellulose membrane using the method developed by Towbin *et al.* (1979). The membrane is then incubated with a primary antibody specific for the protein of interest. A number of washing and blocking steps are performed before applying the secondary antibody, as well as horseradish peroxidase-conjugated streptavidin which binds to the biotinylated secondary antibody, causing the formation of a brown colour. The membrane can then be imaged for greater visibility of the protein bands.

6.1.2.1 Primary PAI-1 antibody selection

A number of different supplier catalogues were searched in order to find a bovine specific anti-PAI-1 primary antibody. However, no such product could be located. Several human-targeted antibodies were available which were found to have cross-reactivity with multiple other species. To check the sequence similarly between human and bovine PAI-1 proteins a sequence alignment was conducted using the Clustal Omega online sequence alignment programme. The EMBOSS Matcher function was used within the Pairwise sequence alignment tool. This used an algorithm to identify local similarities between the human and bovine amino acid input sequences. The result from the sequence alignment showed PAI-1 to be highly conserved, with a 92% sequence similarity, and indicated that a human PAI-1 antibody was highly likely to react with bovine PAI-1 (See Figure 6.7 for results).

6.1.2.2 Western blot sample preparation

Due to the presence of PAI-1 in plasma, non-coated scaffolds were used to investigate PAI-1 secretion from bSCs. Non-coated scaffolds were cut to 3.5 cm before being dynamically seeded with 3×10^5 bSCs according to the method in section 3.1.2. Cell-seeded scaffolds which were destined for loading were clamped into the bioreactor chambers as described in section 4.1.4.2, and were covered with 3 ml of DMEM containing 10% FBS. The following

day cyclic tensile strain of 5% at a frequency of 1 Hz was applied for 1 hour. This was repeated each day. Media was removed from constructs at day 5 of the culture period (prior to the application of that day's loading session) and was immediately frozen at -80˚C. The samples were thawed on the day the western blot was performed. The total protein concentration of each sample was measured using a Bradford assay (Pierce™ Coomassie (Bradford) Protein Assay Kit, ThermoFisher Scientific) as per the manufacturer's instructions. Briefly, bovine serum albumin (BSA) protein standards ranging from 0-200 µg/ml were made up in PBS. 5 µl of each sample and standard was added to 250 µl of Coomassie (Thermo Scientific) in a flat-bottom, 96-well microplate and the plate was incubated at room temperature for 10 minutes. Following incubation, the absorbance was measured at 595 nm using a Varioskan Flash plate reader (Thermo Scientific). A four parametric logistic curve was used to calculate the sample protein concentrations. Samples were diluted in sample buffer (Bio-Rad) so that there was a total of 10 µg of protein in 15 µl. Each sample was combined 1:1 with 2 × Laemmli sample buffer supplemented with 100 mM 2-mercaptoethanol (Bio-Rad). The samples were boiled at 95˚C for 5 minutes prior to loading.

6.1.2.3 Running the western blot gel

A pre-cast Mini-PROTEAN TGX Stain Free Gel 4-15% (Bio-Rad) was used for western blotting. 30 µl of sample was loaded into wells and Precision Plus Protein WesternC standards (Bio-Rad) was loaded as a calibration ladder. The gel was run for 75 minutes at 120 V, in 1 × Tris/Glycine/SDS buffer (Bio-Rad) before transferring to a polyvinylidene difluoride (PVDF) membrane (Trans-Blot Tubro transfer pack, 7 × 8.5 cm) (Bio-Rad) using a Trans-Blot ® Turbo™ transfer system (Bio-Rad).

The membranes were blocked with 25 ml of 5% milk in Tris Buffered Saline (Bio-Rad) with 1% Tween-20 (TBS+T), for at least 1 hour on a rocking shaker, at room temperature. This prevents non-specific binding of the primary antibody. The blocking solution was removed and anti-PAI-1 primary antibody (ab66705, Abcam) was diluted 1:1000 in 0.25% milk powder in TBS+T. The membrane was incubated with the diluted primary antibody overnight at 4˚C, on a rocking shaker. The membrane was then washed 3 times by covering with TBS+T for 5 minutes at room temperature, on a rocking shaker. The membrane was blocked again as previously described, and washed 3 times, before being incubated with HRP conjugated anti-rabbit (ab6721, Abcam) secondary antibody diluted 1:10,000 in 0.25% milk in TBS+T with 1:10,000 StrepTactin-Hrp conjugate (Bio-Rad) for 1 hour, at room temperature. The membrane was washed 3 times, for 5 minutes in TBS+T, to remove any unbound antibody, before incubating for 5 minutes in SuperSignal™ WestFemto Maximum Sensitivity Substrate

(Fisher Scientific), which acts as a chemiluminescent substrate for horseradish peroxidase. A Molecular Imager® Gel Doc™ XR+ System (Bio-Rad) was used to view and image the gel.

6.2 Results

The following section presents the findings from the methods described in sections 6.1.1-6.1.2, in which changes in the expression of tPA and PAI-1, in the response to the application of cyclic tensile strain, were investigated. Observation of P100 constructs undergoing daily sessions of cyclic strain showed a marked increase in construct stability in comparison with non-loaded constructs (see Figure 4.18). It was theorised that by loading the construct, the process of fibrinolysis was being inhibited. The most likely causes of this are a downregulation of tissue-type plasminogen activator (tPA), and/or an upregulation of its inhibitor, plasminogen activator inhibitor-1 (PAI-1) (Saed and Diamond, 2003). It was hoped that these investigations would give an insight into the mechanism by which cyclic strain appeared to enhance the longevity of the P100 coating. Initially, the expression of *tPA* and *PAI-1* genes were compared under non-loaded and loaded conditions using qRT-PCR. Results from this investigation led to the assessment of PAI-1 secretion at the protein level, using western blot.

6.2.1 Clamping constructs in the bioreactor chambers had no significant effect on *tPA* or *PAI-1* gene expression

To determine whether the clamping process had any effect on *tPA* or *PAI-1* expression, qRT-PCR was carried out using mRNA isolated from non-loaded (non-clamped) and non-loaded (clamped) non-coated scaffolds after 15 days of culture. These scaffolds were not exposed to the cyclic strain regime. The expression levels of *tPA* and PAI-1 under clamped and non-clamped conditions are presented in Figure 6.2. Results were analysed using the ΔΔ Ct methods (described in section 4.1.5.5), and are presented as the fold change in expression relative to non-clamped scaffolds. Values are normalised to *GAPDH* expression.

A slight increase (1.2-fold) in *tPA* expression was measured in clamped scaffolds, although this was not found to be statistically significant. In contrast, *PAI-1* expression in cells on clamped scaffolds was approximately 3-fold lower than in cells on non-clamped scaffolds. Although slight differences in *tPA* and *PAI-1* expression were measured between clamped and non-clamped scaffolds, statistical analysis revealed no significant difference in expression between clamped and non-clamped conditions in either gene. As such, culturing non-loaded control constructs in culture wells, rather than under clamped conditions, was considered to be suitable. By clamping only the constructs destined for loading, twice as many constructs could be maintained at one time. Furthermore, to be associated with the observed reduction in fibrinolytic activity, *tPA* expression would need to decrease and/or *PAI-1* expression should increase when cells were subjected to cyclic tensile strain. Because clamping caused a slight

increase in *tPA* expression and a slight decrease in *PAI-1* expression, this reduces the risk of false positives (ie. incorrectly identifying an anti-fibrinolytic phenotype).

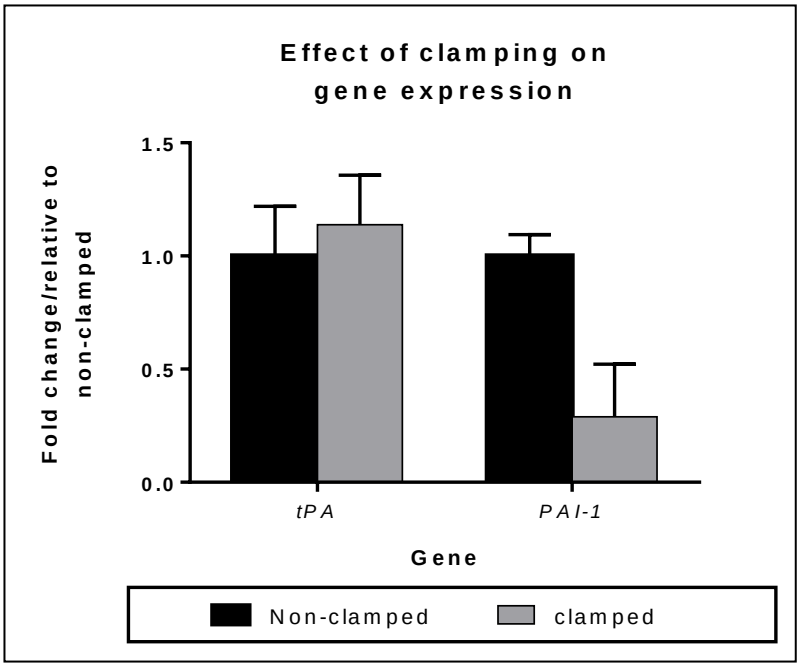

Figure 6.2 The effect of clamping on expression of genes of the fibrinolytic system.
Data is presented for the expression levels of *tPA* and *PAI-1* mRNA in bSCs cultured on non-coated (NC) scaffolds which were either clamped or non-clamped. No forces were applied to either treatment group. Values are normalised to *GAPDH* expression. Bars represent the mean of the fold change in expression, relative to non-clamped scaffolds ± relative standard deviation (n=3). Statistical significance was determined using a t-test and revealed no significant difference in expression of both *tPA* and *PAI-1* mRNA between cells cultured on non-clamped and clamped scaffolds.

6.2.2 The effect of cyclic tensile strain on tPA and PAI-1 gene expression

Expression of *tPA* and *PAI-1* was measured using qRT-PCR and cDNA samples were used from all constructs to which cyclic tensile strain was applied. This includes P100, C50, A25 coated and non-coated constructs subjected to 3 and 15 days of cyclic tensile strain (5% strain at a frequency of 1 Hz, for 1 hour every day) as detailed in Chapter 4, as well as the constructs assessed in Chapter 5 (0.5% FBS, 10% FBS, PPP coated and PRP coated) which were subjected to 3 days of cyclic strain. Results were analysed using the Δ Ct and ΔΔ Ct methods (described in section 4.1.5.5) and are presented as both the absolute mRNA expression level under non-loaded and loaded conditions, and as a fold change in expression level relative to the non-loaded control for each construct. Values were normalised to *GAPDH* expression for each condition. The data presented in this section was generated from bSCs isolated from 2 bovines (donors 1 and 2).

6.2.2.1 The application of cyclic tensile strain induced no significant change in *tPA* gene expression

Figure 6.3 shows the effect of cyclic tensile strain (5% strain at a frequency of 1Hz, for 1 hour every day) on the expression of *tPA* in bSCs cultured in non-coated, P100, C50 and A25 coated constructs. Results are presented for 3 days and 15 days of culture. A significant 3-fold upregulation ($p \leq 0.001$) was measured in donor 1 cells in C50 coated constructs by 15 days. No significant difference in expression was seen at 3 days in donor 1 cells in C50 coated constructs. No other significant change in expression was seen in donor 1 in other constructs. A significant 2-fold upregulation ($p \leq 0.05$) was seen in donor 2 at 3 days in C50 constructs. No other significant change in expression was measured in donor 2 in other constructs.

Figure 6.4 represents the effect of cyclic tensile strain on the expression of *tPA* in bSCs cultured on scaffolds supplemented with 0.5% FBS, 10% FBS and those coated with PPP or PRP. Cyclic strain induced a significant 3-fold upregulation ($p \leq 0.0001$) in donor 1 cells on non-coated scaffolds supplemented with 10% FBS. Donor 2 cells on non-coated scaffolds supplemented with 5% FBS also showed a significant 2-fold upregulation ($p \leq 0.05$) in the presence of strain. No other significant changes in *tPA* expression was measured in either donor under any conditions. These findings are inconsistent with the expectation that *tPA* expression would be reduced as a result of applying cyclic tensile strain to cell-seeded constructs.

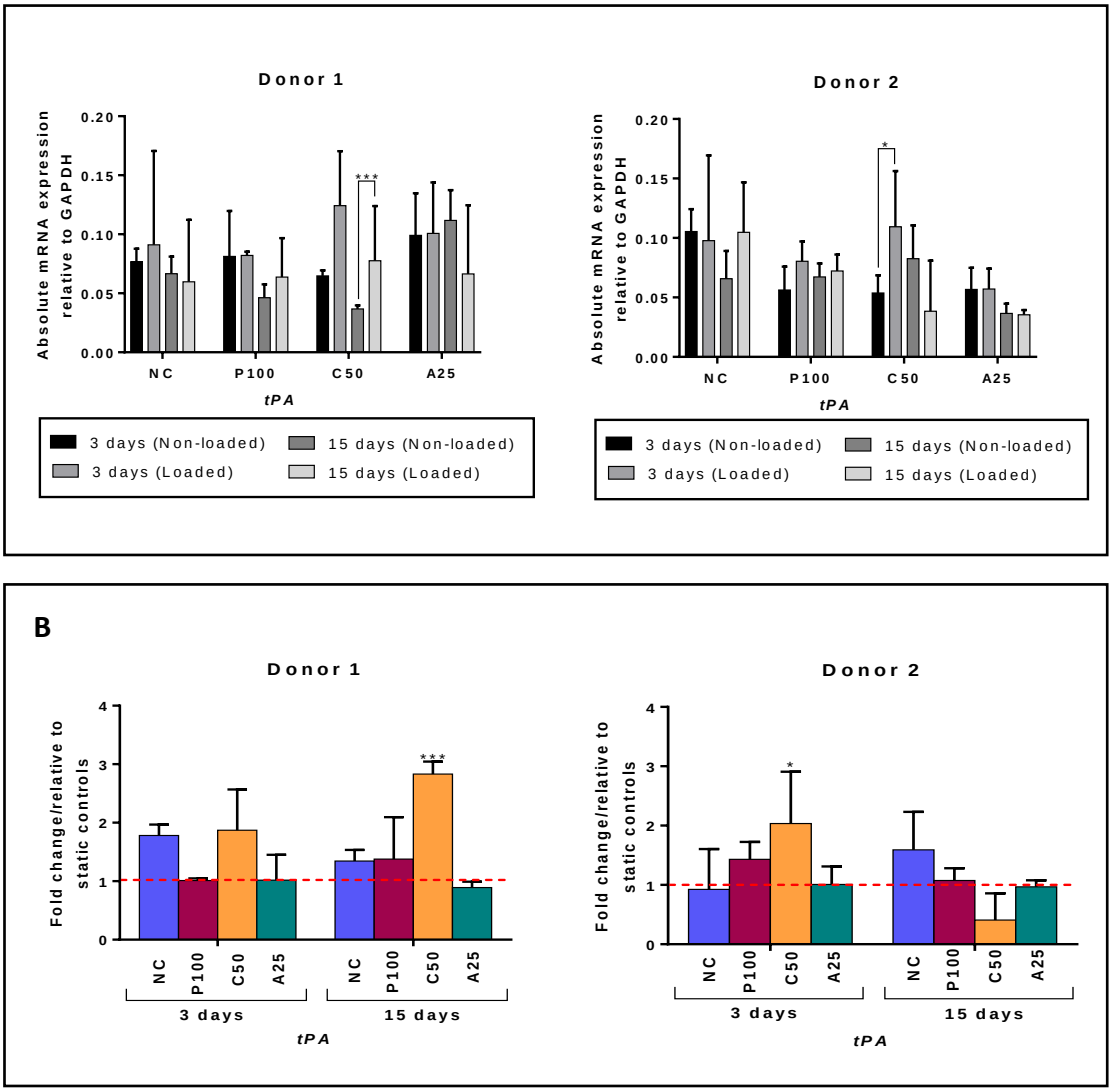

Figure 6.3 Effect of cyclic tensile strain on *tPA* mRNA expression of bSCs in P100, C50 and A25 coated constructs.

The figure demonstrates the effect of applying cyclic tensile strain of 5% at a frequency of 1 Hz (for 1 hour every day) on *tPA* expression of bSCs within each construct (NC, P100, C50 and A25). Data is presented for 3 days and 15 days of culture with DMEM supplemented with 10% FBS, for two donors. Values are normalised to *GAPDH* expression. Statistical significance was determined using a one-way ANOVA. * = $p \leq 0.05$, *** = $p \leq 0.001$.

A) Bars represent the mean absolute mRNA expression (Δ Ct) of non-loaded and loaded constructs ± relative standard deviation (n=3).

B) Bars represent the mean of the fold change (ΔΔ Ct) relative to corresponding non-loaded controls (indicated by the dotted line) ± relative standard deviation (n=3).

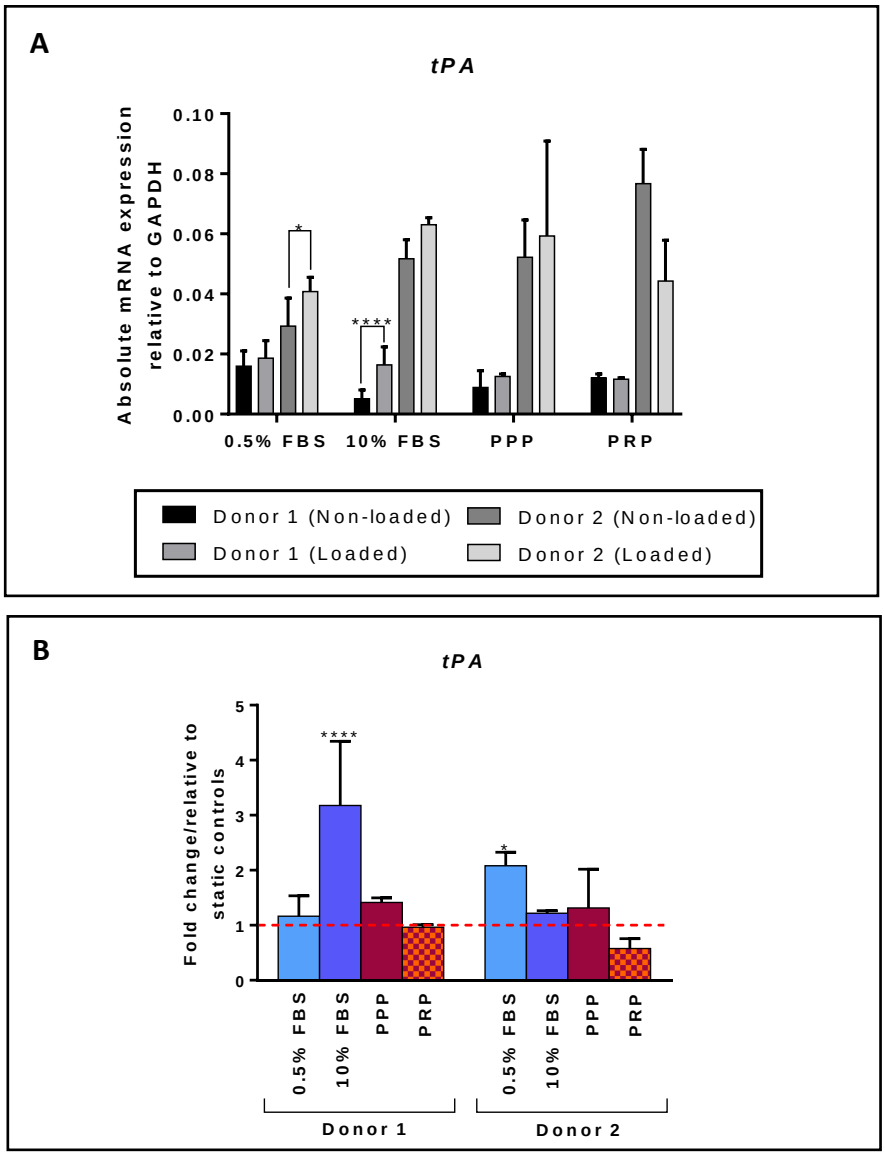

Figure 6.4 Effect of cyclic tensile strain on *tPA* expression of bSCs in PPP and PRP coated constructs.

The figure demonstrates the effect of applying cyclic tensile strain of 5% at a frequency of 1 Hz on *tPA* expression of cells within each construct (0.5% FBS, 10% FBS, PPP and PRP). All constructs were cultured for a total of 4 days and loaded constructs were subjected to 3 strain sessions (for 1 hour per day). Data is presented for donors 1 and 2. Values are normalised to *GAPDH* expression. Statistical significance was determined using a one-way ANOVA. * = $p \leq 0.05$, **** = $p \leq 0.0001$.

A) Bars represent the mean absolute mRNA expression (Δ Ct) of non-loaded and loaded constructs ± relative standard deviation (n=3).

B) Bars represent the mean of the fold change (ΔΔ Ct) relative to corresponding non-loaded controls (indicated by the dotted line) ± relative standard deviation (n=3).

6.2.2.2 Cyclic tensile strain significantly upregulates *PAI-1* gene expression in bSCs at all time points

Figure 6.5 shows the effect of cyclic tensile strain on the expression of *PAI-1* in bSCs cultured in non-coated, P100, C50 and A25 coated constructs. Both donors showed a significant upregulation of *PAI-1* in response to cyclic strain (5% strain at frequency of 1 Hz, for 1 hour every day), in all constructs, at both 3 days and 15 days. Levels of upregulation ranged from 3-fold ($p \leq 0.01$) to 23-fold ($p \leq 0.01$) and did not appear to be affected by construct type, nor time point.

The effect of cyclic tensile strain on *PAI-1* expression in bSCs cultured on scaffolds treated with 0.5% FBS, 10% FBS or those coated with PPP or PRP is shown in Figure 6.6. Application of cyclic tensile strain (5% strain at a frequency of 1 Hz) resulted in a significant upregulation in expression in all supplementation groups, in both donors. Upregulation ranged from 4.5-fold ($p \leq 0.05$) to 8-fold ($p \leq 0.01$). Treatment type (0.5% FBS, 10% FBS, PPP or PRP) did not appear to have any effect on the level of upregulation induced by the application of cyclic strain.

A summary of the effect of cyclic tensile strain on *tPA* and *PAI-1* expression can be found in Tables 11a and 11b.

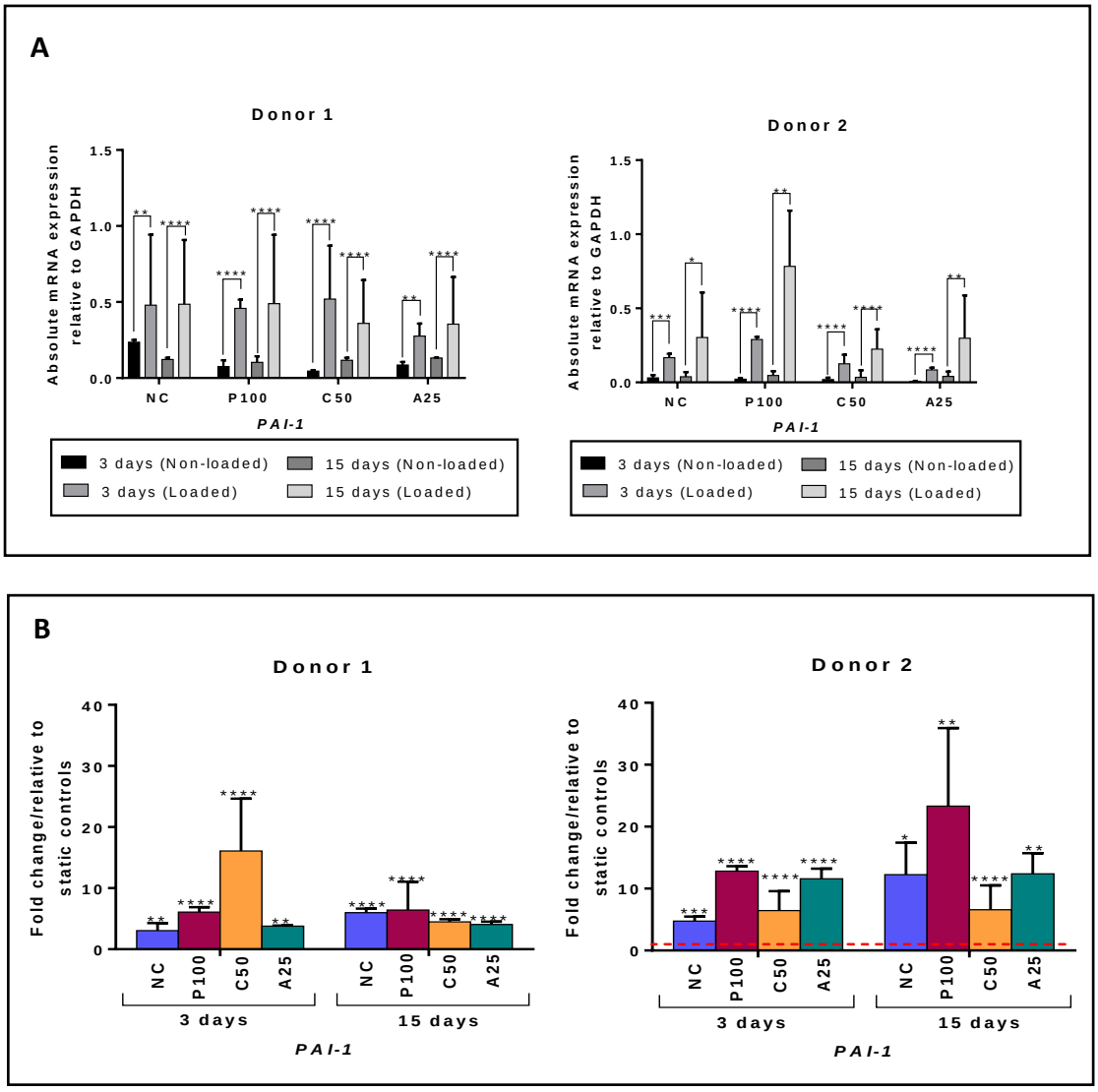

Figure 6.5 Effect of cyclic tensile strain on *PAI-1* mRNA expression of bSCs in P100, C50 and A25 coated constructs.

The figure demonstrates the effect of applying cyclic tensile strain of 5% at a frequency of 1 Hz (for 1 hour every day) on *PAI-1* expression of bSCs within each construct (NC, P100, C50 and A25). Data is presented for 3 days and 15 days of culture with DMEM supplemented with 10% FBS, for two donors. Values are normalised to *GAPDH* expression. Statistical significance was determined using a one-way ANOVA. * = $p \leq 0.05$, ** = $p \leq 0.01$, *** = $p \leq 0.001$, **** = $p \leq 0.0001$.

A) Bars represent the mean absolute mRNA expression (Δ Ct) of non-loaded and loaded constructs ± relative standard deviation (n=3).

B) Bars represent the mean of the fold change (ΔΔ Ct) relative to corresponding non-loaded controls (indicated by the dotted line) ± relative standard deviation (n=3).

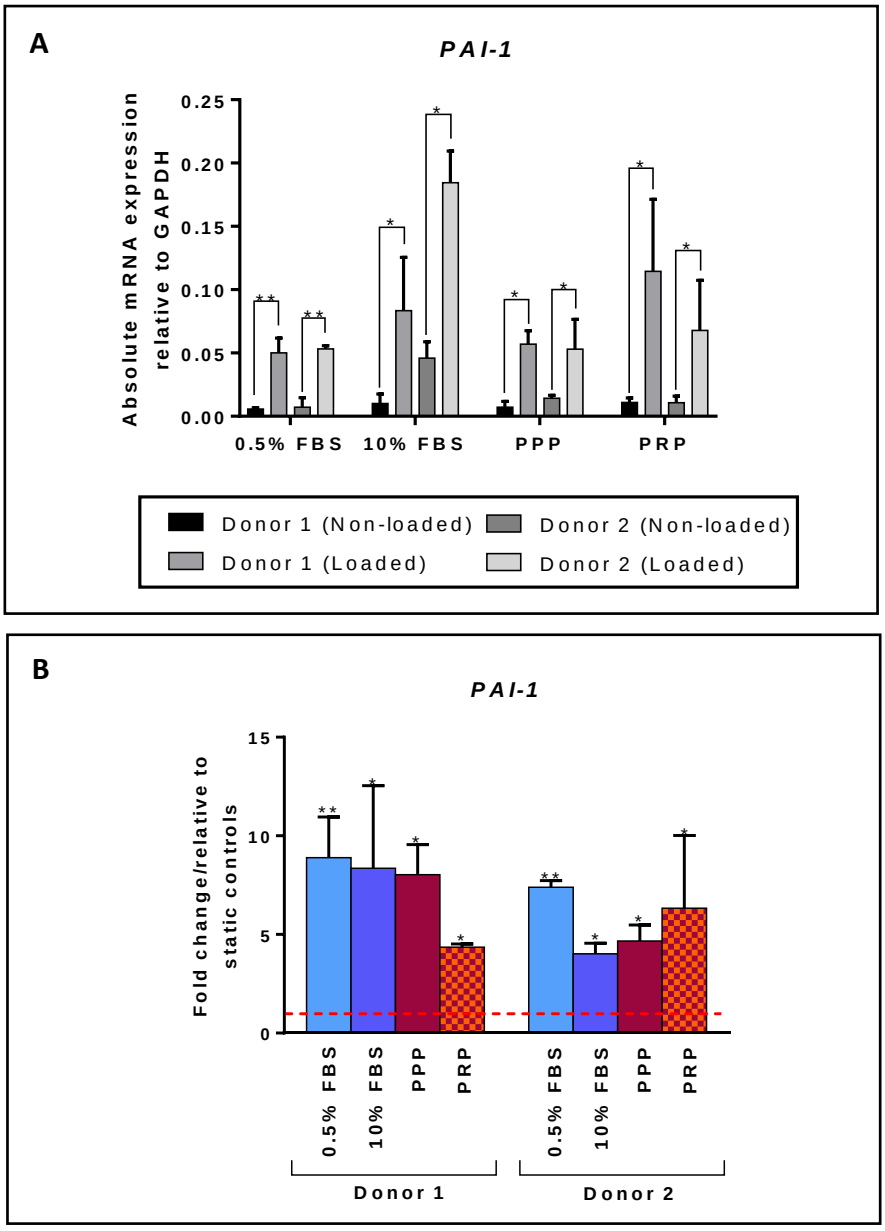

Figure 6.6 Effect of cyclic tensile strain on *PAI-1* expression of bSCs in PPP and PRP coated constructs.

The figure demonstrates the effect of applying cyclic tensile strain of 5% at a frequency of 1 Hz on *PAI-1* expression of cells within each construct (0.5% FBS, 10% FBS, PPP and PRP). All constructs were cultured for a total of 4 days and loaded constructs were subjected to 3 strain sessions (for 1 hour per day). Data is presented for donors 1 and 2. Values are normalised to *GAPDH* expression. Statistical significance was determined using a one-way ANOVA. * = $p \leq 0.05$, ** = $p \leq 0.01$.

A) Bars represent the mean absolute mRNA expression (Δ Ct) of non-loaded and loaded constructs ± relative standard deviation (n=3).

B) Bars represent the mean of the fold change (ΔΔ Ct) relative to corresponding non-loaded controls (indicated by the dotted line) ± relative standard deviation (n=3).

Table 11a Summary of the effect of cyclic tensile strain on *tPA* and *PAI-1* expression of cells in NC, P100, C50 and A25 coated scaffolds.

		NC		P100		C50		A25	
	Gene	Donor 1	Donor 2	Donor 1	Donor 2	Donor 1	Donor 2	Donor 1	Donor 2
3 days	*tPA*	NS	NS	NS	NS	NS	2 (p≤0.05)	NS	NS
	PAI-1	3 (p≤0.01)	4.7 (p≤0.001)	6 (p≤0.0001)	12 (p≤0.0001)	16 (p≤0.0001)	6.4 (p≤0.0001)	3.7 (p≤0.01)	11.6 (p≤0.0001)
15 days	*tPA*	NS	NS	NS	NS	3 (p≤0.001)	NS	NS	NS
	PAI-1	6 (p≤0.0001)	12 (p≤0.05)	6.4 (p≤0.0001)	23 (p≤0.01)	4.5 (p≤0.0001)	6.6 (p≤0.0001)	4 (p≤0.0001)	12 (p≤0.01)

Table 11a summarises the changes in *tPA* and *PAI-1* gene expression resulting from the application of cyclic tensile strain to NC, P100, C50 and A25 constructs, after 3 and 15 days, in cells from donors 1 and 2. Values indicate the fold change in gene expression relative to non-loaded controls (green cells indicate statistically significant upregulation). Statistical significance is presented in brackets. NS indicates no statistically significant difference. Cyclic tensile strain induced a significant upregulation of *PAI-1* expression in all groups.

Table 11b Summary of the effect of cyclic tensile strain on *tPA* and *PAI-1* expression of cells in 0.5% FBS, 10% FBS supplemented annd PPP and PRP coated scaffolds.

	0.5% FBS		10% FBS		PPP		PRP	
Gene	Donor 1	Donor 2	Donor 1	Donor 2	Donor 1	Donor 2	Donor 1	Donor 2
tPA	NS	2 (p≤0.05)	3 (p≤0.0001)	NS	NS	NS	NS	NS
PAI-1	9 (p≤0.01)	7.3 (p≤0.01)	8 (p≤0.05)	4 (p≤0.01)	8 (p≤0.05)	4.7 (p≤0.05)	4 (p≤0.05)	6.3 (p≤0.05)

Table 11b summarises the changes in *tPA* and *PAI-1* gene expression resulting from the application of 3 sessions of cyclic tensile strain to scaffolds supplemented with 0.5% FBS, 10% FBS, PPP and PRP, in cells from donors 1 and 2. Values indicate the fold change in gene expression relative to non-loaded controls (green cells indicate statistically significant upregulation). Statistical significance is presented in brackets. NS indicates no statistically significant difference. Cyclic tensile strain induced a significant upregulation of *PAI-1* expression in all groups.

6.2.3 Effect of cyclic tensile strain on PAI-1 secretion at protein level

As shown in section 6.2.2.2, application of cyclic tensile strain caused a significant upregulation of *PAI-1* expression in all constructs and at all time points measured. To determine whether this resulted in increased translation into active protein, a western blot was performed. Due to a lack of commercially available bovine specific PAI-1 antibodies, a sequence alignment was performed using the Clustal Omega online sequence alignment programme to determine whether a human PAI-1 antibody would be likely to react with bovine PAI-1 protein.

6.2.3.1 Sequence alignment results indicated a 92% amino acid sequence similarity between human and bovine PAI-1 proteins

A sequence alignment was performed to compare the amino acid sequences of human and bovine PAI-1. The results showed a 92% sequence similarity (Figure 6.7) indicating that a human targeted PAI-1 antibody would be highly likely to also react with bovine PAI-1. As a result, a human anti-PAI-1 antibody was used for subsequent western blot analysis.

6.2.3.2 Cyclic tensile strain increased PAI-1 protein secretion from bSCs

Western blotting was performed on extracted proteins from the culture media of non-coated (NC) scaffolds under non-loaded and loaded conditions, after 5 days of culture (according to the methods detailed in sections 6.1.2.2 and 6.1.2.3). Figure 6.8 shows images of the western blot membranes after incubation with the secondary antibody only (which served as the negative control) (B), and after incubation with both the primary and secondary antibodies (A). Lanes 1-3 were loaded with precipitated media (prepared according to section 6.1.2.2) from scaffolds which had been subjected to 4 sessions of cyclic tensile strain (for 1 hour per day). Lanes 5 to 7 were loaded with precipitated media from scaffolds which had been cultured under non-loaded conditions. Immunoreactive bands were clearly visible in lanes 1-3 migrating at 45 KDa, which corresponds with the molecular weight of PAI-1. Bands were visible at this position in lanes 5-7, but were significantly fainter. No non-specific binding of the secondary antibody was detected, indicated by the absence of bands in sample lanes, in Figure 6.8 B. These results confirmed that loading the constructs led to an increase in bSC-secreted PAI-1 protein.

Figure 6.7 Sequence alignment of the human and bovine PAI-1 amino acid sequences. Results from a human/bovine PAI-1 sequence alignment analysis performed using the Clustal Omega programme provided by the European Bioinformatics Institute (EMBL-EBI). The programme calculated a 92% similarity between sequences.

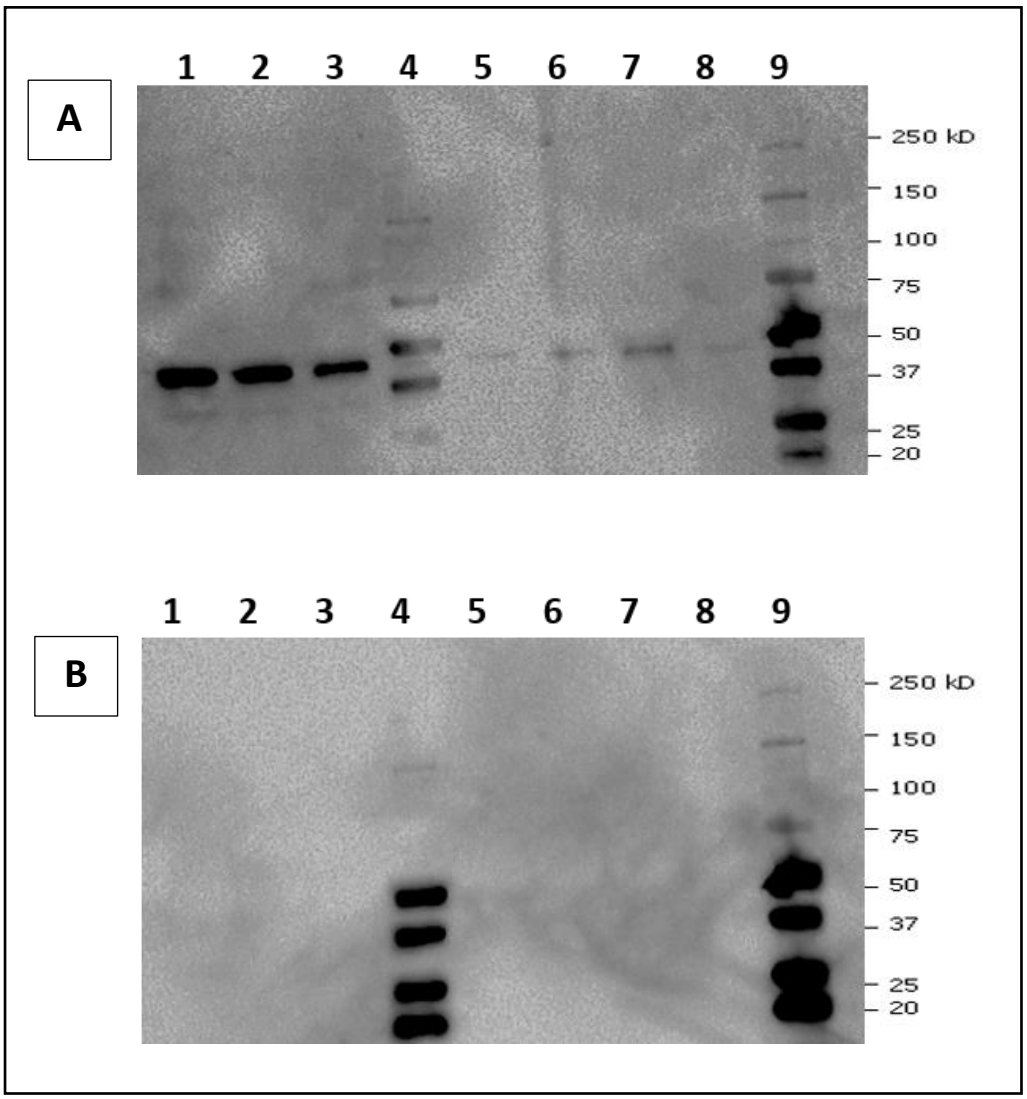

Figure 6.8 Western blot of PAI-1 secretion under non-loaded and loaded conditions. Western blot gels tagged with anti-PAI-1 primary and anti-rabbit secondary antibodies (A), and anti-rabbit secondary antibody only (B). Lanes 4 and 9 were loaded with Precision Plus Protein Western C standards. Lanes 1-3 were loaded with media from non-coated scaffolds which had been subjected to 4 loading sessions over a total culture period of 5 days. Lanes 5-7 were loaded with media from non-loaded non-coated scaffolds which had been cultured for a total of 5 days. Lane 8 was left unloaded.

6.3 Discussion

Observation of P100 constructs under non-loaded and loaded conditions showed a substantial increase in plasma gel stability when subjected to cyclic tensile strain (see Figure 4.18). Plasmin is the main proteolytic enzyme responsible for fibrin degradation. It circulates in blood in its inactive form, plasminogen, which can be activated by a number of enzymes, but primarily tissue-type plasminogen activator (tPA). In vascular endothelial cells, the application of 10% cyclic strain causes a significant downregulation of tPA expression, as well as an upregulation of its inhibitor, plasminogen activator inhibitor-1 (PAI-1) (Ulfhammer *et al.,* 2005). Fibroblasts have also been found to express both tPA and PAI-1, and upon application of mechanical stress, PAI-1 upregulation has been induced in fibroblasts (Saed and Diamond, 2003; Kessler *et al.* 2001). Although PAI-1 appears to be consistently upregulated upon application of strain, regardless of time point, changes in tPA expression seem to be more variable, with studies reporting early increase in expression upon application of strain, followed by significant downregulation by around 48 hours (Sumpio *et al.*, 1997; Ulfhammer *et al.,* 2005). This chapter aimed to identify the molecular mechanism by which the longevity of plasma was enhanced when plasma coated PET scaffolds were subjected to cyclic tensile strain using the bioreactor described in this project (section 4.1.4.2, Chapter 4).

Cyclic tensile strain was applied to all constructs. This included P100, C50 and A25 coated and non-coated constructs which were subjected to 3 and 15 days of cyclic tensile strain (5% strain at a frequency of 1 Hz, for 1 hour every day) as detailed in Chapter 4 (section 4.1.4.2), as well as the constructs assessed in Chapter 5 (0.5% FBS, 10% FBS, PPP coated and PRP coated) which were subjected to 3 days of cyclic strain. The effect of cyclic tensile strain on expression of *tPA* and *PAI-1* mRNA was analysed in cells from the 2 donors.

It was hypothesised that by applying cyclic strain to the hybrid constructs, a downregulation of *tPA* would be observed, along with an upregulation of *PAI-1***.** Interestingly, no significant downregulation of *tPA* was found in any of the constructs (P100, C50, A25, NC, 0.5% FBS, 10% FBS, PPP and PRP), at any of the time points measured (see Figures 6.3 and 6.4). Cells in some constructs showed a significant upregulation, but the level of expression varied between donors. This could indicate that *tPA* expression is regulated differently in synovial cells in comparison with endothelial cells, which were found to downregulate *tPA* when exposed to tensile strain (Ulfhammer *et al.*, 2005).

Conversely, *PAI-1* was significantly upregulated (3-24-fold) in response to cyclic strain in all constructs (P100, C50, A25, NC, 0.5% FBS, 10% FBS, PPP and PRP), at all time points (see Figures 6.5 and 6.6). Results from non-coated scaffolds could indicate a time-dependant

increase in *PAI-1* expression, with a greater expression increase in response to cyclic tensile strain at 15 days (donor 1 = 6-fold, donor 2 = 12-fold) than at 3 days (donor 1 = 3-fold, donor 2 = 5-fold). This trend was not evident in coated constructs however, perhaps due to inconsistencies in the transmission of forces through the gels.

Western blotting was used to determine whether this increase in mRNA was translated into elevated PAI-1 protein secretion. Media was only harvested from non-coated cell-seeded scaffolds to analyse PAI-1 secretion as plasma naturally contains PAI-1 (Vaughan, 2005). Using non-coated control scaffolds, it was evident that bSCs subjected to cyclic tensile strain secreted significantly more PAI-1 than those cultured under non-loaded conditions (see Figure 6.8).

This is highly indicative of increased PAI-1 levels being a cause of improved P100 stability in response to cyclic tensile strain. Elevated synthesis of ECM components such as collagen may have also contributed to this effect, by reinforcing the matrix and allowing cells to continue to spread between PET fibres. However, as cyclic tensile strain did not maintain the stability of the C50 construct, any elevated levels of ECM synthesis may not have been sufficient to offset the rate of gel degradation. Furthermore, very few examples of significant upregulation of ECM genes was identified in any construct, as a result of strain application (see Table 7, Chapter 4). Work by Raif (2008), demonstrated that applying 4.5% strain to bovine synovial cells, for 1 hour, induced a 3-fold upregulation of *MMP-3* expression, which is a key protease involved in matrix degradation. An increase in MMP-3 could promote degradation of synthesised ECM components. Furthermore, the same study found that applying cyclic tensile strain to bovine synovial cells induced no change in the expression of *MMP-1* (a collagenase), nor its inhibitor, tissue inhibitor of metalloproteases (*TIMP-1*). Degradation of the collagen component (50%) of C50 constructs would therefore occur to at least the same extend under loaded conditions as it does under non-loaded conditions, leading to significant loss of gel.

On the other hand, a study conducted by Varju *et al.* (2011) subjected acellular fibrin (in the form of human thrombi) to mechanical strain, and found that fibrin breakdown was reduced in comparison with non-stretched samples. This would suggest that reduced fibrin breakdown is not dependant on the increased PAI-1 secretion from cells. The authors concluded that strain promoted a conformational change in the fibrin matrix, increasing its density, and thereby reducing access of plasmin to fibrin binding sites. Furthermore, they also reported reduced binding of tPA to stretched fibrin, resulting in reduced cleavage of plasminogen to active plasmin. Collet *et al*. (2011) also found fibrin stiffness to positively correlate with its stability. In light of this evidence, it is likely that the increased longevity of the P100 coating subjected

to strain is due to a combination of increased fibrin density, along with increased cellular secretion of PAI-1. To quantify the contribution of each of these mechanisms, fibrin degradation should be compared using mechanically strained fibrin gels with and without the addition of cells.

6.4 Summary

In a clinical setting, it is crucial that a ligament construct is stable enough to support growth of a new ECM, and that it maintains this stability until the ECM is mature enough to support itself. Although long-term tests, as well as *in vivo* studies, would be required to fully establish the longevity of the P100 coating, results presented in this study suggest that it holds potential promise as a method for enhancing long-term tissue induction throughout the Xiros PET ligament when exposed to cyclic loading during activities such as walking or the rehabilitation exercises prescribed after ACL reconstructive surgery. This is the first known example of the anti-fibrinolytic effects of mechanical strain being exploited to enhance the stability of a tissue engineered construct.

Chapter 7

Final discussion

This project aimed to address the insufficiencies associated with the Xiros PET ligament by incorporating a biological, platelet-rich gel which would provide a physiologically relevant substrate and growth factor release system to promote cell proliferation and tissue induction, which has previously been identified as a cause of failure following ACL replacement with a Xiros ligament (Schroven *et al*., 1994). Sections of PET scaffold were coated with various mixtures of blood plasma, collagen and alginate, to produce hybrid constructs. It was hypothesised that by coating the PET scaffold with biological polymers, the bioactivity of the scaffold could be enhanced, by providing growth factors from platelets within the coatings, and creating a more physiologically relevant extracellular environment. These constructs were subjected to multiple tests to determine their effect on cell proliferation and infiltration in comparison with the non-coated scaffold, as well comparing the longevity of each gel coating (Chapter 3). Selection of the three most promising coated constructs, with coatings composed of 100% plasma, 50:50 collagen/plasma and 25:75 alginate/plasma, led to additional tests. Cell viability, growth factor release and gene expression was assessed, before then investigating how the application of a physiologically relevant cyclic tensile strain regime affected proliferation and gene expression of cells within each coated construct (Chapter 4). This eventually led to selection of the final coated construct, composed of 100% plasma, based on its superior durability upon strain application. Comparison of platelet-rich and platelet-poor plasma coatings revealed no significant difference in cell proliferation, infiltration or gene expression within constructs (Chapter 5).

The final hybrid construct developed in this project can be produced easily and cheaply using a simple method to coat the PET ligament with a fibrin gel containing platelets. In a clinical setting, it is anticipated that the ligament would be coated using plasma derived from the patient's own blood, to ensure maximum platelet viability (Marx, 2004). Since increasing the platelet density above normal levels did not produce any identifiable benefit, in terms of cell proliferation or gene expression (see Chapter 5), plasma could be isolated using a single centrifugation step, where plasma is separated from the whole blood but is not further processed. However, *in vivo* studies using autologous plasma samples would be required to confirm that concentrating platelets does not induce any effects above that of a normal platelet density. The coated construct can be fabricated by submerging the Xiros ligament in a few millilitres of blood plasma, activated with 23 mM $CaCl_2$, to form a uniform fibrin gel in which platelets are trapped. Gelation occurs within 30 minutes at 37˚C, also making this a relatively fast procedure.

There is little evidence from the results obtained in this project to suggest that coating the PET ligament with a plasma gel will promote cell proliferation or synthesis of ECM proteins to a greater extent than the non-coated PET ligament. However, limitations associated with *in vitro* studies may be partly responsible for this. Firstly, the controls used in this project consisted of non-coated scaffolds supplemented with 0.5% or 10% FBS. It is unclear how these relate to the synovial environment in terms of growth factor concentration. Interestingly, work by Andrish and Holmes (1979) indicated that ACL fibroblasts exposed to 10% synovial fluid *in vitro* demonstrated diminished cell proliferation and increased aggregation. If synovial fluid has negative proliferative effects on cells populating the PET ligament, then the use of a coating could potentially reduce cellular contact with inhibitory components of the synovial fluid. Furthermore, proliferation of synovial cells has also been found to be significantly reduced in the presence of 10% synovial fluid, in comparison with 10% FBS (Zang *et al*., 2008). This might indicate that applying a coating containing platelets (which release the stimulatory proteins found in serum) to the PET ligament would result in a greater proliferation response from coloniser cells than a non-coated ligament. No examples in the literature could be identified where a PET scaffold has been coated with fibrin, although coating a polyglycolic/polylactic acid scaffold with growth factor rich plasma has previously been demonstrated to enhance cell proliferation *in vitro* (Visser *et al.*, 2010). In terms of *in vivo* studies, no examples were identified in which plasma gels were used in an attempt to augment ACL reconstruction with a synthetic ligament, making it difficult to predict whether incorporating a plasma gel into the Xiros ligament *in vivo* would be more likely to demonstrate a significant improvement in tissue cell proliferation and tissue induction than the results from *in vitro* studies. This further supports the requirement for *in vivo* investigations.

The second limitation of the *in vitro* system used for this project is the relatively short duration of each study. Although changes in expression of ECM genes have previously been reported to occur at as early as 7 days, in response to mechanical forces (Subramony *et al*., 2014), a greater understanding of how the plasma coating affects long-term tissue induction within the Xiros ligament could be achieved by extending the culture period, so that a more mature ECM might be formed. This could then allow for histological analysis of the newly synthesised matrix.

The cells isolated and used within this work were from two different donors, and this resulted in substantial variations in gene expression trends between replicate experiments. Variation between donors in terms of gene expression and proliferation have previously been reported, particularly in MSCs, which show differences with no correlation between age nor gender of the donor (Phinney *et al*., 1999; Ketterl *et al*., 2015). This highlights a requirement for a much

greater number of donors if any consistent trends are to be identified. Cells from donor 1 were found to consistently proliferate more slowly than donor 2 cells. It is hypothesised that this may be linked with the variation in gene expression identified between donors.

This work has demonstrated the improved spatial distribution of cells, induced by coating the PET scaffold with a plasma gel. The coating promoted a homogenous distribution of cells throughout the construct (Chapter 5), and prevented the aggregation of cells identified on the non-coated scaffold during static seeding (see Figure 5.2, Chapter 5). Cell distribution has been linked with the uniformity of tissue formation, suggesting that a more uniformly distributed cell population would result in more uniform tissue synthesis (Kim *et al*., 1998). Uneven tissue formation over the PET ligament may leave areas exposed to abrasive forces within the joint, leading to the formation of wear debris so commonly identified as a limitation of synthetic ligaments (Rushton *et al*., 1983; Legnani *et al*., 2010).

The application of cyclic tensile strain has previously been found to enhance ligament tissue synthesis both *in vitro (*Leung *et al*., 1976; Johannes *et al*., 2000; Berry *et al*., 2003) and *in vivo* (Fujikawa et al., 1989; Amiel et al., 1994; Ng, 2002; Beynnon *et al*., 2005), and is therefore an important factor to include in any study which aims to enhance the development of ligament tissue. The results from this project demonstrated a significant increase in cell proliferation, in as early as 3 days, when bSC-seeded PET scaffolds were subjected to 5% cyclic tensile strain, at a frequency of 1 Hz, for 1 hour every day. This supports all previously mentioned studies which indicate that early mobilisation of the knee following ACL reconstruction is vital for stimulating cellular activity. There was very limited evidence to suggest that cyclic tensile strain enhanced matrix synthesis from the results obtained in this project. However, it is possible that supplementing cells with 10% FBS or a plasma gel (containing platelets) resulted in a maximum stimulus, thereby preventing any additional stimulus in expression from the application of strain. Future experimental design for investigation of the effect of cyclic tensile strain on cellular gene expression within coated constructs, should carefully consider levels of serum supplementation. Use of coatings which are entirely free of platelets, as well as a reduction in media serum concentration, may make any changes attributed to strain more detectable.

Cyclic tensile strain induced expression of plasminogen activator inhibitor 1 (PAI-1), which is a possible mechanism by which fibrin breakdown is inhibited in plasma-coated scaffolds that are subjected to strain. Reduced fibrinolysis has previously been reported in acellular fibrin subjected to mechanical strain (Varju *et al.*, 2011), which suggests that the reduced fibrin loss identified in this study could be due to a combination of PAI-1-mediated inhibition of fibrinolysis, and a strain-induced conformational change in the fibrin structure, which

increases the matrix density and reduces the access of fibrinolytic enzymes to fibrin binding sites. Regardless of which mechanism is most accountable for this increase in fibrin stability, this work highlights the importance of regular application of cyclic tensile strain to a plasma-coated ligament construct, in order to maintain the coating. In a clinical setting, this would be in the form of regular exercise of the knee joint.

Coating the Xiros ligament with human plasma is a simple, fast and inexpensive method of incorporating a biological component into this synthetic ligament, which promotes a more uniform distribution of cells throughout the construct. As previously mentioned, there are two possible approaches to the use of this hybrid construct in a tissue engineering setting. The fist involves ACL reconstruction using an acellular plasma-coated ligament directly after fabrication. Another strategy could be to seed patient cells within the plasma-coated Xiros ligament, and to maintain this seeded ligament *in vitro* to promote synthesis of tissue prior to ACL reconstruction. This latter strategy would require the development of large-scale bioreactor systems capable of applying the necessary forces to stimulate ligament tissue development, as well as an improvement in current tissue culture methods. Using either strategy it is likely that the more uniform distribution of cells, promoted by the plasma coating, will be beneficial to tissue induction. The studies conducted in this work involved maximum culture periods of 15 days. Culture of longer duration should be carried out to understand the long-term effect of the plasma gel coating on tissue induction within the Xiros ligament. The limitations associated with the *in-vitro* system demonstrate the necessity of *in-vivo* studies to conclude whether coating the Xiros ligament with an autologous plasma gel will improve tissue induction within the synovial environment.

Summary

The synthetic Xiros PET ligament has been developed to address issues associated with autograft or allograft-based approached to anterior cruciate ligament (ACL) reconstruction. However, the slow rate of tissue induction on the Xiros ligament has been associated with its failure, by leaving areas of scaffold exposed to bone abrasion. The aim of this work was to enhance the bioactivity of the Xiros PET ligament scaffold by incorporating a biological component that may promote cell growth and indicate an increase in tissue induction.

The Xiros PET scaffold has been successfully coated with human plasma, collage type I and alginate, to produce hybrid ligament constructs that support the growth of bovine synovial cells *in vitro*. Coatings with high alginate content were found to inhibit cell proliferation and infiltration, while collagen and plasma coatings promoted a uniform distribution of cells throughout the construct, and induced a similar level of proliferation to the non-coated scaffold. Alginate coatings had superior longevity in comparison with collagen and plasma coatings, which were almost entirely lost by 15 days, leading to the loss of the uniform cell distribution. Application of cyclic tensile strain (5% at a frequency of 1 Hz) resulted in an upregulation of plasminogen activator inhibitor-1 (PAI-1) and a marked increase in longevity of the plasma coating. PAI-1 inhibits fibrin degradation and so the improvement in plasma coating longevity is thought to be linked with increased PAI-1 expression.

Cyclic tensile strain promoted greater cell proliferation within 3 days, but changes in gene expression were inconsistent between donors, making it difficult to draw conclusions on the effects of cyclic strain on cell differentiation. Supplementation with serum may have masked potential strain-induced differences in transcriptional stimulation. Platelet density was not found to significantly affect cell proliferation or gene expression.

A coating consisting of 100% blood plasma was found to be the most promising, of those tested, for the purpose of enhancing tissue growth over the Xiros ligament. The coating promoted cellular infiltration throughout the construct to a greater extent than the non-coated control scaffold, and the application of strain preserved the coating up to conclusion of the experiment, at 15 days. This work indicates that coating the Xiros ligament with blood plasma, derived from the patient, could promote more uniform tissue synthesis, thereby protecting the ligament from abrasive forces *in vivo*. This is the first known example of a biopolymer gel being incorporated into the Xiros ligament scaffold in an attempt to enhance its bioactivity. Long-term studies and *in vivo* investigations will be required to confirm whether the coating induces superior tissue induction.

Limitations

A number of limitations were identified with regard to the work presented. Variations in gene expression between donors led to inconclusive results in terms of how the coatings and the application of strain affected cellular differentiation and matrix synthesis. A greater number of donors should be used to identify transcriptional responses. Time limitations meant that cells from only 2 donors were investigated. Additional genes should also be investigated, including markers of chondrogenic differentiation (e.g. Collagen type II, Aggrecan, SOX9), to ensure that differentiation is not being directed towards a cartilage-like phenotype.

The studies conducted in this work involved maximum culture periods of 15 days, to investigate early changes in cell behaviour. For a greater understanding of how the plasma coating affects tissue induction on the Xiros ligament at later stages, constructs should be cultured to longer time points. Culture periods of 2-3 months should result in more tissue development, which could then be assessed histologically. By 15 days in culture, the gel coatings were still very soft, which would have made processing the samples for histology challenging.

Cell-seeded constructs were supplemented with FBS throughout the project as this is a commonly used method of cell supplementation *in vitro*. However, this may have led to overstimulation of the cells, particularly when used at a concentration of 10%. FBS is derived from blood plasma, and so is not representative of the synovium, in which the Xiros ligament would be implanted. The use of synovial fluid as an *in vitro* supplementation method may produce results more representative of how cells would behave within the synovium.

All investigations within this project were carried out *in vitro*, as preliminary studies, since coating the Xiros ligament has not previously been done. If further investigations reveal greater evidence that the coated scaffold enhances tissue induction, then *in vivo* animal studies should be considered to investigate how the coated ligament behaves within a living system. The coated scaffold may then be compared with the non-coated ligament, as well as an autograft, which is the current gold standard treatment, so that tissue growth and maturation can be assessed.

References

AGLIETTI, P., BUZZI, R., D'ANDRIA, S. & ZACCHEROTTI, G. 1992. Long-term study of anterior cruciate ligament reconstruction for chronic instability using the central one-third patellar tendon and a lateral extraarticular tenodesis. The American Journal of Sports Medicine, 20, 38-45.

ALSBERG, E., ANDERSON, K. W., ALBEIRUTI, A., FRANCESCHI, R. T. & MOONEY, D. J. 2001. Cell-interactive Alginate Hydrogels for Bone Tissue Engineering. Journal of Dental Research, 80, 2025-2029.

ALTMAN, G. H., HORAN, R. L., LU, H. H., MOREAU, J., MARTIN, I., RICHMOND, J. C. & KAPLAN, D. L. 2002. Silk matrix for tissue engineered anterior cruciate ligaments. Biomaterials, 23, 4131-4141.

AMABLE, P. R., CARIAS, R. B. V., TEIXEIRA, M. V. T., DA CRUZ PACHECO, Í., CORRÊA DO AMARAL, R. J. F., GRANJEIRO, J. M. & BOROJEVIC, R. 2013. Platelet-rich plasma preparation for regenerative medicine: optimization and quantification of cytokines and growth factors. Stem Cell Research & Therapy, 4, 67-75.

AMIEL, D., FRANK, C., HARWOOD, F., FRONEK, J. & AKESON, W. 1983. Tendons and ligaments: A morphological and biochemical comparison. Journal of Orthopaedic Research, 1, 257-265.

AMIEL, D., KLEINER, J. B., ROUX, R. D., HARWOOD, F. L. & AKESON, W. H. 1986. The phenomenon of "Ligamentization": Anterior cruciate ligament reconstruction with autogenous patellar tendon. Journal of Orthopaedic Research, 4, 162-172.

AMIEL, D., WALLACE, C. D. & HARWOOD, F. L. 1994. The effects of immobilization on the maturation of the anterior cruciate ligament of the rabbit knee. The Iowa Orthopaedic Journal, 14, 134-140.

AMINI, A. R., LAURENCIN, C. T. & NUKAVARAPU, S. P. 2012. Bone tissue engineering: recent advances and challenges. Crit Rev Biomed Eng, 40, 363-408.

AMIS, A. A. & DAWKINS, G. P. 1991. Functional anatomy of the anterior cruciate ligament. Fibre bundle actions related to ligament replacements and injuries. J Bone Joint Surg Br, 73, 260-267.

ANDERSEN, T., MARKUSSEN, C., DORNISH, M., HEIER-BAARDSON, H., MELVIK, J. E., ALSBERG, E. & CHRISTENSEN, B. E. 2014. In Situ Gelation for Cell Immobilization and Culture in Alginate Foam Scaffolds. Tissue Engineering. Part A, 20, 600-610.

ANDERSON, A., F., SNYDER, R., B. & LIPSCOMB, JR., A. BRANT 2001. Anterior Cruciate Ligament Reconstruction: A Prospective Randomized Study of Three Surgical Methods. The American Journal of Sports Medicine, 29, 272-279.

ANDREWS, R. K., LÓPEZ, J. & BERNDT, M. C. 1997. Molecular mechanisms of platelet adhesion and activation. The International Journal of Biochemistry & Cell Biology, 29, 91-105.

ANDRISH, J. & HOLMES, R. 1979. Effects of synovial fluid on fibroblasts in tissue culture. Clin Orthop Relat Res, 279-283.

ANITUA, E. 1999. Plasma rich in growth factors: preliminary results of use in the preparation of future sites for implants. International journal of Oral and maxillofacial Implants, 14, 529-535.

ANITUA, E., SANCHEZ, M., NURDEN, A. T., ZALDUENDO, M., DE LA FUENTE, M., ORIVE, G., AZOFRA, J. & ANDIA, I. 2006. Autologous fibrin matrices: a potential source of biological mediators that modulate tendon cell activities. J Biomed Mater Res A, 77, 285-293.

ANITUA, E., SÁNCHEZ, M. & ORIVE, G. 2011. The importance of understanding what is platelet-rich growth factor (PRGF) and what is not. Journal of Shoulder and Elbow Surgery, 20, 23-24.

ANITUA, E., SANCHEZ, M., ZALDUENDO, M. M., DE LA FUENTE, M., PRADO, R., ORIVE, G. & ANDIA, I. 2009. Fibroblastic response to treatment with different preparations rich in growth factors. Cell Prolif, 42, 162-170.

ANKER, P., ZAJAC, V., LYAUTEY, J., LEDERREY, C., DUNAND, C., LEFORT, F., MULCAHY, H., HEINEMANN, J. & STROUN, M. 2004. Transcession of DNA from Bacteria to Human Cells in Culture: A Possible Role in Oncogenesis. Annals of the New York Academy of Sciences, 1022, 195-201.

ANNUNZIATA, M., OLIVA, A., BUONAIUTO, C., DI FEO, A., DI PASQUALE, R., PASSARO, I. & GUIDA, L. 2005. In vitro cell-type specific biological response of human periodontally related cells to platelet-rich plasma. Journal of Periodontal Research, 40, 489-495.

ARNAOUT, M. A., MAHALINGAM, B. & XIONG, J. P. 2005. Integrin structure, allostery, and bidirectional signaling. Annu Rev Cell Dev Biol, 21, 381-410.

ARNESON, W. A. B., J 2007. Clinical Chemistry: A Laboratory Perspective. Philadelphia, PA, USA: F.A Davis Company, 100-105.

ATESOK, K., DORAL, N. M., BILGE, O. & SEKIYA, I. 2013. Synovial stem cells in musculoskeletal regeneration. Journal of the American Academy of Orthopaedic Surgeons, 21, 258-259.

BAJPAI, S. K. & SHARMA, S. 2004. Investigation of swelling/degradation behaviour of alginate beads crosslinked with Ca2+ and Ba2+ ions. Reactive and Functional Polymers, 59, 129-140.

BANERJEE, A., ARHA, M., CHOUDHARY, S., ASHTON, R. S., BHATIA, S. R., SCHAFFER, D. V. & KANE, R. S. 2009. The influence of hydrogel modulus on the proliferation and differentiation of encapsulated neural stem cells. Biomaterials, 30, 4695-4699.

BARRALET, J. E., WANG, L., LAWSON, M., TRIFFITT, J. T., COOPER, P. R. & SHELTON, R. M. 2005. Comparison of bone marrow cell growth on 2D and 3D alginate hydrogels. Journal of Materials Science: Materials in Medicine, 16, 515-519.

BEEKHUIZEN, M., GIERMAN, L., CREEMERS, L. B., DHERT, W. J., HUIZINGA, T. W., VAN OSCH, G. J. & ZUURMOND, A. M. A descriptive study of synovial fluid changes in cytokine, chemokine and growth factor levels between osteoarthritis patients and healthy donors. Osteoarthritis and Cartilage, 20, 79-80.

BELL, E., IVARSSON, B. & MERRILL, C. 1979. Production of a tissue-like structure by contraction of collagen lattices by human fibroblasts of different proliferative potential in vitro. Proceedings of the National Academy of Sciences, 76, 1274-1278.

BERNADOTTE, A., MIKHELSON, V. M. & SPIVAK, I. M. 2016. Markers of cellular senescence. Telomere shortening as a marker of cellular senescence. Aging (Albany NY), 8, 3-11.

BERNARD, M., HERTEL, P., HORNUNG, H. & CIERPINSKI, T. 1997. Femoral insertion of the ACL. Radiographic quadrant method. The American journal of knee surgery, 10, 14-21; discussion 21-22.

BERRY, C. C., SHELTON, J. C., BADER, D. L. & LEE, D. A. 2003. Influence of external uniaxial cyclic strain on oriented fibroblast-seeded collagen gels. Tissue Eng, 9, 613-624.

BEYNNON, B. D., FLEMING, B. C., JOHNSON, R. J., NICHOLS, C. E., RENSTROM, P. A. & POPE, M. H. 1995. Anterior cruciate ligament strain behavior during rehabilitation exercises in vivo. Am J Sports Med, 23, 24-34.

BEYNNON, B. D., UH, B. S., JOHNSON, R. J., ABATE, J. A., NICHOLS, C. E., FLEMING, B. C., POOLE, A. R. & ROOS, H. 2005. Rehabilitation after Anterior Cruciate Ligament Reconstruction. The American Journal of Sports Medicine, 33, 347-359.

BI, F., SHI, Z., LIU, A., GUO, P. & YAN, S. 2015. Anterior Cruciate Ligament Reconstruction in a Rabbit Model Using Silk-Collagen Scaffold and Comparison with Autograft. PLoS ONE, 10, 1259-1270.

BIEBACK, K., HECKER, A., KOCAÖMER, A., LANNERT, H., SCHALLMOSER, K., STRUNK, D. & KLÜTER, H. 2009. Human Alternatives to Fetal Bovine Serum for the Expansion of Mesenchymal Stromal Cells from Bone Marrow. STEM CELLS, 27, 2331-2341.

BIR, S. C., ESAKI, J., MARUI, A., YAMAHARA, K., TSUBOTA, H., IKEDA, T. & SAKATA, R. 2009. Angiogenic properties of sustained release platelet-rich plasma: characterization in-vitro and in the ischemic hind limb of the mouse. J Vasc Surg, 50, 870-879.

BLAIR, P. & FLAUMENHAFT, R. 2009. Platelet α–granules: Basic biology and clinical correlates. Blood reviews, 23, 177-189.

BLOMBACK, B., CARLSSON, K., FATAH, K., HESSEL, B. & PROCYK, R. 1994. Fibrin in human plasma: gel architectures governed by rate and nature of fibrinogen activation. Thromb Res, 75, 521-538.

BOONTHEEKUL, T., KONG, H. J. & MOONEY, D. J. 2005. Controlling alginate gel degradation utilizing partial oxidation and bimodal molecular weight distribution. Biomaterials, 26, 2455-2465.

BRANCO DA CUNHA, C., KLUMPERS, D. D., LI, W. A., KOSHY, S. T., WEAVER, J. C., CHAUDHURI, O., GRANJA, P. L. & MOONEY, D. J. 2014. Influence of the stiffness of three-dimensional alginate/collagen-I interpenetrating networks on fibroblast biology. Biomaterials, 35, 8927-8936.

BREEN, A., O'BRIEN, T. & PANDIT, A. 2009. Fibrin as a delivery system for therapeutic drugs and biomolecules. Tissue Eng Part B Rev, 15, 201-214.

BREIDENBACH, A. P., DYMENT, N. A., LU, Y., RAO, M., SHEARN, J. T., ROWE, D. W., KADLER, K. E. & BUTLER, D. L. 2015. Fibrin Gels Exhibit Improved Biological, Structural, and Mechanical Properties Compared with Collagen Gels in Cell-Based Tendon Tissue-Engineered Constructs. Tissue Engineering. Part A, 21, 438-450.

BROWN, A. E. X., LITVINOV, R. I., DISCHER, D. E., PUROHIT, P. K. & WEISEL, J. W. 2009. Multiscale Mechanics of Fibrin Polymer: Gel Stretching with Protein Unfolding and Loss of Water. Science, 325, 741-744.

BROWN, L. F., LANIR, N., MCDONAGH, J., TOGNAZZI, K., DVORAK, A. M. & DVORAK, H. F. 1993. Fibroblast migration in fibrin gel matrices. The American Journal of Pathology, 142, 273-283.

BRUDER, S. P., KURTH, A. A., SHEA, M., HAYES, W. C., JAISWAL, N. & KADIYALA, S. 1998. Bone regeneration by implantation of purified, culture-expanded human mesenchymal stem cells. Journal of Orthopaedic Research, 16, 155-162.

BUSSO, N., PÉCLAT, V., SO, A. & SAPPINO, A.-P. 1997. Plasminogen activation in synovial tissues: differences between normal, osteoarthritis, and rheumatoid arthritis joints. Annals of the Rheumatic Diseases, 56, 550-557.

BUSTAMANTE, M. F., GARCIA-CARBONELL, R., WHISENANT, K. D. & GUMA, M. 2017. Fibroblast-like synoviocyte metabolism in the pathogenesis of rheumatoid arthritis. Arthritis Research & Therapy, 19, 110-116.

BUZANOVSKII, V. A. 2017. Determination of proteins in blood. Part 1: Determination of total protein and albumin. Review Journal of Chemistry, 7, 79-124.

BYUNG-SOO, K., J., P. A., J., K. T. & J., M. D. 1998. Optimizing seeding and culture methods to engineer smooth muscle tissue on biodegradable polymer matrices. Biotechnology and Bioengineering, 57, 46-54.

CALMBACH, W. L. & HUTCHENS, M. 2003. Evaluation of patients presenting with knee pain: Part I. History, physical examination, radiographs, and laboratory tests. Am Fam Physician, 68, 907-912.

CANELÓN, S. P. & WALLACE, J. M. 2016. β-Aminopropionitrile-Induced Reduction in Enzymatic Crosslinking Causes In Vitro Changes in Collagen Morphology and Molecular Composition. PLoS ONE, 11, 529-534.

CARE, T. H. Normal Hematocrit Levels [Online]. Available: http://the-healthcare.org/symptoms-and-diagnosis/lab-results/normal-hematocrit-levels/ [Accessed 25th February 2015].

CAROSI, J. A., MCINTIRE, L. V. & ESKIN, S. G. 1994. Modulation of secretion of vasoactive materials from human and bovine endothelial cells by cyclic strain. Biotechnology and Bioengineering, 43, 615-621.

CERVELLIN, M., DE GIROLAMO, L., BAIT, C., DENTI, M. & VOLPI, P. 2012. Autologous platelet-rich plasma gel to reduce donor-site morbidity after patellar tendon graft harvesting for anterior cruciate ligament reconstruction: a randomized, controlled clinical study. Knee Surgery, Sports Traumatology, Arthroscopy, 20, 114-120.

CESARMAN-MAUS, G. & HAJJAR, K. A. 2005. Molecular mechanisms of fibrinolysis. Br J Haematol, 129, 307-321.

CHAPIN, J. C. & HAJJAR, K. A. 2015. Fibrinolysis and the control of blood coagulation. Blood Rev, 29, 17-24.

CHEN, J., XU, J., WANG, A. & ZHENG, M. 2009. Scaffolds for tendon and ligament repair: review of the efficacy of commercial products. Expert Review of Medical Devices, 6, 61-73.

CHEN, T., JIANG, J. & CHEN, S. 2015. Status and headway of the clinical application of artificial ligaments. Asia-Pacific Journal of Sports Medicine, Arthroscopy, Rehabilitation and Technology, 2, 15-26.

CHEN, Y.-J., HUANG, C.-H., LEE, I. C., LEE, Y.-T., CHEN, M.-H. & YOUNG, T.-H. 2008. Effects of Cyclic Mechanical Stretching on the mRNA Expression of Tendon/Ligament-Related and Osteoblast-Specific Genes in Human Mesenchymal Stem Cells. Connective Tissue Research, 49, 7-14.

CHENG, J. J., CHAO, Y. J., WUNG, B. S. & WANG, D. L. 1996. Cyclic Strain-Induced Plasminogen Activator Inhibitor-1 (PAI-1) Release from Endothelial Cells Involves Reactive Oxygen Species. Biochemical and Biophysical Research Communications, 225, 100-105.

CHIEN, S. 2007. Mechanotransduction and endothelial cell homeostasis: the wisdom of the cell. Am J Physiol Heart Circ Physiol, 292, 1209-1224.

CHIQUET, M., GELMAN, L., LUTZ, R. & MAIER, S. 2009. From mechanotransduction to extracellular matrix gene expression in fibroblasts. Biochim Biophys Acta, 1793, 911-920.

CHIQUET, M., SARASA-RENEDO, A. & TUNÇ-CIVELEK, V. 2004. Induction of tenascin-C by cyclic tensile strain versus growth factors: distinct contributions by Rho/ROCK and MAPK signaling pathways. Biochimica et Biophysica Acta (BBA) - Molecular Cell Research, 1693, 193-204.

CHIQUET, M., TUNC-CIVELEK, V. & SARASA-RENEDO, A. 2007. Gene regulation by mechanotransduction in fibroblasts. Appl Physiol Nutr Metab, 32, 967-973.

CHIQUET-EHRISMANN, R., MACKIE, E. J., PEARSON, C. A. & SAKAKURA, T. 1986. Tenascin: an extracellular matrix protein involved in tissue interactions during fetal development and oncogenesis. Cell, 47, 131-139.

CHIQUET-EHRISMANN, R., TANNHEIMER, M., KOCH, M., BRUNNER, A., SPRING, J., MARTIN, D., BAUMGARTNER, S. & CHIQUET, M. 1994. Tenascin-C expression by fibroblasts is elevated in stressed collagen gels. The Journal of Cell Biology, 127, 2093-2101.

CHIU, C. L., HECHT, V., DUONG, H., WU, B. & TAWIL, B. 2012. Permeability of Three-Dimensional Fibrin Constructs Corresponds to Fibrinogen and Thrombin Concentrations. BioResearch Open Access, 1, 34-40.

CHOI, B. H., ZHU, S. J., KIM, B. Y., HUH, J. Y., LEE, S. H. & JUNG, J. H. 2005. Effect of platelet-rich plasma (PRP) concentration on the viability and proliferation of alveolar bone cells: an in vitro study. International Journal of Oral and Maxillofacial Surgery, 34, 420-424.

CLAUDIO LEGNANI, A. V., CLARA TERZAGHI, ENRICO BORGO, AND WALTER ALBISETTI 2010. Anterior cruciate ligament reconstruction with synthetic grafts. A review of literature. International Orthapaedics, 34, 465–471.

CLAUSS, A. 1957. Gerinnungsphysiologische Schnellmethode zur Bestimmung des Fibrinogens. Acta Haematologica, 17, 237-246.

COLLAS, P., LUND, E. G. & OLDENBURG, A. R. 2014. Closing the (nuclear) envelope on the genome: How nuclear lamins interact with promoters and modulate gene expression. BioEssays, 36, 75-83.

COLLET, J. P., ALLALI, Y., LESTY, C., TANGUY, M. L., SILVAIN, J., ANKRI, A., BLANCHET, B., DUMAINE, R., GIANETTI, J., PAYOT, L., WEISEL, J. W. & MONTALESCOT, G. 2006. Altered Fibrin Architecture Is Associated With Hypofibrinolysis and Premature Coronary Atherothrombosis. Arteriosclerosis, Thrombosis, and Vascular Biology, 26, 2567-2573.

COOPER, J. A., JR., SAHOTA, J. S., GORUM, W. J., 2ND, CARTER, J., DOTY, S. B. & LAURENCIN, C. T. 2007. Biomimetic tissue-engineered anterior cruciate ligament replacement. Proc Natl Acad Sci U S A, 104, 3049-3054.

CORSETTI, J. R. & JACKSON, D. W. 1996. Failure of Anterior Cruciate Ligament Reconstruction: The Biologic Basis. Clinical Orthopaedics and Related Research, 325, 42-49.

CREEPER, F., LICHANSKA, A. M., MARSHALL, R. I., SEYMOUR, G. J. & IVANOVSKI, S. 2009. The effect of platelet-rich plasma on osteoblast and periodontal ligament cell migration, proliferation and differentiation. Journal of Periodontal Research, 44, 258-265.

CRUZ, H. J., MOREIRA, J. H. & CARRONDO, J.T. 1999. Metabolic shifts by nutrient manipulation in continuous cultures of BHK cells. Biotechnology and Bioengineering, 66, 104-113.

CSERJESI, P., BROWN, D., LIGON, K. L., LYONS, G. E., COPELAND, N. G., GILBERT, D. J., JENKINS, N. A. & OLSON, E. N. 1995. Scleraxis: a basic helix-loop-helix protein that prefigures skeletal formation during mouse embryogenesis. Development, 121, 1099-1110.

CUMMINGS, C. L., GAWLITTA, D., NEREM, R. M. & STEGEMANN, J. P. 2004. Properties of engineered vascular constructs made from collagen, fibrin, and collagen–fibrin mixtures. Biomaterials, 25, 3699-3706.

CUMMINGS, C. L., GAWLITTA, D., NEREM, R. M. & STEGEMANN, J. P. 2004. Properties of engineered vascular constructs made from collagen, fibrin, and collagen–fibrin mixtures. Biomaterials, 25, 3699-3706.

CUMMINGS, C. L., GAWLITTA, D., NEREM, R. M. & STEGEMANN, J. P. 2004. Properties of engineered vascular constructs made from collagen, fibrin, and collagen–fibrin mixtures. Biomaterials, 25, 3699-3706.

CZAPIGA, M., GAO, J.-L., KIRK, A. & LEKSTROM-HIMES, J. 2005. Human platelets exhibit chemotaxis using functional N-formyl peptide receptors. Experimental hematology, 33, 73-84.

GRASSL, E. D., OEGEMA, T. R. & TRANQUILLO, R. T. 2002. Fibrin as an alternative biopolymer to type-I collagen for the fabrication of a media equivalent. Journal of Biomedical Materials Research, 60, 607-612.

D'ANGELO, F., TIRIBUZI, R., ARMENTANO, I., KENNY, J. M., MARTINO, S. & ORLACCHIO, A. 2011. Mechanotransduction: tuning stem cells fate. J Funct Biomater, 2, 67-87.

DARGEL, J., GOTTER, M., MADER, K., PENNIG, D., KOEBKE, J. & SCHMIDT-WIETHOFF, R. 2007. Biomechanics of the anterior cruciate ligament and implications for surgical reconstruction. Strategies in Trauma and Limb Reconstruction, 2, 1-12.

DE BARI, C., DELL'ACCIO, F., TYLZANOWSKI, P. & LUYTEN, F. P. 2001. Multipotent mesenchymal stem cells from adult human synovial membrane. Arthritis Rheum, 44, 1928-1942.

DE DONATIS, A., COMITO, G., BURICCHI, F., VINCI, M. C., PARENTI, A., CASELLI, A., CAMICI, G., MANAO, G., RAMPONI, G. & CIRRI, P. 2008. Proliferation versus migration in platelet-derived growth factor signaling: the key role of endocytosis. J Biol Chem, 283, 19948-19956.

DE LA PUENTE, P. & LUDEÑA, D. 2014. Cell culture in autologous fibrin scaffolds for applications in tissue engineering. Experimental Cell Research, 322, 1-11.

DENTI, M., BIGONI, M., DODARO, G., MONTELEONE, M. & AROSIO, A. 1995. Long-term results of the Leeds-Keio anterior cruciate ligament reconstruction. Knee Surg Sports Traumatol Arthrosc, 3, 75-77.

DHILLON, M. S., BEHERA, P., PATEL, S. & SHETTY, V. 2014. Orthobiologics and platelet rich plasma. Indian J Orthop, 48, 1-9.

DHURAT, R. & SUKESH, M. S. 2014. Principles and Methods of Preparation of Platelet-Rich Plasma: A Review and Author's Perspective. Journal of Cutaneous and Aesthetic Surgery, 7, 189-197.

DO AMARAL, R. J., MATSIKO, A., TOMAZETTE, M. R., ROCHA, W. K., CORDEIRO-SPINETTI, E., LEVINGSTONE, T. J., FARINA, M., O'BRIEN, F. J., EL-CHEIKH, M. C. & BALDUINO, A. 2015. Platelet-rich plasma releasate differently stimulates cellular commitment toward the chondrogenic lineage according to concentration. Journal of Tissue Engineering, 6, 1123-1130.

DUNN, M. G. 1998. Anterior Cruciate Ligament Prostheses. Encyclopedia of Sports Medicine and Science, 65, 201-208.

DUONG, H., WU, B. & TAWIL, B. 2009. Modulation of 3D Fibrin Matrix Stiffness by Intrinsic Fibrinogen–Thrombin Compositions and by Extrinsic Cellular Activity. Tissue Engineering. Part A, 15, 1865-1876.

DURANTE, C., AGOSTINI, F., ABBRUZZESE, L., TOFFOLA, R. T., ZANOLIN, S., SUINE, C. & MAZZUCATO, M. 2013. Growth factor release from platelet concentrates: analytic quantification and characterization for clinical applications. Vox Sang, 105, 129-136.

DUTHON, V. B., BAREA, C., ABRASSART, S., FASEL, J. H., FRITSCHY, D. & MÉNÉTREY, J. 2006. Anatomy of the anterior cruciate ligament. Knee Surgery, Sports Traumatology, Arthroscopy, 14, 204-213.

ELLIS, A. J., CURRY, V. A., POWELL, E. K. & CAWSTON, T. E. 1994. The Prevention of Collagen Breakdown in Bovine Nasal Cartilage by TIMP, TIMP-2 and a Low Molecular Weight Synthetic Inhibitor. Biochemical and Biophysical Research Communications, 201, 94-101.

ENGLER, A. J., SEN, S., SWEENEY, H. L. & DISCHER, D. E. 2006. Matrix elasticity directs stem cell lineage specification. Cell, 126, 677-689.

ENGSTROM, B., WREDMARK, T. & WESTBLAD, P. 1993. Patellar tendon or Leeds-Keio graft in the surgical treatment of anterior cruciate ligament ruptures. Intermediate results. Clin Orthop Relat Res, 190-197.

ESCAMILLA, R. F., MACLEOD, T. D., WILK, K. E., PAULOS, L. & ANDREWS, J. R. 2012. Anterior cruciate ligament strain and tensile forces for weight-bearing and non-weight-bearing exercises: a guide to exercise selection. J Orthop Sports Phys Ther, 42, 208-220.

FELLER, L., KHAMMISSA, R. A. G. & LEMMER, J. 2017. Biomechanical cell regulatory networks as complex adaptive systems in relation to cancer. Cancer Cell International, 17, 16-20.

FERRARA, N. & DAVIS-SMYTH, T. 1997. The biology of vascular endothelial growth factor. Endocr Rev, 18, 4-25.

FERRARA, N., GERBER, H.-P. & LECOUTER, J. 2003. The biology of VEGF and its receptors. Nat Med, 9, 669-676.

FOSTER, T. E., PUSKAS, B. L., MANDELBAUM, B. R., GERHARDT, M. B. & RODEO, S. A. 2009. Platelet-Rich Plasma:From Basic Science to Clinical Applications. The American Journal of Sports Medicine, 37, 2259-2272.

FOX, D. B. & WARNOCK, J. J. 2011. Cell-based Meniscal Tissue Engineering: A Case for Synoviocytes. Clinical Orthopaedics and Related Research®, 469, 2806-2816.

FRANK, C. 2004. Ligament structure, physiology and function. Journal of Musculoskeletal and Neuronal Interactions, 4, 199-128.

FREDRIKSSON, L., LI, H. & ERIKSSON, U. 2004. The PDGF family: four gene products form five dimeric isoforms. Cytokine Growth Factor Rev, 15, 197-204.

FU, F. H., BENNETT, C. H., MA, C. B., MENETREY, J. & LATTERMANN, C. 2000. Current Trends in Anterior Cruciate Ligament Reconstruction. The American Journal of Sports Medicine, 28, 124-130.

FUFA, D., SHEALY, B., JACOBSON, M., KEVY, S. & MURRAY, M. M. 2008. Activation of platelet-rich plasma using soluble type I collagen. J Oral Maxillofac Surg, 66, 684-690.

FUJIKAWA, K., ISEKI, F. & SEEDHOM, B. B. 1989. Arthroscopy after anterior cruciate reconstruction with the Leeds-Keio ligament. Bone & Joint Journal, 71, 566-570.

FUJIKAWA, K., KOBAYASHI, T., SASAZAKI, Y., MATSUMOTO, H. & SEEDHOM, B. B. 2000. Anterior cruciate ligament reconstruction with the Leeds-Keio artificial ligament. Journal of long-term effects of medical implants, 10, 341-350.

PHINNEY, D. G., KOPEN, G., RIGHTER, W., WEBSTER, S., TREMAIN, N. & PROCKOP, P. D. 1999. Donor variation in the growth properties and osteogenic potential of human marrow stromal cells. Journal of Cellular Biochemistry, 75, 424-436.

GHALAYINI, S. R. A., HELM, A. T., BONSHAHI, A. Y., LAVENDER, A., JOHNSON, D. S. & SMITH, R. B. 2010. Arthroscopic anterior cruciate ligament surgery: Results of autogenous patellar tendon graft versus the Leeds-Keio synthetic graft: Five year follow-up of a prospective randomised controlled trial. The Knee, 17, 334-339.

GHAZANFARI, S., TAFAZZOLI-SHADPOUR, M. & SHOKRGOZAR, M. A. 2009. Effects of cyclic stretch on proliferation of mesenchymal stem cells and their differentiation to smooth muscle cells. Biochemical and Biophysical Research Communications, 388, 601-605.

GIRGIS, F. G., MARSHALL, J. L. & MONA JEM, A. R. S. A. 1975. The Cruciate Ligaments of the Knee Joint: Anatomical. Functional and Experimental Analysis. Clinical Orthopaedics and Related Research, 106, 216-231.

GIUSTI, I., D'ASCENZO, S., MANCO, A., DI STEFANO, G., DI FRANCESCO, M., RUGHETTI, A., DAL MAS, A., PROPERZI, G., CALVISI, V. & DOLO, V. 2014. Platelet Concentration in Platelet-Rich Plasma Affects Tenocyte Behavior In Vitro. BioMed Research International, 2014, 12-21.

GOEDECKE, A., WOBUS, M., KRECH, M., MÜNCH, N., RICHTER, K., HÖLIG, K. & BORNHAUSER, M. 2011. Differential effect of platelet-rich plasma and fetal calf serum on bone marrow-derived human mesenchymal stromal cells expanded in vitro. Journal of Tissue Engineering and Regenerative Medicine, 5, 648-654.

GOODLAD, R. A. & WRIGHT, N. A. 1996. Epidermal growth factor (EGF). Baillière's Clinical Gastroenterology, 10, 33-47.

GREILING, D. & CLARK, R. A. 1997. Fibronectin provides a conduit for fibroblast transmigration from collagenous stroma into fibrin clot provisional matrix. Journal of Cell Science, 110, 861-870.

GRINNELL, F. 2003. Fibroblast biology in three-dimensional collagen matrices. Trends in Cell Biology, 13, 264-269.

GUILLUY, C. & BURRIDGE, K. 2015. Nuclear mechanotransduction: Forcing the nucleus to respond. Nucleus, 6, 19-22.

GUILLUY, C., OSBORNE, L. D., VAN LANDEGHEM, L., SHAREK, L., SUPERFINE, R., GARCIA-MATA, R. & BURRIDGE, K. 2014. Isolated nuclei adapt to force and reveal a mechanotransduction pathway in the nucleus. Nat Cell Biol, 16, 376-381.

GUTHOLD, M., LIU, W., SPARKS, E. A., JAWERTH, L. M., PENG, L., FALVO, M., SUPERFINE, R., HANTGAN, R. R. & LORD, S. T. 2007. A Comparison of the Mechanical and Structural Properties of Fibrin Fibers with Other Protein Fibers. Cell biochemistry and biophysics, 49, 165-181.

HAGERTY, P., LEE, A., CALVE, S., LEE, C. A., VIDAL, M. & BAAR, K. 2012. The effect of growth factors on both collagen synthesis and tensile strength of engineered human ligaments. Biomaterials, 33, 6355-6361.

HAIRFIELD-STEIN, M., ENGLAND, C., PAEK, H. J., GILBRAITH, K. B., DENNIS, R., BOLAND, E. & KOSNIK, P. 2007. Development of self-assembled, tissue-engineered ligament from bone marrow stromal cells. Tissue engineering, 13, 703-710.

HALL, M., STEVERMER, C. A. & GILLETTE, J. C. 2012. Gait analysis post anterior cruciate ligament reconstruction: Knee osteoarthritis perspective. Gait & Posture, 36, 56-60.

HANNAFIN, J. A., ATTIA, E. T., WARREN, R. F. & BHARGAVA, M. M. 1999. Characterization of chemotactic migration and growth kinetics of canine knee ligament fibroblasts. Journal of Orthopaedic Research, 17, 398-404.

HANNINK, M. & DONOGHUE, D. J. 1989. Structure and function of platelet-derived growth factor (PDGF) and related proteins. Biochimica et Biophysica Acta (BBA) - Reviews on Cancer, 989, 1-10.

HEID, C. A., STEVENS, J., LIVAK, K. J. & WILLIAMS, P. M. 1996. Real time quantitative PCR. Genome Res, 6, 986-994.

HENRY, T. D., ANNEX, B. H., MCKENDALL, G. R., AZRIN, M. A., LOPEZ, J. J., GIORDANO, F. J., SHAH, P. K., WILLERSON, J. T., BENZA, R. L., BERMAN, D. S., GIBSON, C. M., BAJAMONDE, A., RUNDLE, A. C., FINE, J. & MCCLUSKEY, E. R. 2003. The VIVA trial: Vascular endothelial growth factor in Ischemia for Vascular Angiogenesis. Circulation, 107, 1359-1365.

HEO, S.-J., NERURKAR, N. L., BAKER, B. M., SHIN, J.-W., ELLIOTT, D. M. & MAUCK, R. L. 2011. Fiber Stretch and Reorientation Modulates Mesenchymal Stem Cell Morphology and Fibrous Gene Expression on Oriented Nanofibrous Microenvironments. Annals of Biomedical Engineering, 39, 2780-2789.

HERVY, M., HOFFMAN, L. & BECKERLE, M. C. 2006. From the membrane to the nucleus and back again: bifunctional focal adhesion proteins. Curr Opin Cell Biol, 18, 524-532.

HEY GROVES, E. 1917. Operation for the repair of the crucial ligaments. The Lancet, 190, 674-676.

HOFFMAN, B. D., GRASHOFF, C. & SCHWARTZ, M. A. 2011. Dynamic molecular processes mediate cellular mechanotransduction. Nature, 475, 316-323.

HSIEH, A. H., SAH, R. L. & SUNG, K. L. P. 2002. Biomechanical regulation of type I collagen gene expression in ACLs in organ culture. Journal of Orthopaedic Research, 20, 325-331.

HSIEH, A. H., TSAI, C. M. H., MA, Q. J., LIN, T., BANES, A. J., VILLARREAL, F. J., AKESON, W. H. & PAUL SUNG, K. L. 2000. Time-dependent increases in type-III collagen gene expression in medial collateral ligament fibroblasts under cyclic strains. Journal of Orthopaedic Research, 18, 220-227.

HUANG, D., CHANG, T. R., AGGARWAL, A., LEE, R. C. & EHRLICH, H. P. 1993. Mechanisms and dynamics of mechanical strengthening in ligament-equivalent fibroblast-populated collagen matrices. Ann Biomed Eng, 21, 289-305.

HUMPHREY, J. D., DUFRESNE, E. R. & SCHWARTZ, M. A. 2014. Mechanotransduction and extracellular matrix homeostasis. Nat Rev Mol Cell Biol, 15, 802-812.

HUNT, N. C. & GROVER, L. M. 2010. Cell encapsulation using biopolymer gels for regenerative medicine. Biotechnology Letters, 32, 733-742.

HWANG, J. H., BYUN, M. R., KIM, A. R., KIM, K. M., CHO, H. J., LEE, Y. H., KIM, J., JEONG, M. G., HWANG, E. S. & HONG, J.-H. 2015. Extracellular Matrix Stiffness Regulates Osteogenic Differentiation through MAPK Activation. PLOS ONE, 10, 519-530.

VARJU, I., SOTONYI, P., MACHOVICH, R., SZABO, L., TENEKEDJIEV, K., SILVA, M., LONGSTAFF, C. & KOLEV, K. 2011. Hindered dissolution of fibrin formed under mechanical stress. Journal of Thrombosis and Haemostasis, 9, 979-986.

ISHIDA, K., KURODA, R., MIWA, M., TABATA, Y., HOKUGO, A., KAWAMOTO, T., SASAKI, K., DOITA, M. & KUROSAKA, M. 2007. The regenerative effects of platelet-rich plasma on meniscal cells in vitro and its in vivo application with biodegradable gelatin hydrogel. Tissue Eng, 13, 1103-1112.

ISKRATSCH, T., WOLFENSON, H. & SHEETZ, M. 2014. Appreciating force and shape [mdash] the rise of mechanotransduction in cell biology. Nat Rev Mol Cell Biol, 15, 825-833.

JACKSON, D. W., SIMON, T. M., KURZWEIL, P. R. & ROSEN, M. A. 1992. Survival of cells after intra-articular transplantation of fresh allografts of the patellar and anterior cruciate ligaments. DNA-probe analysis in a goat model. J Bone Joint Surg Am, 74, 112-118.

JAHED, Z., SOHEILYPOUR, M., PEYRO, M. & MOFRAD, M. R. K. 2016. The LINC and NPC relationship – it's complicated! Journal of Cell Science, 129, 3219-3229.

JANMEY, P. A., WINER, J. P. & WEISEL, J. W. 2009. Fibrin gels and their clinical and bioengineering applications. Journal of The Royal Society Interface, 6, 1-10.

JARVINEN, T. A., JOZSA, L., KANNUS, P., JARVINEN, T. L., KVIST, M., HURME, T., ISOLA, J., KALIMO, H. & JARVINEN, M. 1999. Mechanical loading regulates tenascin-C expression in the osteotendinous junction. Journal of Cell Science, 112, 3157-3166.

JENKINS, D. H., FORSTER, I. W., MCKIBBIN, B. & RALIS, Z. A. 1977. Induction of tendon and ligament formation by carbon implants. J Bone Joint Surg Br, 59, 53-57.

JENNER, J. M., VAN EIJK, F., SARIS, D. B., WILLEMS, W. J., DHERT, W. J. & CREEMERS, L. B. 2007. Effect of transforming growth factor-beta and growth differentiation factor-5 on proliferation and matrix production by human bone marrow stromal cells cultured on braided poly lactic-co-glycolic acid scaffolds for ligament tissue engineering. Tissue Eng, 13, 1573-82.

JO, C. H., KIM, J. E., YOON, K. S. & SHIN, S. 2012. Platelet-Rich Plasma Stimulates Cell Proliferation and Enhances Matrix Gene Expression and Synthesis in Tenocytes from Human Rotator Cuff Tendons with Degenerative Tears. The American Journal of Sports Medicine, 40, 1035-1045.

JONES, P. L. & JONES, F. S. 2000. Tenascin-C in development and disease: gene regulation and cell function. Matrix Biology, 19, 581-596.

JU, Y. J., TOHYAMA, H., KONDO, E., YOSHIKAWA, T., MUNETA, T., SHINOMIYA, K. & YASUDA, K. 2006. Effects of Local Administration of Vascular Endothelial Growth Factor on Properties of the in Situ Frozen-Thawed Anterior Cruciate Ligament in Rabbits. The American Journal of Sports Medicine, 34, 84-91.

KADLER, K. E., HOLMES, D. F., TROTTER, J. A. & CHAPMAN, J. A. 1996. Collagen fibril formation. Biochemical Journal, 316, 1-11.

KADRMAS, J. L. & BECKERLE, M. C. 2004. The LIM domain: from the cytoskeleton to the nucleus. Nat Rev Mol Cell Biol, 5, 920-931.

KAKUDO, N., MINAKATA, T., MITSUI, T., KUSHIDA, S., NOTODIHARDJO, F. Z. & KUSUMOTO, K. 2008. Proliferation-promoting effect of platelet-rich plasma on human adipose-derived stem cells and human dermal fibroblasts. Plast Reconstr Surg, 122, 1352-1360.

KANG, H., WEN, Q., JANMEY, P. A., TANG, J. X., CONTI, E. & MACKINTOSH, F. C. 2009. Nonlinear Elasticity of Stiff Filament Networks: Strain Stiffening, Negative Normal Stress, and Filament Alignment in Fibrin Gels. The Journal of Physical Chemistry B, 113, 3799-3805.

KANG, Y.-H., JEON, S. H., PARK, J.-Y., CHUNG, J.-H., CHOUNG, Y.-H., CHOUNG, H.-W., KIM, E.-S. & CHOUNG, P.-H. 2010. Platelet-rich fibrin is a Bioscaffold and reservoir of growth factors for tissue regeneration. Tissue Engineering Part A, 17, 349-359.

KANNO, T., TAKAHASHI, T., TSUJISAWA, T., ARIYOSHI, W. & NISHIHARA, T. 2005. Platelet-rich plasma enhances human osteoblast-like cell proliferation and differentiation. Journal of Oral and Maxillofacial Surgery, 63, 362-369.

KANNO, T., TAKAHASHI, T., TSUJISAWA, T., ARIYOSHI, W. & NISHIHARA, T. 2005. Platelet-rich plasma enhances human osteoblast-like cell proliferation and differentiation. Journal of Oral and Maxillofacial Surgery, 63, 362-369.

KARAMICHOS, D., BROWN, R. A. & MUDERA, V. 2007. Collagen stiffness regulates cellular contraction and matrix remodelling gene expression. Journal of Biomedical Materials Research Part A, 83A, 887-894.

KARAMICHOS, D., SKINNER, J., BROWN, R. & MUDERA, V. 2008. Matrix stiffness and serum concentration effects matrix remodelling and ECM regulatory genes of human bone marrow stem cells. Journal of Tissue Engineering and Regenerative Medicine, 2, 97-105.

KARTUS, J., MAGNUSSON, L., STENER, S., BRANDSSON, S., ERIKSSON, B. I. & KARLSSON, J. 1999. Complications following arthroscopic anterior cruciate ligament reconstruction a 2–5-year follow-up of 604 patients with special emphasis on anterior knee pain. Knee Surgery, Sports Traumatology, Arthroscopy, 7, 2-8.

KESSLER, D., DETHLEFSEN, S., HAASE, I., PLOMANN, M., HIRCHE, F., KRIEG, T. & ECKES, B. 2001. Fibroblasts in mechanically stressed collagen lattices assume a "synthetic" phenotype. J Biol Chem, 276, 36575-36585.

KETTERL, N., BRACHTL, G., SCHUH, C., BIEBACK, K., SCHALLMOSER, K., REINISCH, A. & STRUNK, D. 2015. A robust potency assay highlights significant donor variation of human mesenchymal stem/progenitor cell immune modulatory capacity and extended radio-resistance. Stem Cell Research & Therapy, 6, 236-252.

KIAPOUR, A. M. & MURRAY, M. M. 2014. Basic science of anterior cruciate ligament injury and repair. Bone and Joint Research, 3, 20-31.

KIM, B.-S., KIM, H.-J., CHOI, J.-G., YOU, H.-K. & LEE, J. 2014. The effects of fibrinogen concentration on fibrin/atelocollagen composite gel: an in vitro and in vivo study in rabbit calvarial bone defect. Clinical Oral Implants Research, 12, 27-35.

KIM, J. 2009. Anterior Cruciate Ligament Injury (ACL). Sports Medicine [Online]. Available: http://orthosurg.ucsf.edu/patient-care/divisions/sports-medicine/conditions/knee/anterior-cruciate-ligament-injury-acl/.

KIM, S. A., RYU, H. W., LEE, K. S. & CHO, J. W. 2013. Application of platelet-rich plasma accelerates the wound healing process in acute and chronic ulcers through rapid migration and upregulation of cyclin A and CDK4 in HaCaT cells. Mol Med Rep, 7, 476-480.

KIM, S. G., AKAIKE, T., SASAGAW, T., ATOMI, Y. & KUROSAWA, H. 2002. Gene expression of type I and type III collagen by mechanical stretch in anterior cruciate ligament cells. Cell structure and function, 27, 139-144.

KIM, Y. S., LEE, H. J., YEO, J. E., KIM, Y. I., CHOI, Y. J. & KOH, Y. G. 2015. Isolation and characterization of human mesenchymal stem cells derived from synovial fluid in patients with osteochondral lesion of the talus. Am J Sports Med, 43, 399-406.

KJAERGARD, H. K. & WEIS-FOGH, U. S. 1994. Important Factors Influencing the Strength of Autologous Fibrin Glue; the Fibrin Concentration and Reaction Time – Comparison of Strength with Commercial Fibrin Glue. European Surgical Research, 26, 273-276.

KNIGHTON, D. R., CIRESI, K. F., FIEGEL, V. D., AUSTIN, L. L. & BUTLER, E. L. 1986. Classification and treatment of chronic nonhealing wounds. Successful treatment with autologous platelet-derived wound healing factors (PDWHF). Annals of surgery, 204, 322.

KNOTT, L. & BAILEY, A. J. 1998. Collagen cross-links in mineralizing tissues: A review of their chemistry, function, and clinical relevance. Bone, 22, 181-187.

KOBAYASHI, E., FLÜCKIGER, L., FUJIOKA-KOBAYASHI, M., SAWADA, K., SCULEAN, A., SCHALLER, B. & MIRON, R. J. 2016. Comparative release of growth factors from PRP, PRF, and advanced-PRF. Clinical Oral Investigations, 20, 2353-2360.

KOMORI, T. 2008. Regulation of bone development and maintenance by Runx2. Front Biosci, 13, 898-903.

KOOK, S.-H., JANG, Y.-S. & LEE, J.-C. 2011. Involvement of JNK-AP-1 and ERK-NF-κB signaling in tension-stimulated expression of Type I collagen and MMP-1 in human periodontal ligament fibroblasts. Journal of Applied Physiology, 111, 1575-1583.

KORBLING, M., PRZEPIORKA, D., HUH, Y., ENGEL, H., VAN BESIEN, K., GIRALT, S., ANDERSSON, B., KLEINE, H., SEONG, D. & DEISSEROTH, A. 1995. Allogeneic blood stem cell transplantation for refractory leukemia and lymphoma: potential advantage of blood over marrow allografts. Blood, 85, 1659-1665.

KRAEMER, B. F., BORST, O., GEHRING, E.-M., SCHOENBERGER, T., URBAN, B., NINCI, E., SEIZER, P., SCHMIDT, C., BIGALKE, B., KOCH, M., MARTINOVIC, I., DAUB, K., MERZ, T., SCHWANITZ, L., STELLOS, K., FIESEL, F., SCHALLER, M., LANG, F., GAWAZ, M. & LINDEMANN, S. 2010. PI3 kinase-dependent stimulation of platelet migration by stromal cell-derived factor 1 (SDF-1). Journal of Molecular Medicine, 88, 1277-1288.

KRISMER, A. M., CABRA, R. S., MAY, R. D., FRAUCHIGER, D. A., KOHL, S., AHMAD, S. S. & GANTENBEIN, B. Biologic response of human anterior cruciate ligamentocytes on collagen-patches to platelet-rich plasma formulations with and without leucocytes. Journal of Orthopaedic Research, 42, 197-204.

KUHBECK, D., MAYR, J., HARING, M., HOFMANN, M., QUIGNARD, F. & DIAZ DIAZ, D. 2015. Evaluation of the nitroaldol reaction in the presence of metal ion-crosslinked alginates. New Journal of Chemistry, 39, 2306-2315.

LAI, V. K., LAKE, S. P., FREY, C. R., TRANQUILLO, R. T. & BAROCAS, V. H. 2012. Mechanical Behavior of Collagen-Fibrin Co-Gels Reflects Transition From Series to Parallel Interactions With Increasing Collagen Content. Journal of Biomechanical Engineering, 134, 1132-1150.

LAMMERDING, J., FONG, L. G., JI, J. Y., REUE, K., STEWART, C. L., YOUNG, S. G. & LEE, R. T. 2006. Lamins A and C but not lamin B1 regulate nuclear mechanics. J Biol Chem, 281, 25768-25780.

LARON, Z. 2001. Insulin-like growth factor 1 (IGF-1): a growth hormone. Molecular Pathology, 54, 311-316.

LAURENCIN, C. T., AMBROSIO, A. M. A., BORDEN, M. D. & J. A. COOPER, J. 1999. Tissue engineering: Orthopedic applications. Annual review of biomedical engineering, 1, 19-46.

LAURENCIN, C. T. & FREEMAN, J. W. 2005. Ligament tissue engineering: An evolutionary materials science approach. Biomaterials, 26, 7530-7536.

LAVAGNINO, M., ARNOCZKY, S. P., TIAN, T. & VAUPEL, Z. 2003. Effect of Amplitude and Frequency of Cyclic Tensile Strain on the Inhibition of MMP-1 mRNA Expression in Tendon Cells: An In Vitro Study. Connective Tissue Research, 44, 181-187.

LEE, K., SILVA, E. A. & MOONEY, D. J. 2011. Growth factor delivery-based tissue engineering: general approaches and a review of recent developments. 8, 341-362.

LEE, K. Y. & MOONEY, D. J. 2012. Alginate: properties and biomedical applications. Progress in polymer science, 37, 106-126.

LEGNANI, C., VENTURA, A., TERZAGHI, C., BORGO, E. & ALBISETTI, W. 2010. Anterior cruciate ligament reconstruction with synthetic grafts. A review of literature. International Orthopaedics, 34, 465-471.

LEONG, N. L., KABIR, N., ARSHI, A., NAZEMI, A., WU, B., PETRIGLIANO, F. A. & MCALLISTER, D. R. 2015. Evaluation of polycaprolactone scaffold with basic fibroblast growth factor and fibroblasts in an athymic rat model for anterior cruciate ligament reconstruction. Tissue Eng Part A, 21, 1859-68.

LEUNG, D., GLAGOV, S. & MATHEWS, M. 1976. Cyclic stretching stimulates synthesis of matrix components by arterial smooth muscle cells in vitro. Science, 191, 475-477.

LI, D., ZHOU, J., CHOWDHURY, F., CHENG, J., WANG, N. & WANG, F. 2011. Role of mechanical factors in fate decisions of stem cells. Regenerative medicine, 6, 229-240.

LI, Y., RAMCHARAN, M., ZHOU, Z., LEONG, D. J., AKINBIYI, T., MAJESKA, R. J. & SUN, H. B. 2015. The Role of Scleraxis in Fate Determination of Mesenchymal Stem Cells for Tenocyte Differentiation. 5, 13149-13156.

LILJENSTEN, E., GISSELFALT, K., EDBERG, B., BERTILSSON, H., FLODIN, P., NILSSON, A., LINDAHL, A. & PETERSON, L. 2002. Studies of polyurethane urea bands for ACL reconstruction. J Mater Sci Mater Med, 13, 351-359.

LIU, Y., SUEN, C.-W., ZHANG, J.-F. & LI, G. 2017. Current concepts on tenogenic differentiation and clinical applications. Journal of Orthopaedic Translation, 9, 28-42.

LODISH H, B. A., ZIPURSKY SL, ET AL. 2000. Molecular Cell Biology. 4th edition ed. New York: W. H. Freeman, 14, 553-560.

LOWENHAUPT, R. W. 1982. Human platelet chemotaxis can be induced by low molecular substance(s) derived from the interaction of plasma and collagen. Progress in clinical and biological research, 89, 269-280.

LOWENHAUPT, R. W., GLUECK, H. I., MILLER, M. A. & KLINE, D. L. 1977. Factors which influence blood platelet migration. J Lab Clin Med, 90, 37-45.

LOWENHAUPT, R. W., MILLER, M. A. & GLUECK, H. I. 1973. Platelet migration and chemotaxis demonstrated in vitro. Thrombosis Research, 3, 477-487.

LU, H. H., VO, J. M., CHIN, H. S., LIN, J., COZIN, M., TSAY, R., EISIG, S. & LANDESBERG, R. 2008. Controlled delivery of platelet-rich plasma-derived growth factors for bone formation. J Biomed Mater Res A, 86, 1128-36.

LUKIANOV, A. V., RICHMOND, J. C., BARRETT, G. R. & GILLQUIST, J. 1989. A multicenter study on the results of anterior cruciate ligament reconstruction using a Dacron ligament prosthesis in "salvage" cases. Am J Sports Med, 17, 380-5; discussion 385-386.

LUQUE-SERON, J. A. & MEDINA-PORQUERES, I. 2016. Anterior Cruciate Ligament Strain In Vivo: A Systematic Review. Sports Health, 8, 451-455.

MA, J., SMIETANA, M. J., KOSTROMINOVA, T. Y., WOJTYS, E. M., LARKIN, L. M. & ARRUDA, E. M. 2011. Three-Dimensional Engineered Bone–Ligament–Bone Constructs for Anterior Cruciate Ligament Replacement. Tissue Engineering Part A, 18, 103-116.

MA, K., TITAN, A. L., STAFFORD, M., ZHENG, C. H. & LEVENSTON, M. E. 2012. Variations in chondrogenesis of human bone marrow-derived mesenchymal stem cells in fibrin/alginate blended hydrogels. Acta Biomaterialia, 8, 3754-3764.

MAJHAIL, N. S., DOUGLAS RIZZO, J., LEE, S. J., ALJURF, M., ATSUTA, Y., BONFIM, C., BURNS, L. J., CHAUDHRI, N., DAVIES, S., OKAMOTO, S., SEBER, A., SOCIE, G., SZER, J., VAN LINT, M. T., WINGARD, J. R. & TICHELLI, A. 2012. Recommended Screening and Preventive Practices for Long-Term Survivors after Hematopoietic Cell Transplantation. Hematology/Oncology and Stem Cell Therapy, 5, 1-30.

MANCINI, M., MORESI, M. & RANCINI, R. 1999. Mechanical properties of alginate gels: empirical characterisation. Journal of Food Engineering, 39, 369-378.

MANIOTIS, A. J., CHEN, C. S. & INGBER, D. E. 1997. Demonstration of mechanical connections between integrins, cytoskeletal filaments, and nucleoplasm that stabilize nuclear structure. Proc Natl Acad Sci U S A, 94, 849-854.

MARTINELLO, T., BRONZINI, I., PERAZZI, A., TESTONI, S., DE BENEDICTIS, G. M., NEGRO, A., CAPORALE, G., MASCARELLO, F., IACOPETTI, I. & PATRUNO, M. 2013. Effects of in vivo applications of peripheral blood-derived mesenchymal stromal cells (PB-MSCs) and platlet-rich plasma (PRP) on experimentally injured deep digital flexor tendons of sheep. Journal of Orthopaedic Research, 31, 306-314.

MARUI, T., NIYIBIZI, C., GEORGESCU, H. I., CAO, M., KAVALKOVICH, K. W., LEVINE, R. E. & WOO, S. L. Y. 1997. Effect of growth factors on matrix synthesis by ligament fibroblasts. Journal of Orthopaedic Research, 15, 18-23.

MARX, R. E. 2001. Platelet-Rich Plasma (PRP): What Is PRP and What Is Not PRP? Implant Dentistry, 10, 225-228.

MARX, R. E. 2004. Platelet-Rich Plasma: Evidence to Support Its Use. J Oral Maxillofac Surg, 62, 489-496.

MARX, R. E., CARLSON, E. R., EICHSTAEDT, R. M., SCHIMMELE, S. R., STRAUSS, J. E. & GEORGEFF, K. R. 1998. Platelet-rich plasma: Growth factor enhancement for bone grafts. Oral Surg Oral Med Oral Pathol Oral Radiol Endod, 85, 638-646.

MASSAGUÉ, J. 2012. TGFβ signalling in context. Nature reviews. Molecular cell biology, 13, 616-630.

MATSUMOTO, H. & FUJIKAWA, K. 2001. Leeds-Keio artificial ligament: a new concept for the anterior cruciate ligament reconstruction of the knee. The Keio Journal of Medicine, 50, 161-166.

MATSUNAGA, D., AKIZUKI, S., TAKIZAWA, T., OMAE, S. & KATO, H. 2013. Compact platelet-rich fibrin scaffold to improve healing of patellar tendon defects and for medial collateral ligament reconstruction. Knee, 20, 545-550.

MAZZOCCA, A. D., MCCARTHY, M. B., CHOWANIEC, D. M., DUGDALE, E. M., HANSEN, D., COTE, M. P., BRADLEY, J. P., ROMEO, A. A., ARCIERO, R. A. & BEITZEL, K. 2012. The positive effects of different platelet-rich plasma methods on human muscle, bone, and tendon cells. Am J Sports Med, 40, 1742-1749.

MCCARREL, T. & FORTIER, L. 2009. Temporal growth factor release from platelet-rich plasma, trehalose lyophilized platelets, and bone marrow aspirate and their effect on tendon and ligament gene expression. Journal of Orthopaedic Research, 27, 1033-1042.

MCWILLIAM, H., LI, W., ULUDAG, M., SQUIZZATO, S., PARK, Y. M., BUSO, N., COWLEY, A. P. & LOPEZ, R. 2013. Analysis Tool Web Services from the EMBL-EBI. Nucleic Acids Research, 41, 597-600.

MEUNIER, A., ODENSTEN, M. & GOOD, L. 2007. Long-term results after primary repair or non-surgical treatment of anterior cruciate ligament rupture: a randomized study with a 15-year follow-up. Scandinavian Journal of Medicine & Science in Sports, 17, 230-237.

MIESBACH, W., SCHENK, J., ALESCI, S. & LINDHOFF-LAST, E. 2010. Comparison of the fibrinogen Clauss assay and the fibrinogen PT derived method in patients with dysfibrinogenemia. Thrombosis Research, 126, 428-433.

MISHRA, A. & PAVELKO, T. 2006. Treatment of Chronic Elbow Tendinosis with Buffered Platelet-Rich Plasma. The American Journal of Sports Medicine, 34, 1774-1778.

MISHRA, A. K., SKREPNIK, N. V., EDWARDS, J. C., JONES, G. L., SAMPSON, S., VERMILLION, D. A., RAMSEY, M. L., KARLI, D. C. & RETTIG, A. C. 2014. Efficacy of Platelet-Rich Plasma for Chronic Tennis Elbow:A Double-Blind, Prospective, Multicenter, Randomized Controlled Trial of 230 Patients. The American Journal of Sports Medicine, 42, 463-471.

MOLLOY, T., WANG, Y. & MURRELL, G. A. C. 2003. The Roles of Growth Factors in Tendon and Ligament Healing. Sports Medicine, 33, 381-394.

MONA, N.-N., GHASEM, A., ABBAS, N., MAHMOUD, A., N., A. M., SOMAYEH, E.-B., HOOSHANG, S., ARMIN, A. & JAFAR, A. 2014. Enhancing neuronal growth from human endometrial stem cells derived neuron-like cells in three-dimensional fibrin gel for nerve tissue engineering. Journal of Biomedical Materials Research Part A, 102, 2533-2543.

MOR-COHEN, R., ROSENBERG, N., AVERBUKH, Y., SELIGSOHN, U. & LAHAV, J. 2014. Disulfide bond exchanges in integrins αIIbβ3 and αvβ3 are required for activation and post-ligation signaling during clot retraction. Thrombosis Research, 133, 826-836.

MOREAU, J. E., BRAMONO, D. S., HORAN, R. L., KAPLAN, D. L. & ALTMAN, G. H. 2008. Sequential biochemical and mechanical stimulation in the development of tissue-engineered ligaments. Tissue Engineering Part A, 14, 1161-1172.

MORITO, T., MUNETA, T., HARA, K., JU, Y. J., MOCHIZUKI, T., MAKINO, H., UMEZAWA, A. & SEKIYA, I. 2008. Synovial fluid-derived mesenchymal stem cells increase after intra-articular ligament injury in humans. Rheumatology, 47, 1137-1143.

MOSESSON, M. W. 2005. Fibrinogen and fibrin structure and functions. J Thromb Haemost, 3, 1894-1904.

MURPHY, P. G., LOITZ, B. J., FRANK, C. B. & HART, D. A. 1994. Influence of exogenous growth factors on the synthesis and secretion of collagen types I and III by explants of normal and healing rabbit ligaments. Biochemistry and Cell Biology, 72, 403-409.

MURRAY, A. W. & MACNICOL, M. F. 2004. 10-16 year results of Leeds-Keio anterior cruciate ligament reconstruction. Knee, 11, 9-14.

MURRAY, M. M., PALMER, M., ABREU, E., SPINDLER, K. P., ZURAKOWSKI, D. & FLEMING, B. C. 2009. Platelet-rich plasma alone is not sufficient to enhance suture repair of the ACL in skeletally immature animals: An in vivo study. Journal of Orthopaedic Research, 27, 639-645.

MURRAY, M. M. & SPECTOR, M. 1999. Fibroblast distribution in the anteromedial bundle of the human anterior cruciate ligament: The presence of α-smooth muscle actin-positive cells. Journal of Orthopaedic Research, 17, 18-27.

MURRAY, M. M., SPINDLER, K. P., ABREU, E., MULLER, J. A., NEDDER, A., KELLY, M., FRINO, J., ZURAKOWSKI, D., VALENZA, M., SNYDER, B. D. & CONNOLLY, S. A. 2007. Collagen-platelet rich plasma hydrogel enhances primary repair of the porcine anterior cruciate ligament. Journal of Orthopaedic Research, 25, 81-91.

MURRAY, M. M., SPINDLER, K. P., BALLARD, P., WELCH, T. P., ZURAKOWSKI, D. & NANNEY, L. B. 2007. Enhanced histologic repair in a central wound in the anterior cruciate ligament with a collagen–platelet-rich plasma scaffold. Journal of Orthopaedic Research, 25, 1007-1017.

MURRAY, M. M., SPINDLER, K. P., DEVIN, C., SNYDER, B. S., MULLER, J., TAKAHASHI, M., BALLARD, P., NANNEY, L. B. & ZURAKOWSKI, D. 2006. Use of a collagen-platelet rich plasma scaffold to stimulate healing of a central defect in the canine ACL. Journal of Orthopaedic Research, 24, 820-830.

NAKAMURA, N., SHINO, K., NATSUUME, T., HORIBE, S., MATSUMOTO, N., KANEDA, Y. & OCHI, T. 1998. Early biological effect of in vivo gene transfer of platelet-derived growth factor (PDGF)-B into healing patellar ligament. Gene therapy, 5, 1165-1170.

NAKATSUKA, H., SOKABE, T., YAMAMOTO, K. & ANDO, J. Shear Stress Induces Hepatocyte PAI-1 Gene Expression through Cooperative Sp1/Ets-1 Activation of Transcription. 2006 IEEE International Symposium on Micro Nano Mechanical and Human Science, 5. 1-6.

NEUSS, S., SCHNEIDER, R. K. M., TIETZE, L., KNÜCHEL, R. & JAHNEN-DECHENT, W. 2010. Secretion of Fibrinolytic Enzymes Facilitates Human Mesenchymal Stem Cell Invasion into Fibrin Clots. Cells Tissues Organs, 191, 36-46.

NG, G. Y. F. 2002. Ligament Injury and Repair: Current Concepts. Hong Kong Physiotherapy Journal, 20, 22-29.

NHS. 2013. Knee ligament surgery [Online]. NHS. Available: http://www.nhs.uk/conditions/repairtotendon/Pages/Introduction.aspx [Accessed 21st October 2014].

NIES, D. E., HEMESATH, T. J., KIM, J. H., GULCHER, J. R. & STEFANSSON, K. 1991. The complete cDNA sequence of human hexabrachion (Tenascin). A multidomain protein containing unique epidermal growth factor repeats. J Biol Chem, 266, 2818-2823.

NOMI, M., ATALA, A., COPPI, P. D. & SOKER, S. 2002. Principals of neovascularization for tissue engineering. Molecular Aspects of Medicine, 23, 463-483.

O'BRIEN, F. J. 2011. Biomaterials & scaffolds for tissue engineering. Materials Today, 14, 88-95.

OKAMOTO, T., PATIL, A., NISSINEN, T. & MANN, S. 2017. Self-Assembly of Colloidal Nanocomposite Hydrogels Using 1D Cellulose Nanocrystals and 2D Exfoliated Organoclay Layers. Gels, 3, 11-15.

OLMAN, M. A., HAGOOD, J. S., SIMMONS, W. L., FULLER, G. M., VINSON, C. & WHITE, K. E. 1999. Fibrin Fragment Induction of Plasminogen Activator Inhibitor Transcription Is Mediated by Activator Protein-1 Through a Highly Conserved Element. Blood, 94, 2029-2038.

OLSON, E. J., KANG, J. D., FU, F. H., GEORGESCU, H. I., MASON, G. C. & EVANS, C. H. 1988. The biochemical and histological effects of artificial ligament wear particles: In vitro and in vivo studies. The American Journal of Sports Medicine, 16, 558-570.

ORTEL, T. L., MERCER, M. C., THAMES, E. H., MOORE, K. D. & LAWSON, J. H. 2001. Immunologic Impact and Clinical Outcomes after Surgical Exposure to Bovine Thrombin. Annals of Surgery, 233, 88-96.

OSBORNE, C. S., REID, W. H. & GRANT, M. H. 1999. Investigation into the biological stability of collagen/chondroitin-6-sulphate gels and their contraction by fibroblasts and keratinocytes: the effect of crosslinking agents and diamines. Biomaterials, 20, 283-290.

OSWALD, M. W., HUNT, H. H. & LAZARCHICK, J. 1983. Normal range of plasma fibrinogen. Am J Med Technol, 49, 57-59.

PARAFIORITI, A., ARMIRAGLIO, E., DEL BIANCO, S., TIBALT, E., OLIVA, F. & BERARDI, A. C. 2011. Single injection of platelet-rich plasma in a rat Achilles tendon tear model. Muscles Ligaments Tendons J, 1, 41-47.

PAXTON, J. Z., GROVER, L. M. & BAAR, K. 2010. Engineering an in vitro model of a functional ligament from bone to bone. Tissue Engineering Part A, 16, 3515-3525.

PETERSEN, W. & TILLMANN, B. 2002. Anatomy and function of the anterior cruciate ligament. Der Orthopäde, 31, 710-718.

PIETRAMAGGIORI, G., KAIPAINEN, A., HO, D., ORSER, C., PEBLEY, W., RUDOLPH, A. & ORGILL, D. P. 2007. Trehalose lyophilized platelets for wound healing. Wound Repair Regen, 15, 213-220.

PIFER, M. A., MAERZ, T., KEVIN C., B. & ANDERSON, K. 2014. Matrix Metalloproteinase Content and Activity in Low-Platelet, Low-Leukocyte and High-Platelet, High-Leukocyte Platelet Rich Plasma (PRP) and the Biologic Response to PRP by Human Ligament Fibroblasts. The American Journal of Sports Medicine, 42, 1211-1218.

PODESTA, L., CROW, S. A., VOLKMER, D., BERT, T. & YOCUM, L. A. 2013. Treatment of Partial Ulnar Collateral Ligament Tears in the Elbow with Platelet-Rich Plasma. The American Journal of Sports Medicine, 41, 1689-1694.

PRESTA, M., RUSNATI, M., GUALANDRIS, A., DELL'ERA, P., URBINATI, C., COLTRINI, D., TANGHETTI, E. & BELLERI, M. 1994. Human Basic Fibroblast Growth Factor: Structure-Function Relationship of an Angiogenic Molecule. In: MARAGOUDAKIS, M. E., GULLINO, P. M. & LELKES, P. I. (eds.) Angiogenesis: Molecular Biology, Clinical Aspects. Boston, MA: Springer US, 632-650.

RADICE, F., YÁNEZ, R., GUTIÉRREZ, V., ROSALES, J., PINEDO, M. & CODA, S. 2010. Comparison of Magnetic Resonance Imaging Findings in Anterior Cruciate Ligament Grafts With and Without Autologous Platelet-Derived Growth Factors. Arthroscopy: The Journal of Arthroscopic & Related Surgery, 26, 50-57.

RADING, J. & PETERSON, L. 1995. Clinical experience with the Leeds-Keio artificial ligament in anterior cruciate ligament reconstruction. A prospective two-year follow-up study. Am J Sports Med, 23, 316-319.

RAEISSADAT, S. A., SEDIGHIPOUR, L., RAYEGANI, S. M., BAHRAMI, M. H., BAYAT, M. & RAHIMI, R. 2014. Effect of Platelet-Rich Plasma (PRP) versus Autologous Whole Blood on Pain and Function Improvement in Tennis Elbow: A Randomized Clinical Trial. Pain Research and Treatment, 2014, 191525-191534.

RAIF EL, M. 2008. Effect of cyclic tensile load on the regulation of the expression of matrix metalloproteases (MMPs -1, -3) and structural components in synovial cells. J Cell Mol Med, 12, 2439-48.

RAIF EL, M., SEEDHOM, B. B., PULLAN, M. J. & TOYODA, T. 2007. Cyclic straining of cell-seeded synthetic ligament scaffolds: development of apparatus and methodology. Tissue Eng, 13, 629-40.

RAÏF, E. M. & SEEDHOM, B. B. 2005. Effect of cyclic tensile strain on proliferation of synovial cells seeded onto synthetic ligament scaffolds—an in vitro simulation. Bone, 36, 433-443.

RAO, R. R., PETERSON, A. W., CECCARELLI, J., PUTNAM, A. J. & STEGEMANN, J. P. 2012. Matrix composition regulates three-dimensional network formation by endothelial cells and mesenchymal stem cells in collagen/fibrin materials. Angiogenesis, 15, 253-264.

RATNOFF, O. D. & MENZIE, C. 1951. A new method for the determination of fibrinogen in small samples of plasma. J Lab Clin Med, 37, 316-320.

RICARD-BLUM, S. 2011. The Collagen Family. Cold Spring Harbor Perspectives in Biology, 3, 978-990.

RICHARDSON, L. E., DUDHIA, J., CLEGG, P. D. & SMITH, R. 2013. Stem cells in veterinary medicine; attempts at regenerating equine tendon after injury. Trends in Biotechnology, 25, 409-416.

RODRIGUES, C. V. M., SERRICELLA, P., LINHARES, A. B. R., GUERDES, R. M., BOROJEVIC, R., ROSSI, M. A., DUARTE, M. E. L. & FARINA, M. 2003. Characterization of a bovine collagen–hydroxyapatite composite scaffold for bone tissue engineering. Biomaterials, 24, 4987-4997.

ROSC, D., POWIERZA, W., ZASTAWNA, E., DREWNIAK, W., MICHALSKI, A. & KOTSCHY, M. 2002. Post-traumatic plasminogenesis in intraarticular exudate in the knee joint. Med Sci Monit, 8, 371-378.

ROSEN, M. A., JACKSON, D. W. & ATWELL, E. A. 1992. The efficacy of continuous passive motion in the rehabilitation of anterior cruciate ligament reconstructions. The American Journal of Sports Medicine, 20, 122-127.

ROSS, R., GLOMSET, J., KARIYA, B. & HARKER, L. 1974. A Platelet-Dependent Serum Factor That Stimulates the Proliferation of Arterial Smooth Muscle Cells In Vitro. Proceedings of the National Academy of Sciences, 71, 1207-1210.

ROWE, S. L., LEE, S. & STEGEMANN, J. P. 2007. Influence of thrombin concentration on the mechanical and morphological properties of cell-seeded fibrin hydrogels. Acta Biomaterialia, 3, 59-67.

ROWLEY, J. A., MADLAMBAYAN, G. & MOONEY, D. J. 1999. Alginate hydrogels as synthetic extracellular matrix materials. Biomaterials, 20, 45-53.

RUBIO-AZPEITIA, E. & ANDIA, I. 2014. Partnership between platelet-rich plasma and mesenchymal stem cells: in vitro experience. Muscles Ligaments Tendons J, 4, 52-62.

RUGHETTI, A., GIUSTI, I., D'ASCENZO, S., LEOCATA, P., CARTA, G., PAVAN, A., DELL'ORSO, L. & DOLO, V. 2008. Platelet gel-released supernatant modulates the angiogenic capability of human endothelial cells. Blood Transfus, 6, 12-17.

RUIJTENBERG, S. & VAN DEN HEUVEL, S. 2016. Coordinating cell proliferation and differentiation: Antagonism between cell cycle regulators and cell type-specific gene expression. Cell Cycle, 15, 196-212.

RUSHTON, N., DANDY, D. J. & NAYLOR, C. P. 1983. The clinical, arthroscopic and histological findings after replacement of the anterior cruciate ligament with carbon-fibre. J Bone Joint Surg Br, 65, 308-309.

RUSZCZAK, Z. 2003. Effect of collagen matrices on dermal wound healing. Advanced Drug Delivery Reviews, 55, 1595-1611.

SADOGHI, P., LOHBERGER, B., AIGNER, B., KALTENEGGER, H., FRIESENBICHLER, J., WOLF, M., SUNUNU, T., LEITHNER, A. & VAVKEN, P. 2013. Effect of platelet-rich plasma on the biologic activity of the human rotator-cuff fibroblasts: A controlled in vitro study. Journal of Orthopaedic Research, 31, 1249-1253.

SAED, G. M. & DIAMOND, M. P. 2003. Modulation of the expression of tissue plasminogen activator and its inhibitor by hypoxia in human peritoneal and adhesion fibroblasts. Fertility and Sterility, 79, 164-168.

SAKAGUCHI, Y., SEKIYA, I., YAGISHITA, K. & MUNETA, T. 2005. Comparison of human stem cells derived from various mesenchymal tissues: Superiority of synovium as a cell source. Arthritis & Rheumatism, 52, 2521-2529.

SAMPSON, S., GERHARDT, M. & MANDELBAUM, B. 2008. Platelet rich plasma injection grafts for musculoskeletal injuries: a review. Current Reviews in Musculoskeletal Medicine, 1, 165-174.

SÁNCHEZ, M., ANITUA, E., AZOFRA, J., PRADO, R., MURUZABAL, F. & ANDIA, I. 2010. Ligamentization of Tendon Grafts Treated With an Endogenous Preparation Rich in Growth Factors: Gross Morphology and Histology. Arthroscopy: The Journal of Arthroscopic & Related Surgery, 26, 470-480.

SASAKI, K., TAKAGI, M., KONTTINEN, Y. T., SASAKI, A., TAMAKI, Y., OGINO, T., SANTAVIRTA, S. & SALO, J. 2007. Upregulation of matrix metalloproteinase (MMP)-1 and its activator MMP-3 of human osteoblast by uniaxial cyclic stimulation. Journal of Biomedical Materials Research Part B: Applied Biomaterials, 80B, 491-498.

SAUCEDO, J. M., YAFFE, M. A., BERSCHBACK, J. C., HSU, W. K. & KALAINOV, D. M. 2012. Platelet-Rich Plasma. Journal of Hand Surgery, 37, 587-589.

SAUER, S. & LIND, M. 2017. Bone Tunnel Enlargement after ACL Reconstruction with Hamstring Autograft Is Dependent on Original Bone Tunnel Diameter. The Surgery Journal, 3, 96-100.

SCAPINELLI, R. 1997. Vascular anatomy of the human cruciate ligaments and surrounding structures. Clinical Anatomy, 10, 151-162.

SCHERPING, S. C., SCHMIDT, C. C., GEORGESCU, H. I., KWOH, C. K., EVANS, C. H. & WOO, S. L. Y. 1997. Effect of Growth Factors on the Proliferation of Ligament Fibroblasts from Skeletally Mature Rabbits. Connective Tissue Research, 36, 1-8.

SCHMIDT, C. C., GEORGESCU, H. I., KWOH, C. K., BLOMSTROM, G. L., ENGLE, C. P., LARKIN, L. A., EVANS, C. H. & WOO, S. L. Y. 1995. Effect of growth factors on the proliferation of fibroblasts from the medial collateral and anterior cruciate ligaments. Journal of Orthopaedic Research, 13, 184-190.

SCHMITTGEN, T. D. & LIVAK, K. J. 2008. Analyzing real-time PCR data by the comparative C(T) method. Nat Protoc, 3, 1101-1108.

SCHOR, S. L., ALLEN, T. D. & HARRISON, C. J. 1980. Cell migration through three-dimensional gels of native collagen fibres: collagenolytic activity is not required for the migration of two permanent cell lines. Journal of Cell Science, 46, 171-186.

SCHROVEN, I. T. J., GEENS, S., BECKERS, L., LAGRANGE, W. & FABRY, G. 1994. Experience with the Leeds-Keio artificial ligament for anterior cruciate ligament reconstruction. Knee Surgery, Sports Traumatology, Arthroscopy, 2, 214-218.

SCHULZE-TANZIL, G., MOBASHERI, A., CLEGG, P. D., SENDZIK, J., JOHN, T. & SHAKIBAEI, M. 2004. Cultivation of human tenocytes in high-density culture. Histochemistry and Cell Biology, 122, 219-228.

SCHWEITZER, R., CHYUNG, J. H., MURTAUGH, L. C., BRENT, A. E., ROSEN, V., OLSON, E. N., LASSAR, A. & TABIN, C. J. 2001. Analysis of the tendon cell fate using Scleraxis, a specific marker for tendons and ligaments. Development, 128, 3855-3866.

SCIENTIFIC, T. 2015. LIVE/DEAD® Viability/Cytotoxicity Kit, for mammalian cells [Online]. Available: https://www.thermofisher.com/order/catalog/product/L3224 [Accessed 27th April 2016].

SCOTT, A., DANIELSON, P., ABRAHAM, T., FONG, G., SAMPAIO, A. & UNDERHILL, T. 2011. Mechanical force modulates scleraxis expression in bioartificial tendons. J Musculoskelet Neuronal Interact, 11, 124-132.

SCREEN, H. R. C., SHELTON, J. C., BADER, D. L. & LEE, D. A. 2005. Cyclic tensile strain upregulates collagen synthesis in isolated tendon fascicles. Biochemical and Biophysical Research Communications, 336, 424-429.

SEITZ, H., PICHL, W., MATZI, V. & NAU, T. 2013. Biomechanical evaluation of augmented and nonaugmented primary repair of the anterior cruciate ligament: an in vivo animal study. International Orthopaedics, 37, 2305-2311.

SELL, S. A., WOLFE, P. S., ERICKSEN, J. J., SIMPSON, D. G. & BOWLIN, G. L. 2011. Incorporating platelet-rich plasma into electrospun scaffolds for tissue engineering applications. Tissue Eng Part A, 17, 2723-2737.

SHAERF, D. A., PASTIDES, P. S., SARRAF, K. M. & WILLIS-OWEN, C. A. 2014. Anterior cruciate ligament reconstruction best practice: A review of graft choice. World Journal of Orthopedics, 5, 23-29.

SHAH, J. V. & JANMEY, P. A. 1997. Strain hardening of fibrin gels and plasma clots. Rheologica Acta, 36, 262-268.

SHAHDADFAR, A., FRØNSDAL, K., HAUG, T., REINHOLT, F. P. & BRINCHMANN, J. E. 2005. In Vitro Expansion of Human Mesenchymal Stem Cells: Choice of Serum Is a Determinant of Cell Proliferation, Differentiation, Gene Expression, and Transcriptome Stability. STEM CELLS, 23, 1357-1366.

SHARMA, R. I. & SNEDEKER, J. G. 2010. Biochemical and biomechanical gradients for directed bone marrow stromal cell differentiation toward tendon and bone. Biomaterials, 31, 7695-7704.

SHENGDA, Z., ZHANFENG, C. & JILL, U. 2011. Dead cell counts during serum cultivation are underestimated by the fluorescent live/dead assay. Biotechnology Journal, 6, 513-518.

SHIKANOV, A., XU, M., WOODRUFF, T. K. & SHEA, L. D. 2009. Interpenetrating Fibrin-Alginate Matrices for in vitro Ovarian Follicle Development. Biomaterials, 30, 5476-5485.

SIERRA, D. H. 1993. Fibrin sealant adhesive systems: a review of their chemistry, material properties and clinical applications. J Biomater Appl, 7, 309-352.

SMITH, C. W., YOUNG, I. S. & KEARNEY, J. N. 1996. Mechanical Properties of Tendons: Changes with Sterilization and Preservation. Journal of Biomechanical Engineering, 118, 56-61.

SMITH, J. D., CHEN, A., ERNST, L. A., WAGGONER, A. S. & CAMPBELL, P. G. 2007. Immobilization of Aprotinin to Fibrinogen as a Novel Method for Controlling Degradation of Fibrin Gels. Bioconjugate Chemistry, 18, 695-701.

SPIERING, D. & HODGSON, L. 2011. Dynamics of the Rho-family small GTPases in actin regulation and motility. Cell Adhesion & Migration, 5, 170-180.

SPINDLER, K. P., MURRAY, M. M., DETWILER, K. B., TARTER, J. T., DAWSON, J. M., NANNEY, L. B. & DAVIDSON, J. M. 2003. The biomechanical response to doses of TGF-β2 in the healing rabbit medial collateral ligament. Journal of Orthopaedic Research, 21, 245-249.

STAMOV, D. R., STOCK, E., FRANZ, C. M., JÄHNKE, T. & HASCHKE, H. 2015. Imaging collagen type I fibrillogenesis with high spatiotemporal resolution. Ultramicroscopy, 149, 86-94.

STARR, D. A. & HAN, M. 2002. Role of ANC-1 in tethering nuclei to the actin cytoskeleton. Science, 298, 406-409.

STÄUBLI, H. U., SCHATZMANN, L., BRUNNER, P., RINCÓN, L. & NOLTE, L.-P. 1999. Mechanical Tensile Properties of the Quadriceps Tendon and Patellar Ligament in Young Adults. The American Journal of Sports Medicine, 27, 27-34.

STEENFOS, H. 1989. Insulin-like growth factor I has a major role in wound healing. Surg Forum, 68-71.

STEINERT, A. F., WEBER, M., KUNZ, M., PALMER, G. D., NÖTH, U., EVANS, C. H. & MURRAY, M. M. 2008. In situ IGF-1 gene delivery to cells emerging from the injured anterior cruciate ligament. Biomaterials, 29, 904-916.

STROCCHI, R., DE PASQUALE, V., GUBELLINI, P., FACCHINI, A., MARCACCI, M., BUDA, R., ZAFFAGNINI, S. & RUGGERI, A. 1992. The human anterior cruciate ligament: histological and ultrastructural observations. Journal of Anatomy, 180, 515-519.

SU, C. Y., KUO, Y. P., TSENG, Y. H., SU, C.-H. & BURNOUF, T. 2009. In vitro release of growth factors from platelet-rich fibrin (PRF): a proposal to optimize the clinical applications of PRF. Oral Surgery, Oral Medicine, Oral Pathology, Oral Radiology, and Endodontology, 108, 56-61.

SUBRAMONY, S. D., DARGIS, B. R., CASTILLO, M., AZELOGLU, E. U., TRACEY, M. S., SU, A. & LU, H. H. 2013. The guidance of stem cell differentiation by substrate alignment and mechanical stimulation. Biomaterials, 34, 1942-1953.

SUBRAMONY, S. D., SU, A., YEAGER, K. & LU, H. H. 2014. Combined effects of chemical priming and mechanical stimulation on mesenchymal stem cell differentiation on nanofiber scaffolds. Journal of biomechanics, 47, 2189-2196.

SUMPIO, B. E., CHANG, R., XU, W.-J., WANG, X.-J. & DU, W. 1997. Regulation of tPA in endothelial cells exposed to cyclic strain: role of CRE, AP-2, and SSRE binding sites. American Journal of Physiology - Cell Physiology, 273, 1441-1448.

SUN, L., QU, L., ZHU, R., LI, H., XUE, Y., LIU, X., FAN, J. & FAN, H. 2016. Effects of Mechanical Stretch on Cell Proliferation and Matrix Formation of Mesenchymal Stem Cell and Anterior Cruciate Ligament Fibroblast. Stem cells international, 2016.

SUN, Y., FENG, Y., ZHANG, C. Q., CHEN, S. B. & CHENG, X. G. 2010. The regenerative effect of platelet-rich plasma on healing in large osteochondral defects. International Orthopaedics, 34, 589-597.

TAKAGI, J. 2004. Structural basis for ligand recognition by RGD (Arg-Gly-Asp)-dependent integrins. Biochem Soc Trans, 32, 403-406.

TAN, R., FENG, Q., SHE, Z., WANG, M., JIN, H., LI, J. & YU, X. 2010. In vitro and in vivo degradation of an injectable bone repair composite. Polymer Degradation and Stability, 95, 1736-1742.

TAN, S., FANG, J. Y., YANG, Z., NIMNI, M. E. & HAN, B. 2014. The synergetic effect of hydrogel stiffness and growth factor on osteogenic differentiation. Biomaterials, 35, 5294-5306.

TANDETER, H. B. & SHVARTZMAN, P. 1999. Acute knee injuries: use of decision rules for selective radiograph ordering. Am Fam Physician, 60, 2599-2608.

TEXTOR, J. A., WILLITS, N. H. & TABLIN, F. 2013. Synovial fluid growth factor and cytokine concentrations after intra-articular injection of a platelet-rich product in horses. The Veterinary Journal, 198, 217-223.

TØNNESEN, H. H. & KARLSEN, J. 2002. Alginate in Drug Delivery Systems. Drug Development and Industrial Pharmacy, 28, 621-630.

TORBATI, M., LELE, T. P. & AGRAWAL, A. 2016. An unresolved LINC in the nuclear envelope. Cellular and molecular bioengineering, 9, 252-257.

TOWBIN, H., STAEHELIN, T. & GORDON, J. 1979. Electrophoretic transfer of proteins from polyacrylamide gels to nitrocellulose sheets: procedure and some applications. Proceedings of the National Academy of Sciences of the United States of America, 76, 4350-4354.

TRAUB, W. & PIEZ, K. A. 1971. The Chemistry and Structure of Collagen. In: ANFINSEN, C. B., EDSALL, J. T. & RICHARDS, F. M. (eds.) Advances in Protein Chemistry. Academic Press, 15, 1320-1329.

TSAY, R. C., VO, J., BURKE, A., EISIG, S. B., LU, H. H. & LANDESBERG, R. 2005. Differential growth factor retention by platelet-rich plasma composites. Journal of Oral and Maxillofacial Surgery, 63, 521-528.

TYAGI, S. C., LEWIS, K., PIKES, D., MARCELLO, A., MUJUMDAR, V. S., SMILEY, L. M. & MOORE, C. K. 1998. Stretch-induced membrane type matrix metalloproteinase and tissue plasminogen activator in cardiac fibroblast cells. Journal of Cellular Physiology, 176, 374-382.

ULFHAMMER, E., RIDDERSTRÅLE, W., ANDERSSON, M., KARLSSON, L., HRAFNKELSDÓTTIR, T. & JERN, S. 2005. Prolonged cyclic strain impairs the fibrinolytic system in cultured vascular endothelial cells. Journal of Hypertension, 23, 1551-1557.

VAN DOREN, S. R. 2015. Matrix metalloproteinase interactions with collagen and elastin. Matrix Biology, 44–46, 224-231.

VAN EIJK, F., SARIS, D. B., RIESLE, J., WILLEMS, W. J., VAN BLITTERSWIJK, C. A., VERBOUT, A. J. & DHERT, W. J. 2004. Tissue engineering of ligaments: a comparison of bone marrow stromal cells, anterior cruciate ligament, and skin fibroblasts as cell source. Tissue Eng, 10, 893-903.

VASSALLI, J. D., SAPPINO, A. P. & BELIN, D. 1991. The plasminogen activator/plasmin system. Journal of Clinical Investigation, 88, 1067-1072.

VAUGHAN, D. E. 2005. PAI-1 and atherothrombosis. J Thromb Haemost, 3, 1879-1883.

VELNAR, T., BAILEY, T. & SMRKOLJ, V. 2009. The Wound Healing Process: An Overview of the Cellular and Molecular Mechanisms. Journal of International Medical Research, 37, 1528-1542.

VERNON, R. B. & SAGE, E. H. 1999. A Novel, Quantitative Model for Study of Endothelial Cell Migration and Sprout Formation within Three-Dimensional Collagen Matrices. Microvascular Research, 57, 118-133.

VISSER, L. C., ARNOCZKY, S. P., CABALLERO, O., KERN, A., RATCLIFFE, A. & GARDNER, K. L. 2010. Growth factor-rich plasma increases tendon cell proliferation and matrix synthesis on a synthetic scaffold: an in vitro study. Tissue Eng Part A, 16, 1021-1029.

W., D. J., P., R. T., M., S. R., YA-QI, L. & M., D. R. 1996. Effect of calcium alginate on cellular wound healing processes modeled in vitro. Journal of Biomedical Materials Research, 32, 561-568.

WANG, J. H., JIA, F., GILBERT, T. W. & WOO, S. L. 2003. Cell orientation determines the alignment of cell-produced collagenous matrix. J Biomech, 36, 97-102.

WANG, L., BRESEE, C. S., JIANG, H., HE, W., REN, T., SCHWEITZER, R. & BRIGANDE, J. V. 2011. Scleraxis is Required for Differentiation of the Stapedius and Tensor Tympani Tendons of the Middle Ear. JARO: Journal of the Association for Research in Otolaryngology, 12, 407-421.

WANG, N., TYTELL, J. D. & INGBER, D. E. 2009. Mechanotransduction at a distance: mechanically coupling the extracellular matrix with the nucleus. Nat Rev Mol Cell Biol, 10, 75-82.

WEBB, K., HITCHCOCK, R. W., SMEAL, R. M., LI, W., GRAY, S. D. & TRESCO, P. A. 2006. Cyclic strain increases fibroblast proliferation, matrix accumulation, and elastic modulus of fibroblast-seeded polyurethane constructs. J Biomech, 39, 1136-1144.

WEBSTER, K. E., FELLER, J. A., HARTNETT, N., LEIGH, W. B. & RICHMOND, A. K. 2016. Comparison of Patellar Tendon and Hamstring Tendon Anterior Cruciate Ligament Reconstruction. The American Journal of Sports Medicine, 44, 83-90.

WEISEL, J. W. 2004. The mechanical properties of fibrin for basic scientists and clinicians. Biophysical Chemistry, 112, 267-276.

WEISEL, J. W. & LITVINOV, R. I. 2013. Mechanisms of fibrin polymerization and clinical implications. Blood, 121, 1712-1719.

WILLIAMS, I. F., HEATON, A. & MCCULLAGH, K. G. 1980. Cell morphology and collagen types in equine tendon scar. Research in veterinary science, 28, 302-310.

WOLBERG, A. S. 2007. Thrombin generation and fibrin clot structure. Blood Reviews, 21, 131-142.

WOLFMAN, N. M., HATTERSLEY, G., COX, K., CELESTE, A. J., NELSON, R., YAMAJI, N., DUBE, J. L., DIBLASIO-SMITH, E., NOVE, J., SONG, J. J., WOZNEY, J. M. & ROSEN, V. 1997. Ectopic induction of tendon and ligament in rats by growth and differentiation factors 5, 6, and 7, members of the TGF-beta gene family. Journal of Clinical Investigation, 100, 321-330.

WOO, S. L., DEBSKI, R. E., WITHROW, J. D. & JANAUSHEK, M. A. 1999. Biomechanics of knee ligaments. Am J Sports Med, 27, 533-543.

WOO, S. L., HOLLIS, J. M., ADAMS, D. J., LYON, R. M. & TAKAI, S. 1991. Tensile properties of the human femur-anterior cruciate ligament-tibia complex. The effects of specimen age and orientation. Am J Sports Med, 19, 217-225.

WUDEBWE, U. N. G., BANNERMAN, A., GOLDBERG-OPPENHEIMER, P., PAXTON, J. Z., WILLIAMS, R. L. & GROVER, L. M. 2015. Exploiting cell-mediated contraction and adhesion to structure tissues in vitro. Philosophical Transactions of the Royal Society B: Biological Sciences, 370, 10-18

WUFSUS, ADAM R., RANA, K., BROWN, A., DORGAN, JOHN R., LIBERATORE, MATTHEW W. & NEEVES, KEITH B. 2015. Elastic Behavior and Platelet Retraction in Low- and High-Density Fibrin Gels. Biophysical Journal, 108, 173-183.

XIE, X., WU, H., ZHAO, S., XIE, G., HUANGFU, X. & ZHAO, J. 2013. The effect of platelet-rich plasma on patterns of gene expression in a dog model of anterior cruciate ligament reconstruction. Journal of Surgical Research, 180, 80-88.

XU, J., SUN, M., TAN, Y., WANG, H., WANG, H., LI, P., XU, Z., XIA, Y., LI, L. & LI, Y. 2017. Effect of matrix stiffness on the proliferation and differentiation of umbilical cord mesenchymal stem cells. Differentiation, 96, 30-39.

YAN, L., TENG, M., A., K. D., C., L. L. & SHANG-TIAN, Y. 2001. Effects of Filtration Seeding on Cell Density, Spatial Distribution, and Proliferation in Nonwoven Fibrous Matrices. Biotechnology Progress, 17, 935-944.

YANG, G., CRAWFORD, R. C. & WANG, J. H. C. 2004. Proliferation and collagen production of human patellar tendon fibroblasts in response to cyclic uniaxial stretching in serum-free conditions. Journal of Biomechanics, 37, 1543-1550.

YE, Q., ZÜND, G., BENEDIKT, P., JOCKENHOEVEL, S., HOERSTRUP, S. P., SAKYAMA, S., HUBBELL, J. A. & TURINA, M. 2000. Fibrin gel as a three dimensional matrix in cardiovascular tissue engineering. European Journal of Cardio-Thoracic Surgery, 17, 587-591.

YILGOR, C., YILGOR HURI, P. & HURI, G. 2012. Tissue engineering strategies in ligament regeneration. Stem Cells Int, 2012, 374676-374680.

YOSHIDA, R. & MURRAY, M. M. 2013. Peripheral blood mononuclear cells enhance the anabolic effects of platelet-rich plasma on anterior cruciate ligament fibroblasts. J Orthop Res, 31, 29-34.

YU, S., HUIWU, L., XIAOLING, Z., YUJIE, F., YAN, H., YEE, L. P. P., TINGTING, T. & KERONG, D. 2011. Continuous cyclic mechanical tension inhibited Runx2 expression in mesenchymal stem cells through RhoA-ERK1/2 pathway. Journal of Cellular Physiology, 226, 2159-2169.

YUAN, T., ZHANG, C. Q. & WANG, J. H. 2013. Augmenting tendon and ligament repair with platelet-rich plasma (PRP). Muscles Ligaments Tendons J, 3, 139-49.

YUAN, T., ZHANG, C.-Q. & WANG, J. H. C. 2013. Augmenting tendon and ligament repair with platelet-rich plasma (PRP). Muscles, Ligaments and Tendons Journal, 3, 139-149.

ZEICHEN, J., VAN GRIENSVEN, M. & BOSCH, U. 2000. The Proliferative Response of Isolated Human Tendon Fibroblasts to Cyclic Biaxial Mechanical Strain. The American Journal of Sports Medicine, 28, 888-892.

ZHANG, L., TRAN, N., CHEN, H.-Q., KAHN, C. J.-F., MARCHAL, S., GROUBATCH, F. & WANG, X. 2008. Time-related changes in expression of collagen types I and III and of tenascin-C in rat bone mesenchymal stem cells under co-culture with ligament fibroblasts or uniaxial stretching. Cell and Tissue Research, 332, 101-109.

ZHANG, S., MUNETA, T., MORITO, T., MOCHIZUKI, T. & SEKIYA, I. 2008. Autologous synovial fluid enhances migration of mesenchymal stem cells from synovium of osteoarthritis patients in tissue culture system. J Orthop Res, 26, 1413-1418.

ZHOU, H. & XU, H. H. K. 2011. The fast release of stem cells from alginate-fibrin microbeads in injectable scaffolds for bone tissue engineering. Biomaterials, 32, 7503-7513.

ZHU, B., CHEN, M., YIN, H., DU, Y. & NING, L. 2016. Enzymatic Hydrolysis of Alginate to Produce Oligosaccharides by a New Purified Endo-Type Alginate Lyase. Marine Drugs, 14, 108-113.

ZUIDEMA, J. M., RIVET, C. J., GILBERT, R. J. & MORRISON, F. A. 2014. A protocol for rheological characterization of hydrogels for tissue engineering strategies. J Biomed Mater Res B Appl Biomater, 102, 1063-1073.

9. Appendix

The following images present the results of amino acid sequence alignments carried out on human vs bovine growth factors. Sequence alignments were performed using the Clustal Omega online sequence alignment programme. The EMBOSS Matcher function was used within the Pairwise sequence alignment tool. This used an algorithm to identify local similarities between the human and bovine amino acid input sequences to predict whether growth factors released from human platelets would be likely to interact with receptors on cells of bovine origin.

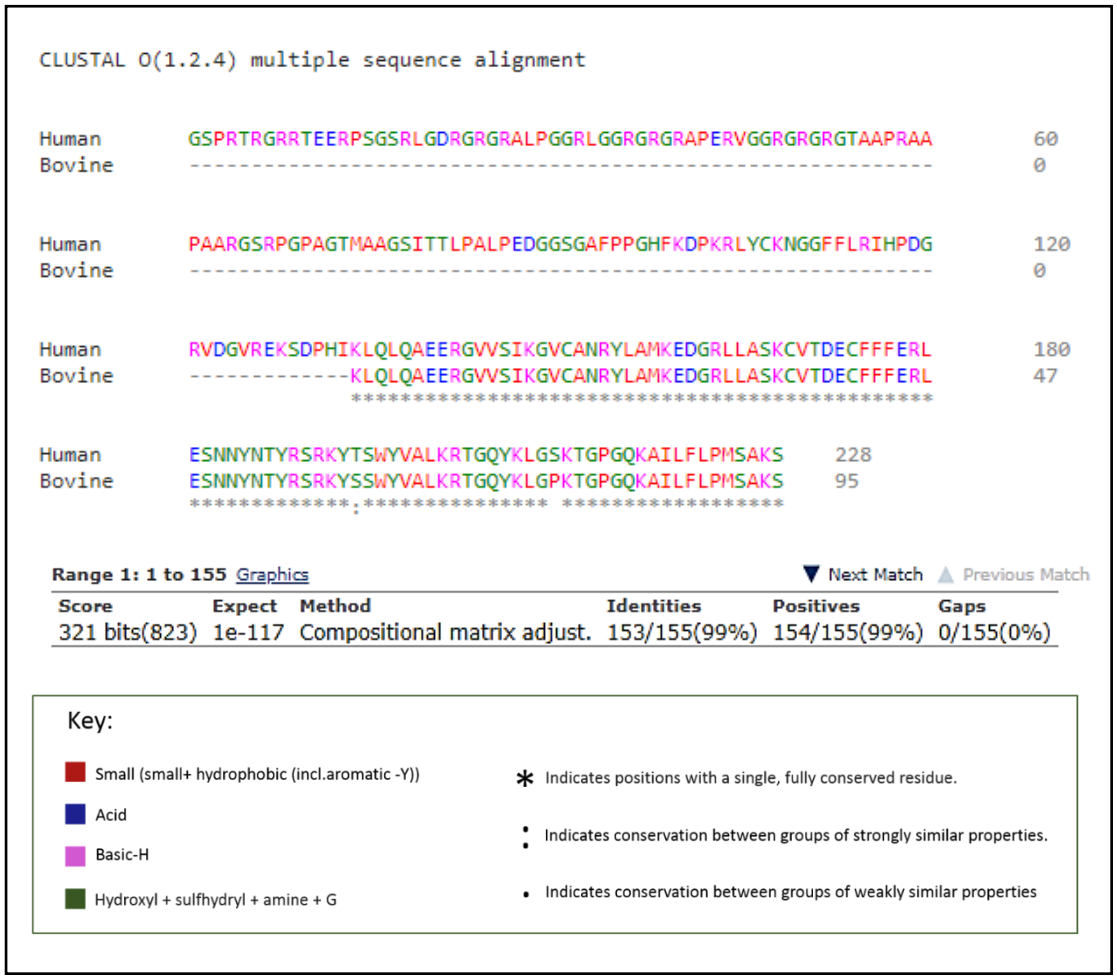

Appendix Figure 1 Basic Fibroblast growth factor (bFGF) human versus bovine sequence alignment.

Sequence alignments were performed using the Clustal Omega online sequence alignment programme. The EMBOSS Matcher function was used within the Pairwise sequence alignment tool.

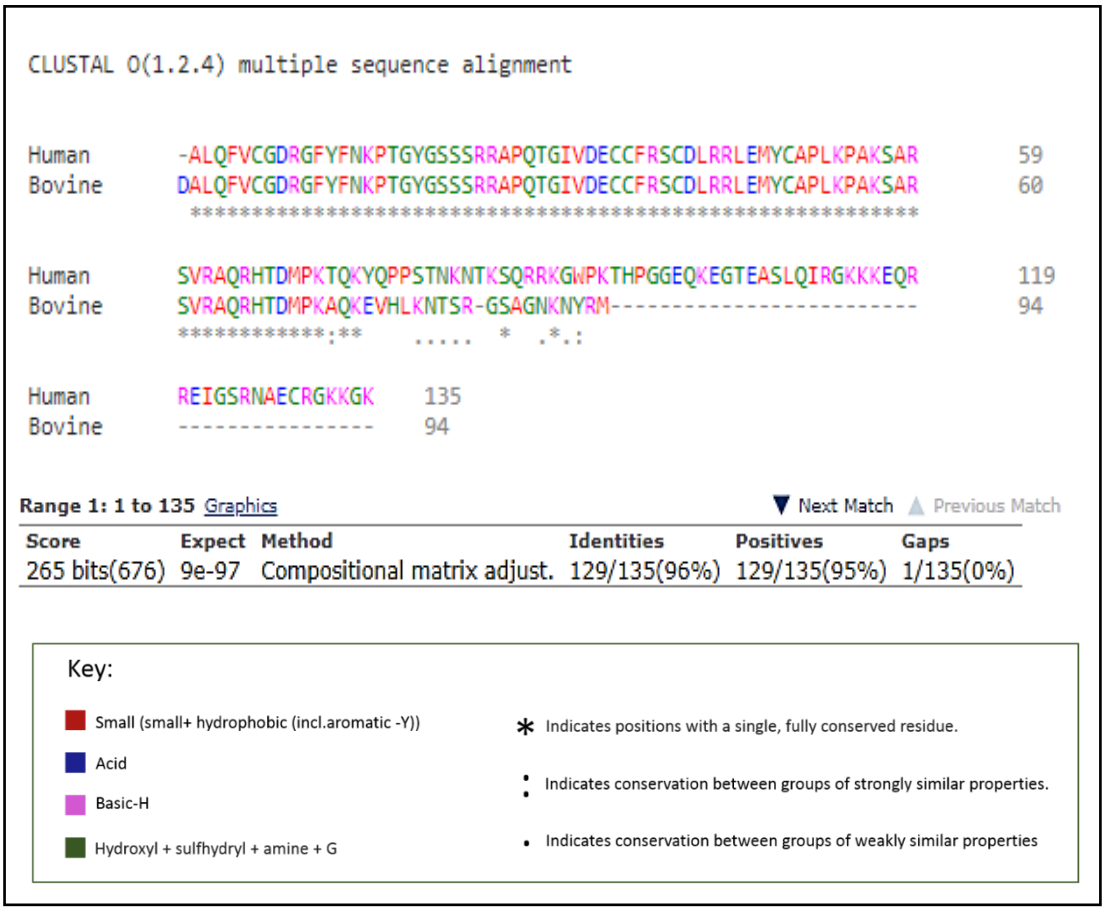

Appendix Figure 2 Insulin-like growth factor-1 (IGF-1) human versus bovine sequence alignment.

Sequence alignments were performed using the Clustal Omega online sequence alignment programme. The EMBOSS Matcher function was used within the Pairwise sequence alignment tool.

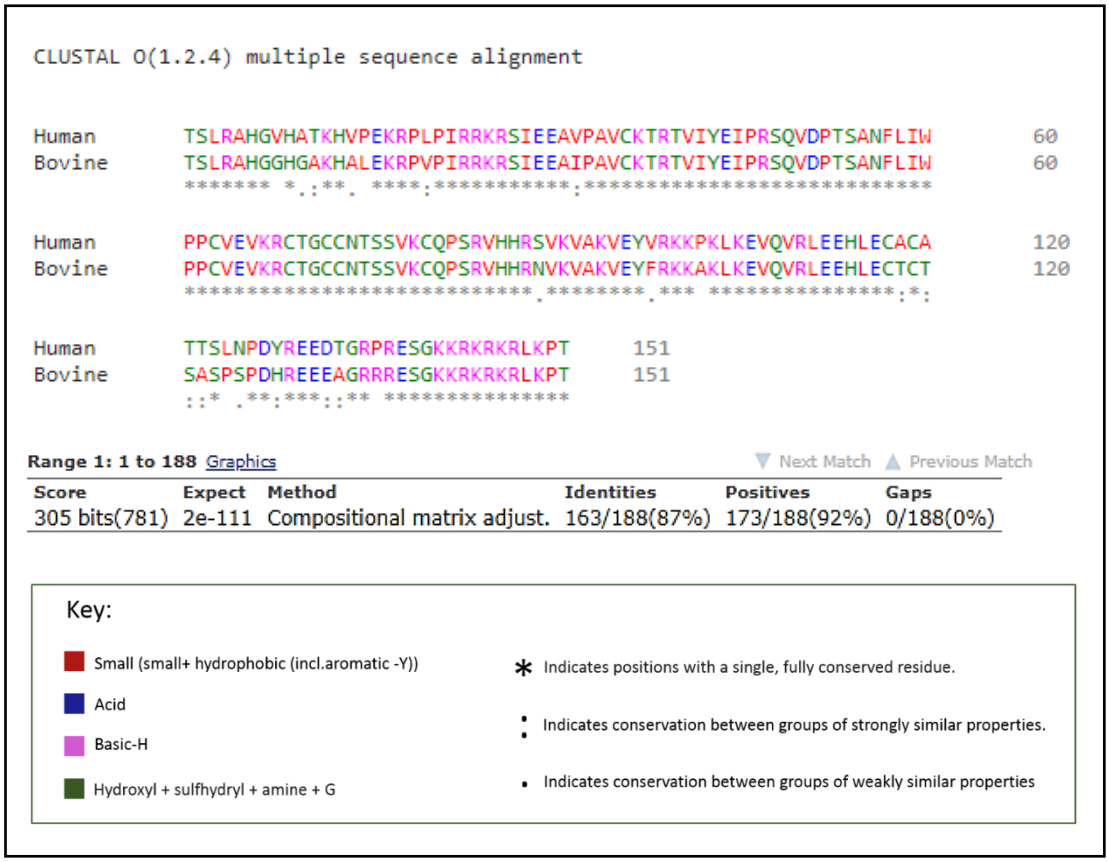

Appendix Figure 3 Platelet-derived growth factor, subunit A (PDGFA) human versus bovine sequence alignment.

Sequence alignments were performed using the Clustal Omega online sequence alignment programme. The EMBOSS Matcher function was used within the Pairwise sequence alignment tool.

Appendix Figure 4 Platelet-derived growth factor, subunit B (PDGFB) human vs bovine sequence alignment.

Sequence alignments were performed using the Clustal Omega online sequence alignment programme. The EMBOSS Matcher function was used within the Pairwise sequence alignment tool.

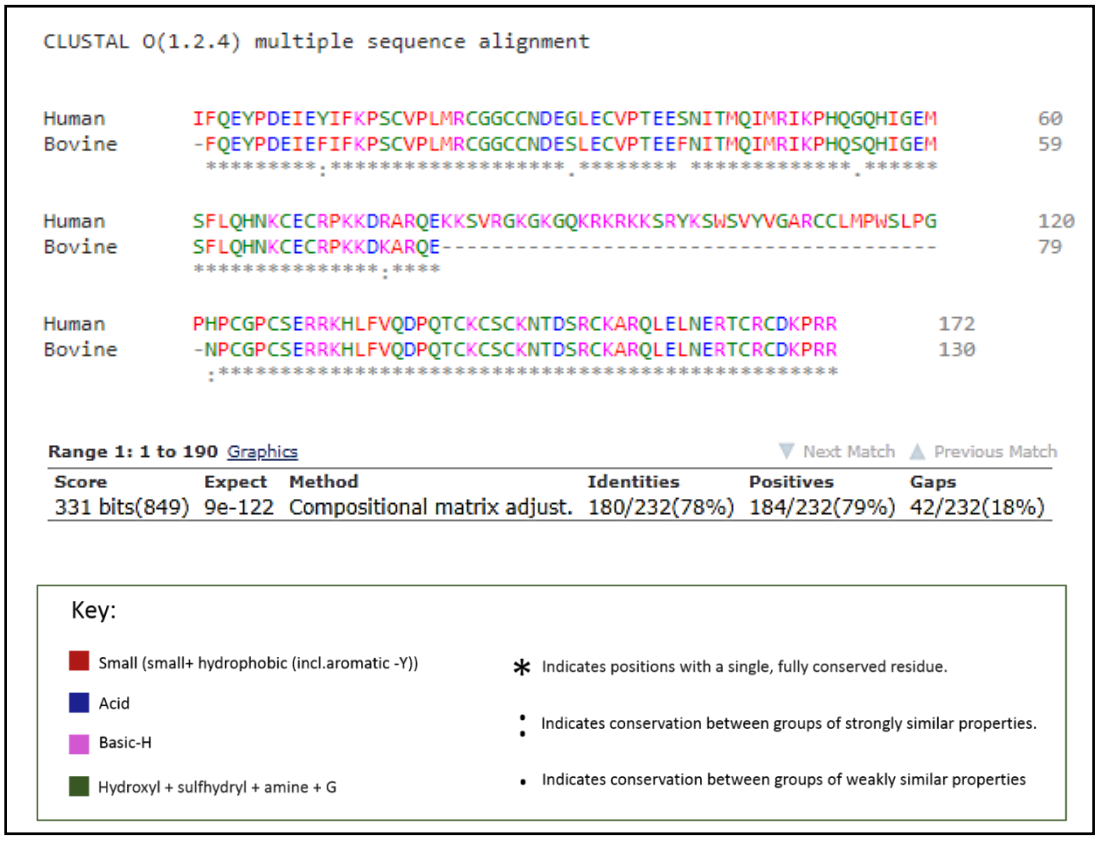

Appendix Figure 5 Vascular endothelial growth factor (VEGF) human versus bovine sequence alignment.

Sequence alignments were performed using the Clustal Omega online sequence alignment programme. The EMBOSS Matcher function was used within the Pairwise sequence alignment tool.

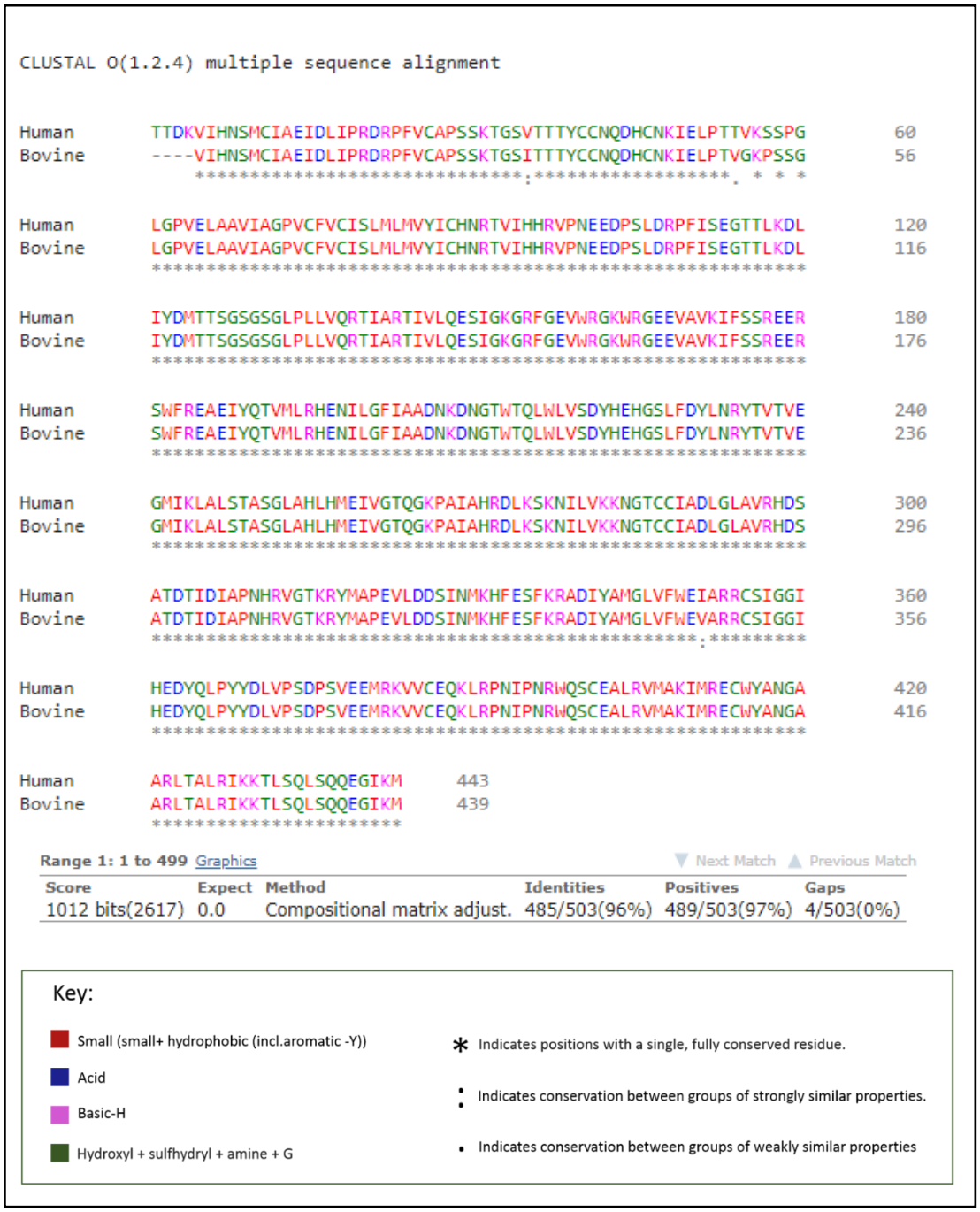

Appendix Figure 6 Transforming growth factor beta (TGF-β) human versus bovine sequence alignment.

Sequence alignments were performed using the Clustal Omega online sequence alignment programme. The EMBOSS Matcher function was used within the Pairwise sequence alignment tool.